Stony Brook University

Comparative Morphology of Primate Distal Phalanges: Implications for Early Primate Evolution and the Origins of the Primate Nail

A Dissertation Presented

by

Stephanie A. Maiolino

to

The Graduate School

in Partial Fulfillment of the

Requirements

for the Degree of

Doctor of Philosophy

in

Anthropology

(Physical Anthropology)

Stony Brook University

May 2015

Stony Brook University

The Graduate School

Stephanie A. Maiolino

We, the dissertation committee for the above candidate for the

Doctor of Philosophy degree, hereby recommend

acceptance of this dissertation.

William L. Jungers – Dissertation Advisor
Distinguished Teaching Professor and Chair, Department of Anatomical Sciences

Brigitte Demes - Chairperson of Defense
Professor, Department of Anatomical Sciences

Doug M. Boyer
Assistant Professor, Evolutionary Anthropology, Duke University

Pierre Lemelin
Associate Professor, Department of Surgery, University of Alberta

This dissertation is accepted by the Graduate School

Charles Taber
Dean of the Graduate School

Abstract of the Dissertation

Comparative Morphology of Primate Distal Phalanges: Implications for Early Primate Evolution and the Origins of the Primate Nail

by

Stephanie A. Maiolino

Doctor of Philosophy

in

Anthropology

(Physical Anthropology)

Stony Brook University

2015

Human manual dexterity is strongly enhanced by the presence of flattened nails associated with well-developed apical pads. However, the presence of nails is not unique to humans; it is one of the few traits that unite all living primates. Further, the form of the keratinous structure (nail, claw, etc.) on the ends of primate digits is often considered to be a diagnostic trait of major primate clades; strepsirrhines (lemurs, lorises, and galagos) possess a grooming claw (a specialized nail or claw used to scratch and clean the fur around the head and neck) on each second pedal digit; tarsiers possess one on each second and third pedal digit; and most anthropoids (monkeys, apes, and humans) lack one. However, relatively little is known about the, origin, diversity, and homologies of primate nails and grooming claws. This dissertation has two major objectives. The first is to determine the distribution, polarities, and homologies of grooming claws in extant and fossil primates and assess their significance for phylogenetic interpretations. The second is to elucidate patterns in distal phalanx morphology among arboreal mammals in order to better understand the circumstances surrounding the origin of primate nails. Data were collected from a sample of preserved digit tips (n=55) and distal phalanges from extant (n=1106) and fossil species (n=53). These were studied using a variety of

methods including traditional and virtual dissection, high resolution imaging techniques, principal components analysis, discriminant function analysis, and ancestral state reconstructions. Major findings can be summarized as follows. Grooming claws are demonstrated to be present in omomyiform primates, and three lineages of platyrrhine monkeys (*Aotus*, *Callicebus*, and *Pithecia*). The likely ancestral condition of the second pedal digit of primates is to bear a grooming claw, and those of strepsirrhines and tarsiers are likely homologous. The presence of primate-like nails in a non-primate mammal that is small bodied (~9g) and inhabits a terminal branch niche (honey possums) is confirmed, and a relationship between primate-like morphology of the distal phalanx and small body size is shown. It is likely that small body size in early primates facilitated the origin of nails.

Dedication Page

For my father, Sebastian Maiolino

Table of Contents

List of Figures ix
List of Tables xii
Acknowledgements xv

Chapter 1: Introduction 1
1.1 Introduction 1
1.2 Background 2
1.2.1 Basic Morphology of the Distal Phalanx 3
1.2.2 The Origins of Ungulae 5
1.2.3 Grooming Ungues 7
1.2.4 Summary 8
1.3 Objectives 8
1.4 Figures 10

Chapter 2: Homologous Features Among Distal Phalanges of Different Forms 15
2.1 Abstract 15
2.2 Introduction 16
2.3 Dissection 18
2.3.1 Materials and Methods 18
2.3.2 Results 20
2.3.2.1 Falculae 20
2.3.2.2 Postaxial Ungulae 22
2.3.2.3 Preaxial Ungulae 23
2.3.2.4 Grooming Ungues 24
2.3.2.5 Tegulae 25
2.3.2.6 Summary 26
2.4 Quantification 26
2.4.1 Materials and Methods 26

2.4.2 Results....28
2.5 Discussion....28
2.6 Figures....31
2.7 Tables....45

Chapter 3: Grooming Unguis Origins - Implications for Primate Systematics....50
3.1 Abstract....50
3.2 Introduction....50
3.3 Materials and Methods....52
3.3.1 Materials....52
3.3.2 Methods....54
3.4 Results....58
3.4.1 PCA of Ray-specific Species Means....58
3.4.2 Classification of Anthropoid Second Pedal Distal Phalanges....59
3.4.3 Classification of Fossil Distal Phalanges....60
3.4.4 Ancestral State Reconstructions....61
3.5 Discussion....63
3.5.1 Anthropoid Grooming Ungues....63
3.5.2 Strepsirrhine and Tarsier Grooming Ungues....63
3.5.3 Omomyiform Grooming Ungues....64
3.5.4 Adapiform Distal Phalanges....65
3.5.5 Ancestral States and Concluding Remarks....66
3.6 Figures....67
3.7 Tables....94

Chapter 4: Nail Origins – Implications for Primate Origins....120
4.1 Abstract....120
4.2 Introduction....120
4.3 Materials and Methods....123
4.4 Results....126
4.4.1 PCA of Ungulae, Falculae, and Tegulae....126

4.4.2 DFA of Ungulae, Falculae, and Tegulae 126
4.4.3 DFA of Locomotor Groups....127
4.5 Discussion....128
4.5.1 Primate-like Morphology in Non-primate Pedal Graspers....128
4.5.2 Early Primate Distal Phalanx Morphology....129
4.5.3 The Transition from Falculae to Ungulae....130
4.6 Figures....132
4.7 Tables....153

Chapter 5: Discussion....177
5.1 Summary of Results....177
5.2 Significance....179
5.2.1 Grooming Ungues in Eocene Primate Phylogenetics....179
5.2.2 The Origins of Primate Nails....180
5.3 Future Directions....182

Works Cited....183

List of Figures

Figure 1.1. Digit forms....10
Figure 1.2. Anatomy of ungular phalanges....11
Figure 1.3. Variation among primate ungular phalanges....12
Figure 1.4. Anatomy of falcula-, ungula-, and tegula-bearing digits....13
Figure 1.5. Grooming ungues and ungulae....14
Figure 2.1. Variation in distal phalanx morphology....31
Figure 2.2. Anatomical terminology....32
Figure 2.3. Similarity of falcular volar process with ungular volar surface....33
Figure 2.4. Dissections of long digital flexor tendon insertions....34
Figure 2.5. Virtual dissections of *Erethizon*, *Callicebus*, and *Theropithecus*....35
Figure 2.6. Virtual dissections of *Hapalemur* and *Lemur*....36
Figure 2.7. Intraosseus ligaments of falcular phalanges....37
Figure 2.8. Intraosseus ligaments of ungular phalanges....38
Figure 2.9. Intraosseus ligaments of grooming and tegular phalanges....39
Figure 2.10. Anatomical structures of the distal phalanx highlighted....40
Figure 2.11. Grooming phalanx variation....41
Figure 2.12. Points used in measurements taken in wet specimens....43
Figure 2.13. Results of regressions....44
Figure 3.1. Variation in external grooming claws and ungulae....67
Figure 3.2. Grooming unguis structure....68
Figure 3.3. Adapiform distal phalanges....69
Figure 3.4. Omomyiform distal phalanges....71
Figure 3.5. Anatomical terminology illustrated....73
Figure 3.6. Measurements used in analyses (1)....74
Figure 3.7. Measurements used in analyses (2)....75
Figure 3.8. Extant phylogeny used for ancestral state reconstructions....76
Figure 3.9. Hypothesized relationships of fossil and extant taxa....77
Figure 3.10. PCA of extant ray-specific species means (1)....78

Figure 3.11. PCA of extant ray-specific species means (2) 79
Figure 3.12. DFA classifying anthropoid second pedal distal phalanges 80
Figure 3.13. DFA classifying fossil distal phalanges 81
Figure 3.14. Boxplots of FH and ETH 82
Figure 3.15. Boxplots of FTH and MPL 83
Figure 3.16. Boxplots of VPL and MSH 84
Figure 3.17. Boxplots of ATH and BW 85
Figure 3.18. Boxplots of MSW and ATW 86
Figure 3.19. Boxplots of WSM and WIM 87
Figure 3.20. Boxplots of SIA and FIA 88
Figure 3.21. Boxplot of FSA 89
Figure 3.22. PCA of second pedal rays 90
Figure 3.23. Bayesian phylomorphospace of extant second pedal rays 91
Figure 3.24. Bayesian phylomorphospace of second pedal rays (Tree 1) 92
Figure 3.25. Bayesian phylomorphospace of second pedal rays (Tree 3) 93
Figure 4.1. Nails and claws 132
Figure 4.2. Extant and fossil distal phalanges 133
Figure 4.3. Anatomical terminology illustrated 134
Figure 4.4. Measurements used in analyses (1) 135
Figure 4.5. Measurements used in analyses (2) 136
Figure 4.6. PCA of ungulae, falculae, and tegulae 137
Figure 4.7. DFA of ungulae, falculae, and tegulae 138
Figure 4.8. Comparison of distal phalanx morphology 139
Figure 4.9. Eocene primate distal phalanges 140
Figure 4.10. Boxplots of FH and ETH 141
Figure 4.11. Boxplots of FTH and MPL 142
Figure 4.12. Boxplots of VPL and MSH 143
Figure 4.13. Boxplots of ATH and BW 144
Figure 4.14. Boxplots of MSW and ATW 145
Figure 4.15. Boxplots of WSM and WIM 146
Figure 4.16. Boxplots of SIA and FIA 147

Figure 4.17. Boxplots of FSA 148
Figure 4.18. DFA of locomotor groups 149
Figure 4.19. Phylogeny in DFA of locomotor groups 150
Figure 4.20. Primate ungular phalanges 151
Figure 4.21. Reduced falculae in small-bodied pedal graspers 152

List of Tables

Table 2.1. Specimens dissected 45
Table 2.2. Specimens virtually dissected 46
Table 2.3. Wet specimens included in regression analyses 47
Table 2.4. Measurement accuracy 48
Table 2.5. Regressions 49
Table 3.1. Extant sample 94
Table 3.2. Institutional abbreviations 100
Table 3.3. Group sample sizes 101
Table 3.4. Fossil specimens analyzed that resemble grooming phalanges 102
Table 3.5. Fossil specimens analyzed resembling ungular phalanges 103
Table 3.6. Dentally known adapiforms from Washakie Basin localities 105
Table 3.7. Dentally known omomyiforms from Washakie Basin localities 106
Table 3.8. Measurements used in this study 107
Table 3.9. Extant sample of second pedal distal phalanges 109
Table 3.10. Principal components 111
Table 3.11. Loadings for PCA (All rays) 112
Table 3.12. Canonical variates 113
Table 3.13. Loadings for DFA (Anth P2s) 114
Table 3.14. Loadings for DFA (Fossils) 115
Table 3.15. Classifications of fossil distal phalanges based on DFA 116
Table 3.16. Group means and standard deviations 118
Table 3.17. Loadings for PCA (P2s) 119
Table 4.1. Extant sample 153
Table 4.2. Group designations for extant species sample 157
Table 4.3. Institutional abbreviations 160
Table 4.4. Group sample sizes 161
Table 4.5. Fossil sample 162
Table 4.6. Dentally known adapiforms from Washakie Basin localities 164

Table 4.7. Dentally known omomyiforms from Washakie Basin localities 165
Table 4.8. Measurements used in this study 166
Table 4.9. Principal components and canonical variates 168
Table 4.10. Loadings for PCA (ungulae, falculae, and tegulae).....169
Table 4.11. Loadings for DFA (ungulae, falculae, and tegulae).....170
Table 4.12 Classifications of pedal grasping non-primates and fossil specimens.....171
Table 4.13. Group (ungulae, faluclae, and tegulae) means and standard deviations.....174
Table 4.14. Loadings for DFA (locomotor group) 175
Table 4.15. Group (locomotor mode) means and standard deviations 176

Acknowledgments

First, I sincerely thank my advisor, Bill Jungers, for his support, advice, and patience over the years. Second, I thank the rest of my committee, Brigitte Demes, Doug Boyer, and Pierre Lemelin for their insight, comments, and feedback which has greatly helped improve my dissertation work. I also thank Doug Boyer, Sergio Almécija, Amanda Kingston, and Biren Patel for generously sharing microCT scans and coveted scanning time. I thank Neil Duncan and especially Eileen Westwig for access to the mammalogy collections at the American Museum of Natural History and John Fleagle and Susan Larson for access to specimens held at Stony Brook University. I also thank Stefan Judex and Clint Ruben for access to the microCT scanner at Stony Brook University. I especially acknowledge Gabe Pagnotti for his calm handling of microCT-related mishaps. I also thank Charlie Nunn and the AnthroTree Workshop for training in phylogenetic comparative methods.

I'd also like to acknowledge the support that I have received from the Stony Brook faculty, staff, and students during my time here. I thank Andreas Koenig for his advice and tips on teaching undergraduates. I, again, sincerely thank Doug Boyer for training in many of the methods used in this dissertation, insightful discussion regarding early primate evolution, and his support. I thank Biren Patel for training in microCT scanning and digital segmentation. I thank Sergio Almécija for his assistance with various analytical methods, for general support, and for the use of his digits in Figure 3.1. I thank Joe Groenke for his assistance with fossils. I would also like to thank the Stony Brook postdocs (Mike D'Emic, Sarah Werning, and Ashley Hammond) for their help in navigating the job application process and feedback on my application materials. I thank all of my fellow students (past and present) for their friendship and support over the years. There are too many of you to list, but I'd particularly like to acknowledge Amanda Kingston, Heather Hassel-Finnegan, Rachel Jacobs, Ian Wallace, Ashley Gosslin-Ildari, Steph Blatch, Stevie Carnation, Julie Winchester, Allison Nesbitt, Kyle Viterbo, Erin Achilles, Jen Everhart, Nathan Thompson, Simone Hoffman, Nick Holowka, Peter Fernandez, Evelyn Pain, Carrie Mongle, Rachel Perlman, James Herrera, Jesse Wolfhagen, Matt Borths, Adam Pritchard, Deming Yang, Fannie Cornejo, Phil Nicodemo, Bonnie Sumner, Kate Corbin, Kate Thompson and Dorien DeVries. Lastly, I thank my family for their love and support.

This material is based upon work supported by the National Science Foundation under Grant nos. BCS-1341075 (SAM), BCS-1317525 (DMB), BCS-14404742 (DMB), BCS-1316947 (SA), BCS-1317047 (BAP); The Leakey Foundation (SAM; BAP); American Association of Physical Anthropologists Professional Development Grants (DMB; SA); and the National Institutes of Health, Grant no. 8 P40 OD012217-25 (Caribbean Primate Research Center).

1. Chapter 1: Introduction

1.1 Introduction

Humans are manually dexterous, an advantage that has allowed our species to use tools and develop complex technology. The tips of human digits facilitate such undertakings as they possess fleshy apical pads and flattened nails rather than claws (Napier, 1993). Flattened nails are present on at least one digit of all living primates, but are rare among other mammals. As such, they are one of the few characters used to define this clade (Mivart, 1873; Clark, 1936; Cartmill, 1992; Dagosto, 2007). Further, the form of the keratinous structures on primate digits varies, and the presence of nails as opposed to another type of structure (grooming ungues or tegulae) on specific digits differs among major primate clades (e.g., strepsirrhines, tarsiers, anthropoids; Bruhns, 1910; Hershkovitz, 1977; Soligo and Müller, 1999; Fleagle, 2013). Therefore, nails are not only a distinctly human and primate feature, but their presence or absence on various digits distinguishes major primate lineages.

Nails are likely to have arisen near the origins of the first primates, but exactly when, why, and how many times is unclear (Cartmill, 1974). Despite this ambiguity, the presence of nails (or absence of claws) features prominently in most hypotheses of the circumstances surrounding primate origins (e.g., Cartmill, 1974; Szalay, 2007; Orkin and Pontzer, 2011). An improved understanding of this trait is needed to better evaluate these hypotheses. Further, the morphology of the nail and the bone that supports it (the distal phalanx) can inform us about early primate evolution and diversification because it is likely related to locomotor and other behavioral activities.

Grooming ungues (sing, unguis; commonly referred to as grooming or toilet claws) are keratinized structures, like nails, that are present in certain primate clades. Strepsirrhines and tarsiers have grooming ungues on their second pedal digits; tarsiers also have them on third pedal digits (Hill, 1953, 1955; Hershkovitz, 1977; Fleagle, 2013). Anthropoids are generally assumed to lack grooming ungues, and, as such, the presumed absence of a grooming unguis has been used to indicate a phylogenetic affinity to anthropoids for certain extinct primates (e.g., adapiforms; Franzen et al., 2009; Gingerich et al., 2010). However, grooming ungues have now been demonstrated to be present in at least one anthropoid genus, *Aotus* (owl monkeys), and is

hinted at in others (Bluntschli, 1929; Hill, 1960; Rosenberger, 1979; Maiolino et al., 2011; Fleagle, 2013). This renders the polarities and homologies of grooming ungues in different groups unclear (Dagosto, 1990; Williams et al., 2010; Maiolino et al., 2011). Thus, a better understanding of the origin or origins of this feature may help elucidate the relationships of fossil primates with living groups.

This dissertation has two main objectives. The first is to determine the distribution, polarities, and homologies of grooming ungues in extant and fossil primates and assess their significance for phylogenetic interpretations. The second is to elucidate patterns in distal phalanx morphology among arboreal mammals in order to better understand the circumstances surrounding the origin of primate nails. Together, these two objectives serve to provide data on key anatomical features that will help paint a more detailed picture of the origins and evolution of early primate groups.

1.2 Background

Living primates possess three categories of keratinized structures or ungues on the tips of their digits: ungulae, tegulae, and grooming ungues. Ungulae are flattened nails, while tegulae are the narrow compressed structures that are present in callitrichines and *Daubentonia* (aye-ayes). Ungulae, tegulae, and grooming ungues differ anatomically from falculae (the claws of non-primate mammals) based on their shape, the morphology of the underlying bone (the distal phalanx; see below), and the position of the apical pad (Bruhns, 1910; Bluntschli, 1929; Clark, 1936; Hershkovitz, 1977; Rosenberger, 1977; Garber, 1980; Spearman, 1985; Soligo and Müller, 1999; Hamrick, 2001; Maiolino et al., 2011). In ungula-bearing digits, most or all of the ungula does not project beyond the distal extremity of the apical pad. Conversely, most of the unguis projects beyond the apical pad in falcula- and grooming unguis-bearing digits. Digits that bear tegulae are intermediate between these two extremes (Rosenberger, 1977; Garber, 1980). Grooming ungues and falculae differ in that grooming ungues project dorsally (point upward) from the apical pad while falculae project more distally (**Fig. 1.1**). A number of studies have sought to identify differences in the histology of unguis forms (e.g., Clark, 1936), but no differences have been found to be consistent (Thorndike, 1968; Soligo and Müller, 1999). Therefore, unguis forms are best differentiated based on gross morphology.

1.2.1 Basic Morphology of the Distal Phalanx

Ungular phalanges (distal phalanges that bear ungulae) are typically divided into three components: the base (proximal epiphysis), the shaft, and the apical tuft (**Fig. 1.2**; Mittra et al., 2007). In humans, as well as most other primates, the base is most often the medio-laterally widest and dorso-ventrally deepest part of the phalanx, flaring beyond the medial and lateral margins of the shaft. It contains the articular facet for the intermediate (or proximal in the case of the hallux and pollex) phalanx. This facet accommodates the two condyles of the trochlea-shaped head of the articulating phalanx, with a blunt keel or intercondylar crest often dividing the facet into two reciprocal concavities (Shrewsbury, 2003). The shaft extends distally from the base, which may be gently canted volarly or dorsally. Compared to falcula-bearing distal phalanges (see below), the shaft is medio-laterally wide and dorso-ventrally shallow (Clark, 1936; Hershkovitz, 1977; Spearman, 1985; Hamrick, 1998; Soligo and Müller, 1999; Maiolino et al., 2011). An expanded bony flange surrounds the distal extremity of the shaft. This structure has been referred to variously as the apical tuft (Susman and Creel, 1979; Aiello and Dean, 1990; Jungers et al., 2005; Mittra et al., 2007; Maiolino et al., 2012), distal phalangeal tuberosity (Walker et al., 2011), ungual tuft (Marzke, 1997), ungual tuberosity (Shrewsbury and Johnson, 1975; Nakatsukasa et al., 2003), or *tuberositas unguicularis* (Wilkinson, 1951; Day and Napier, 1966). Different terms are sometimes used to designate differences in the morphology of the structure among species; for example, some authors reserve the term ‘tuft’ solely for the extremely expanded and rugous structure of humans, while ‘tuberosity’ refers to the condition observed in non-human primates (Shrewsbury and Sonek, 1986). Others have argued that since the term ‘tuft’ does not adequately describe primate morphology, the term ‘shield’ should be used instead (von Koenigswald et al., 2012). Regardless of the preferred nomenclature, this structure is highly variable in shape and shows a great deal of diversity within and across primate taxa (Bruhns, 1910; Shrewsbury, 2003; Mittra et al., 2007; von Koenigswald et al., 2012). It may be rounded or pointed, medio-laterally wide or narrow, and can vary in the degree to which it surrounds the shaft and in the degree of rugosity along its margins (**Fig. 1.3**). The tuft is closely associated with the unguis plate as the distal portion of the unguis bed is firmly attached to its dorsal surface (Shrewsbury et al., 2003). The apical pad may be situated against the volar surface of the tuft (Clark, 1936; Shrewsbury and Johnson, 1975), but in many primates, especially

strepsirrhines, a large portion of the tuft appears to project beyond the apical pad where it is surrounded only by the unguis and associated tissues (Bruhns, 1910; personal observation).

Long flexor tendons (e.g., tendons of *m. flexor digitorum profundus* and *m. flexor digitorum longus*) have their primary insertion on the volar aspect of the shaft and base of ungular phalanges, which may be marked by a roughened tuberosity called the flexor tubercle (Shrewsbury and Johnson, 1975; Susman, 1998; Shrewsbury et al., 2003). This attachment site may be positioned proximally, or even as far distal as the proximal margin of the apical tuft (Shrewsbury et al., 2003). The insertion of a long extensor tendon (e.g., a tendon of *m. extensor digitorum communis* or *m. extensor digitorum longus*) is on the dorsal surface of the ungular phalanx, near or on its base, and typically does not leave a well-distinguished extensor tubercle (Le Gros Clark, 1936).

Postaxial (non-pollical and non-hallucal) ungular phalanges usually cannot be distinguished from one another on the basis of shape alone. However, those of the third and fourth digits tend to be absolutely longer than those of the second and fifth (Susman and Creel, 1979; Ricklan, 1988; Case and Heilman, 2006). Preaxial (pollical and hallucal) ungular phalanges are usually clearly distinguishable from postaxial distal phalanges. The base and articular facet of preaxial distal phalanges are shaped like a kidney bean in proximal view (Susman, 1979), while those of the other digits tend to be more oval. Further, they are often distinguished by a large proximal volar fossa that is often coupled with a V-shaped insertion for the long flexor tendon along its distal margin (Shrewsbury et al., 2003). In the human pollex, this fossa has been suggested to accommodate a sesamoid embedded within the volar plate of the interphalangeal joint during flexion (Marzke et al., 1998). Other primate species have been observed to have such sesamoids (Shrewsbury et al., 2003). When reviewing earlier literature, the reader should be aware that this fossa was once assumed to be the insertion site for the long flexor tendon, a viewpoint that has been rescinded in light of dissection-based evidence (Marzke et al., 1998; Shrewsbury et al., 2003).

As previously noted, callitrichine platyrrhines and aye-ayes (*Daubentonia*) possess specialized claw-like structures on their manual digits called tegulae (Weber, 1904; Le Gros Clark, 1936; Hershkovitz, 1977; Spearman, 1985; Soligo and Müller, 1999). This specialization allows them to cling and climb on relatively large diameter tree trunks (Cartmill, 1974; Garber, 1980; Hamrick, 1998). Tegular phalanges (distal phalanges that bear tegulae) differ in several

ways from those that bear ungulae and falculae. Falcular phalanges (distal phalanges that bear falculae) are relatively narrow and tall, often lack apical tufts, are usually associated with interphalangeal sesamoids, possess nutrient foramina located on the volar aspect of each side of the shaft near its junction with the base, and usually have well-developed tubercles for insertions of the long extensor and flexor tendons (Le Gros Clark, 1936). The flexor tubercle is located on a distinctive, proximally positioned volar process that is associated with a proximally restricted apical pad (Maiolino et al., 2011). Tegular phalanges are narrow and tall, like falcular phalanges, but resemble ungular phalanges in other ways. They possess apical tufts, and typically lack interphalangeal sesamoids, well-defined nutrient foramina, and well-developed extensor tubercles (Le Gros Clark, 1936; Thorndike, 1968; Garber, 1980; Maiolino et al., 2011). The differences among ungular, tegular, and falcular phalanges and associated tissues are illustrated in **Figure 1.4**.

Grooming ungues are used to scratch at the fur surrounding the head and neck. Grooming phalanges (distal phalanges that bear grooming ungues) reflect this function (Maiolino et al., 2011; Gilbert and Maiolino, 2015). They differ from falcular, ungular, and tegular phalanges in that they have shafts that are strongly dorsally canted (**Fig. 1.5**). This facilitates the external grooming unguis in projecting upwards beyond the apical pad where it presumably is of best use for scratching through fur. Grooming phalanges tend to be medio-laterally wider than falcular or tegular phalanges, but less so than ungular phalanges. Interestingly, like tegular and ungular phalanges, grooming phalanges possess an apical tuft surrounding the distal extremity of the shaft.

1.2.2 The Origins of Ungulae

Falculae are an asset for climbing mammals as they allow an animal to cling and climb on relatively large diameter vertical supports (Cartmill, 1972; Cartmill, 1974; Cartmill, 1985). Therefore, their replacement with ungulae in a largely arboreal lineage is unexpected. Some hypotheses have suggested that falculae impede the important grasping functions of primate hands and feet (Clark, 1959; Szalay, 1972; Napier, 1993). In these cases, ungulae are considered to be the natural result of selective pressures against falculae. However, evidence indicates that falcula- and tegula-bearing mammals are still capable to some degree of such behaviors (Cartmill, 1974; Rasmussen, 1990; Iwaniuk et al., 1998; Lemelin and Grafton, 1998; Dagosto,

2007). Further, loss of falculae does not necessarily result in ungulae, as some climbing mammals have lost keratinous structures all together on their grasping halluces (Cartmill, 1974; Szalay, 1994). Other hypotheses explain the presence of ungulae as a passive result of expansion of the apical pad related to exploitation of a terminal branch niche (Rasmussen, 1990; Hamrick, 1998), changes in body size (Soligo and Müller, 1999; Soligo and Martin, 2006), or an increased importance of the role of a tactile digit tip (Lemelin and Grafton, 1998). In general, most hypotheses view the presence of ungulae as the result of selective pressures acting against falculae or acting for expansion of apical pads.

However, the benefits that ungulae may confer must also be considered in order to determine the selective pressures that might have governed their origins. The functions of primate ungulae are poorly understood, but several hypotheses have been offered. Ungulae have been speculated to play a protective role by preventing damage or distortion to the digital pad (Clark, 1936; Baden, 1970; Napier, 1993), but some authors contest this assumption based on an extreme example of the tarsier (Cartmill, 1974; Spearman, 1985). Tarsiers have apical pads that are expanded well beyond the boundaries of their corresponding ungulae. Ungulae have also been suggested to redistribute forces placed on the fingertip (Preuschoft, 1970, 1973), assist in sensing the direction of forces applied to the fingertip (Birznieks et al., 2009), and stabilize insect prey within the hand (Godinot, 2007). Ungulae are certainly useful to primates with increased manual dexterity in behaviors such as picking up small items and peeling fruits (Spearman, 1985; Napier, 1993). Additionally, some strepsirrhines (e.g., *Euoticus elegantulus* and *Phaner furcifer*) use sharply pointed ungulae to aid them in clinging and climbing on relatively large diameter supports (Cartmill, 1972; Charles-Dominique, 1977). Interestingly, similar morphology appears to be present in larger lemur species, but it is unclear if they are used in a similar manner (personal observation). It seems most likely that ungulae play different functional roles in different primates depending on body size, mode of locomotion, and degree of manual dexterity. Therefore, the form of the earliest ungues needs to be considered when determining the possible advantages that they offered to early primates.

Distal phalanges of early fossil primates are known for both major radiations of early primates: adapiforms (e.g., Gregory, 1920; von Koenigswald, 1979; Gebo et al., 1991; Godinot and Beard, 1991; Godinot, 1992; Franzen and Frey, 1993; Godinot and Beard, 1993; Hamrick and Alexander, 1996; Franzen et al., 2009; Maiolino et al., 2012; von Koenigswald et al., 2012;

Boyer et al., 2013) and omomyiforms (e.g., Dagosto, 1988; Rose et al., 2011; Boyer et al., 2013; Ni et al., 2013). Adapiform postaxial distal phalanges have been described as "intermediate in structure" between falcular and ungular phalanges as they possess "claw-like" proximal ends paired with medio-laterally broadened ("nail-like") distal ends (Godinot, 1992; Godinot and Beard, 1993). However, the earliest known postaxial distal phalanges belong to the omomyiform, *Teilhardina brandti* (Rose et al., 2011), and they differ from those of adapiforms by more closely resembling those of extant primates. Thus, the presence of falcular-like aspects in the distal phalanges of adapiforms requires further investigation. If adapiforms are shown to possess transitional morphology while omomyiforms do not, this implies that the origin of modern ungulae differed within the two radiations.

1.2.3 Grooming Ungues

It is generally assumed that anthropoids lack grooming ungues, a notion that is repeated in almost every introductory text book on biological anthropology. This has led some researchers to claim that the assumed absence of a grooming unguis in the fossil adapiform *Darwinius* supports a close taxonomic relationship between adapiforms and anthropoids (Franzen et al., 2009; Gingerich et al., 2010). However, the presence of grooming ungues in platyrrhines (*Aotus* and possibly others) brings into question the utility of this trait for demonstrating such relationships as the polarities and homologies of grooming ungues among different clades are unclear (Maiolino et al., 2011). Further, grooming ungues have now been demonstrated to be present on the second pedal digit of the adapiform *Notharctus tenebrosus* (Maiolino et al., 2012) while additional grooming phalanges have been associated with a number of adapiform taxa (von Koenigswald et al., 2012; Gilbert and Maiolino, 2015). The preservation of the *Darwinius* fossil does not allow for an accurate determination of the presence or absence of a grooming unguis, but the presence of grooming ungues in other adapiforms suggests that it possessed one (Maiolino et al., 2012). Therefore, adapiforms may be strepsirrhine-like in the possession of grooming ungues on the second pedal digit of each foot, but this may also be a trait shared with early anthropoids. If this is the case, then grooming ungues on the second pedal digit cannot be used to indicate the relationships of fossil to extant primate groups.

In order to address the utility of grooming ungues as a synapomorphy, a better understanding of the morphological variation among and within clades is necessary. Strong

morphological differences may help to elucidate independent origins verses shared ancestry. Von Koenigswald et al. (2012) have noted differences in strepsirrhine and tarsier grooming phalanges, while early analysis of the grooming phalanges of owl monkeys suggested similarity to those of extant strepsirrhines (Maiolino et al., 2011). Further, there appears to be a morphological continuum from ungular to grooming phalanges among platyrrhine species (Maiolino et al., 2011), but this was based upon a limited sample and restricted set of measurements. A larger sample and a more detailed set of measurements should better help to elucidate grooming unguis diversity among extant primates.

1.2.4 Summary

In sum, distal phalanges and their accompanying structures have been an important topic in primate evolution. However, relatively little is known about them. There is indication that distal phalanx morphology is linked to function and phylogeny, but an accurate depiction of the morphological correlates of behaviors and clades is required. Further, the presence and absence of grooming ungues in certain lineages needs to be better documented before more solid conclusions about the phylogenetic significance of grooming ungues can be made. Finally, a better understanding of the potentially transitional morphology of adapiform distal phalanges is needed to interpret their significance for ungula origins.

1.3 Objectives

The following dissertation is divided into three sections, each addressing a major topic. Part 1 addresses the question of homologies among distal phalanges that bear different unguis forms. As it has been shown that these bones look quite different from one another, it is unclear as to what features can be used to construct measurements that are meaningful and comparable among forms. Therefore, associations with soft tissue and bony morphology are assessed to identify homologies for use in a comparative context. The major objective of Part 2 is to better document the presence of grooming ungues among platyrrhines and the variation in grooming ungues among different primate groups (both extant and fossil). The resulting data are then used to reconstruct the ancestral conditions of major clades. This allows for a determination of whether or not the presence/absence of grooming phalanges and/or morphological variation among grooming phalanges can be utilized as a synapomorphy of any specific clade. Finally,

Part 3 assesses the evolutionary transition from falculae to ungulae. The relationship between distal phalanx form and function is investigated and non-primate mammals that resemble primates are identified to determine potential selective pressures that lead to ungula-bearing morphology. The potential transitional morphology of adapiforms and their significance is also addressed.

1.4 Figures

Fig. 1.1. Digit forms.
Digits that bear ungulae (*Chlorocebus*), tegulae (*Saguinus*), grooming ungues (*Lemur*), and falculae (*Sciurus*) in lateral (left) and dorsal (right) views. Note that the grooming unguis-bearing digit is flexed at the distal interphalangeal joint so that in lateral view, its dorsal side faces towards the right while those of the other digits face upwards.

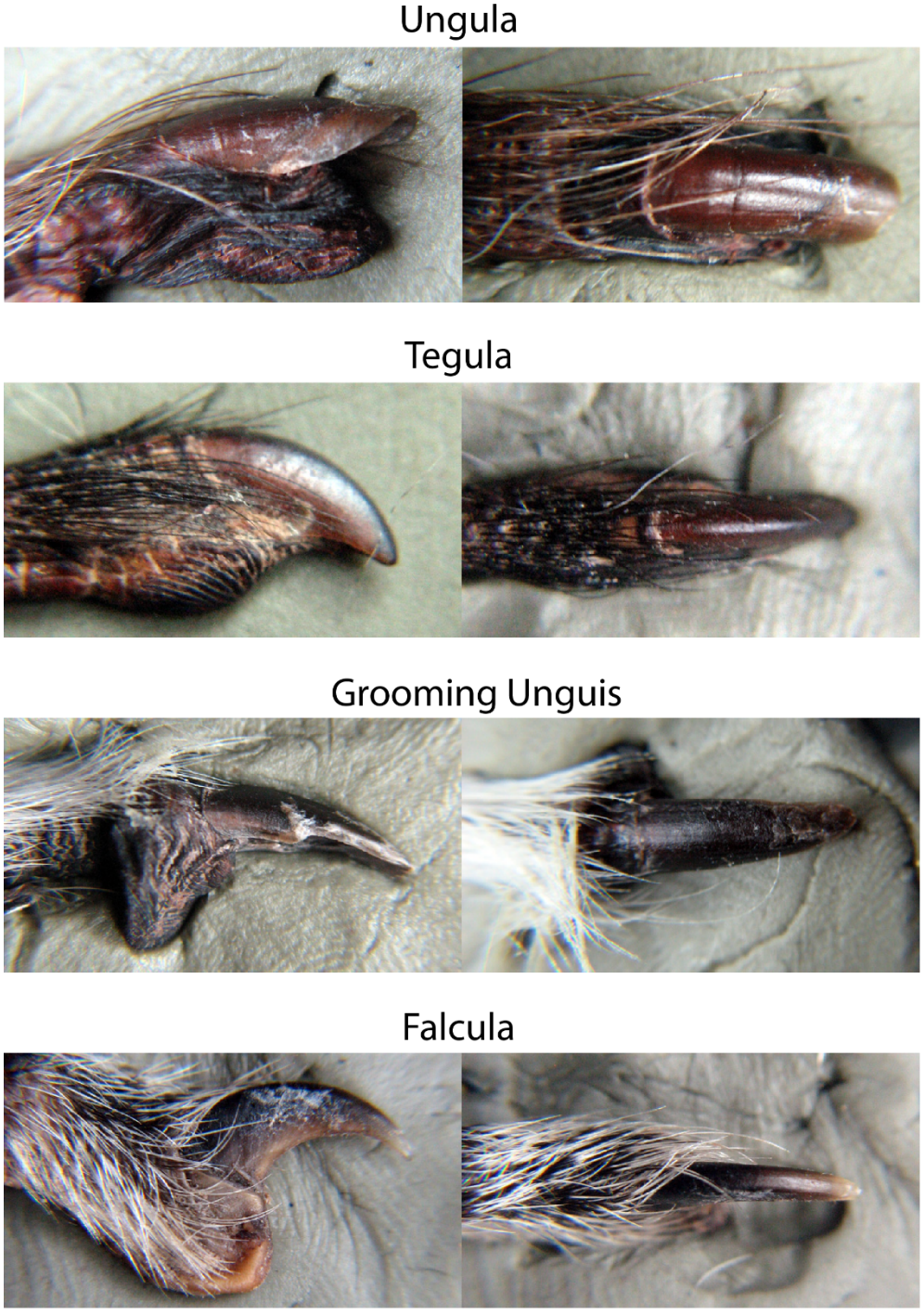

Fig. 1.2. Anatomy of ungular phalanges.
Basic anatomical structures of ungular distal phalanges demonstrated on the human pollical distal phalanx (top, shown in dorsal, volar, and proximal views from left to right respectively) and a postaxial distal phalanx (bottom, same views). Right: the tissues that surround and attach to the distal phalanx demonstrated in sagittal section through the human pollex. Abbreviations: Ap: apical pad; Af: proximal articular facet; At: apical tuft; B: base; Dis: distal interphalangeal sesamoid; Dp: distal phalanx; Ei: insertion of extensor tendon; Et: extensor tendon; Fi: insertion of flexor tendon; Ft: flexor tendon; Ic: intercondylar crest; Np: nail plate; Pp: proximal phalanx; Pvf: proximal volar fossa; S: shaft; Vp: volar plate.

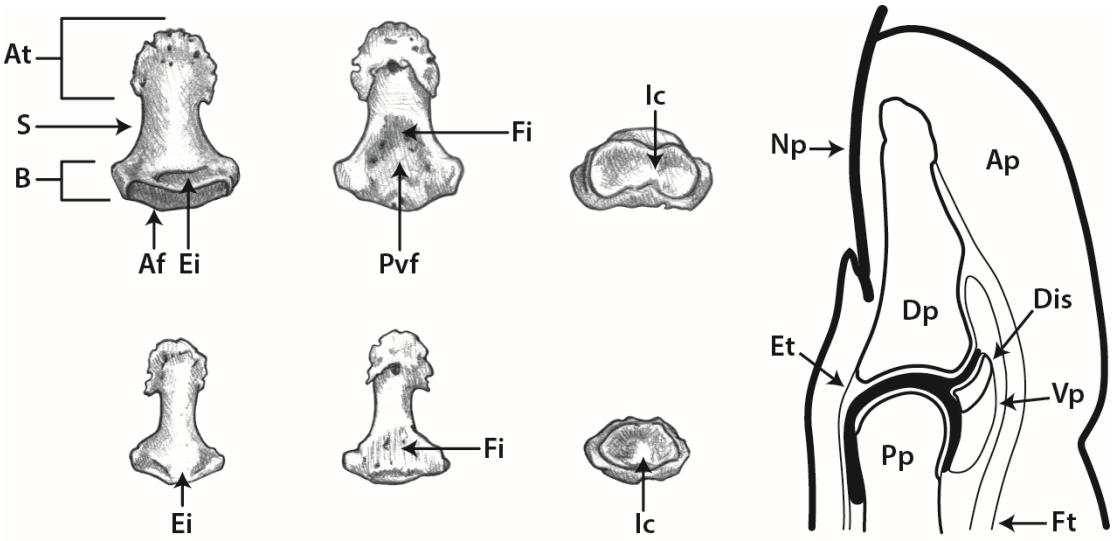

Fig. 1.3. Variation among primate ungular phalanges.
Dorsal view of postaxial distal phalanges from various non-human primates (scaled to the same length) demonstrating variation among primates.

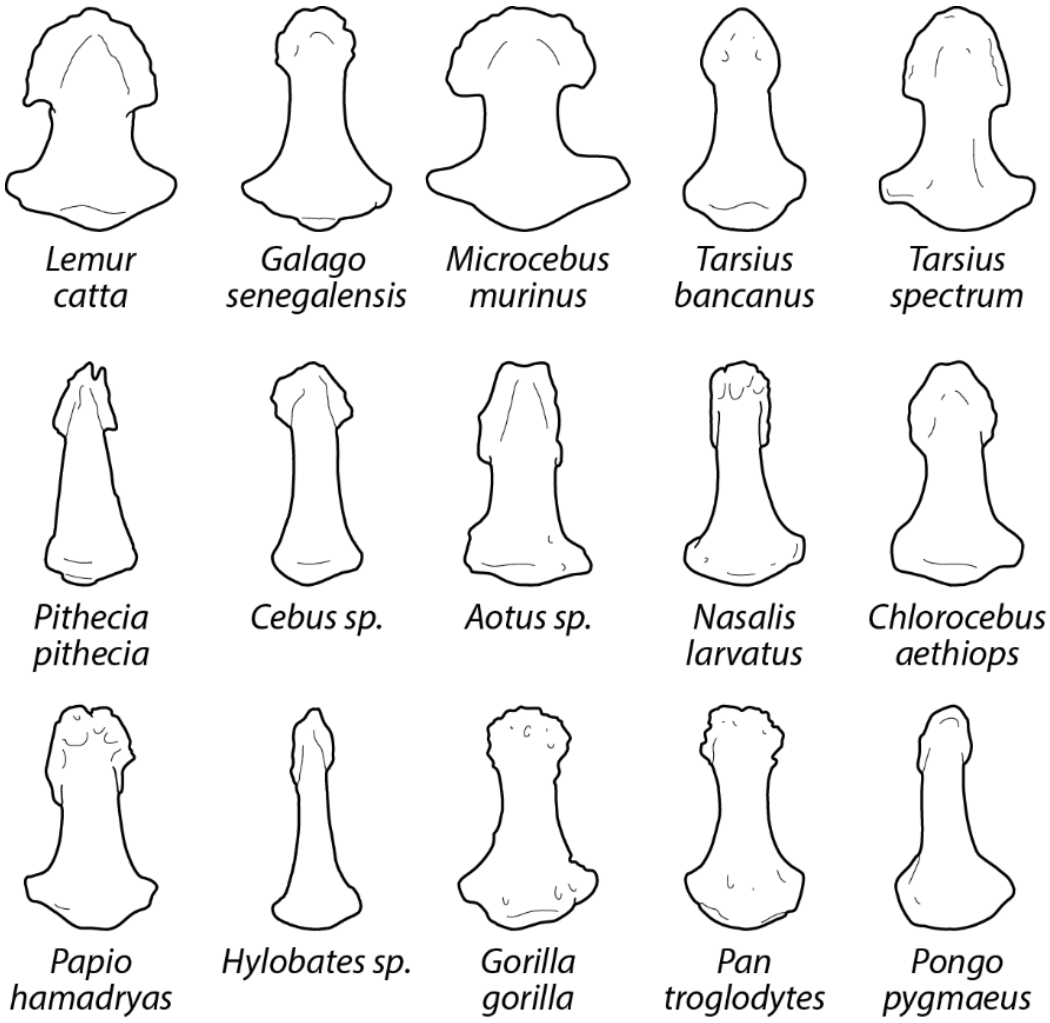

Fig. 1.4. *Anatomy of falcula-, ungula-, and tegula-bearing digits*.
Key anatomical differences among falcular (left), ungular (middle) and tegular (right) distal phalanges and associated structures from postaxial rays. Integument and other soft tissues are indicated by outlines surrounding the distal phalanges. Abbreviations: Ap: apical pad; At: apical tuft; Dis: distal interphalangeal sesamoid; Dp: distal phalanx; F: falcula; Mp: middle phalanx; Nf: nutrient foramen; T: tegula; U: ungula.

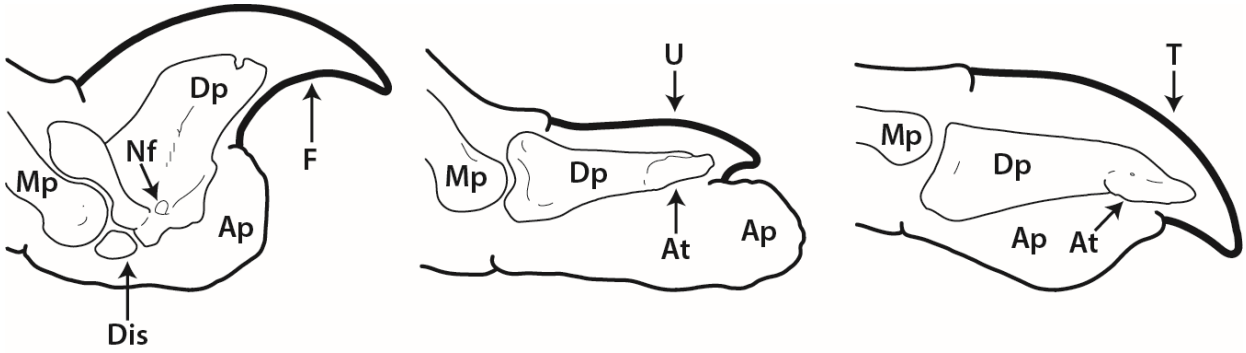

Fig. 1.5. Grooming ungues and ungulae.
The second (grooming unguis-bearing; top) and third (ungula-bearing; bottom) pedal digit tips from *Eulemur fulvus*. Left: external tissue; Middle: external tissue rendered transparent to show position of distal phalanx; Right: isolated distal phalanx. In grooming ungues, the unguis and distal phalanx project dorsally above the apical pad.

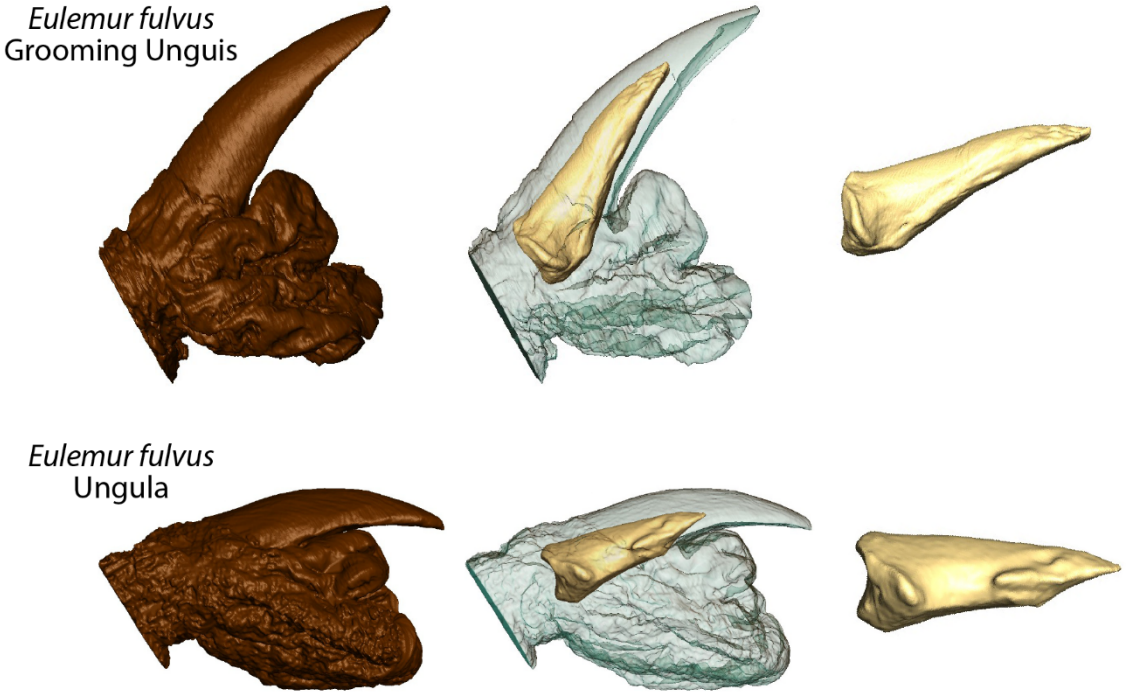

2. Chapter 2: Homologous Features Among Distal Phalanges of Different Form

2.1 Abstract

Distal phalanx morphology can provide critical bearing on questions of primate origins, primate diversification, and the evolution of human manual dexterity. However, distal phalanges are difficult to analyze in a broad comparative and quantitative context as homologous anatomical features among these highly variable bones are not always clear. One possible candidate for a universally identifiable homologous feature is the volar process, a bony structure present in claw-bearing distal phalanges. Similar volar structures have been identified in nail- and tegula-bearing distal phalanges, but are flatter and much more proximo-distally expanded. It has been suggested that these structures may be related to the proximo-distal expansion of the apical pad along the volar surface of the distal phalanx. The first goal of the present study is to determine if the volar process of claw-bearing distal phalanges and the similar structures observed in other distal phalanx forms can be considered homologous. If the volar structures are homologous, it is predicted that they will be associated with the same soft tissue insertions in all taxa that possess them. The second goal is to determine if proximo-distal expansion of the apical pad can be inferred from such a structure/structures. Traditional and virtual dissections were used to assess tissue relationships, while phylogenetic generalized least squares regressions were used to test for a relationship between bony morphology and the apical pad. A bony volar process that typically ends in a rounded eminence was found in almost all observed distal phalanges. It contains insertion sites for the long digital flexor tendon and bilaterally occurring intraosseous ligaments, and lies embedded within the apical pad. Due to its similarity in shape and a conserved relationship with soft tissue structures among distantly related taxa, it is likely that this structure is homologous and/or can be considered functionally equivalent. Further, the volar process can be used to distinguish the portion of the distal phalanx that lies embedded within the apical pad versus the portion that projects distally or dorsally to it. Therefore, the volar process provides useful landmarks than can be used to both compare distal phalanges and infer the proximo-distal extent of the apical pad along the length of the distal phalanx. Since the apical pad features prominently in theories of primate origins as well as the evolution of human manual

dexterity, these results can help inform interpretations of fossil distal phalanges that have bearing on these and related questions.

2.2 Introduction

Distal phalanges have been an important topic when considering many of the critical questions concerning primate (and human) evolution. For example, distal phalanx morphology plays a prominent role in the debate surrounding the origin of the precision grip in the human lineage (Susman and Creel, 1979; Marzke, 1997; Moyà-Solà et al., 1999; Almécija et al., 2014). Further, the presence of ungulae (nails, supported by the bony phalanx) is one of the few traits that unites all living primates(Mivart, 1873), and therefore, the circumstances surrounding the evolution of primate ungulae from non-primate falculae (claws) can provide information bearing on our understanding of primate origins (Cartmill, 1972). In the past, the presence of claw-like structures on some digits of callitrichine platyrrhines and the strepsirrhine *Daubentonia*, termed tegulae (present on all manual digits of both groups, pedal digits 2-5 in callitrichines, and pedal digits 3-5 in *Daubentonia*), presented a significant question: are they retentions of the ancestral falculae or are they ungulae that have been secondarily modified into a falcula-like form? After much debate, analyses relying upon histological studies of the unguis (i.e., keratinized sheath that drapes over the dorsum of the distal phalanx; falcula, tegula, ungula, etc.) and distal phalanx morphology have led to a general agreement that tegulae are derived from ungulae (e.g., Garber, 1980; Soligo and Müller, 1999) rather than falculae (e.g., Clark, 1936; Thorndike, 1968). Therefore, they most likely have been independently derived in the two lineages. More recently, attention has turned toward primate grooming ungues (commonly referred to as grooming claws, which are present on the second pedal digits of strepsirrhines and *Aotus*, and on the second and third pedal digits of tarsiers) due to their presumed cladistic significance when interpreting the phylogenetic affinities of fossil taxa (Franzen et al., 2009; Gingerich et al., 2010; Williams et al., 2010; Maiolino et al., 2011; Gingerich, 2012; Maiolino et al., 2012; von Koenigswald et al., 2012). In particular, the diagnosis of grooming ungues in the fossil record has become a contentious topic, in part due to a lack of understanding of the significance of particular morphological aspects. These and related topics can be challenging to address using a broad comparative and quantitative approach because distal phalanges bearing different unguis forms (e.g., falcular, ungular, tegular, and grooming phalanges), and even those of different taxa that

possess the same general form demonstrate stark morphological differences (**Fig. 2.1**). This renders it difficult to determine meaningful and homologous landmarks and measurements.

Further, distal phalanx morphology (see **Fig. 2.2** for an illustration of morphological terms on ungular phalanges) has a history of misinterpretation that is likely due to its complex nature. Today, in light of evidence from dissection, it is well known that the long flexor tendon of primate pollical and hallucal (preaxial) digits typically inserts onto a v-shaped or gabled ridge distal to a small fat-filled fossa (called the proximal volar fossa; note that this configuration differs from that of non-pollical/non-hallucal ungular phalanges as well as those of other distal phalanx forms); in the past, this fossa was assumed to be the tendon's insertion site (Marzke et al., 1998; Shrewsbury et al., 2003). Ungual spines and their related intraosseous ligaments, structures suggested to be related to a precision grip in humans, have also been subject to contradictory interpretations and descriptions. Ungual spines are described as small, proximally directed spines situated at the lateral edges of the apical tuft (i.e., expansion of bone surrounding the distal shaft of certain distal phalanges, also referred to as ungual tuberosities, ungual tufts, or shields) that serve as attachment sites for bilaterally occurring ligaments originating from the base (proximal epiphysis) of the phalanx (also known as interosseous, lateral intraosseous, or tuberospinous ligaments; Shrewsbury and Johnson, 1975). The presence of ungual spines in non-human taxa has been contested as some authors claim that they are only found in humans and the occasional baboon (Shrewsbury and Sonek, 1986; Shrewsbury et al., 2003), while others suggest that their presence is more widespread among primates (Susman, 1998). Further, the associated intraosseous ligaments are described as being present only in humans and several baboon individuals while a "dense fibrous continuation of the pulp [fleshy pad of the fingertip]" takes its place in other taxa (Shrewsbury et al., 2003:39). Interestingly, several baboon individuals were described as lacking intraosseous ligaments while possessing their insertion sites, the ungual spines. Ambiguity and contradictory interpretations of distal phalanx morphology necessitates the use of a careful, broad, and well-illustrated approach to understand the presence and significance of morphological features.

One such feature that warrants closer attention is a distinct bony process located along the volar surface of the proximal region of falcular (claw-bearing) distal phalanges. This structure contains the insertion of the long digital flexor tendon (often called the flexor tubercle). However, it is often expanded beyond the flexor insertion and interestingly, may bear superficial

resemblance to ungular (nail-bearing) distal phalanges from postaxial (non-hallucal/non-pollical) digits. It may even possess proximally directed spines at the lateral edges of a tuft-like expansion (**Fig 2.3**). This region has been referred to as the volar process to emphasize its expansion beyond the flexor tubercle (**Fig. 2.1**). It lies embedded within the apical pad while the more dorsal and distal portions of the phalanx are surrounded only by the unguis and related tissue (Maiolino et al., 2011). Maiolino et al. (2011) also identified similar structures among ungular, tegular, and grooming phalanges. It is possible that the volar process and these similar structures are homologues of one another. Further, since these structures lie embedded within the apical pad, they may be related to its proximo-distal expansion.

The first goal of the present study is to determine if the volar processes of falcular phalanges are homologous to the similar structures observed in ungular, tegular, and grooming phalanges. This is addressed in the section, Dissection. If the volar structures are homologous, it is predicted that they will be associated with the same soft tissue insertions in all taxa that possess them (i.e., they will contain the same type I landmarks). The second goal is to determine if expansion of the apical pad along the distal phalanx can be inferred from such a structure/structures and therefore would be relevant to the interpretations of fossil distal phalanges. This is addressed in the section Quantification.

2.3 Dissection

2.3.1 Materials and Methods

Dissections were conducted on preserved specimens of primate and non-primate species (**Table 2.1**). Preserved specimens are either wet (formalin-fixed and stored in a formalin-based solution) or dry. Dry specimens were obtained from several sources. *Erethizon dorsatum* specimens were obtained from a trapper and were cured using salt. Others are part of a collection of preserved primates and other mammals that had been maintained by the late George E. “Erik” Erikson and was recently acquired by Stony Brook University (SBU). Many of these specimens have become dried and mummified over time. Additionally, it should be noted that the specimen of *Manis* housed at the American Museum of Natural History (AMNH) was not dissected. Rather, it was found with dried ligamentous attachments and is figured in this paper to increase taxonomic diversity. Since fresh or frozen specimens were not available at the time of study,

only anatomical structures which preserve well (tendons and ligaments) were inspected. Further, dried specimens were preferred as thin, delicate ligaments have become hardened and are less susceptible to accidental damage.

In addition to traditional dissection, several specimens were virtually dissected using high resolution imaging methods (**Table 2.2**). Preserved specimens (wet and dry) were scanned using micro x-ray computed tomography scanners at either SBU (VivaCT75 microCT scanner), Duke University (Nikon XT H 225 ST microCT scanner), or AMNH (GE Phoenix Vtome x S scanner) at voxel sizes ranging from 18 – 68μ. For each scan, each structure of interest was individually segmented out and a 3D model was generated using the software Avizo 7.1. Segmentation was done using a combination of the magic wand tool and the paintbrush tool with "limited range only" selected in Avizo's segmentation editor. In some circumstances, a portion of a structure's boundary could not be discerned from adjacent structures of similar density. In these cases, the structure was visually interpolated based on results from a related traditional dissection. No virtual dissections were conducted on structures for which the boundary could not be determined in the scan nor could be confirmed with traditional dissections.

Along with traditional and virtual dissections, a large number of clean osteological specimens were surveyed in order to assess the amount of variation in extant mammalian distal phalanges. Most specimens were housed at the AMNH and SBU. About 1,800 falcular, ungular, tegular, and grooming distal phalanx specimens from ~260 species of 18 mammalian orders representing Laurasiatheria (Eulipotyphla, Chiroptera, Carnivora and Pholidota), Afrotheria (Macroscelidea, Afrosoricida, and Tubulidentata), Euarchontaglires (Primates, Scandentia, Dermoptera, Rodentia, and Lagomorpha), Xenarthra (Cingulata and Pilosa), Metatheria (Didelphimorphia, Dasyuromorphia, and Diprotodontia), and Monotremata were studied. All major primate groups were included, encompassing 61 of the 73 extant primate genera currently recognized by the International Union for Conservation of Nature. Specimens were either photographed in several views or microCT scanned and are stored in a database for ease of access and review.

2.3.2 Results

Insertions for the long flexor tendon were confirmed to be at the proximal aspect of the volar surface of the phalanx for falcular, tegular, grooming, and postaxial ungular phalanges and along a more distally located site for preaxial ungular phalanges (**Figs. 2.4, 2.5, 2.6**). The term long flexor tendon is used here to refer to any arrangement of flexor tendons that insert upon the distal phalanx. These tendons may be comprised solely of or formed from conjoined subsidiary tendons of *m. flexor digitorum profundus*/*m. flexor pollicis longus*, *m. flexor digitorum tibialis*/*m. flexor hallucis longus*, or *m. flexor digitorum fibularis*/*m. flexor digitorum longus* depending on the ray and organism. It should also be noted that some flexor tendons may also contain tendinous slips from muscles not listed above. For example, in *Erethizon dorsatum*, the long flexor tendon of ray 1 is formed by the conjoined subsidiary tendons of *m. flexor digitorum tibialis* and *m. abductor hallucis brevis* (McEvoy, 1982). Comprehensive descriptions of the flexor tendon arrangements in organisms dissected in this paper can be found in the literature (McClearn; Lewis, 1962; McEvoy, 1982; Aversi-Ferreira et al., 2011; Diogo et al., 2012). Bilaterally occurring intraosseous ligaments were found to be present on all distal phalanx forms (**Figs 2.5-2.9**). These ligaments arise from an insertion site on the base (the proximal epiphysis) of the distal phalanx and, in most cases, attach to the lateral sides of a rounded eminence located somewhere along the volar surface of the phalanx. Specific variations are described below for each unguis form and further illustrated in **Fig. 2.10**.

2.3.2.1 Falculae

Four falcular digits were traditionally dissected, one osteological specimen with preserved ligaments was inspected (*Erethizon*, *Nasua*, and *Manis*, **Table 2.1**), and one was virtually dissected (*Erethizon*, **Table 2.2**). The insertion for the long flexor tendons were confirmed to be located on the proximal aspect of the volar surface (commonly referred to as the flexor tubercle) in both *Erethizon* and *Nasua* (**Figs. 2.4, 2.5**). A flexor tendon was not preserved in the *Manis* specimen, but its insertion is assumed to also be on the proximal aspect of the volar surface. Intraosseous ligaments were found in all three species (**Figs. 2.5, 2.7**). They are positioned deep to the volar edge of the falcula, originate on the base of the phalanx, and insert on the lateral sides of the volar process. In *Erethizon* and *Nasua*, the intraosseous ligaments are

more dorsally positioned and angled such that their volar margins face proximo-volarly, while those of *Manis* more closely parallel the volar surface of the volar process. In *Erethizon* and *Nasua*, the volar process is proximally restricted and dorso-volarly deep, but in *Manis* it is proximo-distally longer and dorso-volarly flatter.

A distinct volar process was observed on all surveyed specimens sampled from therian mammals. The distal ends of these processes end in distally-directed, rounded or blunt eminences and are accompanied by bilaterally occurring nutrient foramina positioned just superior to the process (e.g., *Erethizon* and *Nasua*, **Figs. 2.4**; *Erethizon*, **Fig. 2.5**; *Tupaia*, **Fig. 2.10**). A vascular groove on each side of the phalanx can be seen extending dorsally and distally from most foramina (e.g., *Manis*, **Fig. 2.7**; *Tupaia*, **Fig. 2.10**). This groove has been shown to accommodate the main vasculature of the dermal claw bed (Homberger et al., 2009). It is likely that the vasculature passes between the intraosseous ligament and the phalanx, gives off a branch that enters into the nutrient foramen and continues on in the vascular groove. The shape of the volar processes otherwise varies considerably among taxa, particularly in the degree of its distal expansion along the phalanx and in its dorso-volar depth. Some species have medio-laterally wide processes that possess spine-like extensions similar to those figured for *Myocastor* (**Fig. 2.3**), while others have medio-laterally compressed processes (e.g., *Tupaia*, **Fig. 2.10**). In some specimens, particularly feliform carnivorans, a broad crest of bone (sometimes called an ungual crest or unguicular hood) can be seen extending from the margin of the base of the phalanx and the lateral sides of the volar process. A portion of it occupies the position that the intraosseous ligament takes in other species and therefore in these taxa, it is inferred that the ligament is absent, or perhaps calcified/ossified as part of the crest. Monotreme distal phalanges differ from those of therian mammals. They possess something that is reminiscent of the therian volar process, but it does not end in a rounded eminence and is interrupted by a single large foramen in its volar surface. Consequently, these phalanges lack the bilaterally and more superiorly placed foramina of therian taxa. While there is a high degree of interspecies variation within mammals, observations from multiple individuals of the same species reveals that there is a very low degree of intraspecific variation.

2.3.2.2 Postaxial Ungulae

Two postaxial ungular distal phalanges were traditionally dissected (*Eulemur* and *Cebus*, **Table 2.1**) and two were virtually dissected (*Callicebus* and *Theropithecus*, **Table 2.2**). The flexor tendon insertion was confirmed to be at the proximal region of the volar surface of the phalanx (*Cebus* postaxial distal phalanx, **Fig. 2.4**; *Callicebus* and *Theropithecus*, **Fig. 2.5**). Contrary to the findings of Shrewsbury and Sonek (1986), intraosseous ligaments were found in each specimen (**Fig. 2.5, 2.8**) and were located deep to the volar edges of the ungula which had to be carefully peeled away to reveal their presence. As in falcular phalanges they originate from the base of the phalanx, but insert more distally on the volar aspect of the lateral sides of the phalanx. An examination of the volar surfaces of the *Eulemur* (**Fig. 2.3**, **2.8**) and *Callicebus* (**Fig. 2.7**) distal phalanges show that a large portion of it is formed by a process of bone that contains the flexor insertion proximally and distally ends in a rounded eminence (*Macaca mulatta* orange highlights, **Fig. 2.10**). The remainder of the phalanx projects distally beyond it (*Macaca mulatta* green highlights in volar view, **Fig. 2.10**). The lateral extremities of the rounded eminence provides the insertion points for the intraosseous ligaments. In *Cebus*, the volar surface of the distal phalanx ends in a rounded eminence, but the shaft does not project beyond this as in *Eulemur* and *Callicebus* (**Fig. 2.8**). The intraosseous ligaments can be seen inserting onto the lateral sides of this eminence near its volar surface (**Fig. 2.8**). *Theropithecus* shows a morphological configuration similar to that of *Cebus*, with the exception that the insertion points for the intraosseous ligaments are more proximally positioned and the rounded eminence of the volar surface is much more extensive and rugous (**Fig. 2.5**).

Osteological specimens from all major primate clades show a process containing a proximally positioned flexor tendon insertion and ending in a distally-directed rounded or blunt eminence. In some species, this process ends proximally to the distal-most extent of the phalanx (as in *Eulemur* and *Callicebus*) and in others, it accounts for the entirety of the volar surface of the bone (as in *Cebus* and *Theropithecus*). Some specimens show spine-like insertions for the intraosseous ligament (e.g., *Theropithecus* and *Eulemur*), while others are more rounded (e.g., *Cebus*). The ungular specimens typically lack the bilateral nutrient foramina seen in falcular phalanges, although small, perforating foramina may be present at various locations along the shaft of the bone. A neurovascular bundle has been described to pass deep to the intraosseous ligament (Shrewsbury and Johnson, 1975) and a vascular groove can sometimes be observed on

the lateral sides of many specimens running from the space deep to the ligament and continuing distally along the sides of the phalanx (**Fig. 2.10**). Observing specimens from different individuals, there does not appear to be a high degree of intraspecific variation, although some individuals may have longer or more pronounced ungual spines than others.

2.3.2.3 Preaxial Ungulae

One hallucal ungular distal phalanx was traditionally dissected (*Cebus*, **Table 2.1**) and one pollical ungular distal phalanx was virtually dissected (*Hapalemur*, **Table 2.2**). As previously described, the long flexor tendon was confirmed to insert on a v-shaped ridge which formed the distal margin of a large volar fossa (*Hapalemur*, **Fig. 2.6**). Again contrary to dissection results of Shrewsbury et al. (2003), intraosseous ligaments were observed running from the base of the phalanx to the lateral sides of a rounded eminence of the volar surface of both the *Hapalemur* pollex (**Fig. 2.6**) and the *Cebus* hallux (not preserved).

Again, cleaned osteological specimens from the hallux and pollex of all major primate clades were inspected. Specimens showed a similar configuration as described for postaxial ungular phalanges, but with the exception of the presence of a volar fossa and distally placed insertion for the long flexor tendon. In most specimens, the process ending in a rounded eminence accounts for the entirety or nearly the entirety of the volar surface of the phalanx. It should be noted that some individuals of hominoid species which are known to variably lack a long flexor tendon also lack a fossa and insertion scar on preaxial phalanges (Susman, 1998). As noted by Shrewsbury et al. (2003), the extent of the volar fossa and the position of insertion for the flexor tendon varies per species, and in some specimens it is positioned very far distally. Finally in a few specimens, the intraosseous ligaments were observed to be completely ossified (e.g. *Cercocebus*, **Fig. 2.8**). Overall, there does not appear to be a high degree of intraspecific variation among the observed sample with the exception of the extent of ossification/calcification of the intraosseous ligaments. It is possible that this is related to the age of the individual.

2.3.2.4 Grooming Ungues

One grooming phalanx was traditionally dissected and one was both traditionally and virtually dissected (*Eulemur* and *Lemur*, **Tables 2.1 and 2.2**). In both specimens, the long flexor tendon was seen inserting onto the proximal region of the volar surface of the phalanx (**Figs. 2.4, 2.6**), but only in *Lemur catta* was the presence of intraosseous ligaments confirmed (**Figs. 2.6, 2.9**). These were seen running from the base to spines located on its volar surface, and as in other forms, were positioned deep to the unguis (a bit of which can be seen still attaching to the ligament in **Fig. 2.9**). An asymmetrical bony process that contains the insertions for the long flexor tendon and one of the intraosseous ligaments is present on the volar surface of this phalanx (best seen in **Fig. 2.6**; *Lemur catta* orange highlights in **Fig. 2.10**). The other intraosseous ligament inserts onto a spine that is separated from the rest of the process. In *Eulemur*, no intraosseus ligament could be dissected, but it is not clear if they do not exist or were simply broken during the dissection process. The volar surface of *Eulemur* shows a proximo-distally short bony process that does not expand beyond the insertion of the flexor tendon and does not possess any clear indications as to where intraosseous ligaments might insert (*Eulemur*, **Fig. 2.11**).

Observations of strepsirrhine, tarsier, and *Aotus* grooming phalanges show a variety of volar morphologies (**Fig. 2.11**). Some specimens possess an asymmetrical process of bone which is expanded somewhat beyond the flexor insertion (as in the *Lemur* phalanx described above), while others lack any obvious expansion (similar to the *Eulemur* phalanx described above). Some specimens possess a medio-laterally compressed expansion of bone distal to the flexor tubercle which ends in a small, rounded eminence (e.g., *Propithecus* in **Fig. 2.11**) or a similar, but medio-laterally wider process of bone that ends in a rounded, but slightly asymmetrical eminence (e.g., *Aotus*, *Cephalopachus*, and *Otolemur* in **Fig. 2.11**). However, when observing different individuals of the same species, there appears to be a high degree of intraspecific variation in volar morphology. For example one individual of *Lemur catta* has the morphology described above (**Figs. 2.6, 2.10, 2.11**), while another individual (not figured) shows the condition observed in *Eulemur fulvus* (**Fig. 2.11**). It is not clear what these differences are related to. It seems likely that specimens which have a process that is expanded beyond the flexor tubercle also possess intraosseous ligaments (likely insertions indicated by black arrows on *Aotus*, *Cephalopachus*, *Otolemur*, and *Propithecus* in **Fig. 2.11**) because they are

morphologically similar to falcular volar processes and appear as less extensive versions of the structures seen in ungular phalanges on which the ligaments insert. If specimens which lack an expansion beyond the flexor tubercle do in fact possess intraosseous ligaments, they may insert on small bumps seen on the volar surface of the shaft (indicated by black arrows on *Eulemur* and *Microcebus* in **Fig. 2.11**) or on the more distally placed proximal edges of the apical tuft (blue arrows). Insertions on the proximal edges of the apical tuft seem less likely as these edges may be present, but separate from the actual insertions of the intraosseous ligaments (e.g., blue and black arrows on *Lemur catta* in **Fig 2.11** and *Callicebus* in **Fig.2.6**) and from the inferred insertions of the intraosseous ligaments (blue and black arrows on *Aotus*, *Cephalopachus*, *Otolemur*, and *Propithecus* in **Fig. 2.11**). Finally, no consistent falcula-like nutrient foramina were observed, although one *Eulemur* specimen was seen to possess a small foramen in a similar area (**Fig. 2.11**), but vascular grooves are present along the shafts of many specimens (e.g., *Otolemur* and *Aotus*, **Fig. 2.11**).

2.3.2.5 Tegulae

One postaxial tegular phalanx was traditionally dissected (*Saguinus*, **Table 2.1**). Insertions for the flexor tendon and intraosseous ligaments were confirmed (**Figs. 2.3, 2.6**). The volar surface of this specimen shows a process of bone containing the flexor tubercle and ending in a small, rounded eminence. The intraosseous ligaments originate on the base and insert on the lateral sides of the eminence.

Since, tegulae are believed to be independently acquired in two primate lineages the platyrrhine callitrichines and the strepsirrhine *Daubentonia* (e.g., Garber, 1980; Soligo and Müller, 1999), specimens from both lineages were examined. Callitrichine postaxial phalanges tend to have elongated processes that occasionally possess spines at the insertion site of the intraosseous ligament (*Leontopithecus*, **Fig. 2.9**). In some cases, the process ends in an asymmetrical eminence that is difficult to discern in volar view. *Daubentonia* differs in having a proximo-distally shorter and medio-laterally wider process. Pollical tegular phalanges of both lineages appear to be similar to preaxial ungular phalanges in possessing a volar fossa, but otherwise resemble their postaxial counterparts with the exception of being medio-laterally wider. No consistent falcula-like nutrient foramina were observed in either taxon although deep vascular grooves were observed in most specimens. The only intraspecific variation identified in

the observed osteological collection, was in the presence and extent of spines at the insertion sites of the intraosseous ligaments.

2.3.2.6 Summary

In summary, a process of bone that ends in a rounded eminence and receives the insertions of the long flexor tendon and intraosseous ligaments was observed for the majority of distal phalanx specimens. This structure will hereafter be referred to as the volar process in all phalanx forms. In many ungular phalanges, the volar process accounted for the entirety of the volar surface of the phalanx, but in other forms was more proximally restricted. Finally, it is not clear that intraosseous ligaments are present in grooming phalanges that lack the rounded eminence that receives their insertions in other specimens.

2.4 Quantification

2.4.1 Materials and Methods

Following dissection, a relationship between the volar process and apical pad was tested, specifically to determine if the volar process is the portion of the distal phalanx which lies embedded within the apical pad (the remainder of the phalanx rising distally and dorsally beyond the pad).

Measurements were collected on a set of wet specimens preserved in a formalin-based solution housed at SBU (**Table 2.3**). All specimens were sampled from pedal rays and included falcular, tegular, grooming, postaxial ungular and hallucal ungular phalanges. These specimens were microCT scanned using a VivaCT75 microCT scanner at SBU at voxel sizes ranging from 20 - 70μ. For each specimen, the external soft tissue and distal phalanx were segmented separately and a 3D model was generated for each using the software Amira 5.0 or Avizo 7.1. Segmentation was performed primarily using the magic wand tool in Amira's/Avizo's segmentation editor.

Four measurements were collected on each specimen using Amira's/Avizo's 2D linear measurement tool. Two measurements, volar process length (VPL) and pad association length (PAL) were taken in lateral view. VPL was defined as the distance from the inferior margin of the articular facet (or most proximal portion on the inferior aspect of the facet in the case of

hallucal phalanges for which the articular facet is convex rather than concave) to the distal end of the volar process (A to B in **Fig. 2.12**). The end of the volar process was considered to be at the distal-most extremity of the rounded eminence (distal to the flexor tubercle) described in the previous results section. For grooming phalanges that do not have a clear expansion beyond the flexor tubercle, this was taken at the distal-most extremity of the flexor tubercle. PAL is the length of the portion of the phalanx that lies embedded within the apical pad. This was measured as the distance from the inferior margin of the articular facet (or most proximal portion on the inferior aspect of the facet) to the point where the dorsal margin of the apical pad meets the volar border of the phalanx (A to C in **Fig. 2.12**). PAL was taken by rendering the external tissue transparent using the transparency option in the surface view module of Amira/Avizo. Two additional measurements were taken in proximal view: the maximum height (MH) and width (MW) of the articular facet, these measurements were used to estimate the surface area of the articular facet (SA). SA was calculated as the product of MH and MW and was used as a proxy for size.

Measurement accuracy was assessed for both VPL and PAL. Each measurement was taken 5 times on a small subset of the data set: a falcular phalanx from *Tupaia glis* [SBU (17)], a grooming unguis from *Lemur catta* [SBU (14)], a hallucal ungular phalanx from *Hapalemur griseus* [SBU (12)], and postaxial ungular phalanges from *Chlorocebus aethiops* [SBU (5)] and *Lemur catta* [SBU (14)]. VPL and PAL were measured (using Avizo 7.1) 5 times at intervals of at least 8 hours. The coefficient of variation (CV) was calculated for each measurement set on each specimen. Values lower than 5% were considered to be accurate and repeatable.

Phylogenetic generalized least squares (PGLS) regression using maximum likelihood estimates of lambda (λ) were run using the function 'pgls' in the package caper (Orme, 2013) to assess whether volar process length can accurately predict the portion of the distal phalanx which lies embedded within the apical pad (PAL regressed on VPL). Such a predictive relationship would be useful in analyzing fossil distal phalanges for which no soft tissue is preserved. Three separate PGLS regressions were performed: one for falcular/grooming/tegular digits, one for postaxial ungular digits, and one for hallucal ungular digits. Phylogenetic trees for the analyses were adapted from the maximum likelihood tree based on a molecular supermatrix and divergence times based on autocorrelated rates and soft-bound constraints of Springer et al. (2012). The non-primate taxa, *Tamandua*, *Sciurus*, and *Didelphis* were grafted onto the tree

using divergence times based on molecular data with fossil calibration points presented in Bininda-Emonds et al. (2007) using the software Tree Graph 2 (Stöver and Müller, 2010). To assess all distal phalanx forms together, a least squares regression was also run using the 'lm' function in R (PGLS could not be used in this case as the dataset contains multiple specimens of different form that cannot be averaged for a single species).

The relationship of PAL to VPL was also assessed in relation to body size (e.g., to determine if there is a closer relationship between PAL and VPL in species with a smaller body size versus those of a larger size or vice versa). Since body masses are not available for the individuals in this analysis, the estimated surface area of the articular facet (SA, see above) was used as a rough proxy for size. To determine if there is a significant relationship, the natural log of PAL/VPL was regressed on the natural log of SA using the same methods as for the regressions of PAL on VPL.

2.4.2 Results

The results of the accuracy study are reported in **Table 2.4**. In all cases the CV was less than 3.2% and in 8 out of 10 cases less than 1%. This demonstrates that these measurements are repeatable with a high degree of accuracy.

The results of the least squares regression on all data points and the three PGLS regressions on digits bearing different unguis forms are presented in **Fig. 2.13** and summarized in **Table 2.5**. Each analysis shows a significant predictive relationship between PAL and VPL. This demonstrates that the volar process is related to the extent of the apical pad along the distal phalanx and can be used to predict the portion of the distal phalanx that lies embedded within the apical pad with a high degree of certainty. Further regressions of PAL/VPL on SA are all non-significant demonstrating that the relationship of PAL to VPL does not vary with size (**Table 2.5**).

2.5 Discussion

In all distal phalanx forms, there is a structure that ends in a rounded eminence, is associated with the insertion of the flexor tendon and intraosseous ligaments, and largely lies embedded within the apical pad which is here termed the volar process (**Fig. 2.10, 2.14**). Nearly all specimens observed in this study possessed this clearly defined structure with the exception of

some phalanges that bear grooming ungues and the falcular phalanges of monotreme mammals. Excepting these specimens, there is a pattern of traits (a volar process and soft tissue) that is conserved among therian mammals. Therefore, the volar process and associated tissues can be considered homologous among therian mammals and/or functionally equivalent as an insertion site for the long digital flexor tendon and intraosseous ligaments. However, in the few specimens that lack a clearly defined volar process, it is unclear as to where the homologous region might end.

Previous authors have described the intraosseous ligaments as inserting onto proximally directed spines at the lateral edges of an apical tuft or ungual tuberosity (Shrewsbury and Johnson, 1975; Shrewsbury et al., 2003), while this chapter describes the insertion to be on the lateral sides of the volar process. Shrewsbury and colleagues discussed intraosseous ligaments in humans and baboons, taxa for which the apical tuft appears to be formed by a dorsal expansion of the shaft that is fused with the volar process, a fusion that is so complete that there is often no clear indications as to where one starts and the other stops (e.g., *Theropithecus*, **Fig. 2.7**). Therefore in these taxa, the ungual spines of the apical tuft are the lateral sides of the volar process. However in other primates, there is more of a distinction between a dorsal tuft and the volar process (e.g., *Callicebus*, **Fig. 2.5**; some grooming phalanges, **Fig. 2.11**) as the dorsal tuft projects distally beyond the distal margin of the volar process. In these taxa, it is more accurate to describe the insertions as on the lateral margins of the volar process as the apical tuft may be separated from it.

Shrewsbury and colleagues state that no intraosseous ligament was found in non-human primates with the exception of several baboon specimens (Shrewsbury and Sonek, 1986; Shrewsbury, 2003). Their dissections included some of the same species for which the presence of intraosseous ligaments is demonstrated in this paper (e.g., *Lemur*, *Cebus*, and *Saguinus*). It is unclear as to what caused the discrepancies in results, but it is possible that it is related to the preservation of specimens. Accidental breakage most often occurred in wet specimens while attempting to peel the unguis or apical pad away from the ligaments; dried specimens were easier to dissect due to a hardening of the ligaments. In Shrewsbury et al. (2003), the non-human primates dissected were nearly all fresh specimens, while Shrewsbury and Sonek (1986) dissected frozen specimens that had been thawed. It could be that these tiny ligaments are more

susceptible to accidental damage when fresh and could have easily been peeled away along with the unguis or pad.

Returning to the widespread presence of a volar process in non-primate and primate taxa, the identification of an anatomical structure that is related to the proximo-distal extent of the apical pad is useful for comparative analyses of distal phalanges. First, it provides a basis for the selection of homologous measurements and landmarks needed for quantitative analyses. Second, its relationship to the apical pad allows for inferences to be made about soft tissue anatomy. This will prove particularly useful for the interpretations of enigmatic fossil distal phalanges and the transition from falculae to ungulae in primate evolution.

2.6 Figures

Fig. 2.1. Variation in distal phalanx morphology.
An example of the morphological variation in distal phalanges bearing different unguis forms shown in lateral or medial view. Top row: falcular (claw-bearing) phalanges from a tree squirrel (*Sciurus sp.*) and a tree shrew (*Tupaia tana*); Middle row: ungular (nail-bearing) phalanx from the hallux of a lemur (*Lemur catta*) and postaxial (non-hallucal/non-pollical) ungular phalanx from a grivet monkey (*Chlorocebus aethiops*); Bottom row: tegular (tegula-bearing) phalanx from an aye-aye (*Daubentonia madagascariensis*) and a grooming (grooming unguis-bearing) phalanx from a mouse lemur (*Microcebus murinus*). Specimens are not to scale. Arrows denote the location of the insertion of the long digital flexor tendon (note the differences between preaxial and postaxial distal phalanges). Brackets denote the region of falcular distal phalanges called the volar process.

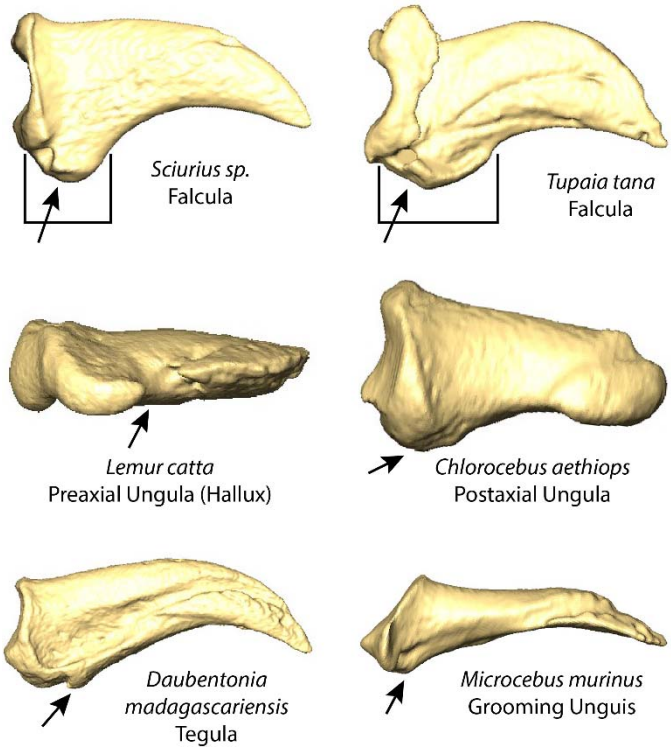

Fig. 2.2. Anatomical terminology.
Illustration of some of the anatomical terms used in this chapter demonstrated on a human pollical distal phalanx (top) and manual postaxial distal phalanx (bottom) in dorsal (left) and volar (right) views. Abbreviations: Af: proximal articular facet; At: apical tuft; B: base; Ei: insertion of extensor tendon; Fi: insertion of flexor tendon; Pvf: proximal volar fossa; S: shaft; Us: ungual spine.

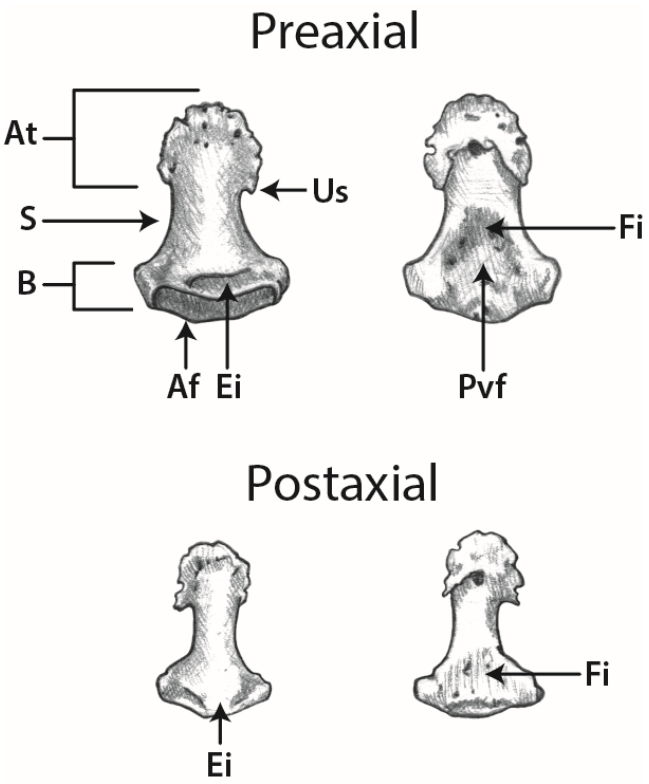

Fig. 2.3. Similarity of falcular volar process with ungular volar surface.
Volar views of a falcular distal phalanx from a nutria (*Myocastor coypus*) and postaxial ungular distal phalanx from a ruffed lemur (*Varecia variegata*). Note that the falcula (keratinized claw) is still attached to the nutria phalanx. The falcular volar process is highlighted in yellow and shows an overall similarity in shape with a volar feature of the ungular phalanx of *Varecia* (also highlighted in yellow). Arrows point to spines which resemble the ungual spines described in human distal phalanges. Ovals indicate the general regions of the insertions of the long digital flexor tendons. Images not to scale.

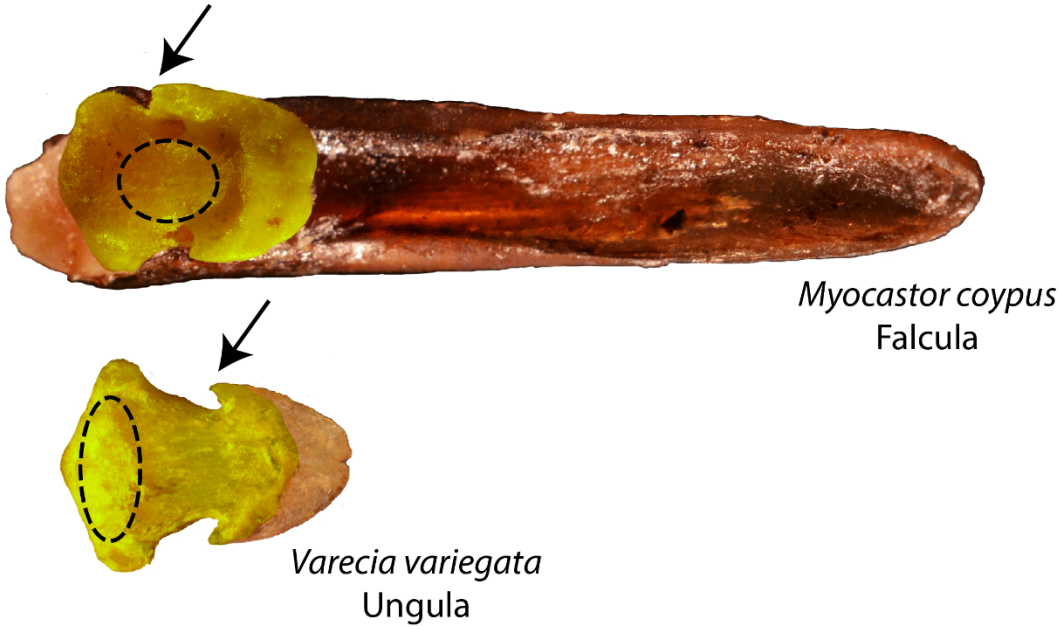

Fig. 2.4. Dissections of long digital flexor tendon insertions.
Lateral or medial views of flexor tendon insertions on distal phalanges that support different unguis forms. Top row: falcular phalanges from a porcupine (*Erethizon dorsatum*) and a coati (*Nasua sp.*), and hallucal (preaxial) ungular phalanx from a capuchin monkey (*Cebus sp.*); Bottom row: grooming phalanx from a common brown lemur (*Eulemur fulvus*), a postaxial ungular phalanx from a capuchin monkey (*Cebus sp.*) and a tegular phalanx from a cotton-top tamarin (*Saguinus oedipus*). Images in which the flexor tendons are highlighted in yellow are shown below the un-edited images. Scale bars are 3mm.

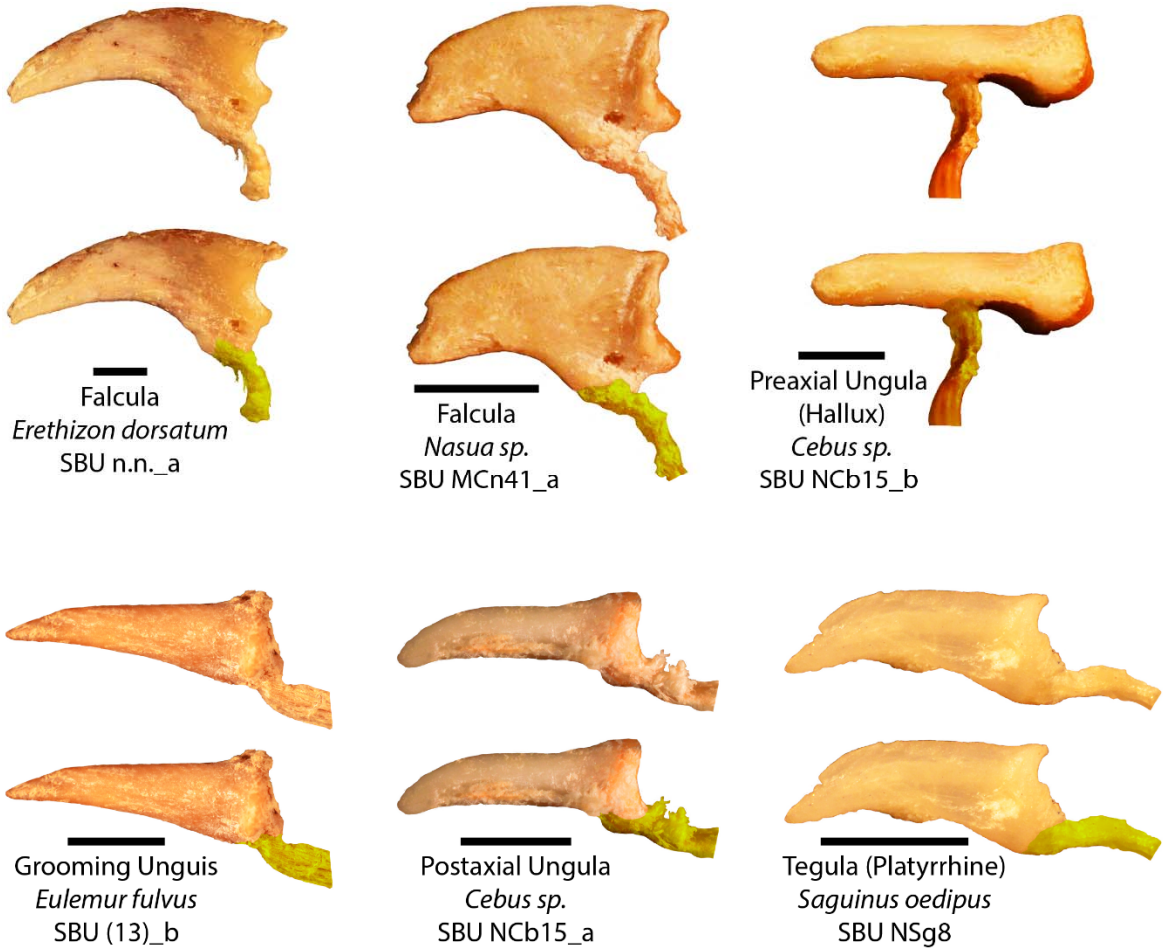

Fig. 2.5. Virtual dissections of Erethizon, Callicebus, and Theropithecus.
Lateral or medial and volar views of virtual dissections of a falcular phalanx of a porcupine (*Erethizon*) and postaxial ungular phalanges of a titi monkey (*Callicebus*) and gelada (*Theropithecus*). Long flexor tendons are shown in brown and intraosseous ligaments in grey. Views of distal phalanx without attaching structures are shown to the right. Scale bars are 3mm.

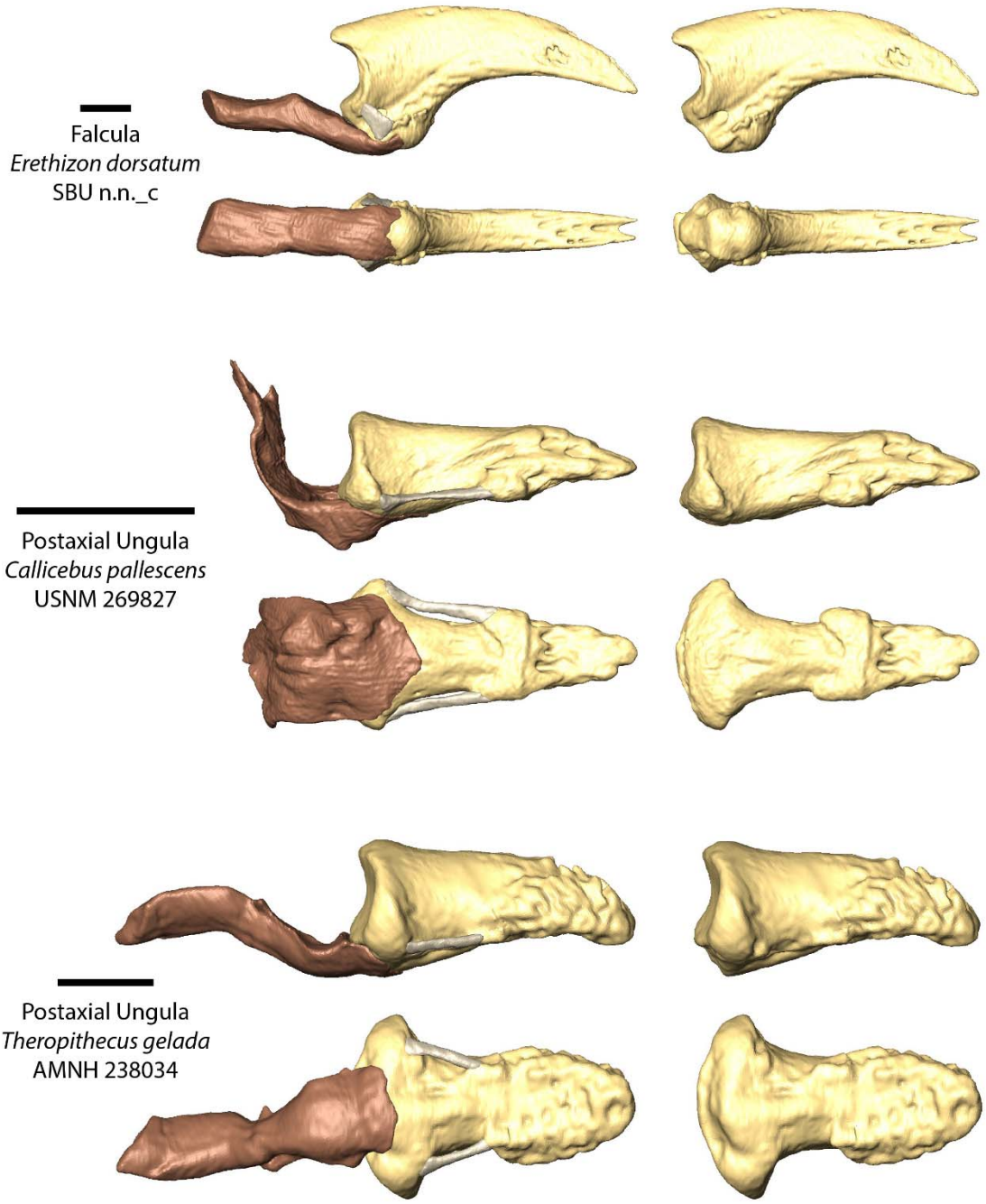

Fig. 2.6. Virtual dissections of Hapalemur and Lemur.
Lateral or medial and volar views of virtual dissections of a pollical (preaxial) ungular phalanx of a bamboo lemur (*Hapalemur*) and grooming phalanx of a ring-tailed lemur (*Lemur*). Long flexor tendons are shown in brown and intraosseous ligaments in grey. Views of distal phalanx without attaching structures are shown to the right. Scale bars are 3mm.

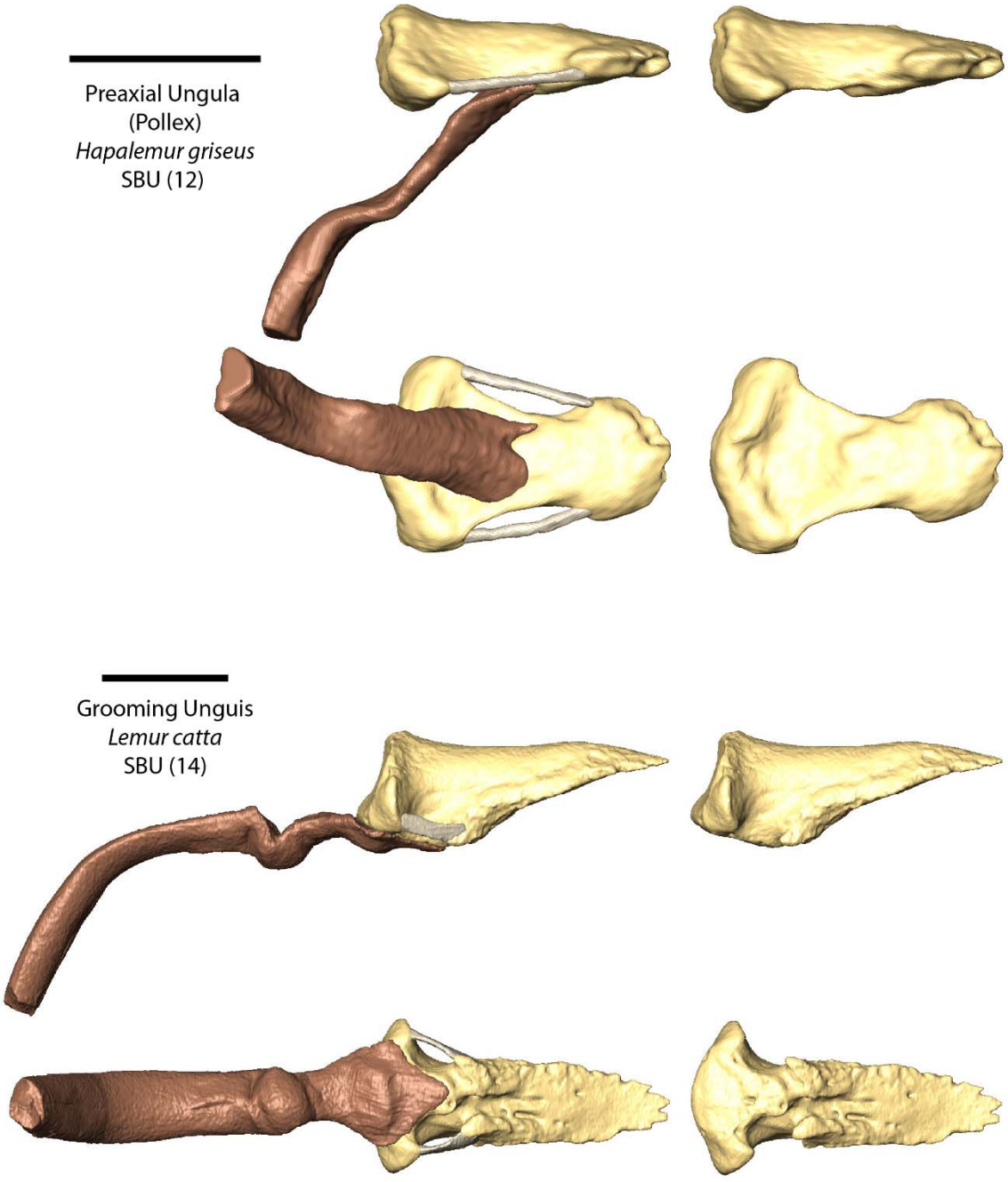

Fig. 2.7. Intraosseus ligaments of falcular phalanges.
Top row: lateral or medial and proximal views of intraosseous ligaments (an intraosseous ligament was present on both sides, but has only been preserved on one) on falcular phalanges from a porcupine (*Erethizon*) and a coati (*Nasua*); Bottom row: lateral and volar views of a pangolin (*Manis*) falcular distal phalanx with preserved intraosseous ligaments and articulated proximal phalanx. Images in which the intraosseous ligaments are highlighted in yellow are shown below the un-edited images. Scale bars are 3mm.

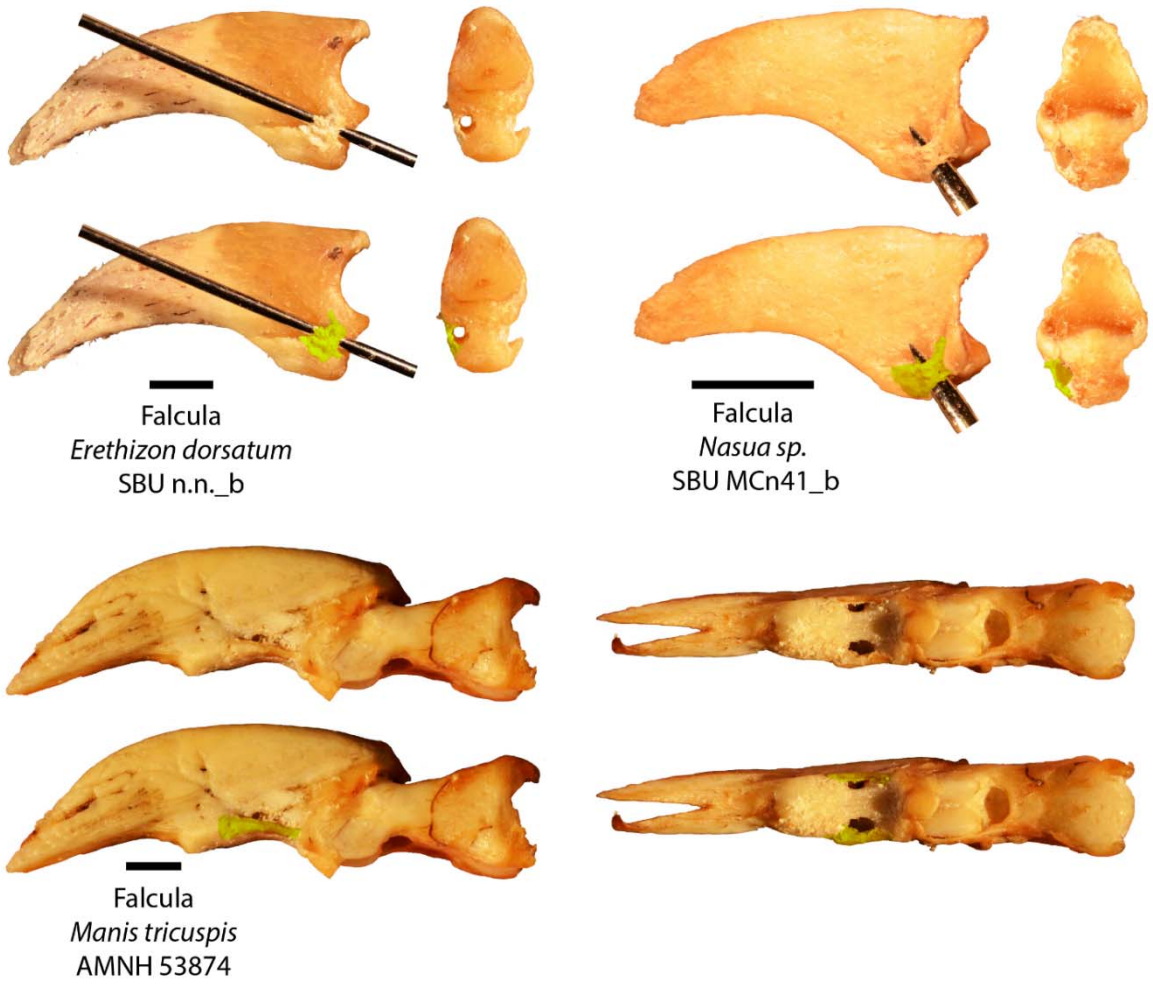

Fig. 2.8. Intraosseus ligaments of ungular phalanges.
Left: lateral and volar views of an intraosseous ligament (an intraosseous ligament was present on both sides, but has only been preserved on one) on a postaxial ungular phalanx of a common brown lemur (*Eulemur*); Top right: lateral and volar views of intraosseous ligaments on a postaxial ungular phalanx of a capuchin monkey (*Cebus*); Bottom right: dorsal view of a hallucal ungular phalanx showing complete ossification of intraosseous ligaments. Images in which the ligaments are highlighted in yellow are shown below the un-edited images. Scale bars are 3mm.

Fig. 2.9. Intraosseus ligaments of grooming and tegular phalanges.
Top: lateral or medial and volar views of intraosseous ligaments (intraosseous ligaments were present on both sides, but have only been preserved on one) on grooming and tegular distal phalanges of a ring-tailed lemur (*Lemur*) and cotton-top tamarin (*Saguinus*); Bottom: lateral and volar view of tegular phalanx from a lion tamarin (*Leontopithecus*) showing spinous insertion sites for intraosseous ligaments. Note that the intraosseous ligament of *Lemur* has attached remnants of the unguis (brown) and that the phalanx of *Saguinus* has been mirror imaged so that it faces in the same direction as the other phalanges. Images in which the ligaments are highlighted in yellow are shown below the un-edited images. Scale bars are 3mm.

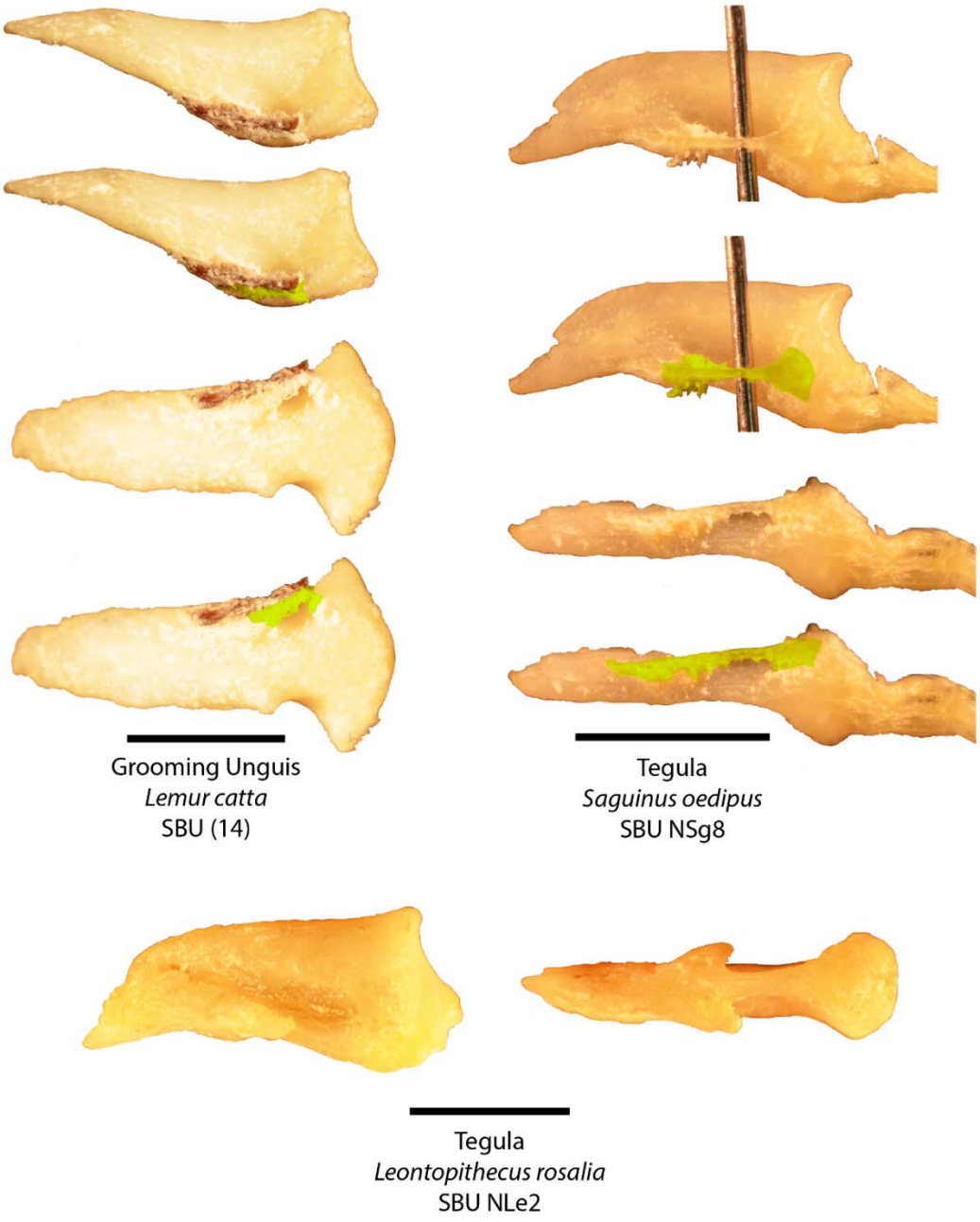

Fig. 2.10. Anatomical structures of the distal phalanx highlighted.
Anatomical structures discussed in the results are highlighted on distal phalanges bearing different unguis forms. Each phalanx is shown in dorsal, lateral, volar, and proximal views. Unmarked images are placed above highlighted images.

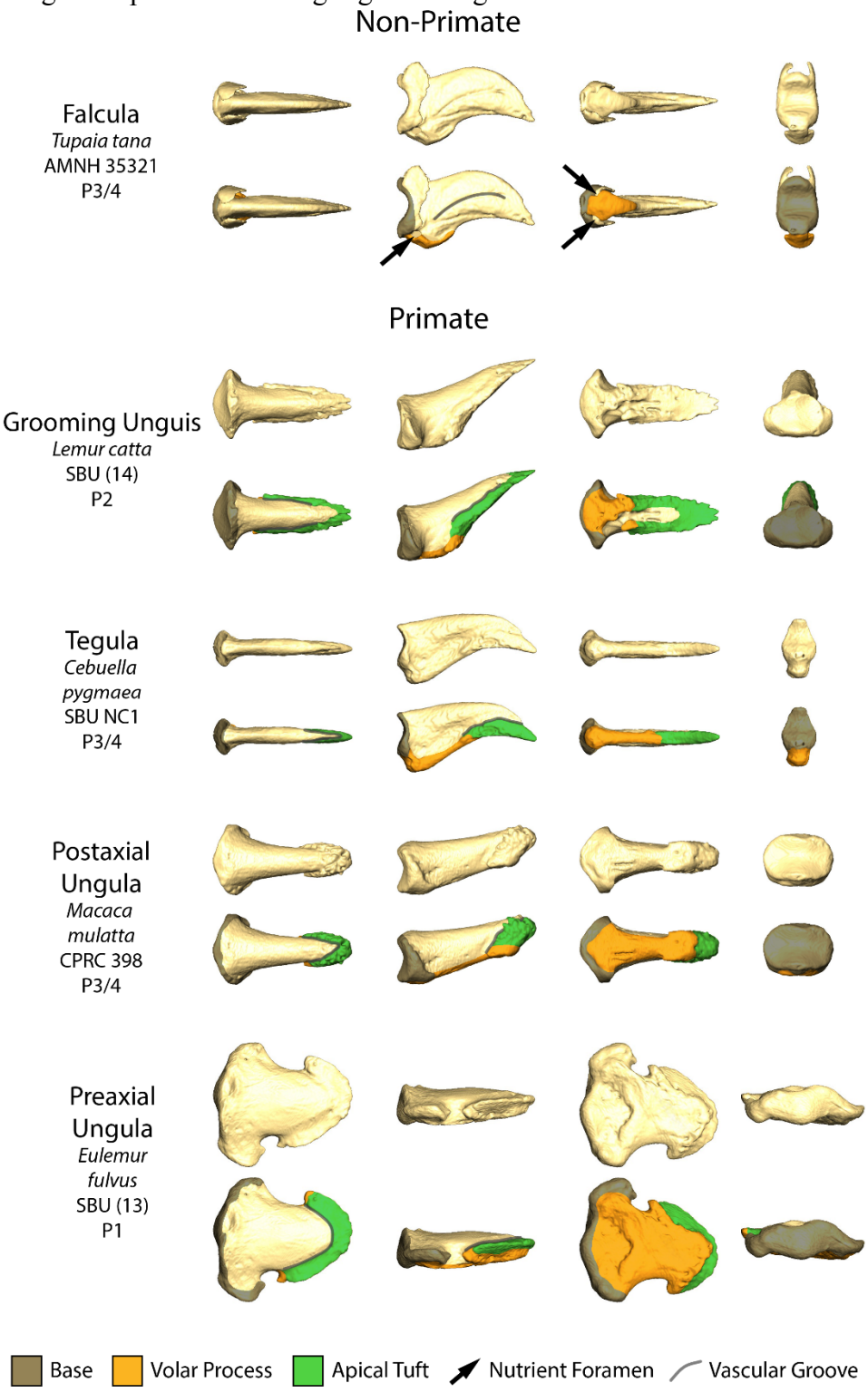

Fig. 2.11. Grooming phalanx variation.
An example of the observed variation in primate grooming phalanges. Dorsal, lateral, medial, and volar views of grooming phalanges from a ring-tailed lemur (*Lemur*; top: same phalanx with attached intraosseous ligaments), owl-monkey (*Aotus*), tarsier (*Cephalopachus*), greater galago (*Otolemur*), diademed sifaka (*Propithecus*), common brown lemur (*Eulemur*), and mouse lemur (*Microcebus*). A variety of volar morphologies can be seen: asymmetrical process expanded beyond the proximally positioned flexor insertion (see **Fig.2.4** and **2.6** for flexor insertion) and separated from the insertion site of one of the intraosseous ligaments (*Lemur*), process expanded beyond the flexor insertion varying in width and degree of asymmetry (*Aotus*, *Cephalopachus*, *Otolemur*, *Propithecus*), and no expansion of a process beyond the flexor insertion (*Eulemur*, *Microcebus*). Black arrows point to insertion sites of intraosseous ligaments in *Lemur*, *Aotus*, *Cephalopachus*, *Otolemur*, and *Propithecus* and to possible insertion sites in *Eulemur* and *Microcebus* if a ligament is present (see text). Blue arrows point to spines sometimes present at the edges of apical tufts in a number of specimens. These spines are separate from the intraosseous insertions in *Lemur* and *Aotus*, and therefore are unlikely to be intraosseous insertions in *Cephalopachus*, *Otolemur*, *Propithecus*, and *Microcebus*. Scale bars are 3mm.

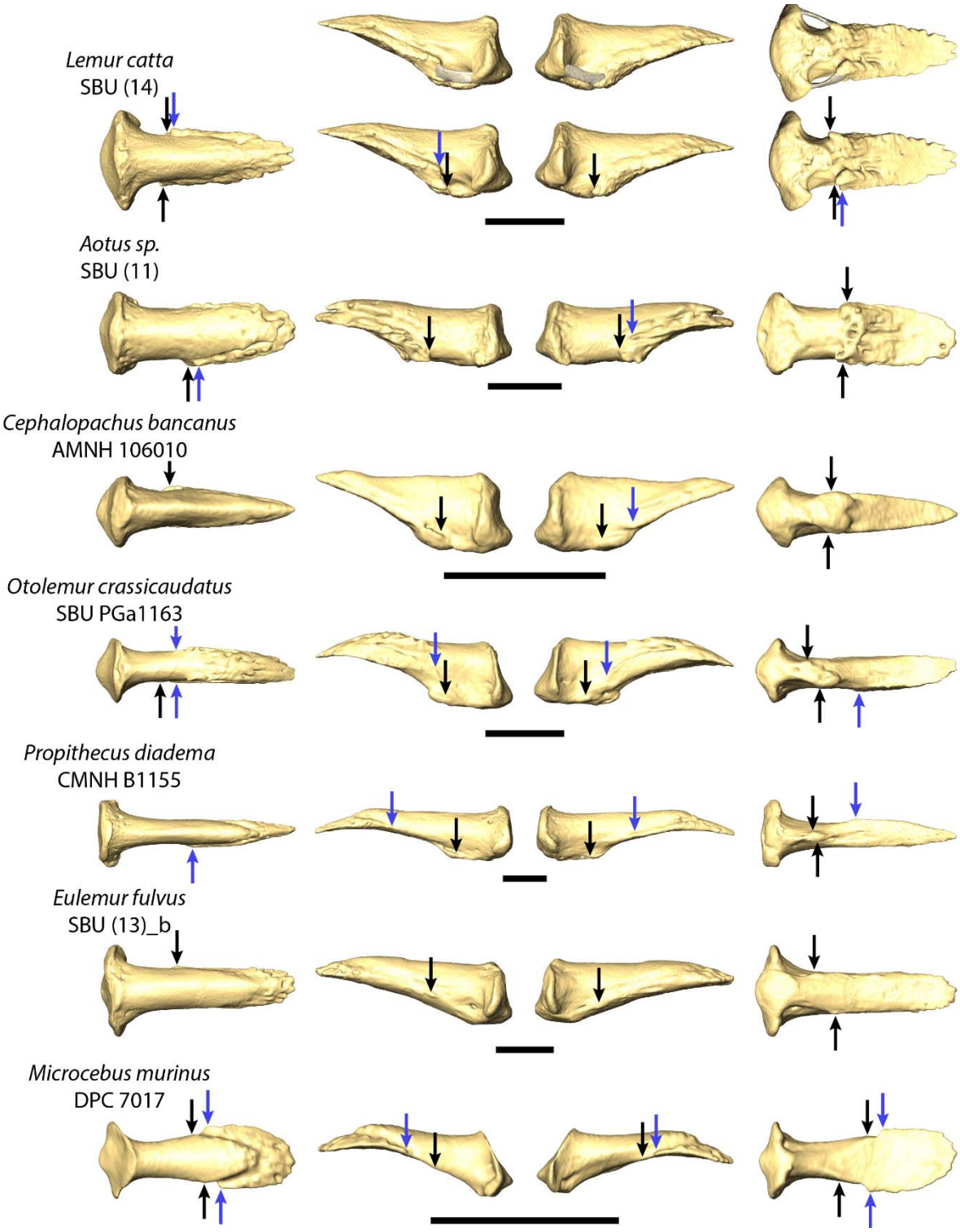
Lemur catta
SBU (14)
Aotus sp.
SBU (11)
Cephalopachus bancanus
AMNH 106010
Otolemur crassicaudatus
SBU PGa1163
Propithecus diadema
CMNH B1155
Eulemur fulvus
SBU (13)_b
Microcebus murinus
DPC 7017

Fig. 2.12. Points used in measurements taken in wet specimens.
Lateral views of microCT reconstructions of common brown lemur (*Eulemur*) digits (for each digit, top left: external tissue; top right: external tissue rendered transparent to show position of phalanx; bottom left: bone without surrounding external tissue with points used for measurements indicated; bottom right: transparent external tissue with dorsal surface of apical pad and edge where unguis emerges from skin of digit darkened to show a point used in measurement). A is the most proximal point on the inferior margin of the articular facet. B is the distal-most extremity of the rounded eminence of the volar process. C is the point where the dorsal margin of the apical pad meets the volar border of the phalanx. VPL (volar process length) is defined as the distance from A to B; PAL (pad association length) is A to C.

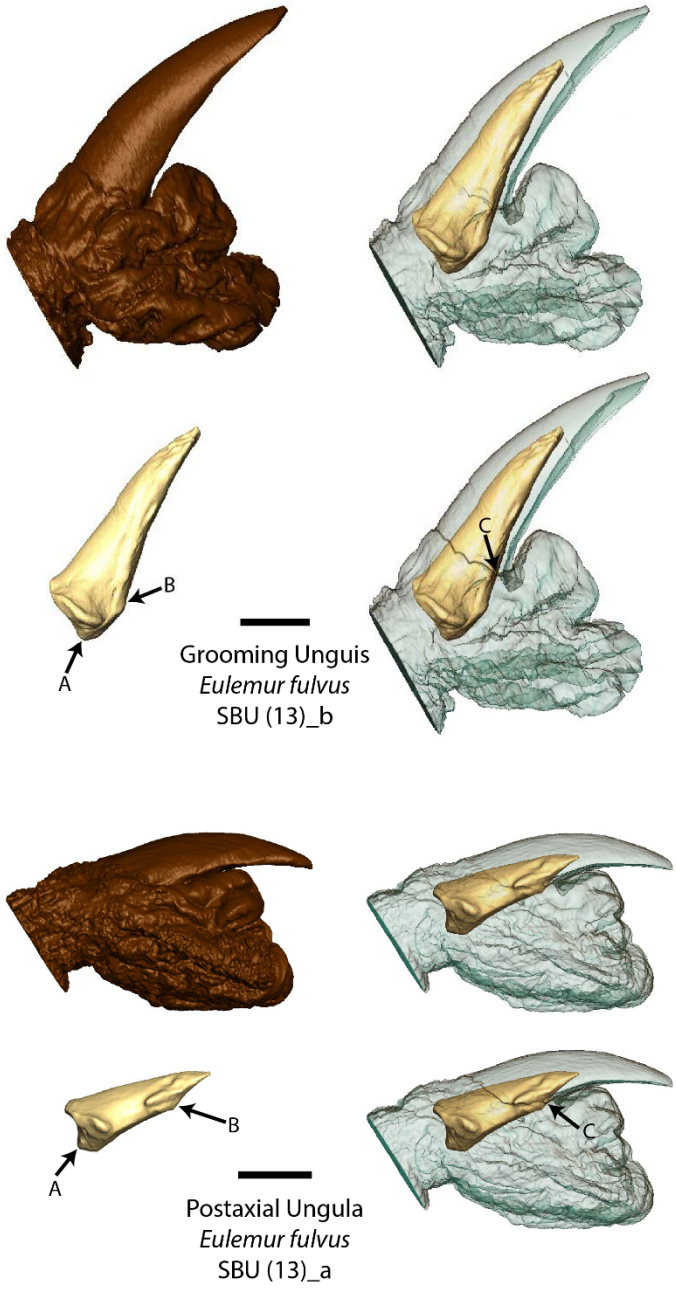

Fig. 2.13. Results of regressions.
Regression analyses demonstrating a relationship between the length of the portion of the bone which lies embedded in the apical pad (PAL) and the length of the volar process (VPL). The close relationship quantitatively demonstrates that the volar process is related to the apical pad's extent along the volar surface of the phalanx in that it lies completely or largely embedded within it and that this aspect of soft tissue morphology (PAL) can be predicted by a bony measurement (VPL).

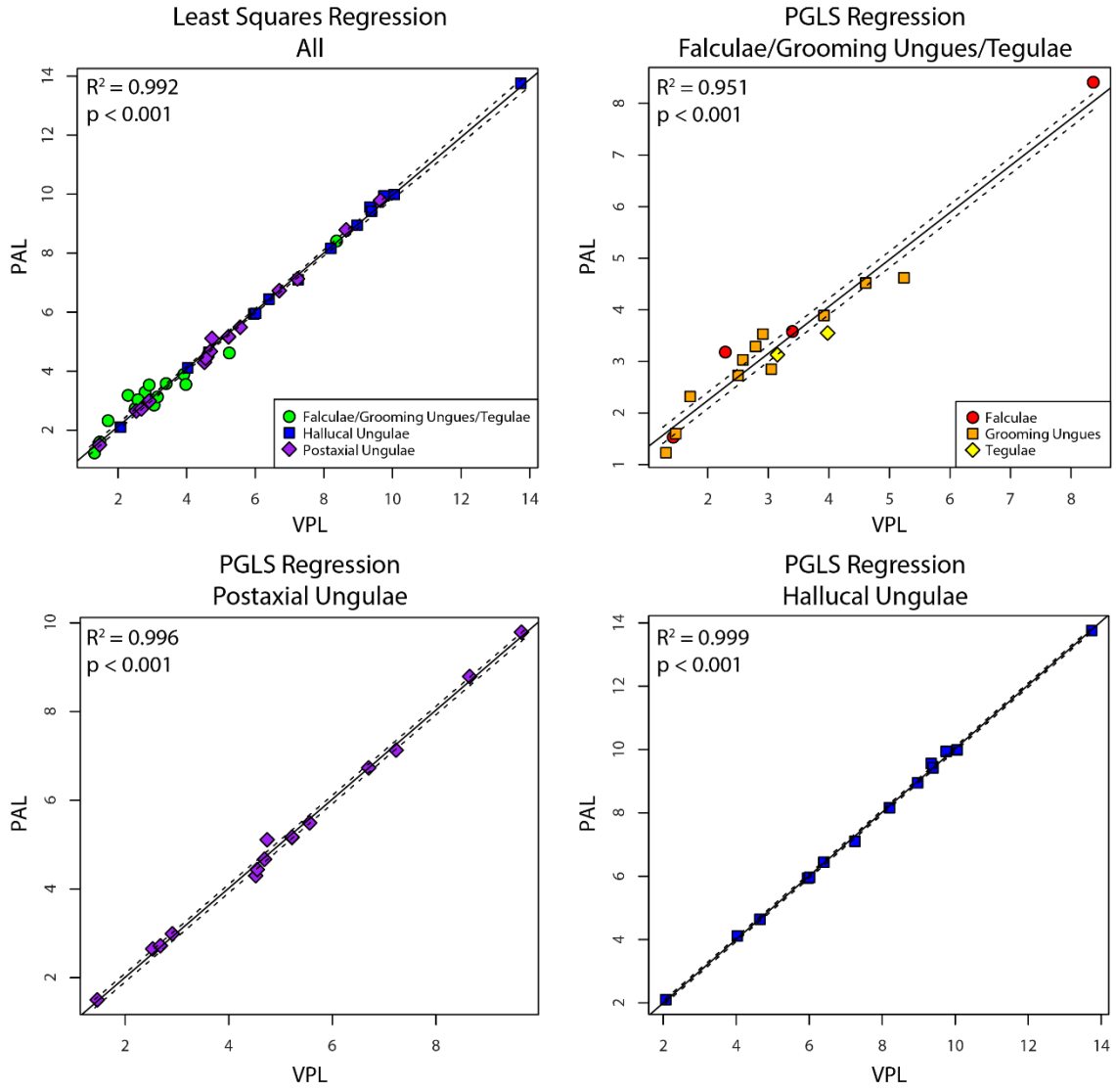

2.7 Tables

Table 2.1. Specimens dissected.
Abbreviations: SBU, Stony Brook University; AMNH, American Museum of Natural History. Element refers to the digit sampled: Manual (M) or Pedal (P), ray indicated by 1-5.

Form	Species	Specimen #	Element	Preparation
Falcula	*Erethizon dorsatum* (Porcupine)	SBU n.n._a	M2	Dry
Falcula	*Erethizon dorsatum*	SBU n.n._b	M3	Dry
Falcula	*Nasua sp.* (Coati)	SBU MCn41_a	M1	Dry
Falcula	*Nasua sp.*	SBU MCn41_b	M2	Dry
Falcula	*Manis tricuspis* (Pangolin)	AMNH 53874*	M3	Dry
Postaxial Ungula	*Cebus sp.* (Capuchin monkey)	SBU NCb15_a	M5	Dry
Postaxial Ungula	*Eulemur fulvus* (Common brown lemur)	SBU (13)_a[1]	P3	Wet
Preaxial Ungula	*Cebus sp.*	SBU NCb15_b	P1	Dry
Grooming Unguis	*Eulemur fulvus*	SBU (13)_b[1]	P2	Wet
Grooming Unguis	*Lemur catta* (Ring-tailed lemur)	SBU (12)[1]	P2	Wet
Tegula	*Saguinus oedipus* (Cotton-top tamarin)	SBU NSg8	M3	Dry

*This specimen was not dissected, but was found in a collection with preserved ligaments attached.
[1]Prior to dissection these specimens were microCT scanned.

Table 2.2. Specimens virtually dissected.
Abbreviations: SBU, Stony Brook University; AMNH, American Museum of Natural History; USNM, National Museum of Natural History.
Element refers to the digit sampled: Manual (M) or Pedal (P), ray indicated by 1-5.
The voxel size at which the specimen was scanned is listed in microns; see text for additional information.

Form	Species	Specimen #	Element	Preparation	Scanner Location	Voxel Size
Falcula	*Erethizon dorsatum* (Porcupine)	SBU n.n._c	M4	Dried	SBU	60µ
Postaxial Ungula	*Theropithecus gelada* (Gelada)	AMNH 238034	P2	Dried	AMNH	68µ
Postaxial Ungula	*Callicebus pallescens* (Titi monkey)	USNM 269827	M2	Dried	Duke	18µ
Prexial Ungula	*Hapalemur griseus* (Bamboo lemur)	SBU (12)	M1	Wet	SBU	39µ
Grooming Unguis	*Lemur catta* (Ring-tailed lemur)	SBU (14)*	P2	Wet	SBU	20µ

*After microCT scan, this specimen was traditionally dissected.

Table 2.3. Wet specimens included in regression analyses.
Abbreviations: SBU, Stony Brook University; DPC, Duke Lemur Center.
Element refers to the digit sampled: Pedal (P), rays indicated by 1-5.

Form	Species	Specimen #	Element
Falcula	*Tamandua sp.*	SBU (1)	P3
Falcula	*Tupaia glis*	SBU (17)	P3
Falcula	*Sciurus sp.*	SBU (2)	P3
Falcula	*Didelphis sp.*	SBU (3)	P3
Grooming Unguis	*Nycticebus coucang*	DPC 1906	P2
Grooming Unguis	*Mirza coquereli*	DPC 2301	P2
Grooming Unguis	*Loris tardigradus*	DPC 2925	P2
Grooming Unguis	*Propithecus coquereli*	DPC 6273	P2
Grooming Unguis	*Eulemur rufus*	DPC 6287	P2
Grooming Unguis	*Eulemur macaco*	DPC 6793	P2
Grooming Unguis	*Microcebus murinus*	DPC 7017	P2
Grooming Unguis	*Aotus sp.*	SBU (11)	P2
Grooming Unguis	*Hapalemur griseus*	SBU (12)	P2
Grooming Unguis	*Eulemur fulvus*	SBU (13)[1]	P2
Grooming Unguis	*Lemur catta*	SBU (14)[1]	P2
Tegula	*Saguinus fuscicollis*	SBU (16)	P3
Tegula	*Saguinus midas*	SBU (21)	P3
Preaxial Ungula	*Loris tardigradus*	DPC 2925	P1
Preaxial Ungula	*Propithecus coquereli*	DPC 6273	P1
Preaxial Ungula	*Eulemur rufus*	DPC 6287	P1
Preaxial Ungula	*Eulemur macaco*	DPC 6793	P1
Preaxial Ungula	*Microcebus murinus*	DPC 7017	P1
Preaxial Ungula	*Aotus sp.*	SBU (11)	P1
Preaxial Ungula	*Hapalemur griseus*	SBU (12)	P1
Preaxial Ungula	*Eulemur fulvus*	SBU (13)[1]	P1
Preaxial Ungula	*Lemur catta*	SBU (14)	P1
Preaxial Ungula	*Chlorocebus sabaeus*	SBU (18)	P1
Preaxial Ungula	*Cercocebus/Lophocebus sp.*	SBU (19)	P1
Preaxial Ungula	*Chlorocebus aethiops*	SBU (5)	P1
Preaxial Ungula	*Cebus sp.*	SBU (7)	P1
Preaxial Ungula	*Saimiri sp.*	SBU (9)	P1
Postaxial Ungula	*Mirza coquereli*	DPC 2301	P4
Postaxial Ungula	*Loris tardigradus*	DPC 2925	P3
Postaxial Ungula	*Propithecus coquereli*	DPC 6273	P4
Postaxial Ungula	*Eulemur rufus*	DPC 6287	P4
Postaxial Ungula	*Eulemur macaco*	DPC 6793	P4
Postaxial Ungula	*Microcebus murinus*	DPC 7017	P3
Postaxial Ungula	*Aotus sp.*	SBU (11)	P3
Postaxial Ungula	*Hapalemur griseus*	SBU (12)	P3
Postaxial Ungula	*Eulemur fulvus*	SBU (13)	P3
Postaxial Ungula	*Lemur catta*	SBU (14)	P3
Postaxial Ungula	*Galago senegalensis*	SBU (15)	P4
Postaxial Ungula	*Chlorocebus sabaeus*	SBU (18)	P3
Postaxial Ungula	*Cercocebus/Lophocebus sp.*	SBU (19)	P3
Postaxial Ungula	*Chlorocebus aethiops*	SBU (5)	P3
Postaxial Ungula	*Saimiri sp*	SBU (9)	P3

[1]After microCT scan, this specimen was traditionally dissected.

Table 2.4. Measurement accuracy.
The means, standard deviations (SD), and coefficients of variation (CV) for each measurement (VPL and PAL) taken 5 times at intervals greater than 8 hours on a subset of specimens.

	SBU (17) Falcula		**SBU (14) Grooming Unguis**		**SBU (12) Hallucal Ungula**		**SBU (5) Postaxial Ungula**		**SBU (14) Postaxial Ungula**	
	VPL	**PAL**	**VPL**	**PAL**	**VPL**	**PAL**	**VPL**	**PAL**	**VPL**	**PAL**
Mean	1.434	1.602	3.946	3.888	7.280	6.990	6.652	6.670	5.250	5.212
SD	0.015	0.051	0.025	0.124	0.021	0.068	0.037	0.045	0.033	0.034
CV	1.058%	3.164%	0.636%	3.189%	0.291%	0.976%	0.556%	0.670%	0.632%	0.656%

Table 2.5. Regressions.
Results from regression analyses. The variables regressed and the dataset from which they were taken (in parentheses) are listed under "Analysis." All refers to all specimens (this dataset contains multiple specimens per species and therefore PGLS could not be used); F, G, T refers to the subset containing falcular, grooming, and tegular phalanges only; H. ungulae refers to the subset containing hallucal ungular phalanges only; and P. ungulae refers to the subset containing postaxial ungular phalanges only. The type of regression analysis run is listed under the "Regression;" LS refers to least squares and PGLS to phylogenetic generalized least squares. For each analysis the R^2 and its associated p-value along with the slope and intercept of the regression line are reported. For PGLS regressions, the maximum likelihood estimate of lambda (λ) is also reported. In all cases λ was close to zero indicating that the data did not exhibit strong phylogenetic structuring.

Analysis	**Regression**	**R^2**	**p-value**	**Slope**	**Intercept**	**λ**
PAL~VPL (all)	LS	0.992	< 2.20e-16	0.981	0.162	n/a
PAL~VPL (F, G, T)	PGLS	0.951	3.12e-11	0.910	0.424	1.00e-6
PAL~VPL (H. ungulae)	PGLS	0.999	< 2.20e-16	1.004	-0.013	1.00e-6
PAL~VPL (P. ungulae)	PGLS	0.996	< 2.20e-16	1.004	0.003	1.00e-6
ln(PAL/VPL)~ln(SA) (all)	LS	0.021	0.333	-0.009	0.042	n/a
ln(PAL/VPL)~ln(SA) (F, G, T)	PGLS	0.003	0.824	-0.009	0.074	1.00e-6
ln(PAL/VPL)~ln(SA) (H. ungulae)	PGLS	0.051	0.437	-0.003	0.010	1.00e-6
ln(PAL/VPL)~ln(SA) (P. ungulae)	PGLS	0.139	0.171	-0.006	0.016	1.00e-6

3. Chapter 3: Grooming Unguis Origins - Implications for Primate Systematics

3.1 Abstract

The presence or absence of grooming claws (specialized structures used for scratching around the head and neck) has been an important character in fossil primate cladistics. Strepsirrhine primates possess a grooming claw on the second ray of each foot while tarsiers have them on both the second and third rays of each foot. Anthropoids are generally assumed to lack them, but recently their presence has been demonstrated in owl monkeys based on a quantitative approach and hinted at in other taxa. An absence of a grooming claw in fossil primates has previously been treated as positive evidence for an anthropoid affiliation. However, the presence of this structure in anthropoids questions the validity of this assumption. The aim of the current study is to test this assumption by surveying a broad range of anthropoid primate distal phalanges to determine if and which primates possess a grooming claw and to compare their morphology to those of strepsirrhines and tarsiers. This data will be used to estimate the ancestral conditions of the second pedal ungues of major primate groups to determine if grooming claws had an independent or a shared origin in different clades. Results show that among anthropoids, the platyrrhines *Aotus*, *Callicebus*, and *Pithecia* all possess grooming claws on second pedal rays. However these structures differ from the grooming claws of strepsirrhines and tarsiers. Grooming claws that strongly resemble those of strepsirrhines and tarsiers are also demonstrated in both adapiform and omomyiform primates. Finally, ancestral state reconstructions suggest that the most recent common ancestor of living primates possessed a grooming claw on its second pedal digit while the ancestral condition of anthropoids was to possess a nail.

3.2 Introduction

Grooming ungues (commonly referred to as grooming or toilet claws) are specialized ungues (nails or claws) that are present on the pedal digits of some primates and are primarily used for scratching through the fur surrounding the head and neck (**Fig. 3.1**). Among living taxa, strepsirrhines are well known to possess these structures on each second pedal digit, while tarsiers possess them on each second and third pedal digit. Anthropoids are generally thought to

lack grooming ungues, although there is now strong evidence that owl monkeys and possibly other platyrrhines possess them (Maiolino et al., 2011). The presence or absence of grooming ungues are often accorded strong phylogenetic significance when assessing relationships of fossil primates with living taxa.

A particularly contentious debate that grooming ungues have played a role in is the phylogenetic affinity of adapiform primates (Franzen et al., 2009; Gingerich et al., 2010) (Seiffert et al., 2009; Williams et al., 2010; Gingerich, 2012; Maiolino et al., 2012; Gilbert and Maiolino, 2015). Adapiforms are early primates from the Eocene of North America, Europe, Asia, and Africa. Two major hypotheses of their phylogenetic placement exist: they are more closely related to strepsirrhines (Seiffert et al., 2009; Williams et al., 2010; Maiolino et al., 2012; Gilbert and Maiolino, 2015) or they are more closely related to anthropoids (Franzen et al., 2009; Gingerich et al., 2010; Gingerich, 2012). One spectacularly preserved fossil adapiform, *Darwinius masillae* has been central to this debate. It was originally described to lack a grooming unguis leading authors to hypothesize a haplorhine or anthropoid affinity for adapiforms (Franzen et al., 2009; Gingerich et al., 2010). Since then, the general consensus is that the view permissible by the preservation of the *Darwinius* fossil does not allow for adequate determination of the presence or absence of a grooming unguis (Maiolino et al., 2012; von Koenigswald et al., 2012; Gilbert and Maiolino, 2015). Further, a number of adapiforms have been shown to possess grooming ungues on the basis of their distal phalanx morphology. This includes *Notharctus tenebrosus*, *Notharctus venticolis*, *Cantius nunienus*, *Europolemur koenigswaldi*, and *Europolemur kelleri* (Maiolino et al., 2012; von Koenigswald et al., 2012; Gilbert and Maiolino, 2015). As many adapiform species possess a grooming unguis, an anthropoid affiliation becomes less likely for adapiforms. However, this issue is compounded by the presence of grooming ungues in some anthropoids and the fact that we do not know the ancestral condition for the group. If strepsirrhines, tarsiers, and some platyrrhines all possess them on second pedal digits, it is certainly possible that early anthropoids also possessed them.

While grooming ungues can best be defined as an unguis (keratinized structure) that projects upwards and outwards beyond the apical pad (**Fig. 3.2**), there does appear to be some differences in their morphology among phylogenetic groups. *Notharctus tenebrosus* grooming phalanges (grooming unguis-bearing distal phalanx) appear to be distally wider than those of strepsirrhines and tarsiers (Maiolino et al., 2012; von Koenigswald et al., 2012). Koenigswald et

al (2012) noted some shape differences between the grooming phalanges of tarsiers and strepsirrhines and suggested that this may be indicative of separate origins in the two clades. The grooming phalanx of *Aotus* was shown to be morphologically similar to strepsirrhine and tarsier grooming phalanges, while a continuum of morphology has been observed in platyrrhines (Maiolino et al., 2011). However, this was based on a limited sample and a restricted set of measurements. To assess the significance of morphological similarities and differences among clades, the continuous variation of a large sample of grooming phalanges must be assessed.

The present study is undertaken to determine what variation may exist among clades and if this variation can be used to indicate shared or independent origins. Distal phalanges from a broad range of anthropoids and Eocene fossil primates are studied in a comparative context using an expanded set of measurements. First, anthropoid species that possess grooming phalanges are identified and compared to those of strepsirrhines and tarsiers. Then, adapiform and omomyiform grooming phalanges are identified and compared to those of extant taxa. Finally, the continuous variation in distal phalanx form is utilized to reconstruct the ancestral states of major primate clades.

3.3 Materials and Methods

3.3.1 Materials

Extant data were collected from distal phalanges (n=1009) of both primates and non-primates and were divided into six groups based on unguis form, ray, and/or phylogenetic group: strepsirrhines/tarsier grooming phalanges, anthropoid second pedal distal phalanges, ungular phalanges, tegular phalanges, non-primate grooming phalanges, and falcular phalanges. See **Table 3.1** for sample, **Table 3.2** for institutional abbreviations, and **Table 3.3** for sample sizes of each group. Strepsirrhine/tarsier grooming phalanges are the distal phalanges of strepsirrhines and tarsiiforms that bear grooming ungues taken from pedal ray II of strepsirrhines and pedal rays II-III of tarsiiforms. Distal phalanges from pedal ray II of anthropoids are placed into their own group to assess the variation among them in comparison to other groups. Ungular phalanges are primate distal phalanges that bear ungulae (nails) and are sampled from manual rays II-V and pedal rays III-V (or IV-V in the case of tarsiers). Tegular phalanges bear tegulae, the claw-like nails of calltrichines and aye-ayes, and are sampled from manual rays II-V and pedal rays III-V.

Non-primate grooming phalanges are the distal phalanges of non-primates that possess grooming ungues. These include pedal rays II and III of diprotodont marsupials and erinacein erinaceomorphs, and pedal rays II of the rodent *Castor* (the beaver). Falcular phalanges are sampled from the non-grooming rays of the falcula-bearing (claw) non-primates from which grooming ungues were sampled. Also included in this group are distal phalanges from non-primate euarchontans and an additional rodent which are included as outgroups for ancestral state reconstructions (see below).

Data were also collected from distal phalanges of Eocene adapiforms and omomyiforms (n=53; **Tables 3.4, 3.5**). UCMP fossils are known from a number of localities within the Washakie Basin, WY. These specimens are isolated distal phalanges that have not been attributed to species. Adapiform and omomyiform distal phalanges in this assemblage are easily distinguished from one another on the basis of size as well as morphology. Overall, the omomyiform postaxial distal phalanges from the Washakie Basin are smaller than those of the adapiforms as they range from about 1.61mm in length to about 3.2mm in length while the adapiforms range from about 5.14mm to about 6.43mm. Further, the adapiform distal phalanges are distinct in having more rugous apical tufts, dorso-ventrally deeper shafts, and much larger nutrient foramina than the omomyiforms (compare ungular specimens in **Figs. 3.3 and 3.4**). **Table 3.6** and **3.7** provides a list of the dentally known species at each locality as it is likely that the distal phalanges are from the same species. The AMNH fossils are from several localities within the Bridger (Green River) Basin, WY. Most adapiform specimens are associated with other skeletal and/or dental materials and have been attributed to a specific taxon. The AMNH omomyiforms are all isolated specimens, some of which were figured and discussed by Dagosto (1988). Based on other postcranial elements, three omomyid taxa are suggested to be present, the largest and most common being *Hemiacodon gracilis* or a similar species. Dagosto suggests that most of the distal phalanges in this collection are attributable to *Hemiacodon* (or a similar species). The UM specimens are also from the Bridger Basin, WY. Most of the indet omomyiform specimens are isolated, but are most likely from either *Hemiacodon gracilis* or *Omomys carteri* (pers comm Gregg Gunnell).

Two adapiform fossil specimens [AMNH FM 129382 (a) and 143612_3] have been included in previous analyses demonstrating that they are grooming phalanges (Maiolino et al., 2012; Gilbert and Maiolino, 2015); three additional specimens also appear to resemble grooming

phalanges (UCMP 217911, 217999, 218000; **Table 3.4; Figs. 3.3, 3.4**). UCMP 217911 is an adapiform based on its similarities to other known adapiform grooming phalanges and its larger size. This specimen is from the v70243 locality of Washakie Basin, WY from which several adapiform genera are dentally known. The majority of dental specimens have been attributed to the genus *Cantius* or *Notharctus venticolis* so it is likely that this distal phalanx is also from one of those taxa (**Table 3.6**). The base of UCMP 217911 is slightly eroded and so has been reconstructed by mirror imaging the unbroken side in proximal view.

UCMP 217999 and 218000 are small distal phalanges (3.15 and 3.22mm in length respectively) that resemble living primate grooming phalanges, but differ in possessing enlarged falcula-like nutrient foramina (similar to those of adapiform grooming phalanges). If these specimens are primate grooming phalanges (as opposed to non-primate falcular or grooming phalanges), then they would most likely belong to omomyiform species based on their small size. UCMP 217999 is from the v70214 locality of the Washakie Basin, WY. Only two omomyiform genera are dentally known from this locality, the overwhelming majority being attributed to *Tetonius*. Therefore, UCMP 217999 would most likely be from this genus (**Table 3.7**). The distal tip and a small portion of the base of this specimen is broken. The distal-most point of the tip is reconstructed as the point of intersection between a straight line following the dorsal contour of the shaft and a straight line following the volar contour of the shaft in lateral view. The missing portion of the base is reconstructed by mirror imaging the undamaged side. UCMP 218000 is from the v74022 locality of the Washakie Basin, WY. The majority of the dental specimens at this site are attributed to the genus *Arapahovius*, so it would be most likely that UCMP 218000 would is from this genus (**Table 3.7**). It should also be noted that no broken ungular phalanges (though figured in **Figs. 3.3, 3.4**) were measured or included in actual analyses. Potential grooming phalanx fossils were included despite some damage because the damage is slight and these specimens are particularly valuable to study.

3.3.2 Methods

Each specimen was sampled in one of two ways. Many extant primates and non-primates were sampled using a high resolution digital SLR camera (Nikon D5100) with a macro lens (Nikon AF-S Micro NIKKOR 40mm 1:2.8G). Photos were taken in dorsal, lateral, volar, and proximal views; a millimeter scale was placed in the same plane as each specimen. Some extant

species and all fossil specimens were sampled using micro computed tomography. Most extant specimens were scanned using either a VivaCT 75 Scanco microCT scanner at SBU, a μCT 50 Scanco scanner at the University of Southern California, a GE phoenix v|tome|x s240 at the AMNH, or a Nikon XT H 225 ST micro x-ray computed tomography scanner at Duke University. Voxel sizes ranged from 10μ (smallest specimens) to 110μ (large specimens). Many of these specimens are left in preserved skins, and microCT scanning allows for non-destructive recovery of their morphology. Very large specimens (e.g., great apes) were scanned using a medical CT scanner (General electric Lightspeed CVT CT) with a voxel size of 200μ. All fossils (except AMNH FM 11474 which was acquired earlier) were scanned with voxel sizes of 4μ to 10μ using a VivaCT 40 Scanco microCT scanner at SBU or the Nikon XT H 225 ST micro x-ray computed tomography scanner at Duke University. Such a range of resolutions was necessary to create comparable 3D reconstructions from very tiny and very large specimens. The resulting scan data was segmented using Avizo 7.1 to generate 3D digital models of each bone. Screen shots with scales were taken of each in dorsal, lateral, volar, and proximal views. Morphological terms referred to in this study are illustrated in **Fig. 3.5**.

A set of 15 measurements was taken from the photos or screenshots of each bone (**Figs. 3.6, 3.7; Table 3.8**). Measurements were taken using the ruler tool in Adobe Photoshop CS6 Extended Edition. All measurements with the exception of SIA, FIA, and FSA are take in millimeters; SIA, FIA, and FSA are in degrees. Calculations of included angles (**Fig. 3.7**) are modified from Jungers et al. (1997). As mentioned previously, three fossils appear to have minimal damage on their bases and/or tips of their shafts. To assess if this slight damage might affect interpretations, measurements of regions that show damage were also taken on reconstructions of the specimens (described above and illustrated in **Figs. 3.3, 3.4**) and analyzed in tandem with measurements taken on the non-reconstructed specimens (BW was estimated for UCMP 217911; MPL, BW, and WSM for UCMP 217999; and MPL, BW, and WIM for UCMP 218000). All non-angular measurements were converted to size-adjusted shape variables through division of their geometric mean (Jungers et al., 1995). After size-adjustment, species means were calculated for each ray [Mdp2, Mdp3/4, Mdp5, Pdp2, Pdp3 (for species that have a grooming unguis on this ray), Pdp3/4 (pooled only when the same unguis form is present on both rays), and Pdp5]. Finally, each measurement was converted into a z-score (subtracting by the variable mean and dividing by the variable's standard deviation) to create a set of variables that

each have a mean of 0 and a standard deviation of 1 for use in ordination methods that expect variables to have similar variances.

Analyses of data were run in R v3.0.3 (R Core Team, 2014). Principal components analyses (PCA) were run using the princomp function in the base stats package of R and linear discriminant functions analyses (DFA) were run using the lda function in the MASS package (Venables and Ripley, 2002). Pearson's correlation coefficients between each variate and each variable were used to determine loadings (using the corr function in the basic stats package). PCAs were used to summarize the maximum amount of variation observed in the dataset, while DFAs were used to determine the combinations of variables which best distinguish among groups and to classify unknown cases into these groups. The classification ability of each analysis was tested by classifying all training cases based on the original analysis and through leave-one-out cross validation (in which each training case is in turn left out of an analysis and then classified based on this newly run analysis). First, anthropoid second pedal distal phalanges were classified based on other groups to determine which species possess grooming ungues and/or grooming unguis-like morphology. Next, fossil distal phalanges were classified to determine if any specimens can be classified as grooming phalanges based on living taxa. Comparisons among primate grooming ungues and distal phalanges of non-primate mammals were used to determine whether or not isolated fossil distal phalanges can be considered primate grooming ungues.

Ancestral state reconstructions were run on species means of second pedal distal phalanges (**Table 3.9**; n=89). The main phylogeny used in this analysis (**Fig. 3.8**) contains only extant taxa and was modified from Springer et al. (2012). All modifications were done using Tree Graph 2 (Stöver and Müller, 2010). *Ptilocercus lowii*, which was not present in Springer et al.'s analysis, was grafted onto the tree in the same manner as described by Boyer and Seiffert (2013). The rodent *Chiropodomys* was added using the revised divergence date for rodents presented by Bininda-Emonds et al. (2007). A PCA was run on the extant sample from **Table 3.9** and the fossils from **Table 3.4** (a species mean is used for *Notharctus tenebrosus*) and ancestral state reconstructions of PC1 and PC2 scores for specific ancestors (**Fig. 3.8**) were run using BayesTraits v2 (Meade and Pagel, 2014). Ancestral states of continuously varying traits were estimated using a phylogenetic generalized least squares approach assuming a Brownian motion model of evolution. The use of PC scores as tip data for ancestral state reconstructions is similar

to a phylomorphospace approach (e.g., Revell, 2014), but here differs in the method of ancestral state reconstruction (using BayesTraits) and that states were only reconstructed for specific nodes of interest (rather than all internal nodes). First, ancestral states were reconstructed using the extant tree (**Fig. 3.8**). Prior to reconstructing the states, it was tested if adjusting the tree by a phylogenetic scaling parameter (δ, κ, and λ) provided a better fit of the data (PC1 and PC2) to the model (a constant-variance random walk model of trait evolution) than when using the untransformed tree. Delta (δ) detects changes in the rate of evolution over time; kappa (κ) detects if trait evolution is associated with branch length; and lambda (λ) detects whether a trait varies with phylogenetic relatedness (Meade and Pagel, 2014). Posterior distributions of the scaling parameters were generated using Markov chain Monte Carlo (MCMC) sampling of 10,050,000 iterations where the first 50,000 iterations were discarded as burn-in under model A (continuous random-walk MCMC). Model B (continuous directional MCMC) was not used as the input tree was ultrametric and this model cannot be used on ultrametric trees. Hypothesis testing was done following (Meade and Pagel, 2014): a likelihood ratio statistic comparing two models was calculated as 2[harmonic mean estimate of marginal likelihood(better fitting model) – harmonic mean estimate of marginal likelihood (worse fitting model)] where a value of two or greater is considered evidence that one model provides a better fit than another. Once an appropriate scaling parameter was identified, two independent MCMC chains were run (30,050,000 iterations with 50,000 discarded as burn in) using the scaling parameter estimates. Mean values were taken from combined results, calculated in Tracer 1.6 (Rambaut et al., 2014). It was also worthwhile to consider how different hypotheses of fossil relationships to extant taxa may affect results. Reconstructions were run using a set of four trees (**Fig. 3.9**) representing the major hypotheses of relationships of fossil to extant taxa (e.g., Rose, 1994): adapiforms as sister to strepsirrhines and omomyiforms as sister to tarsiiformes (**Tree 1, Fig. 3.9**), adapiforms as sister to strepsirrhines and omomyiforms as sister to haplorhines (**Tree 2, Fig. 3.9**), adapiforms as sister to anthropoids and omomyiforms as sister to tarsiiformes (**Tree 3, Fig. 3.9**), and adapiforms as sister to anthropoids and omomyiforms as sister to haplorhines (**Tree 4, Fig. 3.9**). Fossils were added to the extant tree using similar methods as done by Boyer and Seiffert (2013): extinct clades were spaced at 1ma intervals working down from extant nodes to minimize ghost lineages. Branch lengths for fossil taxa were calculated so that they terminate near the age of the specimen's locality or the species/genus that it is from: 47.45ma [Br-2/Br-3 boundary from

Smith et al.'s Fig. 1 (2004) as *Notharctus tenebrosus* is best known from Br-2 (2002)] for *Notharctus tenebrosus* [mean of AMNH FM 129382 (a) and 143612_3], 54.5ma [Wa-3/Wa4 from Smith et al.'s Fig. 8 (2014)] for UCMP 217911 and 217999, and 52.93ma [Wa-5/Wa-6 boundary from Smith et al.'s Fig. 1 (2004)] for UCMP 218000. Using the scaling parameters estimated for the extant tree, two independent MCMC chains were run (30,050,000 iterations with 50,000 discarded as burn in) for each tree. Again, mean values were calculated from the two combined runs for each tree using Tracer 1.6.

3.4 Results

3.4.1 PCA of Ray-specific Species Means

A PCA was run on a dataset comprised of all extant ray-specific species means and fossil individuals to summarize and assess the maximum amount of variation within the dataset. PC scores were calculated for fossil estimates *a posteriori*. See **Table 3.10** for components and **Table 3.11** for component loadings. A plot of the first two PC scores (**Fig. 3.10, top**) for the grouped taxa (anthropoid second pedal distal phalanges and fossils specimens not shown) demonstrate that PC1 separates falcular, non-primate grooming, and tegular phalanges from ungular phalanges. Strepsirrhine/tarsier grooming phalanges fall in the middle, but overlap extensively with ungular phalanges. Loadings demonstrate that falcular, tegular, and non-primate grooming phalanges have relatively dorso-ventrally deeper midshafts (MSH), flexor tubercles (FTH), articular facets (FH), and apical tufts/distal shafts (ATH) coupled with more strongly dorsally convex shafts (SIA) and proximally concave articular facets (FIA). Ungular phalanges, on the other hand, tend to have relatively medio-laterally wider superior articular facet margins (WSM), midshafts (MSW), apical tufts/distal shafts (ATW), and bases (BW). Primate grooming phalanges fall within the midrange for these values, but are more similar to ungular phalanges. Data points with higher scores along PC2 tend to have relatively wider inferior articular facet margins (WIM) and narrower mid-shaft widths (MSW). Within ungular phalanges, strepsirrhines tend to be medio-laterally wider (WIM; MSW) than anthropoids. PC3 separates strepsirrhine/tarsier grooming phalanges from other groups and demonstrates that they are relatively longer (MPL), have relatively medio-laterally narrower inferior articular facet margins (WIM), dorsally canted shafts (FSA) and articular facets that are less proximally concave (FIA;

Fig. 3.10, bottom). Most anthropoid second pedal distal phalanges fall within the ungular phalanx morphospace for PC3 (**Fig. 3.11, top**). All callitrichine platyrrhines fall near or within the tegular morphospace. Two anthropoid second pedal distal phalanges fall intermediate between the ungular and strepsirrhine/tarsier grooming morphospaces: *Aotus trivirgatus* (a genus that has previously been shown to have a grooming unguis) and *Pithecia monachus*. Most omomyiform and adapiform distal phalanges also fall within the ungular morphospace, although the two clades tend to cluster apart from one another (**Fig. 3.11, bottom**). The small specimens (and their estimates) that resemble strepsirrhine/tarsier grooming phalanges (UCMP 217999 and 218000) fall within or on the edge of strepsirrhine/tarsier grooming morphospace. Three adapiform specimens fall within strepsirrhine/tarsier grooming morphospace: the two *Notharctus* grooming ungues [AMNH FM 143612_3 and 129382 (a)] and a *Notharctus* specimen which does not visually resemble a grooming phalanx (AMNH FM 11474). UCMP 217911 and its estimate fall between the ungular and strepsirrhine/tarsier grooming morphospaces.

3.4.2 Classification of Anthropoid Second Pedal Distal Phalanges

A DFA was run on a training set of extant ray-specific species means divided into the following groups: ungular, strepsirrhine/tarsier grooming, tegular, falcular, and non-primate grooming phalanges. Species means of anthropoid second pedal distal phalanges were classified based on this analysis. Four canonical variates (CV) were extracted (**Table 3.12**). A plot of the first two CVs (**Fig. 3.12**) show that there is clear discrimination of ungular, strepsirrhine/tarsier grooming, tegular, and non-primate distal phalanges (there is considerable overlap of the falcular and non-primate grooming morphospaces). CV1 separates ungular, tegular, and non-primate phalanges. The loadings of CV1 show that (**Table 3.13**) non-primate phalanges have relatively dorso-ventrally deeper midshafts (MSH), flexor and extensor tubercles (FTH; ETH), and articular facets (FH) coupled with more strongly dorsally convex shafts (SIA). Ungular phalanges tend to have relatively medio-laterally wider superior articular facet margins (WSM), apical tufts/distal shafts (ATW), and bases (BW) coupled with relatively proximo-distally longer volar processes (VPL). CV 2 distinguishes strepsirrhine/tarsier grooming phalanges from other forms. CV2 loadings show that they tend to have dorsally canted shafts (FSA) and articular facets that are less proximally concave (FIA) than other forms. They also have higher values along CV1 than ungular phalanges demonstrating a tendency to have relatively dorso-ventrally

deeper midshafts (MSH), flexor and extensor tubercles (FTH; ETH), and articular facets (FH); more strongly dorsally convex shafts (SIA); medio-laterally narrower superior articular facet margins (WSM), apical tufts/distal shafts (ATW), and bases (BW); and relatively proximo-distally short volar processes (VPL). 98.4% of the training cases were classified correctly based on the original analysis as were 97.9% under leave-one-out cross validation. Anthropoid second pedal distal phalanges were classified as either ungular or tegular phalanges. All callitrichine platyrrhines were classified as tegular phalanges with a probability of 1.00. *Aotus sp.* (probability of 1.00) and the three *Callicebus* species (probabilities of 0.99) were also classified as tegular phalanges, but occupy their own space on the graph accompanied by *Aotus trivirgatus* and the two *Pithecia* distal phalanges. However, these cases were classified as ungular phalanges with probabilities of 0.99 (*Aotus trivirgatus*), 0.94 (*Pithecia monachus*) and 0.73 (*Pithecia sp*). The *Aotus*, *Callicebus*, and *Pithecia* second pedal distal phalanges do not clearly fit into the ungular or strepsirrhine/tarsier grooming phalanx morphospaces, showing that they are morphologically unique. They tend to have relatively shorter volar processes (VPL) and more strongly dorsally canted shafts (FSA) in comparison to ungular phalanges, but to a lesser degree than do strepsirrhine/tarsier grooming phalanges. All other anthropoid second pedal distal phalanges were classified as ungular phalanges with a probability of 1.00 and fall within or near the ungular phalanx morphospace.

3.4.3 Classification of Fossil Distal Phalanges

A second DFA was run discriminating among six groups: unmodified falcular, non-primate grooming, and strepsirrhine/tarsier grooming phalanx groups as in the first DFA, a tegular phalanx group incorporating callitrichine second pedal distal phalanges (which were classified into this group by the first DFA), a new group called anthropoid grooming phalanges consisting of the second pedal distal phalanges of *Aotus*, *Callicebus*, and *Pithecia* that did not fall into any of the previously defined groups, and an ungular phalanx group incorporating all other anthropoid second pedal distal phalanges (which were classified into this group in the previous DFA). This analysis extracted 5 canonical variates (**Table 3.12**) and a biplot of the first two shows complete (**Fig. 3.13**) separation of all groups with the exception of the non-primate morphospaces. The variate loadings (**Table 3.14**) are very similar to those of the first DFA. 96.9% of training cases were classified correctly based on the original analysis and 95.9% under

leave-one-out cross validation. Almost all omomyiforms were classified as ungular phalanges with a probability of 1.00 and fall within or near the ungular morphospace (**Table 3.15**). The only exceptions are the potential omomyiform grooming phalanges UCMP 217999 and 218000 (and their estimates). These were classified as strepsirrhine/tarsier grooming phalanges (with probabilities of 1.00 for UCMP 217999 and its estimate; 0.83 for UCMP 218000 and 0.94 for its estimate). These specimens fall within or very near to strepsirrhine/tarsier grooming morphospace and differ considerably from non-primate distal phalanges, supporting the contention that they are most likely primate grooming phalanges rather than non-primate phalanges. The omomyiform specimens that were classified as ungular phalanges tend to cluster away from adapiform distal phalanges. Adapiform distal phalanges were classified as either ungular, strepsirrhine/tarsier grooming, or anthropoid grooming phalanges (**Table 3.15**). The two specimens previously identified as grooming phalanges [AMNH FM 129382 (a) and 143612_3] fall within or very near strepsirrhine/tarsier grooming morphospace, but only AMNH FM 143612_3 is classified as a strepsirrhine/tarsier grooming phalanx (with a probability of 0.97); AMNH FM 129382 (a) is classified as an anthropoid grooming phalanx (with a probability of 0.84). The only other adapiform specimen that falls nearest to strepsirrhine/tarsier grooming phalanx space is UCMP 217911 (and its estimate). Despite the close proximity to strepsirrhine/tarsier grooming space, UCMP 217911 and its estimate are classified as anthropoid grooming phalanges with probabilities of 0.37 and 0.82 respectively. No adapiform specimens fall within tegular or anthropoid grooming morphospace, although AMNH FM 131764 (a) falls very close to this space and is classified as an anthropoid grooming phalanx with a probability of 1.00. Other adapiform specimens fall within ungular morphospace or between it and tegular morphospace (see **Table 3.15** for the remaining classifications). See **Figs. 3.14-3.21** for group summaries of each variable demonstrated as boxplots and **Table 3.16** for group means and standard deviations.

3.4.4 Ancestral State Reconstructions

A PCA was run on a subset of the data consisting of species means of extant second pedal distal phalanges (**Table 3.9**) and fossil grooming phalanges (**Table 3.4**). The first two components (**Table 3.10**) show separation of falcular, tegular, ungular, strepsirrhine/tarsier grooming and anthropoid grooming morphospaces (**Fig. 3.22**). Interestingly, there does appear to

be some phylogenetic structuring within grooming morphospace as tarsiers group with lorisiforms and *Daubentonia*, while lemuriform strepsirrhines cluster together. The omomyiform grooming phalanges fall near the tarsier/lorisiform/*Daubentonia* group while the adapiforms fall near the lemuriform group. Loadings (**Table 3.17**) show a similar pattern to those of the discriminant function analyses.

Ancestral states were reconstructed for both PC1 and PC2 scores at 19 nodes of interest (**Fig. 3.8**). The scaling parameter λ provided the best fit of extant PC1 scores to the model and was therefore used for reconstructions of PC1 scores. No scaling parameter provided a better fit of extant PC2 scores than when no parameters were used, so no scaling parameters were utilized in the reconstructions of PC2 scores. Reconstructions of PC1 and PC2 scores utilizing the extant tree (**Fig. 3.23**) plotted in a "Bayesian phylomorphospace" show that the most recent common ancestors of primates and haplorhines likely had a second pedal distal phalanx that resembled those of extant strepsirrhines and tarsiers while those of anthropoids, platyrrhines, and catarrhines likely bore ungulae. Further, these results suggest that anthropoid grooming phalanges evolved in parallel within three platyrrhine lineages: *Aotus*, Callicebinae, and *Pithecia*. Reconstructing ancestral states when adapiforms are placed as stem strepsirrhines (Trees 1 and 2, **Fig. 3.9**) show a similar pattern as do reconstructions based on extant taxa alone. Reconstructions based on Trees 1 and 2 give nearly identical results so only those for Tree 1 are shown (**Fig. 3.24**). Reconstructions when adapiforms are placed as stem anthropoids tell a somewhat different story. Trees 3 and 4 (**Fig. 3.9**) give nearly identical results so only those for Tree 3 are presented (**Fig. 3.25**). The reconstructions of ancestral states for primates and haplorhines fall within extant strepsirrhine/tarsier grooming phalanx morphospace rather than near it and anthropoids are reconstructed as having anthropoid grooming phalanges on their second pedal digits which were then lost in parallel in both platyrrhines and catarrhines. Despite these differences, results based on Trees 3 and 4 also suggest that the anthropoid grooming phalanges of the *Aotus*, Callicebinae, and *Pithecia* evolved in parallel.

3.5 Discussion

3.5.1 Anthropoid Grooming Ungues

These analyses demonstrate the presence of grooming ungues in three platyrrhine genera: *Aotus*, *Pithecia*, and *Callicebus*. Interestingly, anthropoid grooming phalanges are differentiated from both ungular phalanges and the grooming phalanges of strepsirrhines and tarsiers and rather, are morphologically intermediate between the two. Anthropoid grooming phalanges tend to have relatively shorter volar processes with more ventrally canted shafts than most ungular phalanges, but not to the same degree as those of strepsirrhines and tarsiers. Ancestral state reconstructions suggest that the grooming morphology of the platyrrhine genera were independently acquired in parallel along the three lineages. However, the specific selective pressures for grooming ungues are unclear. These results differ from an earlier study by Maiolino et al. (2011) in which *Aotus* plotted near strepsirrhine/tarsier grooming phalanges, *Pithecia* with ungular phalanges, and *Callicebus* between the two in a PCA of shape variables. The differences between results are likely due to a broader sample and additional measurements allowing for more fine-grained differences among phalanges to be detected in the present study.

3.5.2 Strepsirrhine and Tarsier Grooming Ungues

Von Koenigswald et al. (2012) suggested that differences in strepsirrhine and tarsier grooming phalanx shape may indicate that these two lineages acquired grooming ungues independently of one another. Shape does seem to vary with phylogeny, but there is not a clear divide between strepsirrhines and tarsiers. Rather there seems to be a divide between lorisiforms and the chiromyiform *Daubentonia* on one side and the lemuriforms on the other. Tarsiers fall with the lorisiform and *Daubentonia*. Ancestral state reconstructions suggest that the ancestor of living primates possessed morphology of the second pedal distal phalanx that was already quite similar to those of extant tarsiers and strepsirrhines. This implies that grooming ungues (on the second pedal ray) were not acquired independently in strepsirrhines and tarsiers, but rather were inherited from the most recent common ancestor of primates, and subsequently modified along the two lineages.

3.5.3 Omomyiform Grooming Ungues

The specimens UCMP 217999 and 218000 morphometrically resemble the grooming phalanges of tarsiers and strepsirrhines and differ from the distal phalanges of non-primate mammals. This combined with their small size suggest that these specimens are most likely omomyiform grooming phalanges. Further, they likely belong to the anaptomorphine genera of *Tetonius* (UCMP 217999) and *Arapahovius* (UCMP 218000) as these are the most prevalent genera at their respective localities (**Table 3.7**). These specimens look similar to those of tarsiers and lorisiform strepsirrhines and plot near the ancestral state reconstruction of haplorhines. They differ from the grooming phalanges of adapiforms in being relatively narrower, but are similar in possessing enlarged nutrient foramina.

Unfortunately, these are isolated specimens so it is unclear as to which ray they actually belong to. It seems most likely that they were at least present on the second pedal digit. There are no known primates with grooming ungues present on manual digits or any pedal digit more lateral than the third and no cases in which a grooming unguis is found on the third digit in the absence of one on the second. This may be related to the second pedal digit (the most medial of the postaxial rays) being in the best position for scratching at the fur of the body and/or modifications of this ray being the least disruptive for grasping performance.

Currently, tarsiers are the only primates known to possess grooming ungues on both the second and third pedal rays. Von Koenigswald et al. (2012) suggested that *Notharctus tenebrosus* may have possessed a grooming unguis on its third pedal digit based on their assessment of AMNH FM 143612_2 (the distal phalanx from the third pedal ray), but my results did not corroborate this. Rather, this specimen fell between the tegular and ungular phalanx morphospaces and away from other *Notharctus* grooming phalanges (**Fig. 3.13**). Consequently, it seems likely that adapiforms (or at least *Notharctus*) lacked grooming ungues on this digit. Therefore, the more interesting question is whether or not omomyiforms were tarsier-like in possessing grooming ungues on both second and third pedal digits. However, articulated fossil specimens are required to determine this, and additional specimens are needed to better document the distribution of grooming ungues among different omomyiform clades.

3.5.4 Adapiform Distal Phalanges

The presence of grooming ungues is reconfirmed for *Notharctus tenebrosus* and an additional specimen from an early Eocene adapiform (most likely *Cantius* or *Notharctus venticolis*) is identified as a grooming phalanx. Since grooming ungues have now been identified in both North American notharctines and European cercamoniines, it is highly likely that most, if not all adapiforms possessed a grooming unguis (von Koenigswald et al., 2012; Gilbert and Maiolino, 2015).

An earlier study noted a pronounced broadening of the apical tuft in AMNH FM 143612_3 (*Notharctus tenebrosus*) compared to extant taxa and suggested that this may represent transitional morphology between a grooming unguis and nail state (Maiolino et al., 2012). The apical tufts of all the adapiform grooming phalanges are relatively wide, but not to the extreme of AMNH FM 143612_3 (**Fig. 3.3**). In the current study, a much larger sample of extant grooming phalanges is assessed and it shows that AMNH FM 143612_3 falls just outside of the range of extant strepsirrhines/tarsiers, while the other adapiform specimens fall within the range of extant species (although towards the relatively wider side; ATW, **Fig. 3.18** – the highest value of the *Notharctus* grooming box is from AMNH FM 143612_3). Therefore, it seems less likely that AMNH FM 143612_3 is transitional in form, but it is unclear what this morphology is related to.

Interestingly, some adapiform specimens are classified as anthropoid grooming phalanges by the discriminant function analysis. The majority of these are specimens from *Notharctus tenebrosus* (**Table 3.15**). These specimens are not interpreted to be anthropoid grooming phalanges for several reasons. First, many adapiform distal phalanges tend to have relatively shorter volar processes (**VPL, Fig. 3.16**) and dorso-ventrally taller mid-shafts (**MSH, Fig.3.16**); causing them to resemble anthropoid grooming phalanges. Some researchers have suggested that adapiform distal phalanges may demonstrate falcula-like morphology and can possibly be interpreted as intermediate between ungular and falcular phalanges (Godinot and Beard, 1991; Godinot, 1992; Godinot and Beard, 1993). A relatively shorter volar process and deeper mid-shaft may be related to this. Second, the presence of strepsirrhine/tarsier-like grooming phalanges in *Notharctus* suggests that these other morphologies are not grooming phalanges. It seems highly unlikely that one species would have two grooming ungues of very different form.

It is clear from these analyses that many adapiform distal phalanges possess unique morphology, but additional analyses are necessary to interpret its significance.

3.5.5 Ancestral States and Concluding Remarks

Ancestral state reconstructions based on extant taxa alone, as well as several hypotheses of fossil relationships all suggest that platyrrhine grooming ungues have evolved in parallel among three separate lineages of platyrrhine primates. The ancestral state of anthropoids is reconstructed as ungula-bearing based on extant taxa; similar results are obtained when utilizing fossil taxa in which adapiforms are placed as stem-strepsirrhines. However, if adapiforms are considered to be stem-anthropoids, the ancestral anthropoid condition is reconstructed as possessing a grooming unguis like that of *Aotus*, *Callicebus*, and *Pithecia*. These structures were then independently lost in both catarrhine and platyrrhine lineages and re-evolved in parallel among three separate lineages of platyrrhine primates. Since, the relationships of fossil to extant primates are so heavily debated, reconstructions based on fossils are not considered reliable, but they do demonstrate two things. First, the ancestral states of primates, haplorhines, tarsiers, and strepsirrhines can likely be considered accurate because they are unchanged or change very little when reconstructed based on different hypothesized relationships of fossils. Second, the reconstruction of the anthropoid ancestor differs depending on the hypothesis of phylogenetic relationship, and as such, this result is considered less robust. Further analyses are required to better determine the validity of this result.

3.6 Figures

Fig. 3.1. Variation in external grooming ungues and ungulae.
Photos of the toes of preserved skins (and one living human) in lateral and dorsal views. Strepsirrhines possess grooming ungues on each second pedal digit and tarsiers on both second and third (third not shown). Platyrrhines possess a range of morphologies on second pedal digits: grooming ungues (e.g., *Aotus* and *Callicebus*), ungulae (nails, e.g., *Alouatta*), tegulae (e.g., *Callithrix*), and more difficult to define structures (e.g., *Pithecia*). Catarrhines possess ungulae on all digits.

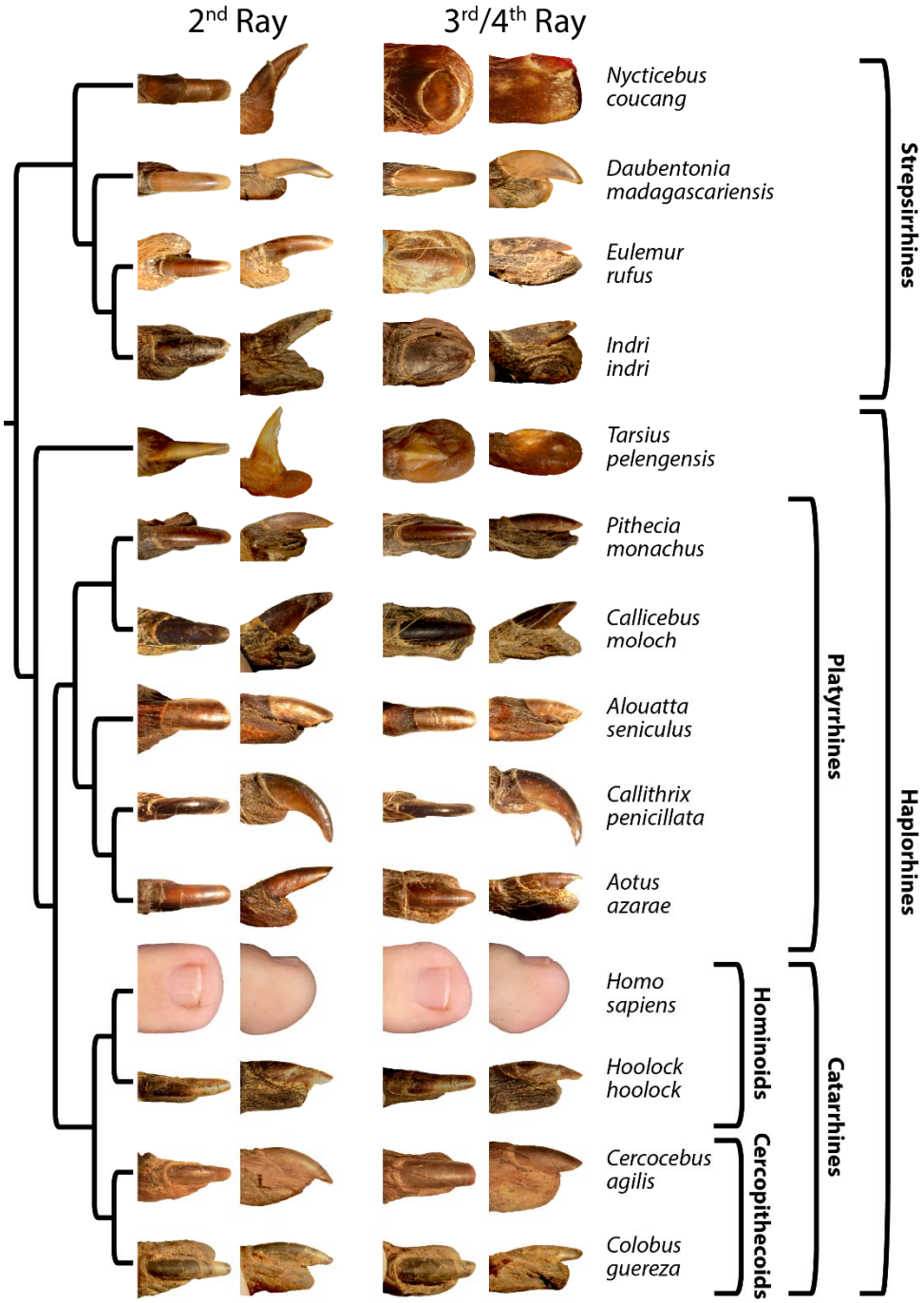

Fig. 3.2. Grooming Unguis Structure.
A comparison of the structure of grooming unguis- and ungula (nail)-bearing digits. Images are lateral views of microCT reconstructions of the second and third pedal digits of SBU (13). Left: External tissues of the digits show that grooming ungues project above and beyond the apical pad to a greater degree than do ungulae. Middle: When external tissue is rendered transparent, it can be seen that grooming phalanges, like the external unguis, also project dorsally and distally beyond the pad. Right: The morphology of the distal phalanx relates to these external differences in two ways. First, grooming phalanges have shafts that are dorsally canted with respect to the articular facet (when the superior and inferior margins of the facet are aligned within the same vertical plane), facilitating the support of a dorsally projecting unguis. Second, grooming phalanges have relatively short volar processes while ungular phalanges possess relatively longer volar processes. The volar process is the portion of the distal phalanx that lies embedded within the apical pad; the relative length of the volar processes in comparison to the total length of the phalanx is indicative of the degree to which a distal phalanx projects above and beyond the apical pad.

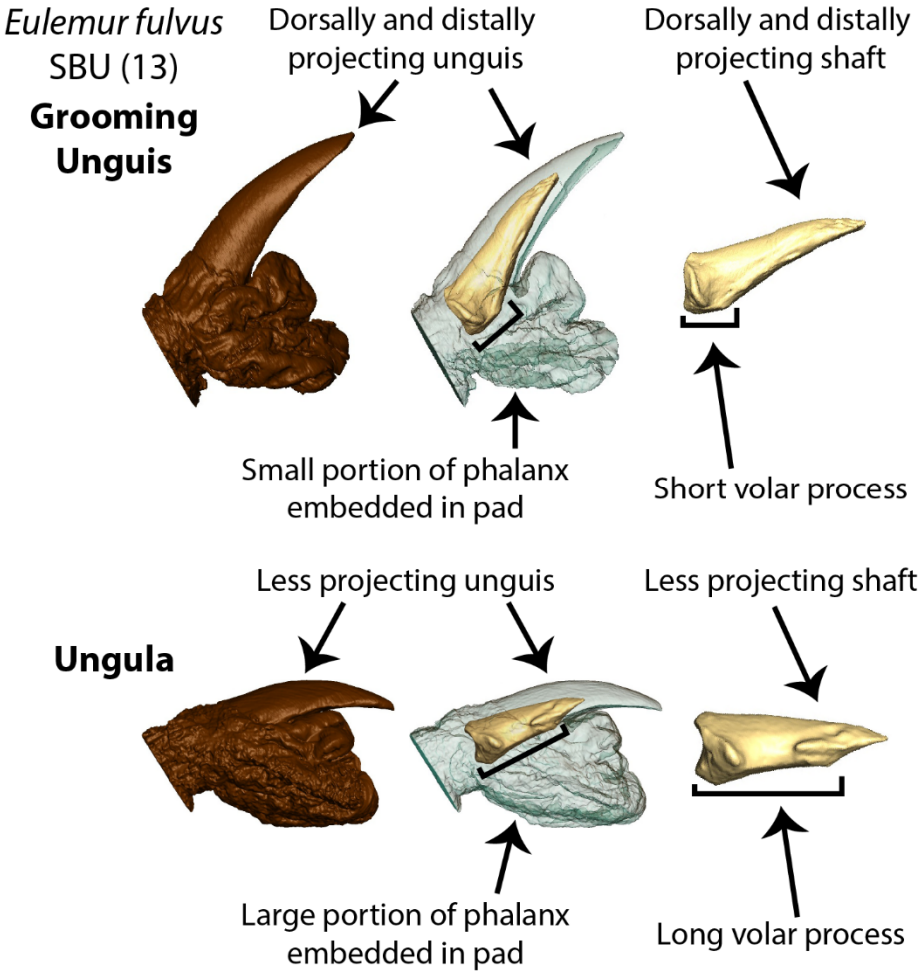

Fig. 3.3. Adapiform distal phalanges.
Adapiform grooming phalanges compared to ungular phalanges. Each distal phalanx is shown in dorsal, lateral, proximal, medial, and volar views. UCMP 217911 and 147533 are isolated distal phalanges from the v70243 locality in the Washakie Basin, WY. They can most likely be attributed to *Cantius* or *Notharctus venticolis* as the majority of dental specimens from this site are attributed to these genera (See **Table 3.6**). One side of the base of UCMP 217911 is slightly damaged; it is reconstructed (black shaded region) by creating a mirror image of the undamaged side of the base. AMNH FM 129382 (a) and 143612_3 are grooming phalanges both attributed to *Notharctus tenebrosus*. These are not isolated specimens and are shown compared to ungular phalanges from the same individual. AMNH FM 129382 (b) is likely from a fifth pedal ray (based on its small size and asymmetrical base), but is heavily damaged. Damaged parts are reconstructed by comparison to undamaged specimens; this specimen was not included in the analyses and is shown for comparison only. The specimens from AMNH FM 143612 were found in semi-articulation and can each be attributed to specific pedal rays; 143612_3 to the 2nd, 143612_2 to the 3rd and 143612_4 to the 4th.

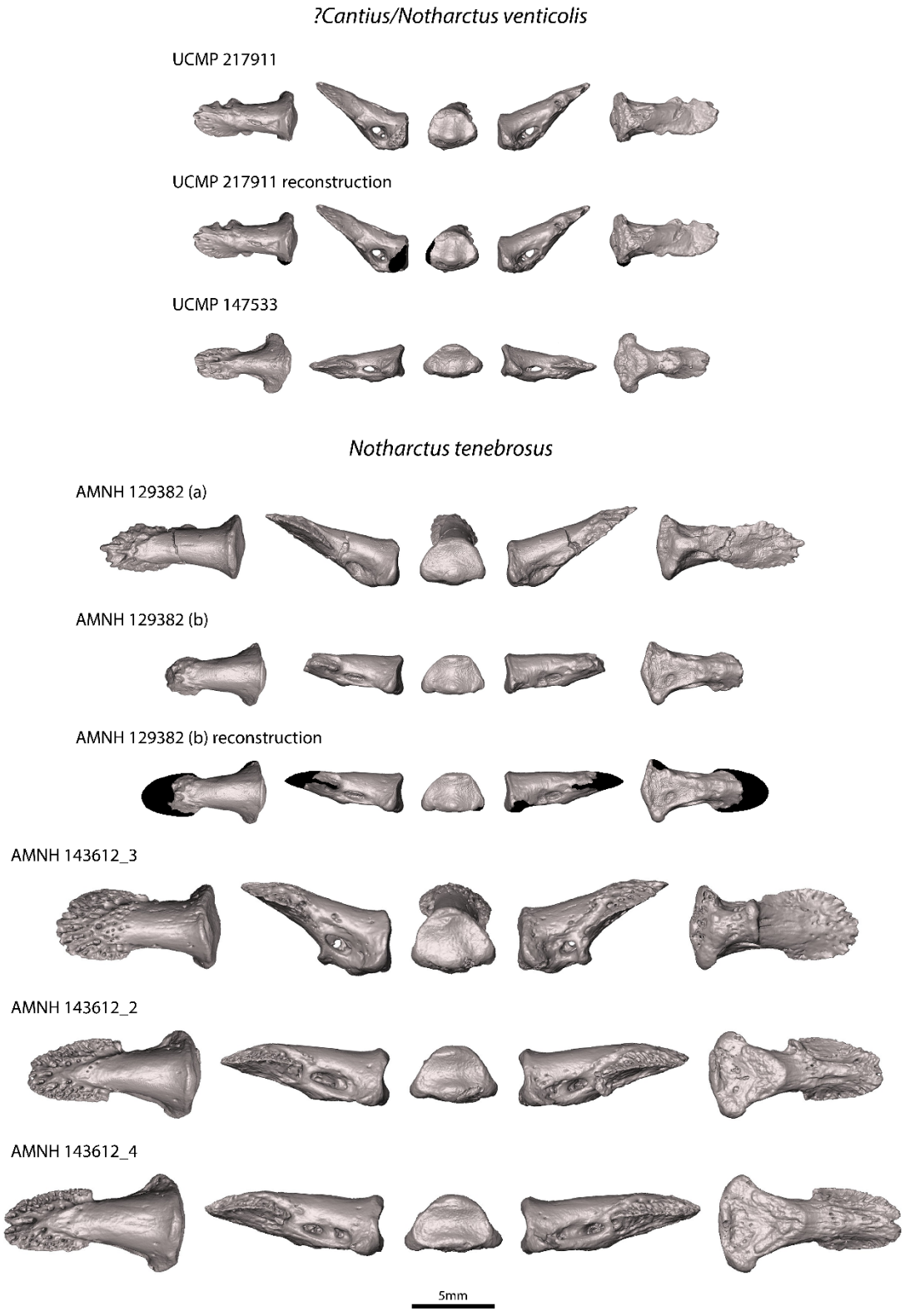
?Cantius/Notharctus venticolis
UCMP 217911
UCMP 217911 reconstruction
UCMP 147533
Notharctus tenebrosus
AMNH 129382 (a)
AMNH 129382 (b)
AMNH 129382 (b) reconstruction
AMNH 143612_3
AMNH 143612_2
AMNH 143612_4
5mm

Fig. 3.4. Omomyiform distal phalanges.
Specimens that are hypothesized to be omomyiform grooming phalanges (UCMP 217999 and 218000) compared to ungular phalanges. Each distal phalanx is shown in dorsal, lateral, proximal, medial, and volar views. UCMP 217999 and 218373 are isolated distal phalanges from the v70214 locality in the Washakie Basin, WY. They can most likely be attributed to *Tetonius* as the vast majority of dental specimens from this site are attributed to this genus (See **Table 3.7**). The tip and base of UCMP 217999 are slightly damaged. The base is reconstructed (black shaded region) by creating a mirror image of the undamaged side of the base. The distal tip is reconstructed in lateral view as the intersection of two straight lines that follow the contours of the dorsal and volar surfaces. The shape of the tip in dorsal and volar view is based on following the contours of the lateral margins, but this choice does not affect any measurements taken from the reconstructed phalanges. UCMP 218373 shows erosion on both its tip and base; it is reconstructed based on similar specimens from other sites (this specimen was not included in the analyses and is shown for comparison only). UCMP 218000 and 218261 are isolated distal phalanges from the v74022 locality in the Washakie Basin, WY. These specimens are most likely from *Arapahovius* as the majority of dental specimens from this locality are attributed to this genus. UCMP 218000 is reconstructed in the same manner as described for 217999.

?Tetonius

UCMP 217999

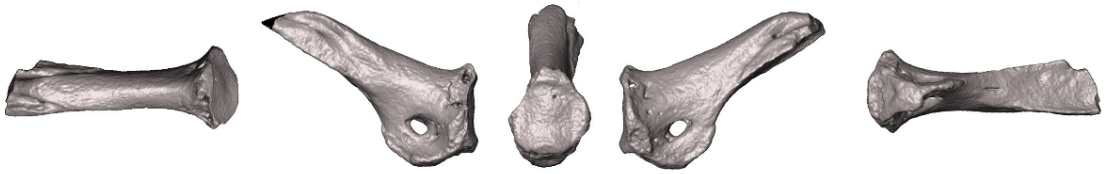

UCMP 217999 reconstruction

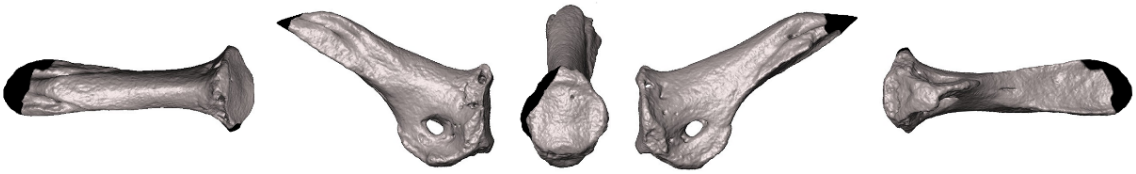

UCMP 218373

UCMP 218373 reconstruction

?Arapahovius

UCMP 218000

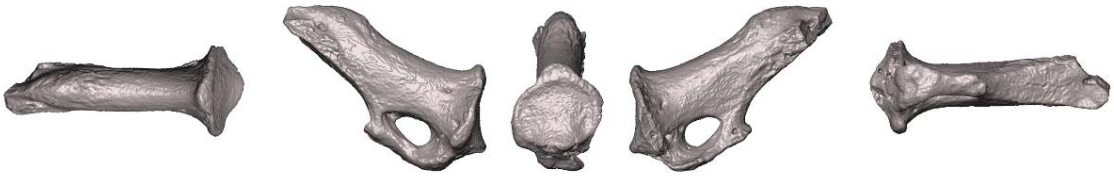

UCMP 218000 reconstruction

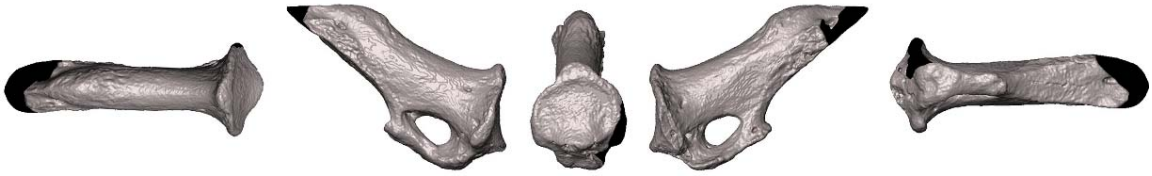

UCMP 218261

1mm

Fig. 3.5. Anatomical terminology illustrated.
Morphological features discussed in this chapter are demonstrated on distal phalanges that bear different unguis forms shown (from left to right) in dorsal, lateral, volar, and proximal views. Unmarked images of each specimen are shown directly above those that are highlighted.

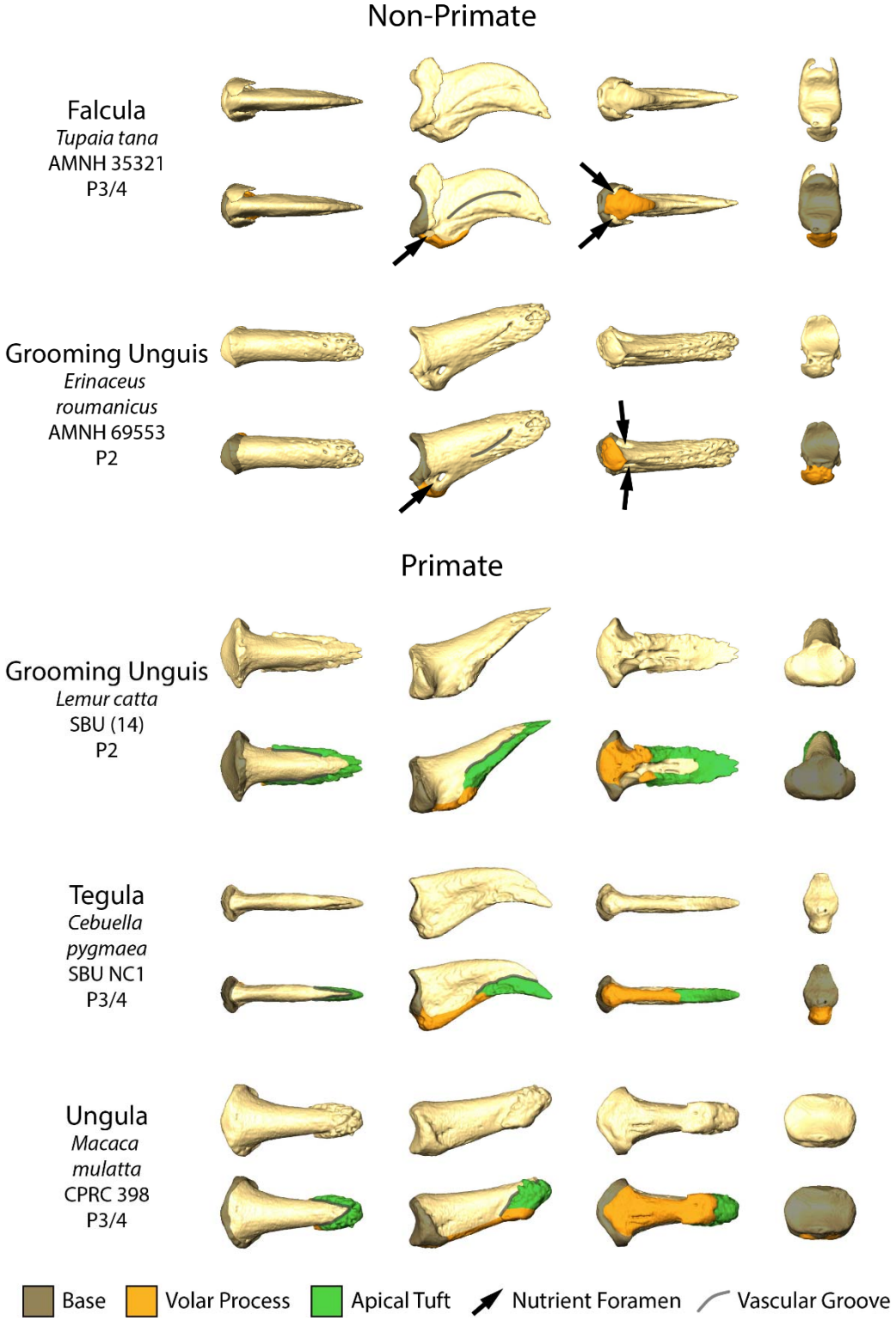

Fig. 3.6. Measurements used in analyses (1).
Illustrations of measurements ETH, FTH, VPL, MSH, ATH, WSM, and WIM taken on a range of distal phalanx shapes. See **Table 3.8** for measurement abbreviations and definitions.

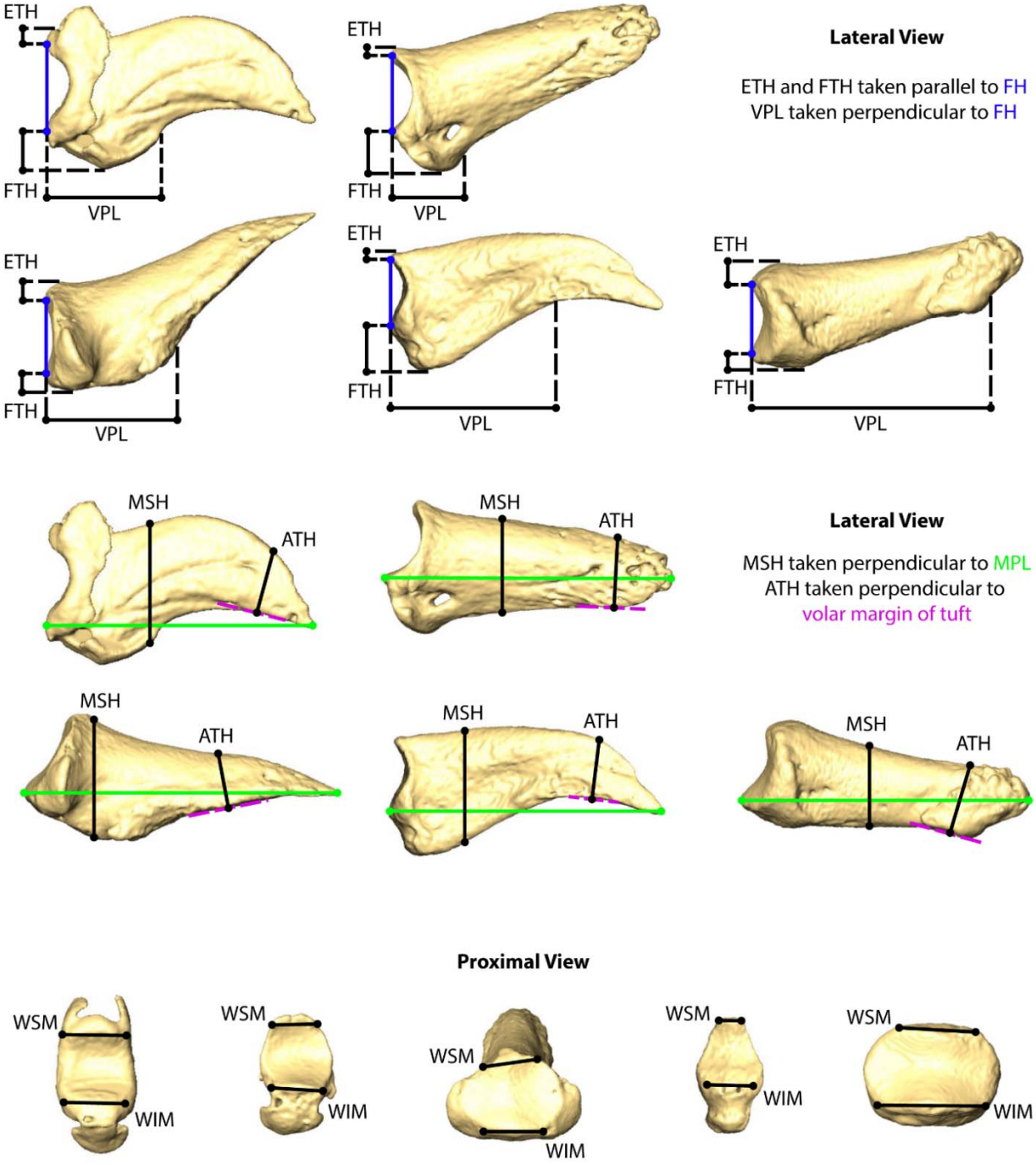

Fig. 3.7. Measurements used in analyses (2).
Illustrations of measurements FH, FIA, SIA, MPL, BW, MSW, and ATW taken on a range of distal phalanx shapes. See **Table 3.8** for measurement abbreviations and definitions.

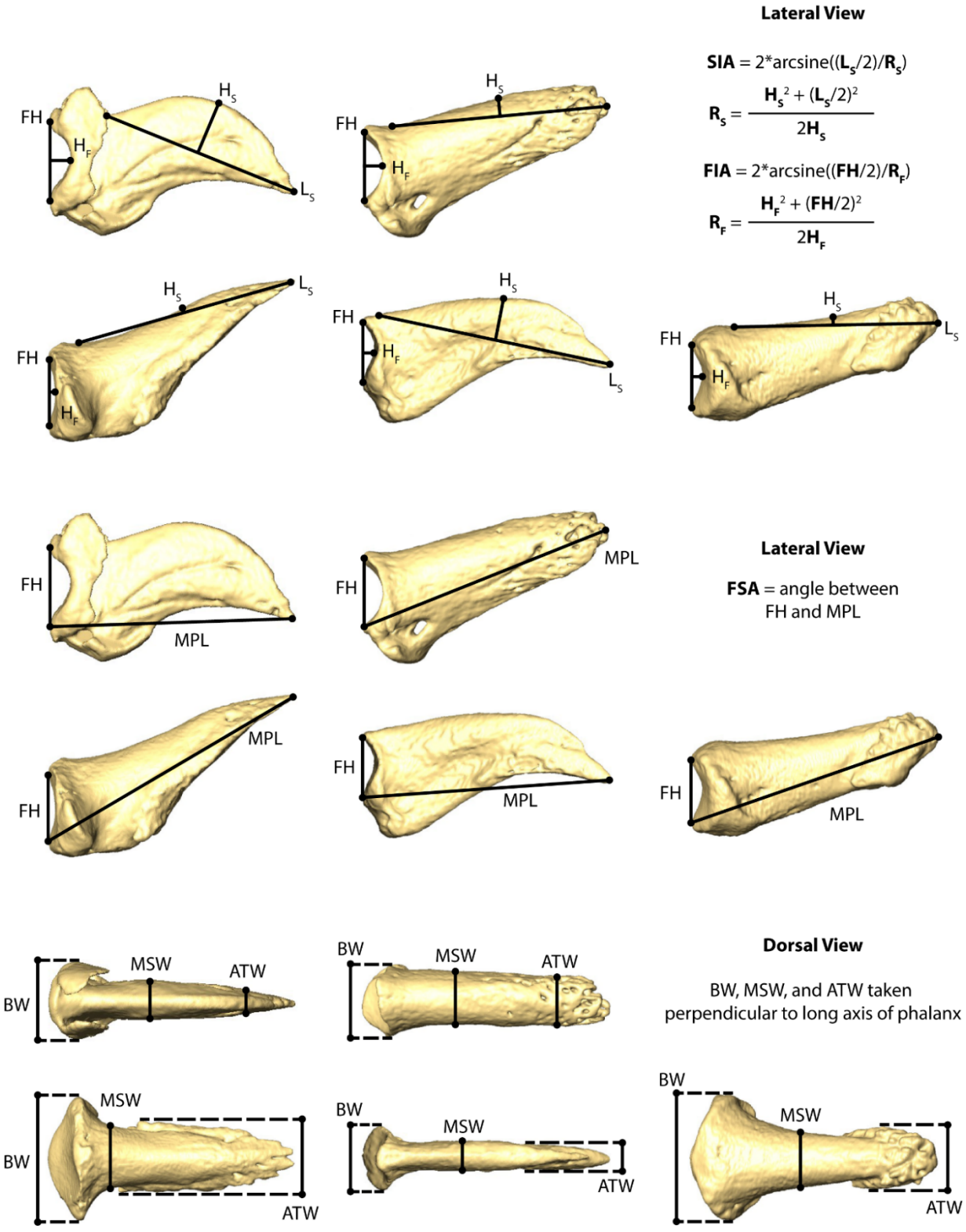

Fig. 3.8. Extant phylogeny used for ancestral state reconstructions.
Stars mark the internal nodes for which ancestral states were reconstructed.

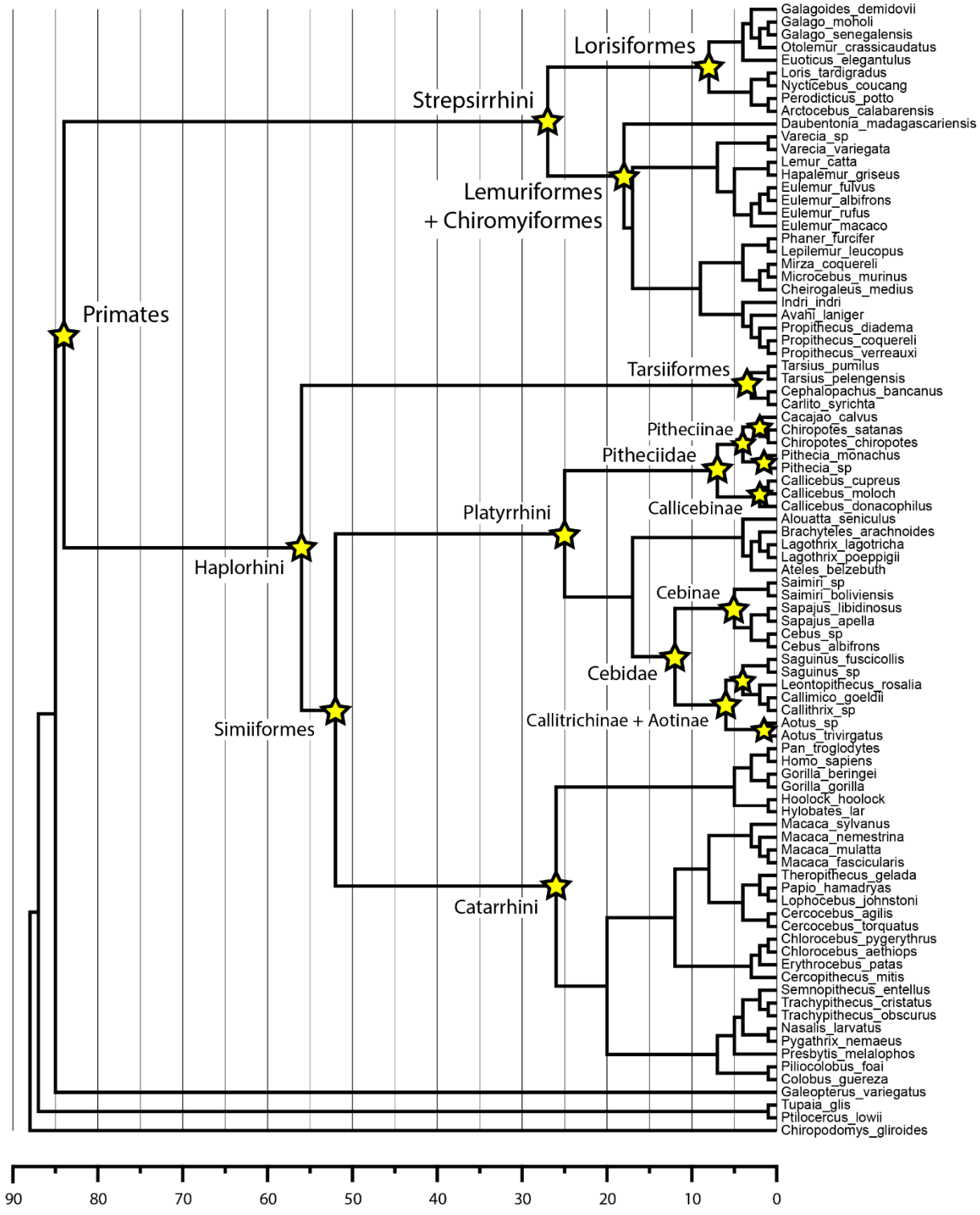

Fig. 3.9. Hypothesized relationships of fossil and extant taxa.
Tree number refers to the specific tree used in ancestral state reconstructions (see text). The robustness of ancestral state reconstructions based on extant taxa are tested in relation to inclusion and placement of fossil taxa by comparing ancestral states reconstructed using these four topologies.

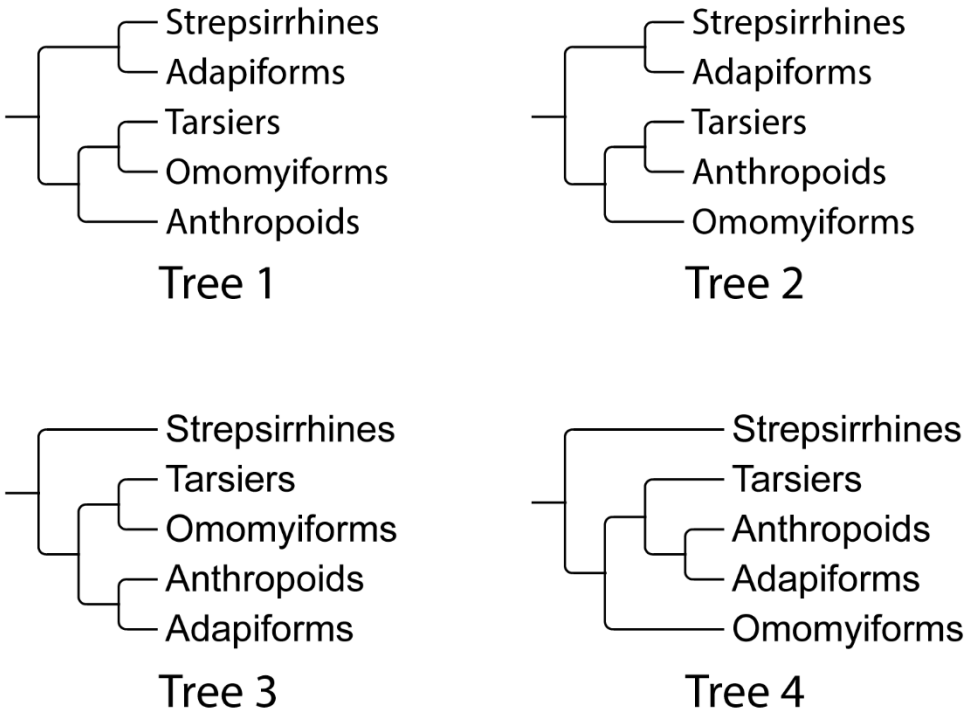

Fig. 3.10. PCA of extant ray-specific species means (1).
Top: bivariate plot of PC1 and PC2. Bottom: bivariate plot of PC1 and PC3. Variables with the highest loadings along each axis are listed along the top and right side of each graph. Anthropoid second pedal distal phalanges and fossils specimens not shown.

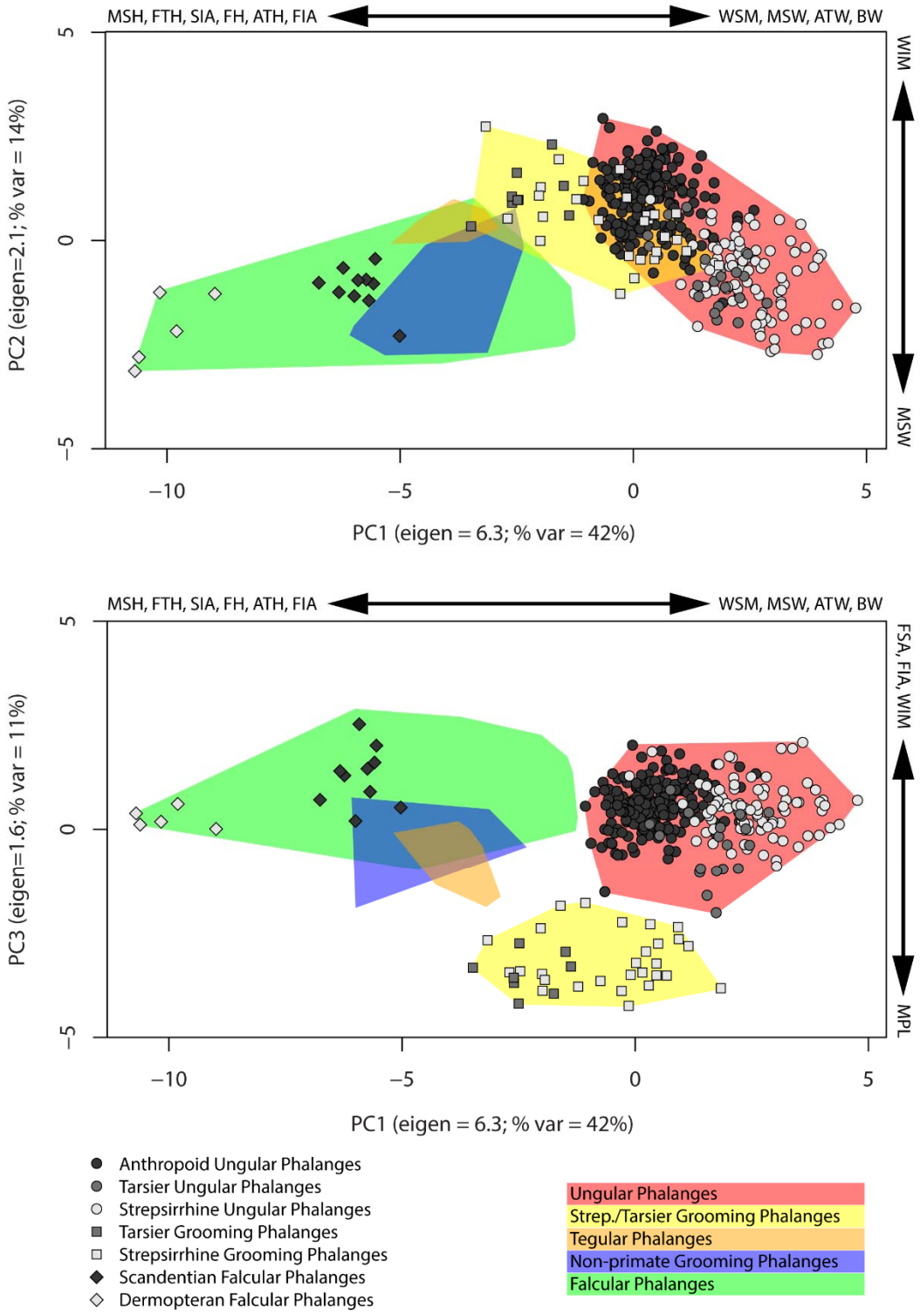

Fig. 3.11. PCA of extant ray-specific species means (2).
Top: bivariate plot of PC1 and PC3 with anthropoid second pedal digits plotted. Bottom: bivariate plot of PC1 and PC3 with fossil specimens plotted. Variables with the highest loadings along each axis are listed along the top and right side of each graph.

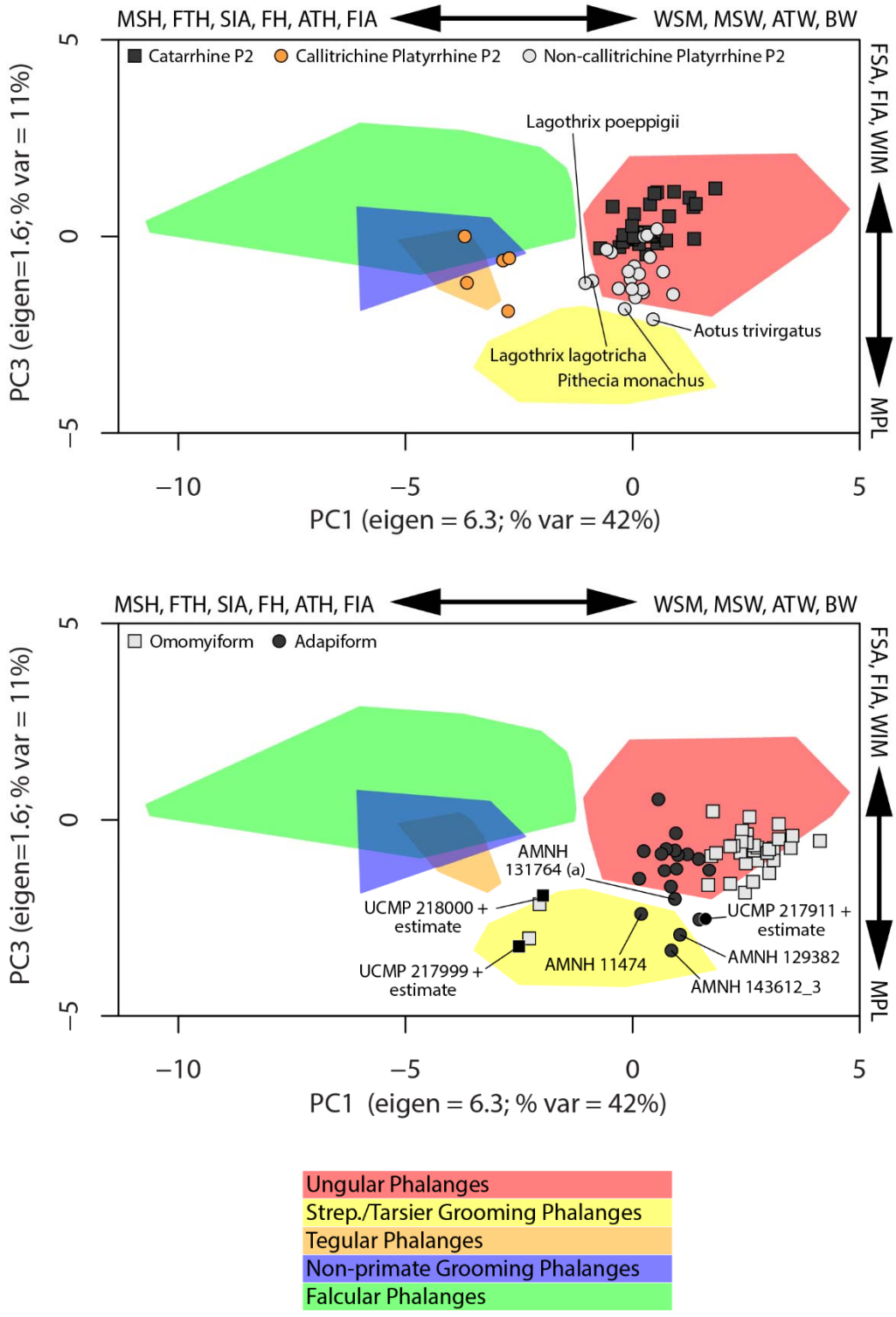

Fig. 3.12. DFA classifying anthropoid second pedal distal phalanges.
The first two canonical variates from a DFA discriminating among ungular, strepsirrhine/tarsier grooming, tegular, falcular, and non-primate grooming phalanges used to classify anthropoid second pedal distal phalanges. Variables with the highest loadings along each axis are listed along the top and right side of the graph.

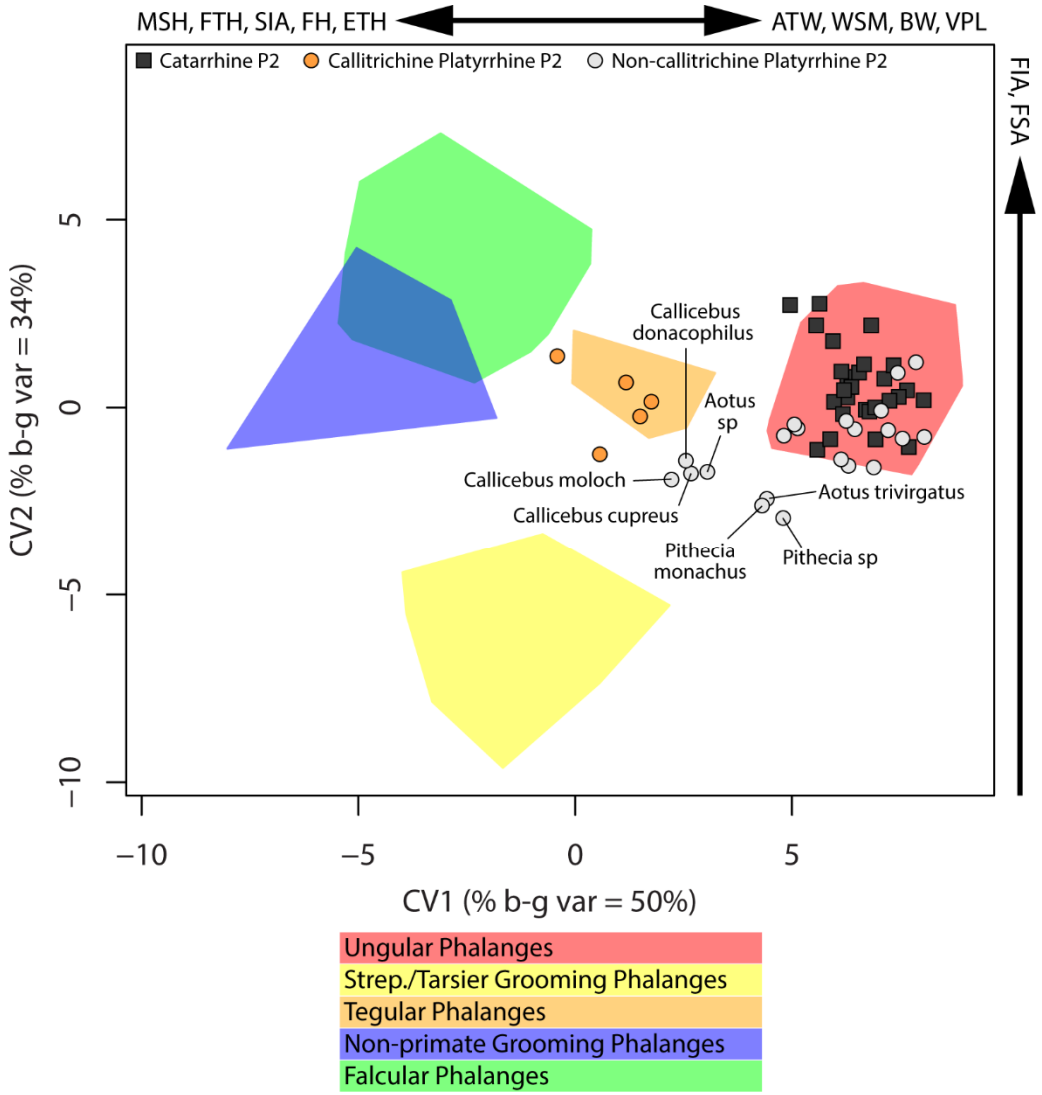

Fig. 3.13. DFA classifying fossil distal phalanges.
A second DFA discriminating among six groups: unmodified falcular, non-primate grooming, and strepsirrhine/tarsier grooming phalanx groups as in the first DFA, a tegular phalanx group incorporating callitrichine second pedal distal phalanges (which were classified into this group by the first DFA), a new group called anthropoid grooming phalanges consisting of the second pedal distal phalanges of *Aotus*, *Callicebus*, and *Pithecia* that did not fall into any of the previously defined groups, and an ungular phalanx group incorporating all other anthropoid second pedal distal phalanges (which were classified into this group in the previous DFA). Variables with the highest loadings along each axis are listed along the top and right side of the graph. Fossil distal phalanges are classified based on this analysis.

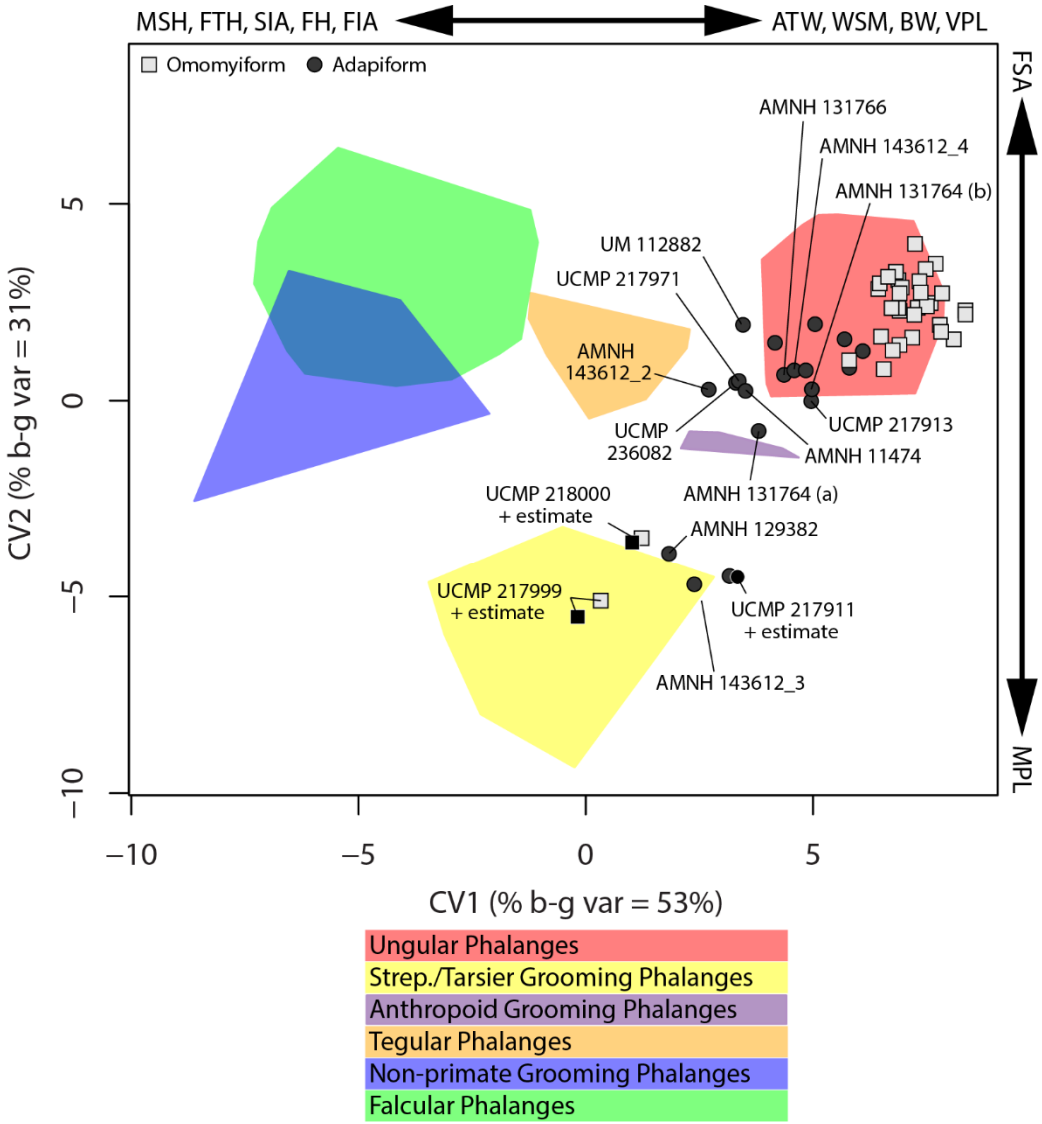

Fig. 3.14. Boxplots of FH and ETH.
Boxplots of Z-scores of FH (top) and ETH (bottom) indicating interquartile range and median with whiskers extending to the most extreme case that is not greater than 1.5x the interquartile range. Data points that fall outside of this are represented by open circles.

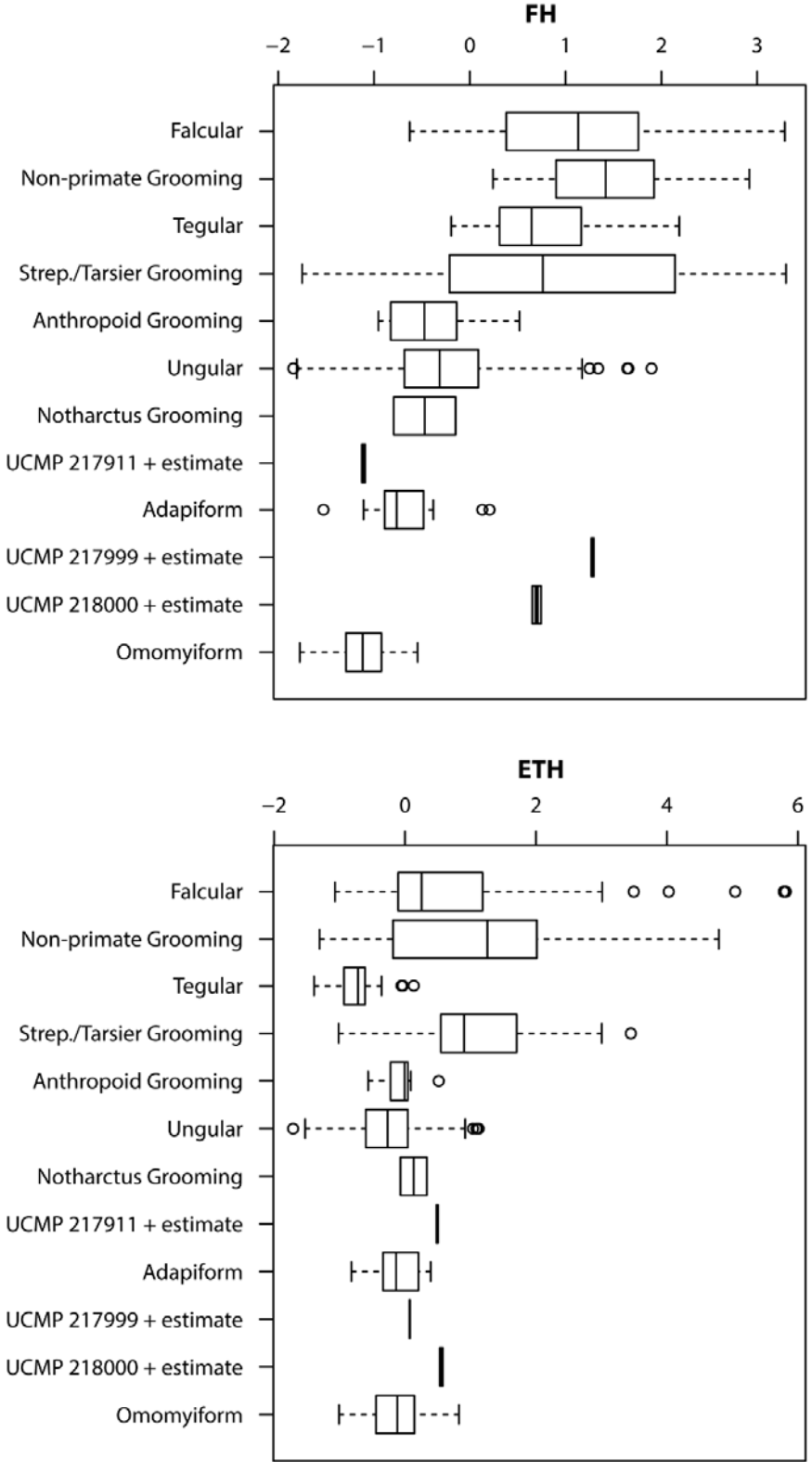

Fig. 3.15. Boxplots of FTH and MPL.
Boxplots of Z-scores of FTH (top) and MPL (bottom) indicating interquartile range and median with whiskers extending to the most extreme case that is not greater than 1.5x the interquartile range. Data points that fall outside of this are represented by open circles.

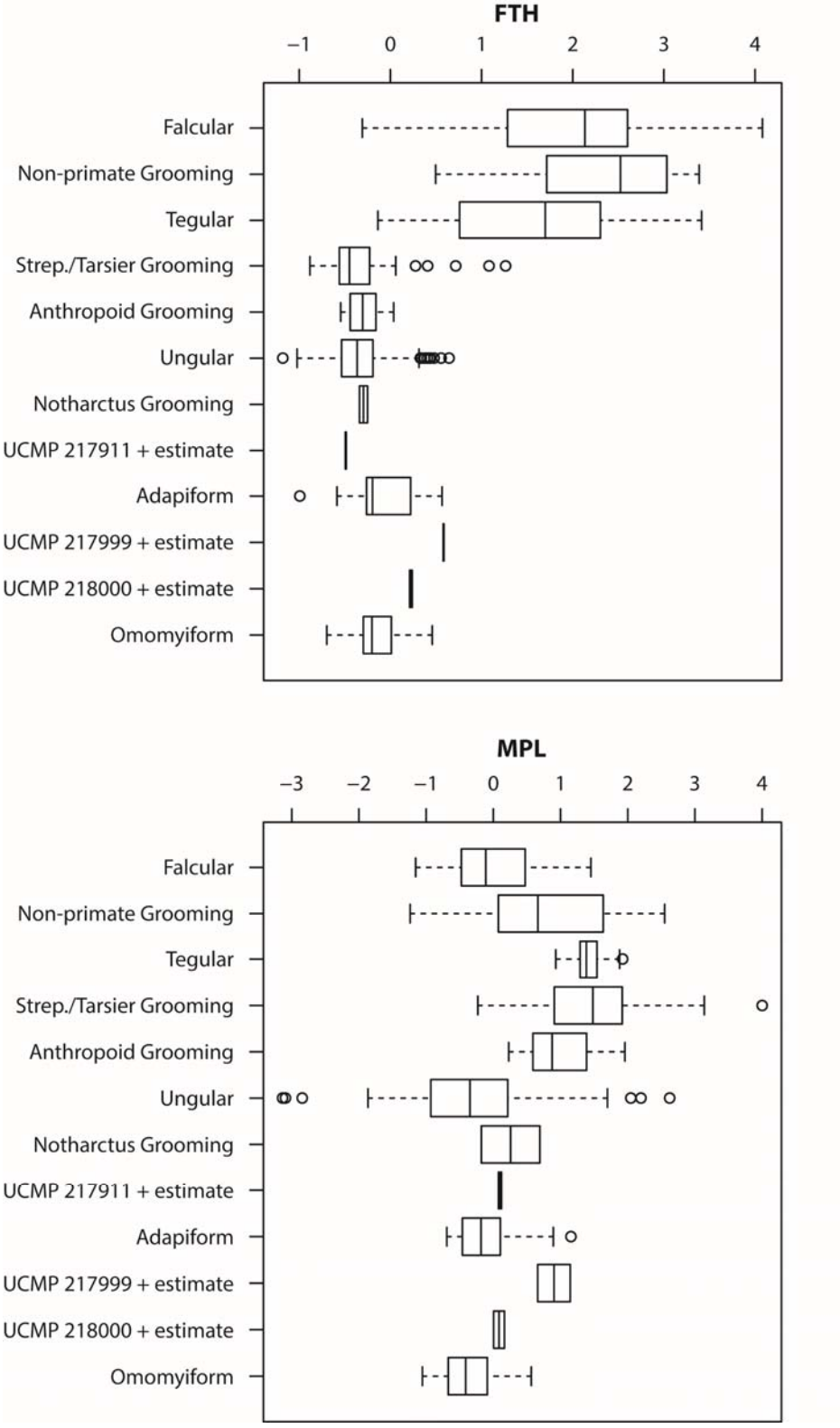

Fig. 3.16. Boxplots of VPL and MSH.
Boxplots of Z-scores of VPL (top) and MSH (bottom) indicating interquartile range and median with whiskers extending to the most extreme case that is not greater than 1.5x the interquartile range. Data points that fall outside of this are represented by open circles.

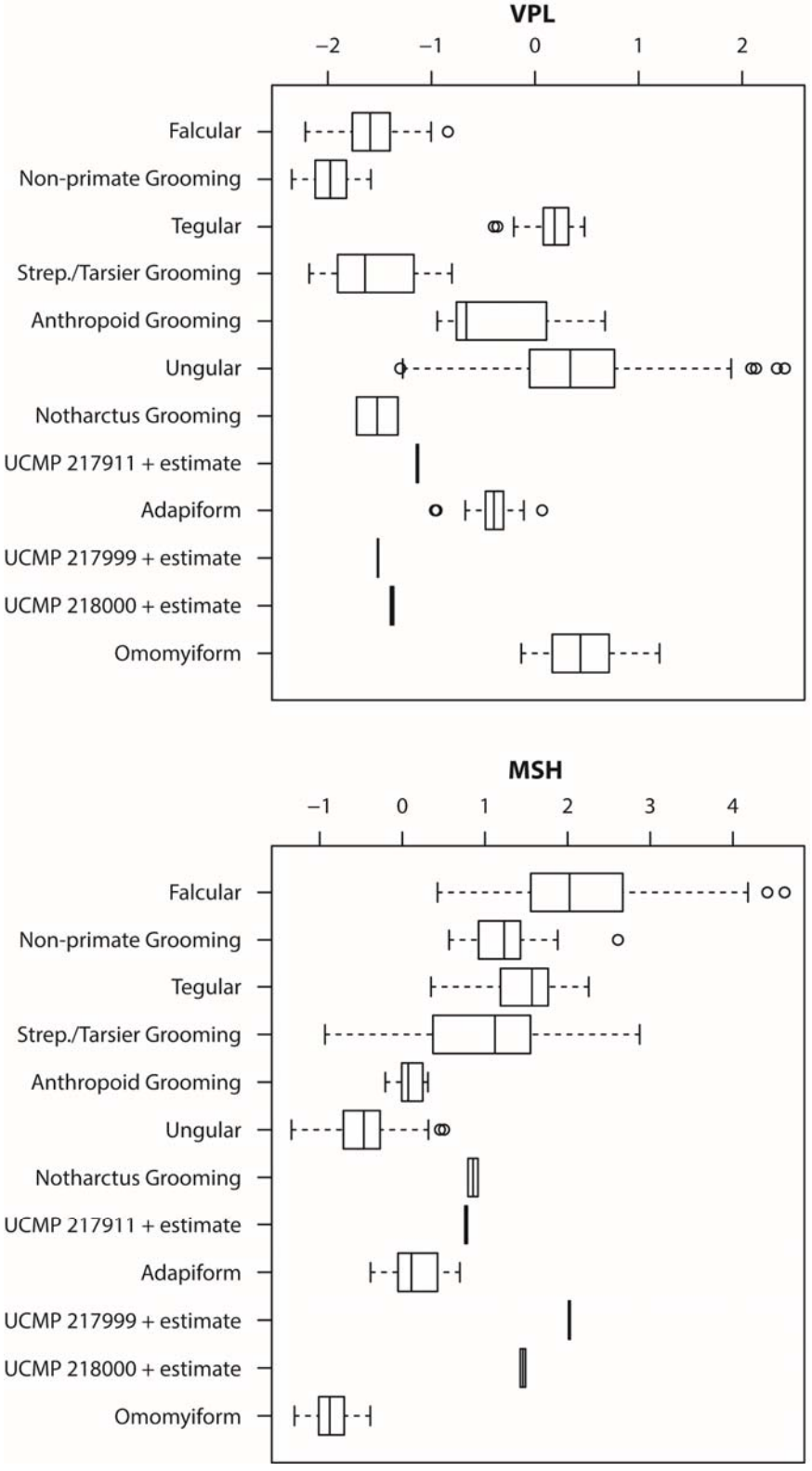

Fig. 3.17. Boxplots of ATH and BW.
Boxplots of Z-scores of ATH (top) and BW (bottom) indicating interquartile range and median with whiskers extending to the most extreme case that is not greater than 1.5x the interquartile range. Data points that fall outside of this are represented by open circles.

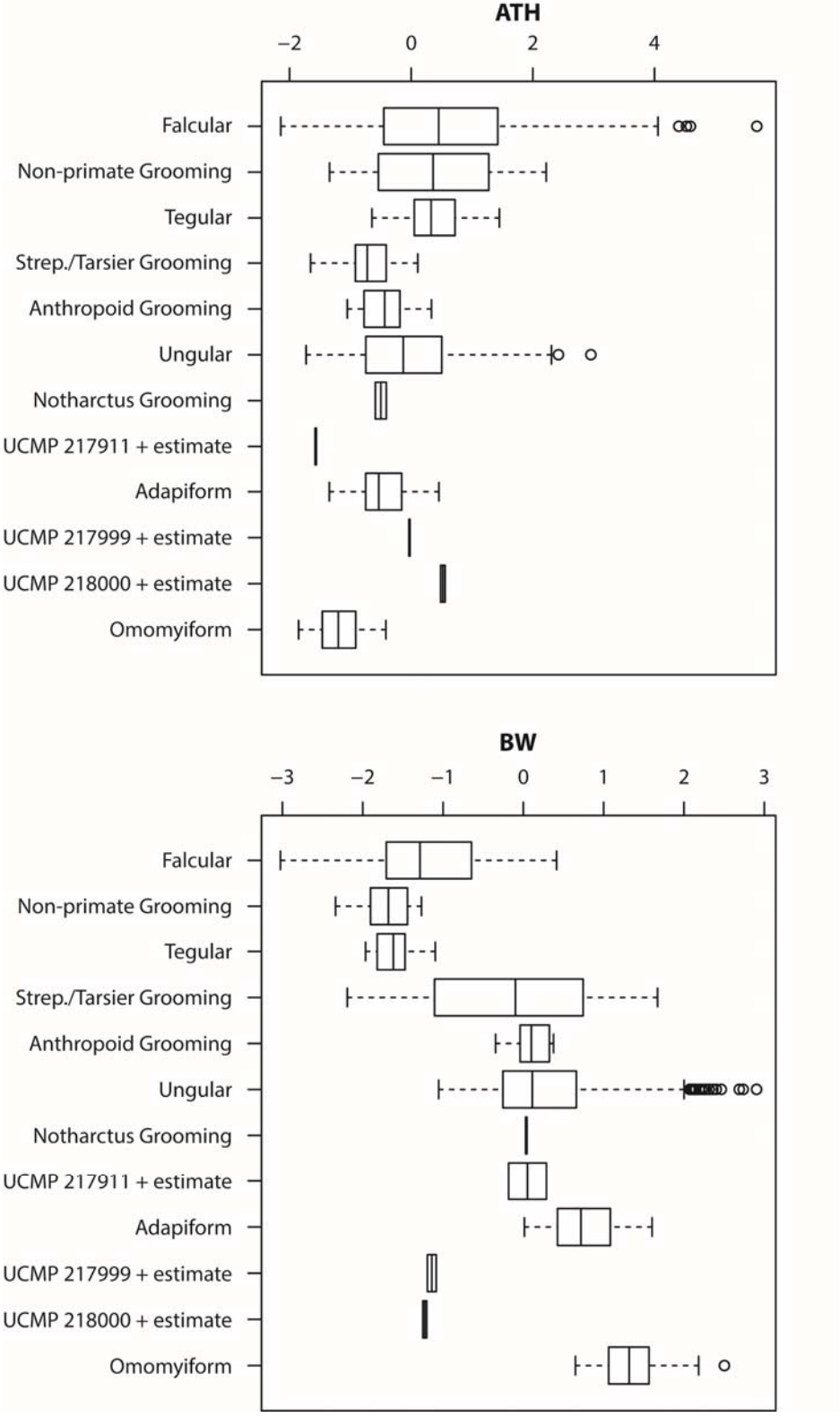

Fig. 3.18. Boxplots of MSW and ATW.
Boxplots of Z-scores of MSW (top) and ATW (bottom) indicating interquartile range and median with whiskers extending to the most extreme case that is not greater than 1.5x the interquartile range. Data points that fall outside of this are represented by open circles.

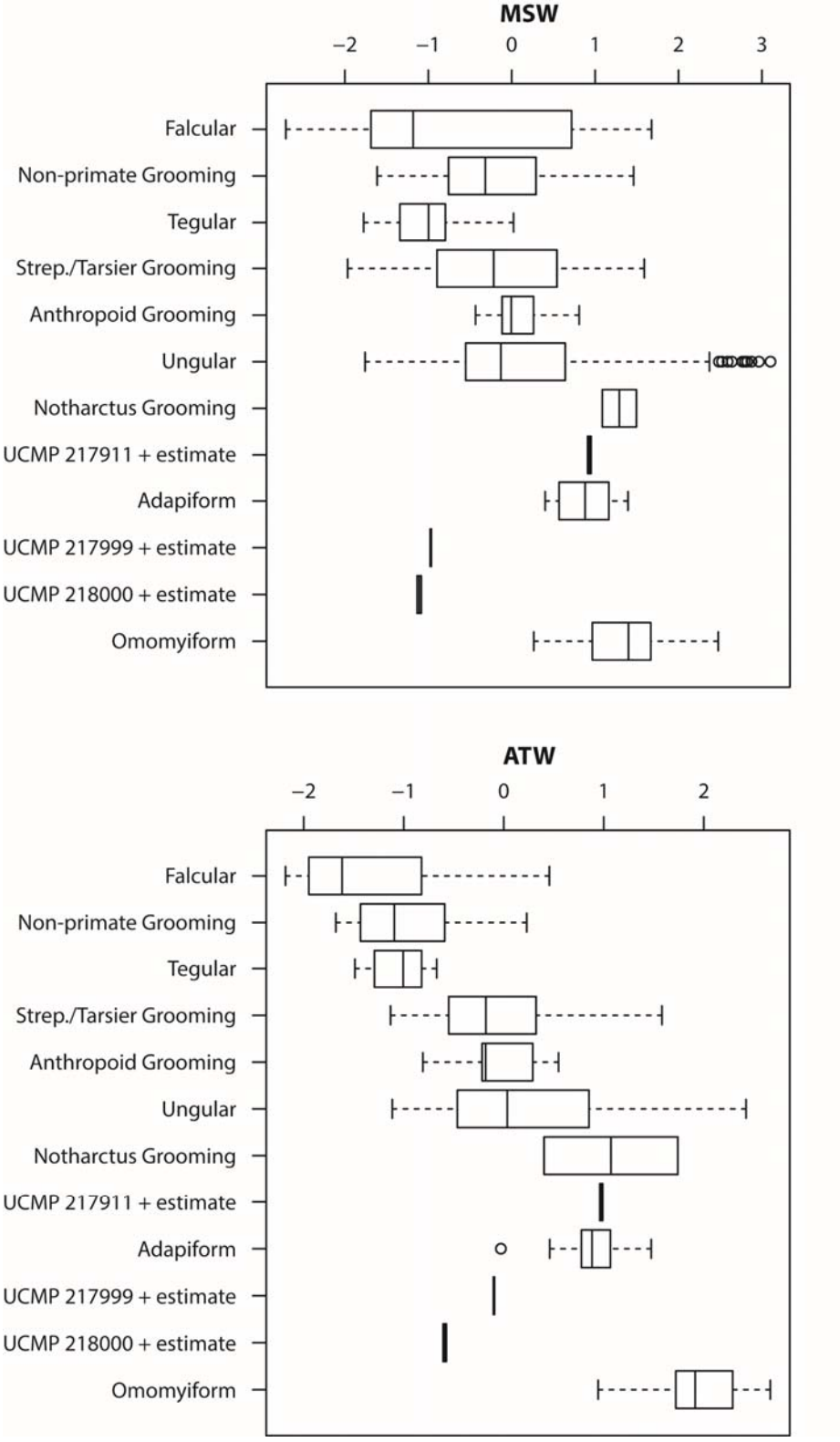

Fig. 3.19. Boxplots of WSM and WIM.
Boxplots of Z-scores of WSM (top) and WIM (bottom) indicating interquartile range and median with whiskers extending to the most extreme case that is not greater than 1.5x the interquartile range. Data points that fall outside of this are represented by open circles.

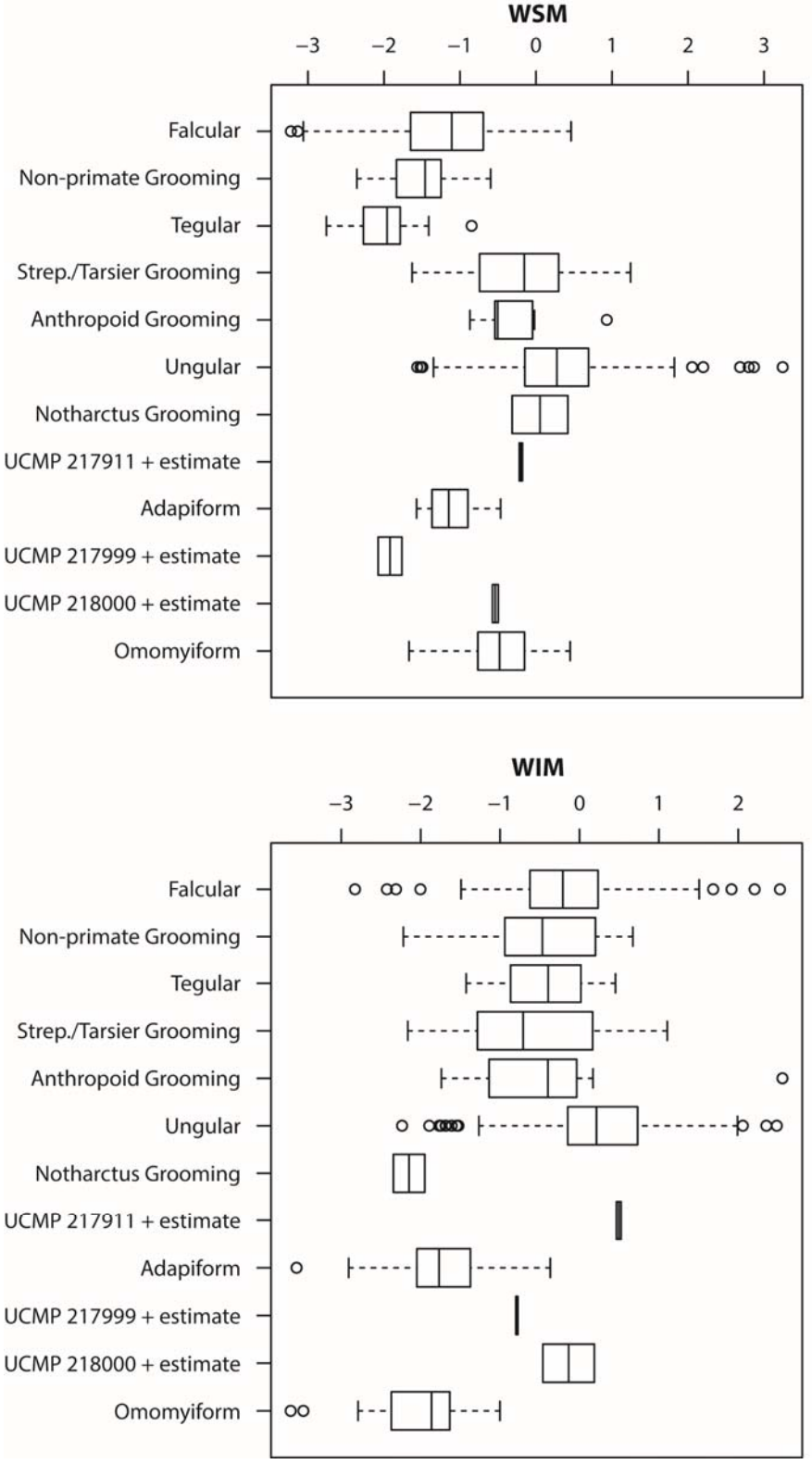

Fig. 3.20. Boxplots of SIA and FIA.
Boxplots of Z-scores of SIA (top) and FIA (bottom) indicating interquartile range and median with whiskers extending to the most extreme case that is not greater than 1.5x the interquartile range. Data points that fall outside of this are represented by open circles.

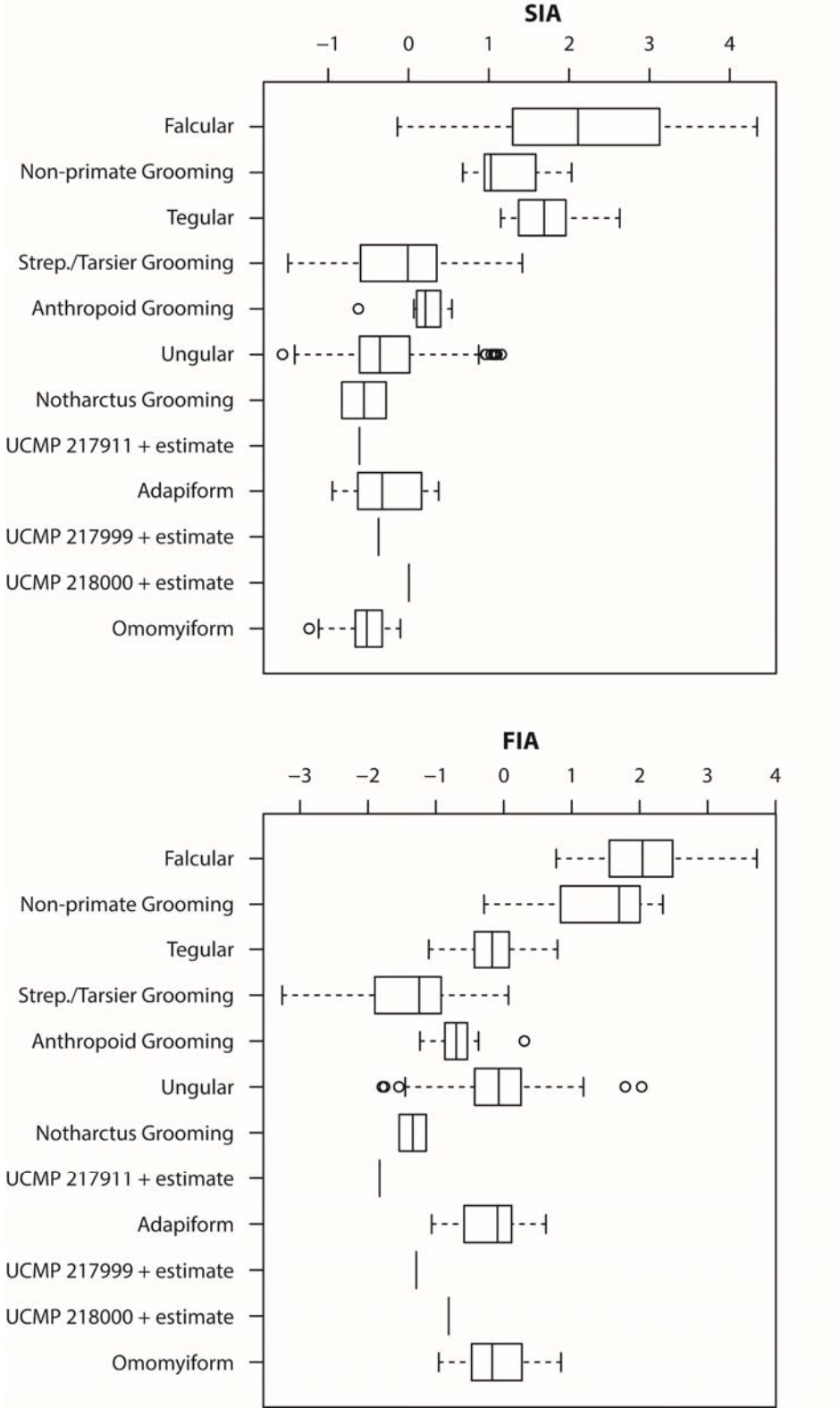

Fig. 3.21. Boxplot of FSA.
Boxplots of Z-scores of FSA indicating interquartile range and median with whiskers extending to the most extreme case that is not greater than 1.5x the interquartile range. Data points that fall outside of this are represented by open circles.

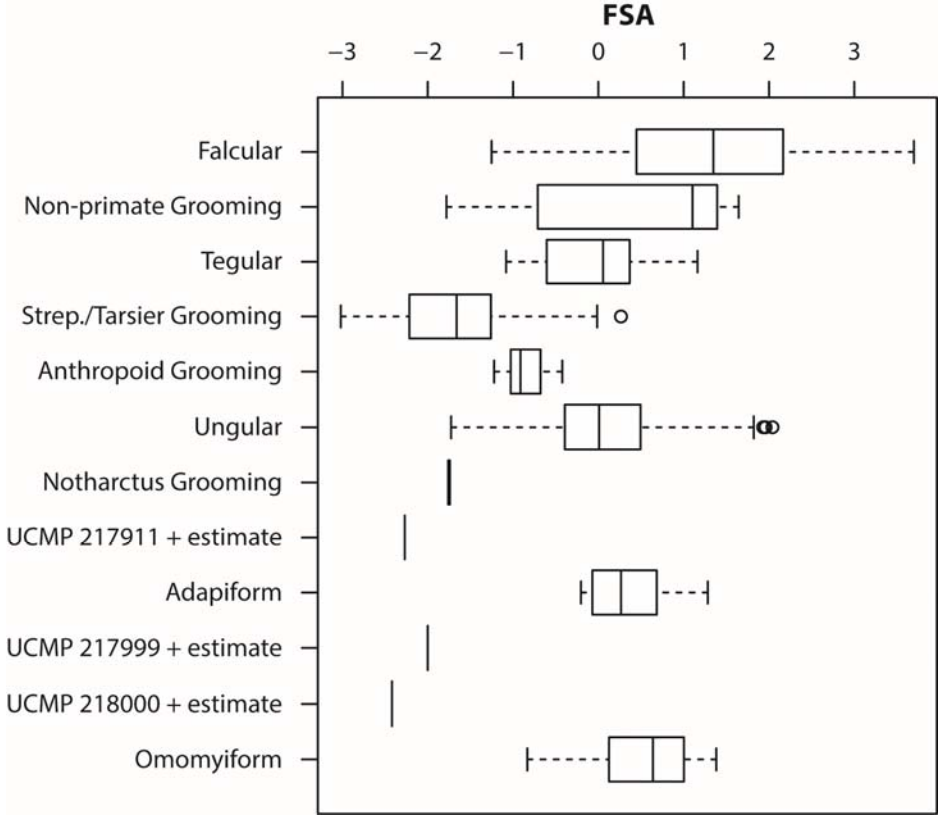

Fig. 3.22. PCA of second pedal rays.
A PCA of second pedal distal phalanx species means (**Table 3.4 and 3.9**). Variables with the highest loadings along each axis are listed along the top and right side of the graph. Grooming distal phalanx symbol shape and color indicate the phylogenetic group from which they come.

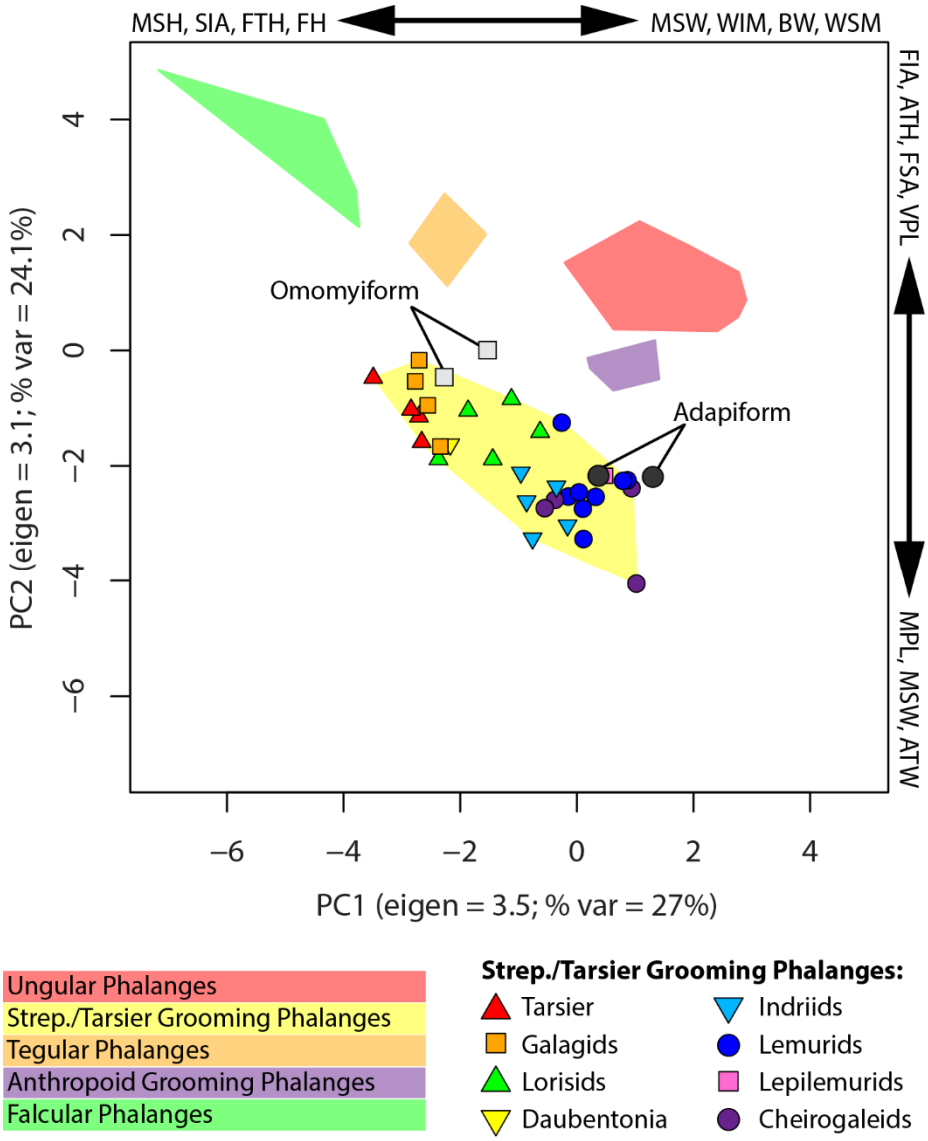

Fig. 3.23. Bayesian phylomorphospace of extant second pedal rays.
PCA from **Fig. 3.22** with reconstructed values of the ancestral states for major clades (stars for higher taxa, closed black circles for lower taxa) based on extant taxa. Variables with the highest loadings along each axis are listed along the top and right side of the graph. Falcular phalanges not shown (see **Fig.3.22** for falcular phalanges).

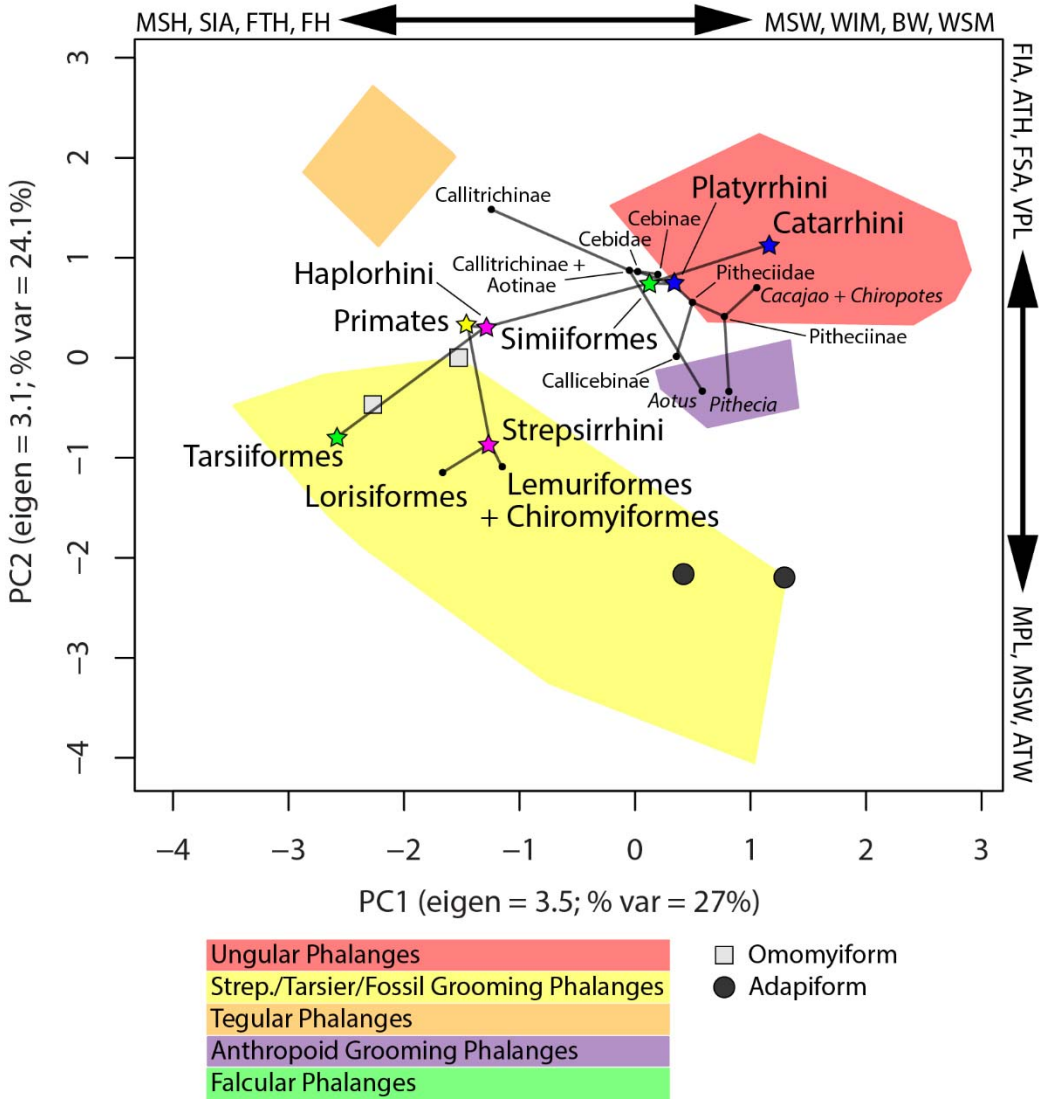

Fig. 3.24. Bayesian phylomorphospace of second pedal rays (Tree 1).
PCA from **Fig. 3.22** with reconstructed values of the ancestral states for major clades (stars for higher taxa, closed black circles for lower taxa) based on Tree 1 (adapiforms as stem strepsirrhines). Tree 2 provides nearly identical results and therefore, is not figured. Variables with the highest loadings along each axis are listed along the top and right side of the graph. Falcular phalanges not shown (see **Fig. 3.22** for falcular phalanges).

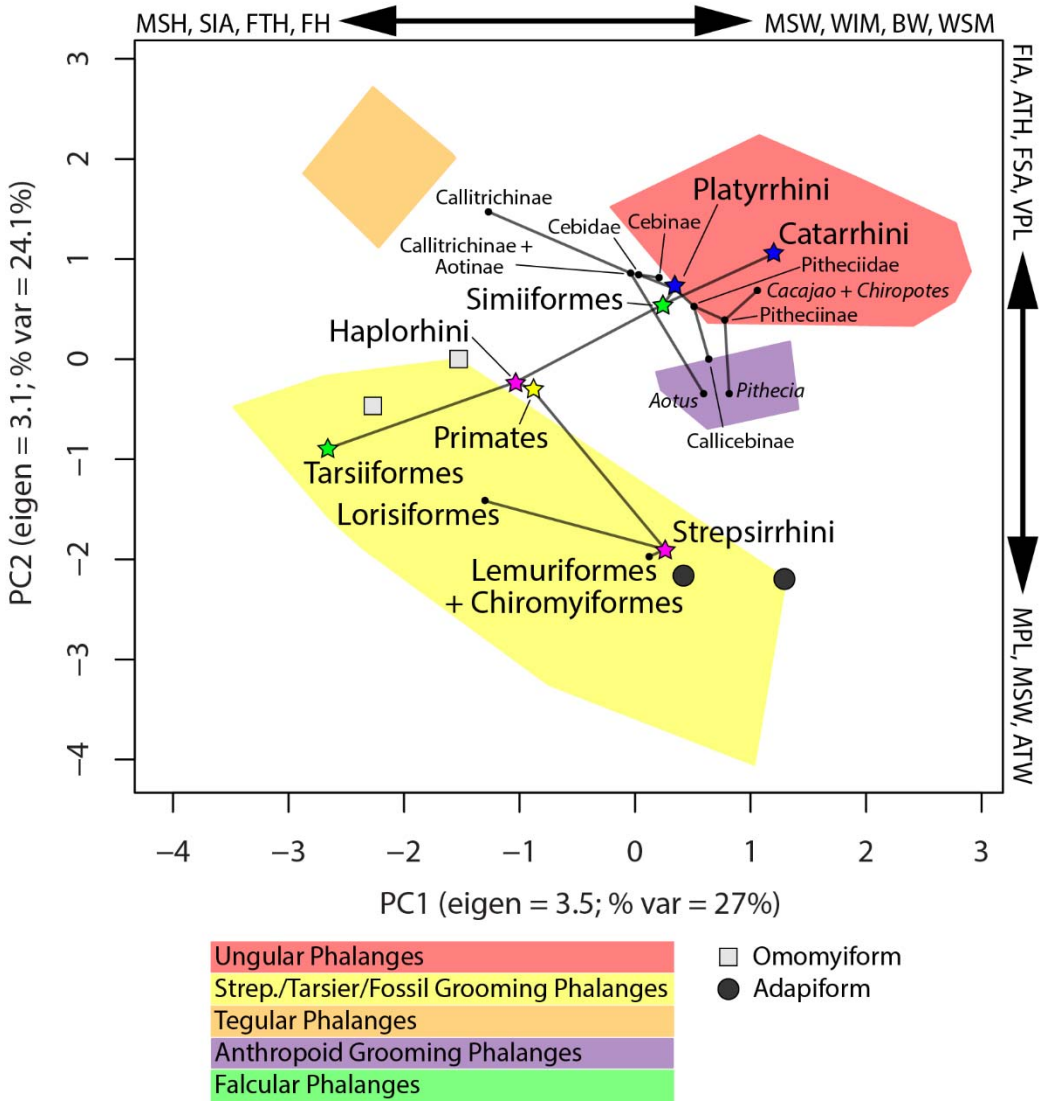

Fig. 3.25. Bayesian phylomorphospace of second pedal rays (Tree 3).
PCA from **Fig. 3.22** with reconstructed values of the ancestral states for major clades (stars for higher taxa, closed black circles for lower taxa) based on Tree 3 (adapiforms as stem anthropoids). Tree 4 provides nearly identical results and therefore, is not figured. Variables with the highest loadings along each axis are listed along the top and right side of the graph. Falcular phalanges not shown (see **Fig. 3.22** for falcular phalanges).

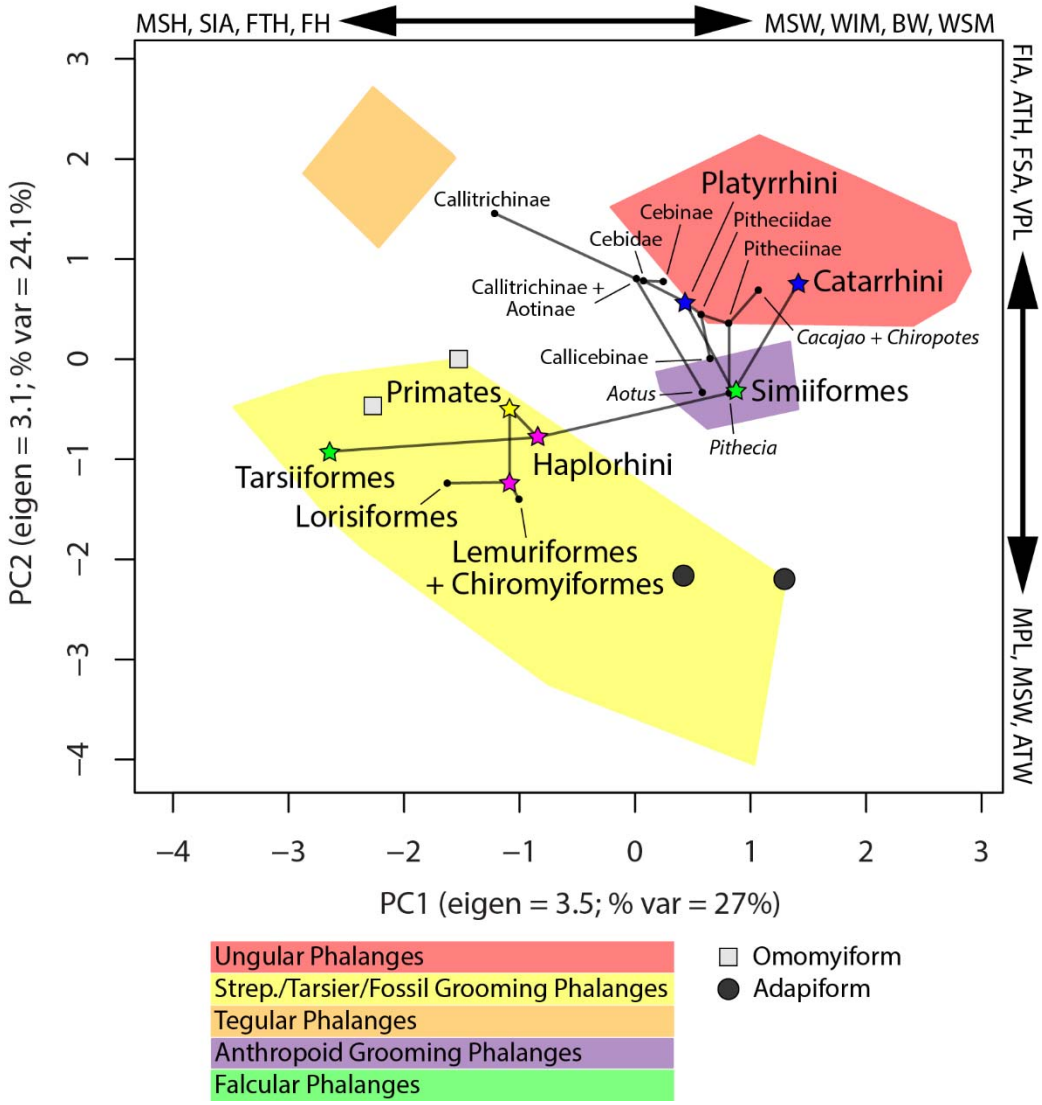

3.7 Tables

Table 3.1. Extant sample.
The elements sampled from each individual listed by institutional abbreviation and specimen number. See **Table 3.2** for institutional abbreviations. Rays: the rays from which distal phalanges were sampled; M, manual; P, pedal.

Specimen	Order/ Suborder	Infraorder/ Suborder	Parvorder/ Superfamily/ Family	Species	Rays
AMNH 52641	Haplorhini	Simiiformes	Cercopithecoidea	*Cercocebus agilis*	M2, M3/4, M3/4, M5, P2, P3/4, P3/4, P5
AMNH 81250	Haplorhini	Simiiformes	Cercopithecoidea	*Cercocebus agilis*	M3/4, P2, P3/4
AMNH 200754	Haplorhini	Simiiformes	Cercopithecoidea	*Cercocebus sp.*	M2, M3/4, M5
AMNH 200872	Haplorhini	Simiiformes	Cercopithecoidea	*Cercocebus torquatus*	M3/4, P2, P3/4
AMNH 200896	Haplorhini	Simiiformes	Cercopithecoidea	*Cercocebus torquatus*	M3/4, P2, P3/4
AMNH 52368	Haplorhini	Simiiformes	Cercopithecoidea	*Cercopithecus mitis*	M2, M3/4, M3/4, M5, P2, P3/4, P3/4, P5
AMNH 52401	Haplorhini	Simiiformes	Cercopithecoidea	*Cercopithecus mitis*	M3/4, P2, P3/4
AMNH 52410	Haplorhini	Simiiformes	Cercopithecoidea	*Cercopithecus mitis*	M3/4, P2, P3/4
SBU (5)	Haplorhini	Simiiformes	Cercopithecoidea	*Chlorocebus aethiops*	M3/4, P2, P3/4
AMNH 54231	Haplorhini	Simiiformes	Cercopithecoidea	*Chlorocebus pygerythrus*	M3/4, P2, P3/4
AMNH 52223	Haplorhini	Simiiformes	Cercopithecoidea	*Colobus guereza*	M2, M3/4, M5, P2, P3/4, P3/4, P5
AMNH 52240	Haplorhini	Simiiformes	Cercopithecoidea	*Colobus guereza*	P2, P3/4
AMNH 52241	Haplorhini	Simiiformes	Cercopithecoidea	*Colobus guereza*	M3/4, P3/4
CPRC 1090	Haplorhini	Simiiformes	Cercopithecoidea	*Erythrocebus patas*	M3/4, P2, P3/4
CPRC 1101	Haplorhini	Simiiformes	Cercopithecoidea	*Erythrocebus patas*	M3/4, P3/4
CPRC 1106	Haplorhini	Simiiformes	Cercopithecoidea	*Erythrocebus patas*	M2, M3/4, M5, P2, P3/4, P5
AMNH 52596	Haplorhini	Simiiformes	Cercopithecoidea	*Lophocebus johnstoni*	M2, M3/4, M3/4, M5, P2, P3/4, P3/4, P5
AMNH 52609	Haplorhini	Simiiformes	Cercopithecoidea	*Lophocebus johnstoni*	M3/4, M5
AMNH 52627	Haplorhini	Simiiformes	Cercopithecoidea	*Lophocebus johnstoni*	M3/4, P2, P2, P3/4
MCZ 35613	Haplorhini	Simiiformes	Cercopithecoidea	*Macaca fascicularis*	P3/4
MCZ 35673	Haplorhini	Simiiformes	Cercopithecoidea	*Macaca fascicularis*	M3/4, P3/4
MCZ 35677	Haplorhini	Simiiformes	Cercopithecoidea	*Macaca fascicularis*	M2, P3/4
MCZ 35681	Haplorhini	Simiiformes	Cercopithecoidea	*Macaca fascicularis*	M3/4, P3/4
MCZ 35693	Haplorhini	Simiiformes	Cercopithecoidea	*Macaca fascicularis*	M3/4, P2, P3/4
MCZ 35729	Haplorhini	Simiiformes	Cercopithecoidea	*Macaca fascicularis*	M2, P3/4
MCZ 35736	Haplorhini	Simiiformes	Cercopithecoidea	*Macaca fascicularis*	M3/4, P3/4
MCZ 37414	Haplorhini	Simiiformes	Cercopithecoidea	*Macaca fascicularis*	M2, P3/4
MCZ 37663	Haplorhini	Simiiformes	Cercopithecoidea	*Macaca fascicularis*	M3/4, P3/4
AMNH 103654	Haplorhini	Simiiformes	Cercopithecoidea	*Macaca fascicularis*	M2, M3/4, M3/4, M5, P2, P3/4, P3/4
AMNH 201014	Haplorhini	Simiiformes	Cercopithecoidea	*Macaca mulatta*	P2, P5
AMNH 201015	Haplorhini	Simiiformes	Cercopithecoidea	*Macaca mulatta*	P3/4
AMNH 201081	Haplorhini	Simiiformes	Cercopithecoidea	*Macaca mulatta*	M3/4
CPRC 323	Haplorhini	Simiiformes	Cercopithecoidea	*Macaca mulatta*	M3/4, P2, P3/4, P5
CPRC 383	Haplorhini	Simiiformes	Cercopithecoidea	*Macaca mulatta*	P2, P3/4
CPRC 398	Haplorhini	Simiiformes	Cercopithecoidea	*Macaca mulatta*	M2, M3/4, P2, P3/4
CPRC 439	Haplorhini	Simiiformes	Cercopithecoidea	*Macaca mulatta*	M3/4, P2, P3/4
CPRC 496	Haplorhini	Simiiformes	Cercopithecoidea	*Macaca mulatta*	M3/4, M5
AMNH 17964	Haplorhini	Simiiformes	Cercopithecoidea	*Macaca nemestrina*	M2, M3/4, M3/4, M5, P2, P3/4, P3/4, P5
MCZ 35361	Haplorhini	Simiiformes	Cercopithecoidea	*Macaca nemestrina*	M3/4, P3/4
MCZ 35602	Haplorhini	Simiiformes	Cercopithecoidea	*Macaca nemestrina*	M3/4, P3/4
MCZ 35649	Haplorhini	Simiiformes	Cercopithecoidea	*Macaca nemestrina*	M3/4, P3/4
MCZ 35670	Haplorhini	Simiiformes	Cercopithecoidea	*Macaca nemestrina*	M2, P3/4
MCZ 35687	Haplorhini	Simiiformes	Cercopithecoidea	*Macaca nemestrina*	M3/4, P3/4
AMNH 202286	Haplorhini	Simiiformes	Cercopithecoidea	*Macaca sylvanus*	M3/4, P2, P3/4, P5
AMNH 202416	Haplorhini	Simiiformes	Cercopithecoidea	*Mandrillus leucophaeus*	M3/4, P3/4
AMNH 235289	Haplorhini	Simiiformes	Cercopithecoidea	*Mandrillus sp.*	M2, M3/4, M3/4, M5, P3/4, P5
ANSP 21743	Haplorhini	Simiiformes	Cercopithecoidea	*Nasalis larvatus*	M2, M3/4, M3/4, M5, P2, P3/4, P3/4, P5

MCZ 37327	Haplorhini	Simiiformes	Cercopithecoidea	*Nasalis larvatus*	M2, M2, M3/4, M3/4, M3/4, M3/4, P2, P2, P3/4, P3/4, P3/4, P3/4
MCZ 37330	Haplorhini	Simiiformes	Cercopithecoidea	*Nasalis larvatus*	M2, M2, M3/4, M3/4, M3/4, M3/4, P2, P2, P3/4, P3/4, P3/4
MCZ 37337	Haplorhini	Simiiformes	Cercopithecoidea	*Nasalis larvatus*	M3/4, P3/4
MCZ 37341	Haplorhini	Simiiformes	Cercopithecoidea	*Nasalis larvatus*	M3/4, P3/4
MCZ 37343	Haplorhini	Simiiformes	Cercopithecoidea	*Nasalis larvatus*	M3/4, P3/4
MCZ 37344	Haplorhini	Simiiformes	Cercopithecoidea	*Nasalis larvatus*	M3/4, P3/4
MCZ 41557	Haplorhini	Simiiformes	Cercopithecoidea	*Nasalis larvatus*	M3/4, P3/4
MCZ 41559	Haplorhini	Simiiformes	Cercopithecoidea	*Nasalis larvatus*	M3/4, P3/4
MCZ 41561	Haplorhini	Simiiformes	Cercopithecoidea	*Nasalis larvatus*	M3/4, P3/4
MCZ 41562	Haplorhini	Simiiformes	Cercopithecoidea	*Nasalis larvatus*	M3/4, M3/4, P3/4
MCZ 41563	Haplorhini	Simiiformes	Cercopithecoidea	*Nasalis larvatus*	M3/4, P3/4
AMNH 200847	Haplorhini	Simiiformes	Cercopithecoidea	*Papio hamadryas*	P2, P3/4, P5
AMNH 200886	Haplorhini	Simiiformes	Cercopithecoidea	*Papio hamadryas*	M2, M3/4, P2, P3/4
AMNH 201055	Haplorhini	Simiiformes	Cercopithecoidea	*Papio hamadryas*	M2, M3/4, M3/4, P2, P3/4, P3/4
AMNH 52262	Haplorhini	Simiiformes	Cercopithecoidea	*Piliocolobus foai*	M2, M3/4
AMNH 52278	Haplorhini	Simiiformes	Cercopithecoidea	*Piliocolobus foai*	M2, M3/4, P2, P3/4, P5
AMNH 52303	Haplorhini	Simiiformes	Cercopithecoidea	*Piliocolobus foai*	M3/4, P2, P3/4
SBU OPr6	Haplorhini	Simiiformes	Cercopithecoidea	*Presbytis melalophos*	M3/4, M5, P2, P3/4, P3/4, P5
SBU OPr7	Haplorhini	Simiiformes	Cercopithecoidea	*Presbytis melalophos*	M2, M3/4, M3/4, M5, P2, P3/4
SBU OPr8	Haplorhini	Simiiformes	Cercopithecoidea	*Presbytis melalophos*	M3/4, P3/4
AMNH 87255	Haplorhini	Simiiformes	Cercopithecoidea	*Pygathrix nemaeus*	M2, M3/4, M3/4, M5, P2, P3/4
AMNH 87256	Haplorhini	Simiiformes	Cercopithecoidea	*Pygathrix nemaeus*	M3/4, P2, P3/4, P5
AMNH 90328	Haplorhini	Simiiformes	Cercopithecoidea	*Semnopithecus entellus*	M2, M3/4, P2, P3/4, P5
AMNH 19006	Haplorhini	Simiiformes	Cercopithecoidea	*Theropithecus gelada*	M2, M3/4
AMNH 200763	Haplorhini	Simiiformes	Cercopithecoidea	*Theropithecus gelada*	M3/4, P2
AMNH 201008	Haplorhini	Simiiformes	Cercopithecoidea	*Theropithecus gelada*	M2, M3/4, M3/4, P2, P3/4, P3/4
AMNH 238034	Haplorhini	Simiiformes	Cercopithecoidea	*Theropithecus gelada*	M3/4, P2, P3/4
SBU 5	Haplorhini	Simiiformes	Cercopithecoidea	*Theropithecus gelada*	M2, M3/4, M3/4, M5, P2, P3/4, P3/4, P5
MCZ 35618	Haplorhini	Simiiformes	Cercopithecoidea	*Trachypithecus cristatus*	M2, M3/4
MCZ 35666	Haplorhini	Simiiformes	Cercopithecoidea	*Trachypithecus cristatus*	M3/4, P3/4
MCZ 35672	Haplorhini	Simiiformes	Cercopithecoidea	*Trachypithecus cristatus*	M3/4, P3/4
MCZ 35678	Haplorhini	Simiiformes	Cercopithecoidea	*Trachypithecus cristatus*	M3/4, P3/4
MCZ 35688	Haplorhini	Simiiformes	Cercopithecoidea	*Trachypithecus cristatus*	M3/4, P3/4
MCZ 35696	Haplorhini	Simiiformes	Cercopithecoidea	*Trachypithecus cristatus*	M3/4, P3/4
MCZ 35709	Haplorhini	Simiiformes	Cercopithecoidea	*Trachypithecus cristatus*	M3/4, P3/4
MCZ 35718	Haplorhini	Simiiformes	Cercopithecoidea	*Trachypithecus cristatus*	P3/4
MCZ 37404	Haplorhini	Simiiformes	Cercopithecoidea	*Trachypithecus cristatus*	P3/4, P3/4
MCZ 37670	Haplorhini	Simiiformes	Cercopithecoidea	*Trachypithecus cristatus*	M3/4, P3/4
MCZ 37675	Haplorhini	Simiiformes	Cercopithecoidea	*Trachypithecus cristatus*	P2, P3/4
MCZ 37388	Haplorhini	Simiiformes	Cercopithecoidea	*Trachypithecus cristatus*	M3/4, P3/4
AMNH 112976	Haplorhini	Simiiformes	Cercopithecoidea	*Trachypithecus obscurus*	P2, P3/4
SBU OPr10	Haplorhini	Simiiformes	Cercopithecoidea	*Trachypithecus obscurus*	M3/4, P2, P3/4, P5
AMNH 115609	Haplorhini	Simiiformes	Hominoidea	*Gorilla beringei*	P2, P3/4
AMNH 54090	Haplorhini	Simiiformes	Hominoidea	*Gorilla beringei*	P2, P3/4
AMNH 54091	Haplorhini	Simiiformes	Hominoidea	*Gorilla beringei*	M2, M3/4, M3/4, M5, P2, P3/4, P5
AMNH 202932	Haplorhini	Simiiformes	Hominoidea	*Gorilla beringei*	M3/4, P2, P3/4
AMNH 167335	Haplorhini	Simiiformes	Hominoidea	*Gorilla gorilla*	M2, M3/4, M3/4, M5, P2, P3/4, P3/4, P5
AMNH 167368	Haplorhini	Simiiformes	Hominoidea	*Gorilla gorilla*	P2
AMNH 81651	Haplorhini	Simiiformes	Hominoidea	*Gorilla gorilla*	P2, P3/4
AMNH 81652	Haplorhini	Simiiformes	Hominoidea	*Gorilla gorilla*	M3/4
AMNH 214103	Haplorhini	Simiiformes	Hominoidea	*Gorilla gorilla*	P3/4
AMNH 69398	Haplorhini	Simiiformes	Hominoidea	*Gorilla gorilla*	M3/4
MCZ 20038	Haplorhini	Simiiformes	Hominoidea	*Gorilla gorilla*	P3/4, P3/4
MCZ 29048	Haplorhini	Simiiformes	Hominoidea	*Gorilla gorilla*	M3/4
MCZ 57482	Haplorhini	Simiiformes	Hominoidea	*Gorilla gorilla*	M3/4
SBU AS-1	Haplorhini	Simiiformes	Hominoidea	*Homo sapiens*	P2, P3/4, P3/4, P5

SBU AS-10	Haplorhini	Simiiformes	Hominoidea	*Homo sapiens*	P2, P3/4
SBU AS-14	Haplorhini	Simiiformes	Hominoidea	*Homo sapiens*	P2, P3/4
SBU AS-15	Haplorhini	Simiiformes	Hominoidea	*Homo sapiens*	P2, P3/4
SBU AS-33	Haplorhini	Simiiformes	Hominoidea	*Homo sapiens*	M3/4
SBU AS-34	Haplorhini	Simiiformes	Hominoidea	*Homo sapiens*	M3/4
SBU AS-44	Haplorhini	Simiiformes	Hominoidea	*Homo sapiens*	M2, M3/4, M3/4, M5
AMNH 11092	Haplorhini	Simiiformes	Hominoidea	*Hoolock hoolock*	M2, M3/4, P3/4
AMNH 112676	Haplorhini	Simiiformes	Hominoidea	*Hoolock hoolock*	M2, M3/4, M5, P2, P3/4
AMNH 200752	Haplorhini	Simiiformes	Hominoidea	*Hylobates lar*	P2, P3/4
AMNH 202384	Haplorhini	Simiiformes	Hominoidea	*Hylobates lar*	P2
MCZ 35950	Haplorhini	Simiiformes	Hominoidea	*Hylobates lar*	M3/4, P3/4
MCZ 35951	Haplorhini	Simiiformes	Hominoidea	*Hylobates lar*	M3/4
MCZ 41412	Haplorhini	Simiiformes	Hominoidea	*Hylobates lar*	M3/4, P3/4
MCZ 41415	Haplorhini	Simiiformes	Hominoidea	*Hylobates lar*	M2, M3/4
MCZ 41424	Haplorhini	Simiiformes	Hominoidea	*Hylobates lar*	M3/4
MCZ 41427	Haplorhini	Simiiformes	Hominoidea	*Hylobates lar*	M3/4, P3/4
MCZ 41431	Haplorhini	Simiiformes	Hominoidea	*Hylobates lar*	M3/4
MCZ 41433	Haplorhini	Simiiformes	Hominoidea	*Hylobates lar*	M2, M3/4
MCZ 41449	Haplorhini	Simiiformes	Hominoidea	*Hylobates lar*	M3/4, P3/4
MCZ 41454	Haplorhini	Simiiformes	Hominoidea	*Hylobates lar*	M3/4, P3/4
MCZ 41456	Haplorhini	Simiiformes	Hominoidea	*Hylobates lar*	M2, M3/4, P3/4
MCZ 41458	Haplorhini	Simiiformes	Hominoidea	*Hylobates lar*	M3/4, P3/4
SBU 87-1	Haplorhini	Simiiformes	Hominoidea	*Pan troglodytes*	M3/4, P2, P3/4
SBU APa9	Haplorhini	Simiiformes	Hominoidea	*Pan troglodytes*	M3/4, P2, P3/4, P3/4, P5
AMNH 167342	Haplorhini	Simiiformes	Hominoidea	*Pan troglodytes*	M3/4, P2, P3/4
AMNH 167343	Haplorhini	Simiiformes	Hominoidea	*Pan troglodytes*	M3/4, P2, P3/4
AMNH 90191	Haplorhini	Simiiformes	Hominoidea	*Pan troglodytes*	M3/4
AMNH 51202	Haplorhini	Simiiformes	Hominoidea	*Pan troglodytes*	M2, M3/4, M3/4, M5
AMNH 51367	Haplorhini	Simiiformes	Hominoidea	*Pan troglodytes*	M2, M3/4, M3/4, M5
AMNH 51381	Haplorhini	Simiiformes	Hominoidea	*Pan troglodytes*	M3/4
AMNH 89351	Haplorhini	Simiiformes	Hominoidea	*Pan troglodytes*	M3/4
AMNH 89353	Haplorhini	Simiiformes	Hominoidea	*Pan troglodytes*	M2, M3/4, M3/4, M5
MCZ 37362	Haplorhini	Simiiformes	Hominoidea	*Pongo pygmaeus*	P3/4
MCZ 37363	Haplorhini	Simiiformes	Hominoidea	*Pongo pygmaeus*	M3/4, P3/4
MCZ 37365	Haplorhini	Simiiformes	Hominoidea	*Pongo pygmaeus*	P3/4
AMNH 187994	Haplorhini	Simiiformes	Platyrrhini	*Alouatta seniculus*	M3/4, P2, P3/4
AMNH 188002	Haplorhini	Simiiformes	Platyrrhini	*Alouatta seniculus*	M3/4, P2, P3/4
AMNH 42316	Haplorhini	Simiiformes	Platyrrhini	*Alouatta seniculus*	M3/4, P2, P3/4
SBU NAl26	Haplorhini	Simiiformes	Platyrrhini	*Alouatta sp.*	M2, M3/4, M3/4, M5
AMNH 94992	Haplorhini	Simiiformes	Platyrrhini	*Aotus infulatos*	M3/4, P3/4
DPC nn	Haplorhini	Simiiformes	Platyrrhini	*Aotus sp.*	P2, P3/4, P3/4
SBU (11)	Haplorhini	Simiiformes	Platyrrhini	*Aotus sp.*	M3/4, P2, P3/4
SBU NAo2	Haplorhini	Simiiformes	Platyrrhini	*Aotus trivirgatus*	M2, M3/4, M3/4
SBU NAo3	Haplorhini	Simiiformes	Platyrrhini	*Aotus trivirgatus*	M2, M5, P2, P3/4, P3/4, P5
AMNH 201294	Haplorhini	Simiiformes	Platyrrhini	*Ateles belzebuth*	M3/4, P2, P3/4
AMNH 259	Haplorhini	Simiiformes	Platyrrhini	*Ateles belzebuth*	M3/4, P2, P3/4
AMNH 260	Haplorhini	Simiiformes	Platyrrhini	*Brachyteles arachnoides*	M3/4, P2, P3/4
AMNH 201122	Haplorhini	Simiiformes	Platyrrhini	*Cacajao calvus*	M3/4, P2, P3/4
SBU NCj1	Haplorhini	Simiiformes	Platyrrhini	*Cacajao calvus*	M2, M3/4, M3/4, M5, P2, P3/4, P5
AMNH 130361	Haplorhini	Simiiformes	Platyrrhini	*Callicebus cupreus*	M2, M3/4, M5, P2, P3/4, P3/4, P5
AMNH 94977	Haplorhini	Simiiformes	Platyrrhini	*Callicebus moloch*	M2, M3/4, M3/4, M3/4, M5, P2, P3/4, P3/4, P3/4, P5
AMNH 136217	Haplorhini	Simiiformes	Platyrrhini	*Callicebus moloch*	P2
USNM 239453	Haplorhini	Simiiformes	Platyrrhini	*Callicebus moloch*	P2, P3/4
USNM 269827	Haplorhini	Simiiformes	Platyrrhini	*Callicebus donacophilus*	M2, M3/4, M5, P2, P5
SBU nn	Haplorhini	Simiiformes	Platyrrhini	*Callimico goeldii*	M3/4, P2, P3/4
AMNH 17574	Haplorhini	Simiiformes	Platyrrhini	*Callithrix sp.*	M3/4, P3/4
AMNH 22994	Haplorhini	Simiiformes	Platyrrhini	*Callithrix sp.*	M3/4, P2, P3/4
SBU NCx1	Haplorhini	Simiiformes	Platyrrhini	*Callithrix sp.*	M3/4, P3/4
SBU NCx2	Haplorhini	Simiiformes	Platyrrhini	*Callithrix sp.*	M3/4
AMNH 244101	Haplorhini	Simiiformes	Platyrrhini	*Cebuella pygmaea*	P3/4, P3/4, P3/4
SBU NC1	Haplorhini	Simiiformes	Platyrrhini	*Cebuella pygmaea*	P3/4, P3/4, P3/4, P3/4
AMNH 188018	Haplorhini	Simiiformes	Platyrrhini	*Cebus albifrons*	M3/4, P3/4
AMNH 188019	Haplorhini	Simiiformes	Platyrrhini	*Cebus albifrons*	P2, P3/4, P5
AMNH 188020	Haplorhini	Simiiformes	Platyrrhini	*Cebus albifrons*	M3/4, P2, P3/4
SBU (7)	Haplorhini	Simiiformes	Platyrrhini	*Cebus sp.*	M3/4, P2, P3/4

SBU NCb15	Haplorhini	Simiiformes	Platyrrhini	*Cebus sp.*	M2, M3/4, M5, P2, P3/4, P3/4, P5
SBU NCh2	Haplorhini	Simiiformes	Platyrrhini	*Chiropotes chiropotes*	M3/4, P2, P3/4, P3/4, P5
AMNH 95760	Haplorhini	Simiiformes	Platyrrhini	*Chiropotes satanas*	M2, M3/4, P2, P3/4
AMNH 201310	Haplorhini	Simiiformes	Platyrrhini	*Lagothrix lagotricha*	M3/4, P2
AMNH 201391	Haplorhini	Simiiformes	Platyrrhini	*Lagothrix lagotricha*	M3/4
AMNH 35752	Haplorhini	Simiiformes	Platyrrhini	*Lagothrix lagotricha*	M3/4, P2, P3/4
AMNH 188155	Haplorhini	Simiiformes	Platyrrhini	*Lagothrix poeppigii*	M3/4, P2, P3/4, P3/4
SBU NLg2	Haplorhini	Simiiformes	Platyrrhini	*Lagothrix sp.*	M2, M3/4, M5, P3/4, P5
SBU NLe1	Haplorhini	Simiiformes	Platyrrhini	*Leontopithecus rosalia*	M3/4, P2
SBU NLe2	Haplorhini	Simiiformes	Platyrrhini	*Leontopithecus rosalia*	M3/4, P3/4, P3/4
AMNH 235275	Haplorhini	Simiiformes	Platyrrhini	*Leontopithecus sp.*	M3/4, P3/4
AMNH 187978	Haplorhini	Simiiformes	Platyrrhini	*Pithecia monachus*	M3/4, P2, P3/4
AMNH 202373	Haplorhini	Simiiformes	Platyrrhini	*Pithecia sp.*	M3/4, P2, P3/4
SBU NSg9	Haplorhini	Simiiformes	Platyrrhini	*Saguinus fuscicollis*	M3/4, P2, P3/4
SBU NSg1	Haplorhini	Simiiformes	Platyrrhini	*Saguinus sp.*	M3/4, P2, P3/4
SBU NSg2	Haplorhini	Simiiformes	Platyrrhini	*Saguinus sp.*	M3/4, P2, P3/4
AMNH 211647	Haplorhini	Simiiformes	Platyrrhini	*Saimiri boliviensis*	M3/4, P2, P3/4
AMNH 211649	Haplorhini	Simiiformes	Platyrrhini	*Saimiri boliviensis*	M3/4, P2, P3/4
AMNH 211653	Haplorhini	Simiiformes	Platyrrhini	*Saimiri boliviensis*	M3/4, P2, P3/4, P5
SBU (9)	Haplorhini	Simiiformes	Platyrrhini	*Saimiri sp.*	M3/4, P2, P3/4
SBU NSm7	Haplorhini	Simiiformes	Platyrrhini	*Saimiri sp.*	M2, M3/4, M3/4, M5, P2, P3/4, P3/4, P5
AMNH 188038	Haplorhini	Simiiformes	Platyrrhini	*Sapajus apella*	M3/4, P3/4
AMNH 188046	Haplorhini	Simiiformes	Platyrrhini	*Sapajus apella*	M3/4, P2, P3/4
AMNH 133813	Haplorhini	Simiiformes	Platyrrhini	*Sapajus libidinosus*	P2
AMNH 166856	Haplorhini	Tarsiiformes	Tarsiidae	*Carlito syrichta*	M2, M3/4, M3/4, M5, P2, P3, P4, P5
AMNH 203296	Haplorhini	Tarsiiformes	Tarsiidae	*Carlito syrichta*	M3/4, P2, P3, P4
AMNH 203297	Haplorhini	Tarsiiformes	Tarsiidae	*Carlito syrichta*	M3/4, P2, P3, P4, P5
AMNH 242091	Haplorhini	Tarsiiformes	Tarsiidae	*Carlito syrichta*	M3/4, P2, P3
AMNH 106649	Haplorhini	Tarsiiformes	Tarsiidae	*Cephalopachus bancanus*	M3/4, P2, P3, P4
AMNH 106010	Haplorhini	Tarsiiformes	Tarsiidae	*Cephalopachus bancanus*	M3/4, P2, P3, P4
AMNH 106754	Haplorhini	Tarsiiformes	Tarsiidae	*Cephalopachus bancanus*	M2, M3/4, M5, P2, P3, P4, P4, P5
AMNH 109216	Haplorhini	Tarsiiformes	Tarsiidae	*Tarsius pelengensis*	M3/4, P2, P3, P4
AMNH 109367	Haplorhini	Tarsiiformes	Tarsiidae	*Tarsius pelengensis*	M2, M3/4, M5, P2, P3, P4, P4, P5
AMNH 109368	Haplorhini	Tarsiiformes	Tarsiidae	*Tarsius pelengensis*	M3/4, P2, P3, P4
AMNH 109369	Haplorhini	Tarsiiformes	Tarsiidae	*Tarsius pelengensis*	M3/4, P2, P3, P4
AMNH 196477	Haplorhini	Tarsiiformes	Tarsiidae	*Tarsius pumilus*	M2, M3/4, M3/4, M5, P2, P3, P4, P5
USNM 199694	Strepsirrhini	Chiromyiformes	Daubentoniidae	*Daubentonia madagascariensis*	M2, M3/4, M5, P2, P3/4, P3/4, P5
AMNH 100654	Strepsirrhini	Lemuriformes	Cheirogaleidae	*Cheirogaleus medius*	M3/4, P2, P3/4, P3/4, P5
DPC 1285	Strepsirrhini	Lemuriformes	Cheirogaleidae	*Cheirogaleus medius*	P2, P3/4
DPC 130	Strepsirrhini	Lemuriformes	Cheirogaleidae	*Cheirogaleus medius*	P2, P3/4
AMNH 174424	Strepsirrhini	Lemuriformes	Cheirogaleidae	*Microcebus murinus*	M3/4, P3/4
AMNH 185627	Strepsirrhini	Lemuriformes	Cheirogaleidae	*Microcebus murinus*	M3/4, P2, P3/4
AMNH 185628	Strepsirrhini	Lemuriformes	Cheirogaleidae	*Microcebus murinus*	M3/4, P2, P3/4
DPC 035	Strepsirrhini	Lemuriformes	Cheirogaleidae	*Microcebus murinus*	P2, P3/4
DPC 7017	Strepsirrhini	Lemuriformes	Cheirogaleidae	*Microcebus murinus*	P2, P3/4, P5
DPC 097	Strepsirrhini	Lemuriformes	Cheirogaleidae	*Mirza coquereli*	P2, P3/4
DPC 137	Strepsirrhini	Lemuriformes	Cheirogaleidae	*Mirza coquereli*	M2, M3/4, M3/4, M5, P2, P5
DPC 2301	Strepsirrhini	Lemuriformes	Cheirogaleidae	*Mirza coquereli*	P2, P3/4, P3/4
AMNH 100645	Strepsirrhini	Lemuriformes	Cheirogaleidae	*Phaner furcifer*	M2, M3/4, M5, P2, P3/4, P3/4, P5
AMNH 100831	Strepsirrhini	Lemuriformes	Cheirogaleidae	*Phaner furcifer*	M3/4
USNM 18437	Strepsirrhini	Lemuriformes	Indriidae	*Avahi laniger*	P3/4, P2, P3/4, P5
USNM 83651	Strepsirrhini	Lemuriformes	Indriidae	*Avahi laniger*	M3/4
USNM 83652	Strepsirrhini	Lemuriformes	Indriidae	*Avahi laniger*	M3/4
AMNH 170494	Strepsirrhini	Lemuriformes	Indriidae	*Avahi laniger*	M2, M3/4, P2, P3/4, P3/4, P5
CMNH 1474	Strepsirrhini	Lemuriformes	Indriidae	*Indri indri*	P2
CMNH B343	Strepsirrhini	Lemuriformes	Indriidae	*Indri indri*	M2, M3/4, M3/4, M5, P2, P3/4, P3/4, P5
DPC 6273	Strepsirrhini	Lemuriformes	Indriidae	*Propithecus coquereli*	P2, P3/4, P5

CMNH B1155	Strepsirrhini	Lemuriformes	Indriidae	*Propithecus diadema*	M3/4, M3/4, M5, P2, P3/4, P5
AMNH 170463	Strepsirrhini	Lemuriformes	Indriidae	*Propithecus verreauxi*	M3/4, P2, P3/4
AMNH 170489	Strepsirrhini	Lemuriformes	Indriidae	*Propithecus verreauxi*	M2, M3/4, M5, P3/4, P5, P5
AMNH 170491	Strepsirrhini	Lemuriformes	Indriidae	*Propithecus verreauxi*	M3/4, P2, P3/4
AMNH 31255	Strepsirrhini	Lemuriformes	Indriidae	*Propithecus verreauxi*	P2, P3/4
DPC 1397	Strepsirrhini	Lemuriformes	Indriidae	*Propithecus verreauxi*	P2, P3/4
AMNH 170708	Strepsirrhini	Lemuriformes	Lemuridae	*Eulemur albifrons*	M3/4, P2, P3/4
AMNH 170711	Strepsirrhini	Lemuriformes	Lemuridae	*Eulemur albifrons*	M5, P2
AMNH 170717	Strepsirrhini	Lemuriformes	Lemuridae	*Eulemur albifrons*	M3/4, P3/4
SBU (13)	Strepsirrhini	Lemuriformes	Lemuridae	*Eulemur fulvus*	M3/4, P2, P3/4
DPC 6793	Strepsirrhini	Lemuriformes	Lemuridae	*Eulemur macaco*	P2, P3/4, P3/4, P5
DPC 6287	Strepsirrhini	Lemuriformes	Lemuridae	*Eulemur rufus*	P2, P3/4, P5
AMNH 170675	Strepsirrhini	Lemuriformes	Lemuridae	*Hapalemur griseus*	M2, M3/4, P3/4
AMNH 170680	Strepsirrhini	Lemuriformes	Lemuridae	*Hapalemur griseus*	M3/4, P2, P3/4
AMNH 170687	Strepsirrhini	Lemuriformes	Lemuridae	*Hapalemur griseus*	P2
AMNH 170689	Strepsirrhini	Lemuriformes	Lemuridae	*Hapalemur griseus*	P2, P3/4, P5
DPC 1359	Strepsirrhini	Lemuriformes	Lemuridae	*Hapalemur griseus*	P2, P3/4, P5
SBU (12)	Strepsirrhini	Lemuriformes	Lemuridae	*Hapalemur griseus*	P2, P3/4
AMNH 200881	Strepsirrhini	Lemuriformes	Lemuridae	*Lemur catta*	M2, M3/4, M3/4, M5, P2, P3/4, P3/4, P5
SBU (14)	Strepsirrhini	Lemuriformes	Lemuridae	*Lemur catta*	M3/4, P2, P3/4
CMNH 1382	Strepsirrhini	Lemuriformes	Lemuridae	*Varecia sp.*	M3/4, M3/4, P2
CMNH 1383	Strepsirrhini	Lemuriformes	Lemuridae	*Varecia sp.*	M2, M5, P2
AMNH 17338	Strepsirrhini	Lemuriformes	Lemuridae	*Varecia variegata*	M3/4, P3/4
AMNH 18040	Strepsirrhini	Lemuriformes	Lemuridae	*Varecia variegata*	M3/4
AMNH 201384	Strepsirrhini	Lemuriformes	Lemuridae	*Varecia variegata*	P2
AMNH 22897	Strepsirrhini	Lemuriformes	Lemuridae	*Varecia variegata*	M3/4, M3/4
AMNH 83955	Strepsirrhini	Lemuriformes	Lemuridae	*Varecia variegata*	P2
AMNH 170557	Strepsirrhini	Lemuriformes	Lepilemuridae	*Lepilemur leucopus*	M3/4, P3/4
AMNH 170560	Strepsirrhini	Lemuriformes	Lepilemuridae	*Lepilemur leucopus*	M3/4
AMNH 170562	Strepsirrhini	Lemuriformes	Lepilemuridae	*Lepilemur leucopus*	P2, P3/4
AMNH 170565	Strepsirrhini	Lemuriformes	Lepilemuridae	*Lepilemur leucopus*	P3/4
USNM 598551	Strepsirrhini	Lorisiformes	Galagidae	*Euoticus elegantulus*	M3/4, M5, P2, P3/4, P3/4
AMNH 86502	Strepsirrhini	Lorisiformes	Galagidae	*Galago moholi*	M3/4, P2
AMNH 87065	Strepsirrhini	Lorisiformes	Galagidae	*Galago moholi*	M3/4, P2, P3/4
DPC 3190	Strepsirrhini	Lorisiformes	Galagidae	*Galago moholi*	M2, M3/4, M3/4, M5
DPC 003	Strepsirrhini	Lorisiformes	Galagidae	*Galago senegalensis*	P2, P3/4
DPC 1063	Strepsirrhini	Lorisiformes	Galagidae	*Galago senegalensis*	P2, P3/4
SBU (15)	Strepsirrhini	Lorisiformes	Galagidae	*Galago senegalensis*	M3/4, M3/4, M5, P2, P3/4, P3/4, P5
SBU PGa4	Strepsirrhini	Lorisiformes	Galagidae	*Galago senegalensis*	M3/4, P2, P3/4
AMNH 215180	Strepsirrhini	Lorisiformes	Galagidae	*Galagoides demidovii*	M3/4, P2, P3/4
AMNH 80801	Strepsirrhini	Lorisiformes	Galagidae	*Otolemur crassicaudatus*	M3/4
DPC 024	Strepsirrhini	Lorisiformes	Galagidae	*Otolemur crassicaudatus*	P2
SBU PGa1163	Strepsirrhini	Lorisiformes	Galagidae	*Otolemur crassicaudatus*	M3/4, P2, P3/4
AMNH 212576	Strepsirrhini	Lorisiformes	Lorisidae	*Arctocebus calabarensis*	M3/4, P2, P3/4
AMNH 212954	Strepsirrhini	Lorisiformes	Lorisidae	*Arctocebus calabarensis*	P3/4
AMNH 34256	Strepsirrhini	Lorisiformes	Lorisidae	*Loris tardigradus*	P2
AMNH 34257	Strepsirrhini	Lorisiformes	Lorisidae	*Loris tardigradus*	M3/4, P2, P3/4
DPC 2925	Strepsirrhini	Lorisiformes	Lorisidae	*Loris tardigradus*	M5, P2, P3/4, P5
AMNH 90381	Strepsirrhini	Lorisiformes	Lorisidae	*Nycticebus coucang*	M3/4, P3/4
AMNH 16615	Strepsirrhini	Lorisiformes	Lorisidae	*Nycticebus coucang*	P2
AMNH 102027	Strepsirrhini	Lorisiformes	Lorisidae	*Nycticebus coucang*	M3/4
AMNH 16591	Strepsirrhini	Lorisiformes	Lorisidae	*Nycticebus coucang*	M3/4, P2, P3/4
DPC 1906	Strepsirrhini	Lorisiformes	Lorisidae	*Nycticebus coucang*	M3/4, M5, P2, P5
AMNH 52682	Strepsirrhini	Lorisiformes	Lorisidae	*Perodicticus potto*	M3/4, P3/4
AMNH 52685	Strepsirrhini	Lorisiformes	Lorisidae	*Perodicticus potto*	M3/4, P2, P5
AMNH 52698	Strepsirrhini	Lorisiformes	Lorisidae	*Perodicticus potto*	M3/4, P2, P3/4
USNM 144662	Dermoptera		Cynocephalidae	*Cynocephalus volans*	M3/4
YPM 963	Dermoptera		Cynocephalidae	*Cynocephalus volans*	P5
USNM 15502	Dermoptera		Cynocephalidae	*Galeopterus variegatus*	M3/4, P2, P3/4
AMNH 192143	Diprotodontia	Macropodiformes	Macropodidae	*Dendrolagus dorianus*	M2, M3/4
AMNH 35642	Diprotodontia	Macropodiformes	Macropodidae	*Dendrolagus lumholtzi*	P2
AMNH 35731	Diprotodontia	Macropodiformes	Macropodidae	*Dendrolagus lumholtzi*	M3/4, P2, P4, P5
AMNH 65256	Diprotodontia	Macropodiformes	Macropodidae	*Dendrolagus lumholtzi*	M3/4, P2, P4
AMNH 35231	Diprotodontia	Macropodiformes	Macropodidae	*Macropus rufus*	P2, P2, P5, P5

AMNH 70284	Diprotodontia	Macropodiformes	Macropodidae	*Macropus rufus*	P2
AMNH 70355	Diprotodontia	Macropodiformes	Macropodidae	*Macropus rufus*	M3/4, M3/4, M3/4, P2, P4, P4
AMNH 257	Diprotodontia	Macropodiformes	Macropodidae	*Petrogale penicillata*	M3/4, P2, P2
AMNH 35023	Diprotodontia	Macropodiformes	Macropodidae	*Petrogale penicillata*	P4
AMNH 35636	Diprotodontia	Macropodiformes	Macropodidae	*Petrogale penicillata*	P4
AMNH 3837	Diprotodontia	Macropodiformes	Macropodidae	*Petrogale penicillata*	M3/4
AMNH 35722	Diprotodontia	Macropodiformes	Macropodidae	*Setonix brachyurus*	P4
AMNH 35744	Diprotodontia	Macropodiformes	Macropodidae	*Setonix brachyurus*	M3/4, P2
AMNH 160105	Diprotodontia	Phalangeriformes	Petauroidea	*Dactylopsila trivirgata*	M3/4, P2, P4
AMNH 42993	Diprotodontia	Phalangeriformes	Petauroidea	*Petaurus breviceps*	M3/4, P4
AMNH 237507	Diprotodontia	Phalangeriformes	Petauroidea	*Petaurus sp.*	M3/4, P3, P4
AMNH 109803	Diprotodontia	Phalangeriformes	Phalangeroidea	*Cercartetus caudatus*	M2, M3/4, M3/4, M5, P2, P3, P4
AMNH 104089	Diprotodontia	Phalangeriformes	Phalangeroidea	*Phalanger gymnotis*	P3/4, P3/4
AMNH 79864	Diprotodontia	Phalangeriformes	Phalangeroidea	*Phalanger orientalis*	M3/4, M3/4, P2, P2, P4, P4
AMNH 35698	Diprotodontia	Phalangeriformes	Phalangeroidea	*Trichosurus vulpecula*	P4
AMNH 35708	Diprotodontia	Phalangeriformes	Phalangeroidea	*Trichosurus vulpecula*	M3/4, P4
AMNH 37708	Diprotodontia	Phalangeriformes	Phalangeroidea	*Trichosurus vulpecula*	P2, P2
AMNH 42996	Diprotodontia	Phalangeriformes	Phalangeroidea	*Trichosurus vulpecula*	M3/4, P4, P4
AMNH 65611	Diprotodontia	Vombatiformes	Phascolarctidae	*Phascolarctos cinerus*	M2, M3/4, P2, P3, P4
AMNH 35512	Diprotodontia	Vombatiformes	Vombatidae	*Vombatus ursinus*	M3/4, P2, P4
AMNH 35701	Diprotodontia	Vombatiformes	Vombatidae	*Vombatus ursinus*	M3/4, P2, P4
AMNH 201230	Erinaceomorpha		Erinaceidae	*Erinaceus europaeus*	P2, P3
AMNH 3770	Erinaceomorpha		Erinaceidae	*Erinaceus europaeus*	M3/4, P2, P4
AMNH 69553	Erinaceomorpha		Erinaceidae	*Erinaceus roumanicus*	M3/4, P2, P3, P4
AMNH 185374	Erinaceomorpha		Erinaceidae	*Hemiechinus auritus*	M3/4, P2, P3, P4
AMNH 35465	Rodentia	Castorimorpha	Castoridae	*Castor canadensis*	P3/4
AMNH 35470	Rodentia	Castorimorpha	Castoridae	*Castor canadensis*	M3/4
AMNH 35474	Rodentia	Castorimorpha	Castoridae	*Castor canadensis*	P2
AMNH 7556	Rodentia	Castorimorpha	Castoridae	*Castor canadensis*	M3/4, P2, P3/4
AMNH 102119	Rodentia	Myomorpha	Muridae	*Chiropodomys gliroides*	P2
USNM 481106	Scandentia		Ptilocercidae	*Ptilocercus lowii*	M3/4, P3/4
USNM 488055	Scandentia		Ptilocercidae	*Ptilocercus lowii*	M3/4, P3/4
USNM 488058	Scandentia		Ptilocercidae	*Ptilocercus lowii*	M3/4, P3/4
USNM 488067	Scandentia		Ptilocercidae	*Ptilocercus lowii*	M3/4, P3/4
USNM 488069	Scandentia		Ptilocercidae	*Ptilocercus lowii*	M3/4, P2, P3/4
USNM 488072	Scandentia		Ptilocercidae	*Ptilocercus lowii*	M3/4, P3/4
AMNH 215175	Scandentia		Tupaiidae	*Tupaia glis*	M3/4, P3/4
AMNH 215176	Scandentia		Tupaiidae	*Tupaia glis*	M3/4, P2
AMNH 215177	Scandentia		Tupaiidae	*Tupaia glis*	M3/4, P3/4
AMNH 35921	Scandentia		Tupaiidae	*Tupaia tana*	M3/4, M3/4, P2, P3/4, P3/4, P3/4, P5

Table 3.2. Institutional abbreviations.
Abbreviations for institutions from which specimens were sampled.

Abbreviation	Institution
AMNH	American Museum of Natural History, New York, NY, USA
ANSP	Academy of Natural Sciences of Philadelphia, Philadelphia, PA, USA
CMNH	Cleveland Museum of Natural History, Cleveland, OH, USA
CPRC	Caribbean Primate Research Center, San Juan, Puerto Rico
DPC	Duke Lemur Center, Durham, NC, USA
MCZ	Museum of Comparative Zoology - Harvard University, Cambridge, MA, USA
SBU	Stony Brook University, Stony Brook, NY, USA
UCMP	University of California Museum of Paleontology, Berkeley, CA, USA
UM	University of Michigan Museum of Paleontology, Ann Arbor, MI, USA
USNM	National Museum of Natural History, Smithsonian Institution, Washington, DC, USA

Table 3.3. Group sample sizes.
The number of specimens, individuals, species, and ray-specific species means sampled for each group.

Group	Specimens	Individuals	Species	Means (n)
Strepsirrhine/tarsier Grooming Phalanges	82	70	32	36
Anthropoid Second Pedal Distal Phalanges	105	102	53	53
Ungular Phalanges	665	256	85	308
Tegular Phalanges	34	14	8	18
Non-primate Grooming Phalanges	31	22	15	17
Falcular Phalanges	92	43	24	50

Table 3.4. Fossil specimens analyzed that resemble grooming phalanges.

Specimen	Taxon	Species	Region/Area/Locality	Relative Age
AMNH FM 129382 (a)	Adapiform	*Notharctus tenebrosus*	Bridger Basin, WY (Butch Hill)	Bridgerian (Br-2)
AMNH FM 143612_3	Adapiform	*Notharctus tenebrosus*	Bridger Basin, WY (ALX-00-02)	Bridgerian (Br-2)
UCMP 217911	Adapiform	?*Cantius*/ *Notharctus venticolis*	Washakie Basin, WY (v70243)	Wasatchian (Wa-3)
UCMP 217999	Omomyiform	?*Tetonius*	Washakie Basin, WY (v70214)	Wasatchian (Wa-3)
UCMP 218000	Omomyiform	?*Arapahovius*	Washakie Basin, WY (v74022)	Wasatchian (Wa-5)

Table 3.5. *Fossil specimens analyzed resembling ungular phalanges*.

Specimen	Taxon	Species	Region/Locality	Relative Age
UM 112882	Adapiform	*Cantius nunienus*	Bridger Basin, WY (SP-98)	Bridgerian (Br-1a)
AMNH FM 11474	Adapiform	*Notharctus tenebrosus*	Bridger Basin, WY (Little Dry Creek)	Bridgerian (Br-2)
AMNH FM 131764 (a)	Adapiform	*Notharctus tenebrosus*	Bridger Basin, WY (Forbidden City)	Bridgerian (Br-2)
AMNH FM 131764 (b)	Adapiform	*Notharctus tenebrosus*	Bridger Basin, WY (Forbidden City)	Bridgerian (Br-2)
AMNH FM 143612_2	Adapiform	*Notharctus tenebrosus*	Bridger Basin, WY (ALX-00-02)	Bridgerian (Br-2)
AMNH FM 143612_4	Adapiform	*Notharctus tenebrosus*	Bridger Basin, WY (ALX-00-02)	Bridgerian (Br-2)
AMNH FM 131763	Adapiform	*Smilodectes gracilis*	Bridger Basin, WY (Hermes Hill)	Bridgerian (Br-2)
AMNH FM 131766	Adapiform	Indet	Bridger Basin, WY (Leahanne's Lintel)	Bridgerian (Br-2)
UCMP 236082	Adapiform	Indet	Mutigny, France (v6167)	Ypresian
UCMP 147533	Adapiform	Indet	Washakie Basin, WY (v70243)	Wasatchian (Wa-3)
UCMP 147534	Adapiform	Indet	Washakie Basin, WY (v70243)	Wasatchian (Wa-3)
UCMP 217913	Adapiform	Indet	Washakie Basin, WY (v70243)	Wasatchian (Wa-3)
UCMP 217971	Adapiform	Indet	Washakie Basin, WY (v74022)	Wasatchian (Wa-5)
UCMP 218139	Adapiform	Indet	Washakie Basin, WY (v74022)	Wasatchian (Wa-5)
UCMP 218367	Adapiform	Indet	Washakie Basin, WY (v71231)	Wasatchian
UCMP 218402	Adapiform	Indet	Washakie Basin, WY (v70215)	Wasatchian (~Wa-3)
UM 32258	Omomyiform	*Omomys carteri*	Bridger Basin, WY (BRW-139)	Bridgerian (Br-3)
USNM 540587	Omomyiform	*Teilhardina brandti*	Bighorn Basin, WY	Wasatchian (Wa-0)
UM 31624	Omomyiform	Indet	Bridger Basin, WY (BRW-14)	Bridgerian (Br-2)
UM 32129	Omomyiform	Indet	Bridger Basin, WY (BRW-14)	Bridgerian (Br-2)
UM 32146 (a)	Omomyiform	Indet	Bridger Basin, WY (BRW-14)	Bridgerian (Br-2)
UM 32146 (b)	Omomyiform	Indet	Bridger Basin, WY (BRW-14)	Bridgerian (Br-2)
UM 32274	Omomyiform	Indet	Bridger Basin, WY (BRW-35)	Bridgerian (Br-2)
UM 32186	Omomyiform	Indet	Bridger Basin, WY (BRW-12)	Bridgerian (Br-3)
UM 32249 (a)	Omomyiform	Indet	Bridger Basin, WY (BRW-10)	Bridgerian (Br-3)
UM 32249 (b)	Omomyiform	Indet	Bridger Basin, WY (BRW-10)	Bridgerian (Br-3)
UM 32249 (c)	Omomyiform	Indet	Bridger Basin, WY (BRW-10)	Bridgerian (Br-3)
UM 32249 (d)	Omomyiform	Indet	Bridger Basin, WY (BRW-10)	Bridgerian (Br-3)
UM 32249 (e)	Omomyiform	Indet	Bridger Basin, WY (BRW-10)	Bridgerian (Br-3)
AMNH FM 126631	Omomyiform	Indet	Bridger Basin, WY (LSV-A)	Bridgerian (Br-3)
AMNH FM 126632	Omomyiform	Indet	Bridger Basin, WY (LSV-A)	Bridgerian (Br-3)
AMNH FM 126637	Omomyiform	Indet	Bridger Basin, WY (LSV-A)	Bridgerian (Br-3)
AMNH FM 126659	Omomyiform	Indet	Bridger Basin, WY (Sage Creek)	Bridgerian (Br-2)
AMNH FM 126663	Omomyiform	Indet	Bridger Basin, WY (Sage Creek)	Bridgerian (Br-2)
AMNH FM 126664	Omomyiform	Indet	Bridger Basin, WY (Sage Creek)	Bridgerian (Br-2)

AMNH FM 126665	Omomyiform	Indet	Bridger Basin, WY (Sage Creek)	Bridgerian (Br-2)
AMNH FM 126674	Omomyiform	Indet	Bridger Basin, WY (Sage Creek)	Bridgerian (Br-2)
AMNH FM 126735	Omomyiform	Indet	Bridger Basin, WY (Mac's Hole)	Bridgerian (~Br-2/3)
UCMP 134993	Omomyiform	Indet	Washakie Basin, WY (v70220)	Wasatchian
UCMP 218416	Omomyiform	Indet	Washakie Basin, WY (v70220)	Wasatchian
UCMP 218183	Omomyiform	Indet	Washakie Basin, WY (v74022)	Wasatchian (Wa-5)
UCMP 218244	Omomyiform	Indet	Washakie Basin, WY (v74022)	Wasatchian (Wa-5)
UCMP 218261	Omomyiform	Indet	Washakie Basin, WY (v74022)	Wasatchian (Wa-5)
UCMP 218295	Omomyiform	Indet	Washakie Basin, WY (v74022)	Wasatchian (Wa-5)
UCMP 218301	Omomyiform	Indet	Washakie Basin, WY (v74022)	Wasatchian (Wa-5)
UCMP 218368	Omomyiform	Indet	Washakie Basin, WY (v71231)	Wasatchian
UCMP 218432	Omomyiform	Indet	Washakie Basin, WY (v70229)	Wasatchian
UCMP 218436	Omomyiform	Indet	Washakie Basin, WY (v70246)	Wasatchian (Wa-3)

Table 3.6. Dentally known adapiforms from Washakie Basin localities.
Lists of the known adapiform taxa and the number of dental specimens attributed to them for each locality (listed along the top). Information was taken from the UCMP online database.

v6167		**v70215**		**v70243**		**v71231**		**v74022**	
*Cantius sp.**	30	*Cantius sp.**	3	*Cantius sp.**	31	*Cantius sp.**	1	*Cantius sp.**	3
Cantius savagei	11			*Copelemur sp.*	18	*Copelemur sp.*	1	*Copelemur australotutus*	4
				Copelemur praetutus	2			*Copelemur feretutus*	2
								Copelemur sp.	2
								Notharctus sp.	1

*These specimens may also be attributed to *Notharctus venticolis* (pers. comm., Doug Boyer)

Table 3.7. Dentally known omomyiforms from Washakie Basin localities.
Lists of the known omomyiform taxa and the number of dental specimens attributed to them for each locality (listed along the top). Information was taken from the UCMP online database.

v70214		**v70220**		**v70229**		**v70246**		**v74022**	
Tetonius sp.	134	*Anemorhysis pearcei*	9	*Anemorhysis sp.*	5	*Arapahovius gazini*	45	*Arapahovius sp.*	93
Anemorhysis sp.	1	*Anemorhysis sp.*	1	*Tetonius sp.*	1	*Arapahovius sp.*	10	*Anemorhysis savagei*	70
Anemorhysis pearcei	1	*Tetonius sp.*	1	*Loveina zephyri*	1	*Anemorhysis sp.*	2	*Arapahovius gazini*	39
								Anemorhysis sp.	5
								Steinius sp.	4
								Tetonius sp.	4

Table 3.8. Measurements used in this study.
See **Fig. 3.5** for illustrations of anatomical terminology and **Figs. 3.6, 3.7** for illustrations of measurements.

Measurement (Abbreviation)	**Definition**	**Significance**
Facet height (FH)	Distance between most proximal point on superior margin of articular facet and that of the inferior margin; Taken in lateral view	Height of articular facet
Extensor tubercle height (ETH)	Distance between most proximal point on superior margin of articular facet and most dorsal point of extensor tubercle; ∥ to FH and taken in lateral view	Related to leverage of long digital extensor tendon; higher values reflect increased lever arm
Flexor tubercle height (FTH)	Distance between most proximal point on inferior margin of articular facet and most volar point of flexor tubercle; ∥ to FH and taken in lateral view	Related to leverage of long digital flexor tendon; higher values reflect increased lever arm
Maximum phalangeal length (MPL)	Distance between most proximal point on inferior margin of articular facet and most distal point on distal tip of phalanx; Taken in lateral view	Total length of the phalanx
Volar process length (VPL)	Distance between most proximal point on inferior margin of articular facet and most distal point of volar process; ⊥ to FH and taken in lateral view	Estimate of the portion of the bone that lies embedded within the apical pad
Mid-shaft height (MSH)	For specimens that have apical tufts: Height of shaft at midpoint between base and tuft For specimens that do not have apical tufts: Height of shaft taken at ¼ of its length (shaft length is considered to be the length of MPL distal to the base of the phalanx); in both cases ⊥ to MPL and taken in lateral view	Higher values are suggested to reflect a shaft that is more resistant to dorso-ventral bending
Apical tuft height (ATH)	For specimens that have apical tufts: Height of shaft at midpoint of apical tuft For specimens that do not have apical tufts: Height of shaft taken at ¾ of its length (shaft length is considered to be the length of MPL distal to the base of the phalanx); in both cases ⊥ to volar margin of tuft/shaft in region where measurement is taken and taken in lateral view	Height of the apical tuft
Base width (BW)	Maximum, medio-lateral width of base; ⊥ to long axis of shaft and taken in dorsal view	May be related to width of unguis
Mid-shaft width (MSW)	For specimens that have apical tufts: Width of shaft at midpoint between base and tuft For specimens that do not have apical tufts: Width of shaft taken at ¼ of its length (shaft length is considered to be the length of MPL distal to the base of the phalanx); in both cases ⊥ to long axis of shaft and taken in dorsal view	Higher values are suggested to reflect a shaft that is more resistant to medio-lateral bending

Apical tuft width (ATW)	For specimens that have apical tufts: Maximum width of apical tuft For specimens that do not have apical tufts: Width of shaft taken at ¾ of its length (shaft length is considered to be the length of MPL distal to the base of the phalanx); in both cases ⊥ to long axis of shaft and taken in dorsal view	May be related to width of unguis
Width of superior margin of articular facet (WSM)	Width of superior margin of articular facet taken in proximal view	Describes shape of facet
Width of inferior margin of articular facet (WIM)	Width of inferior margin of articular facet taken in proximal view	Describes shape of facet
Included angle of shaft (SIA)	Included angle of dorsal surface of shaft calculated based on measurements L_s and H_s as in **Fig. 3.7** L_s = distance from point on dorsal margin where shaft meets base to distalmost tip of shaft H_s = distance from midpoint of L_s to dorsal margin of shaft; ⊥ to L_s If L_s is positioned volar to H_s; angle is scored as positive (dorsally convex) If L_s is position dorsal to H_s, angle is scored as negative (dorsally concave) All measurements taken in lateral view	Curvature of the dorsum of shaft; unguis tends to follow shape of dorsum of shaft; higher degrees of curvature indicative of a more strongly keeled unguis
Included angle of articular facet (FIA)	Included angle of dorsal surface of shaft calculated based on measurements FH and H_F as in **Fig. 3.7** H_F = distance from midpoint of FH to proximal margin of articular surface; ⊥ to FH If FH is positioned proximal to H_F; angle is scored as positive (proximally concave) If FH is positioned distal to H_F, angle is scored as negative (proximally convex) All measurements taken in lateral view	Describes shape of facet
Facet-shaft angle (FSA)	Angle between FH and MPL	Reflects the degree to which the shaft (and unguis) projects dorsally or volarly with respect to the base of the phalanx

Table 3.9. Extant sample of second pedal distal phalanges.
Extant sample used for ancestral state reconstructions.

Species	Taxonomy	n
Galagoides demidovii	Strepsirrhini > Lorisiformes > Galagidae	1
Galago moholi	Strepsirrhini > Lorisiformes > Galagidae	2
Galago senegalensis	Strepsirrhini > Lorisiformes > Galagidae	4
Otolemur crassicaudatus	Strepsirrhini > Lorisiformes > Galagidae	2
Euoticus elegantulus	Strepsirrhini > Lorisiformes > Galagidae	1
Loris tardigradus	Strepsirrhini > Lorisiformes > Lorisidae	3
Nycticebus coucang	Strepsirrhini > Lorisiformes > Lorisidae	3
Perodicticus potto	Strepsirrhini > Lorisiformes > Lorisidae	2
Arctocebus calabarensis	Strepsirrhini > Lorisiformes > Lorisidae	1
Daubentonia madagascariensis	Strepsirrhini > Chiromyiformes > Daubentoniidae	1
Varecia sp.	Strepsirrhini > Lemuriformes > Lemuridae	2
Varecia variegata	Strepsirrhini > Lemuriformes > Lemuridae	2
Lemur catta	Strepsirrhini > Lemuriformes > Lemuridae	2
Hapalemur griseus	Strepsirrhini > Lemuriformes > Lemuridae	5
Eulemur fulvus	Strepsirrhini > Lemuriformes > Lemuridae	1
Eulemur albifrons	Strepsirrhini > Lemuriformes > Lemuridae	2
Eulemur rufus	Strepsirrhini > Lemuriformes > Lemuridae	1
Eulemur macaco	Strepsirrhini > Lemuriformes > Lemuridae	1
Phaner furcifer	Strepsirrhini > Lemuriformes > Cheirogaleidae	1
Lepilemur leucopus	Strepsirrhini > Lemuriformes > Lepilemuridae	1
Mirza coquereli	Strepsirrhini > Lemuriformes > Cheirogaleidae	3
Microcebus murinus	Strepsirrhini > Lemuriformes > Cheirogaleidae	4
Cheirogaleus medius	Strepsirrhini > Lemuriformes > Cheirogaleidae	3
Indri indri	Strepsirrhini > Lemuriformes > Indriidae	2
Avahi laniger	Strepsirrhini > Lemuriformes > Indriidae	2
Propithecus diadema	Strepsirrhini > Lemuriformes > Indriidae	1
Propithecus coquereli	Strepsirrhini > Lemuriformes > Indriidae	1
Propithecus verreauxi	Strepsirrhini > Lemuriformes > Indriidae	4
Tarsius pumilus	Haplorhini > Tarsiiformes > Tarsiidae	1
Tarsius pelengensis	Haplorhini > Tarsiiformes > Tarsiidae	4
Cephalopachus bancanus	Haplorhini > Tarsiiformes > Tarsiidae	3
Carlito syrichta	Haplorhini > Tarsiiformes > Tarsiidae	4
Cacajao calvus	Haplorhini > Simiiformes > Platyrrhini > Pitheciidae > Pitheciinae	2
Chiropotes satanas	Haplorhini > Simiiformes > Platyrrhini > Pitheciidae > Pitheciinae	1
Chiropotes chiropotes	Haplorhini > Simiiformes > Platyrrhini > Pitheciidae > Pitheciinae	1
Pithecia monachus	Haplorhini > Simiiformes > Platyrrhini > Pitheciidae > Pitheciinae	1
Pithecia sp.	Haplorhini > Simiiformes > Platyrrhini > Pitheciidae > Pitheciinae	1
Callicebus cupreus	Haplorhini > Simiiformes > Platyrrhini > Pitheciidae > Callicebinae	1
Callicebus moloch	Haplorhini > Simiiformes > Platyrrhini > Pitheciidae > Callicebinae	3
Callicebus donacophilus	Haplorhini > Simiiformes > Platyrrhini > Pitheciidae > Callicebinae	1
Alouatta seniculus	Haplorhini > Simiiformes > Platyrrhini > Atelidae > Alouattinae	3
Brachyteles arachnoides	Haplorhini > Simiiformes > Platyrrhini > Atelidae > Atelinae	1
Lagothrix lagotricha	Haplorhini > Simiiformes > Platyrrhini > Atelidae > Atelinae	2
Lagothrix poeppigii	Haplorhini > Simiiformes > Platyrrhini > Atelidae > Atelinae	1
Ateles belzebuth	Haplorhini > Simiiformes > Platyrrhini > Atelidae > Atelinae	2

Saimiri sp.	Haplorhini > Simiiformes > Platyrrhini > Cebidae > Cebinae	2
Saimiri boliviensis	Haplorhini > Simiiformes > Platyrrhini > Cebidae > Cebinae	3
Sapajus libidinosus	Haplorhini > Simiiformes > Platyrrhini > Cebidae > Cebinae	1
Sapajus apella	Haplorhini > Simiiformes > Platyrrhini > Cebidae > Cebinae	1
Cebus sp.	Haplorhini > Simiiformes > Platyrrhini > Cebidae > Cebinae	2
Cebus albifrons	Haplorhini > Simiiformes > Platyrrhini > Cebidae > Cebinae	2
Saguinus fuscicollis	Haplorhini > Simiiformes > Platyrrhini > Cebidae > Callitrichinae	1
Saguinus sp.	Haplorhini > Simiiformes > Platyrrhini > Cebidae > Callitrichinae	2
Leontopithecus rosalia	Haplorhini > Simiiformes > Platyrrhini > Cebidae > Callitrichinae	1
Callimico goeldii	Haplorhini > Simiiformes > Platyrrhini > Cebidae > Callitrichinae	1
Callithrix sp	Haplorhini > Simiiformes > Platyrrhini > Cebidae > Callitrichinae	1
Aotus sp.	Haplorhini > Simiiformes > Platyrrhini > Cebidae > Aotinae	2
Aotus trivirgatus	Haplorhini > Simiiformes > Platyrrhini > Cebidae > Aotinae	1
Pan troglodytes	Haplorhini > Simiiformes > Catarrhini > Hominoidea > Hominidae	4
Homo sapiens	Haplorhini > Simiiformes > Catarrhini > Hominoidea > Hominidae	4
Gorilla beringei	Haplorhini > Simiiformes > Catarrhini > Hominoidea > Hominidae	4
Gorilla gorilla	Haplorhini > Simiiformes > Catarrhini > Hominoidea > Hominidae	3
Hoolock hoolock	Haplorhini > Simiiformes > Catarrhini > Hominoidea > Hylobatidae	1
Hylobates lar	Haplorhini > Simiiformes > Catarrhini > Hominoidea > Hylobatidae	2
Macaca sylvanus	Haplorhini > Simiiformes > Catarrhini > Cercopithecoidea > Cercopithecinae	1
Macaca nemestrina	Haplorhini > Simiiformes > Catarrhini > Cercopithecoidea > Cercopithecinae	1
Macaca mulatta	Haplorhini > Simiiformes > Catarrhini > Cercopithecoidea > Cercopithecinae	5
Macaca fascicularis	Haplorhini > Simiiformes > Catarrhini > Cercopithecoidea > Cercopithecinae	2
Theropithecus gelada	Haplorhini > Simiiformes > Catarrhini > Cercopithecoidea > Cercopithecinae	4
Papio hamadryas	Haplorhini > Simiiformes > Catarrhini > Cercopithecoidea > Cercopithecinae	3
Lophocebus johnstoni	Haplorhini > Simiiformes > Catarrhini > Cercopithecoidea > Cercopithecinae	2
Cercocebus agilis	Haplorhini > Simiiformes > Catarrhini > Cercopithecoidea > Cercopithecinae	2
Cercocebus torquatus	Haplorhini > Simiiformes > Catarrhini > Cercopithecoidea > Cercopithecinae	2
Chlorocebus pygerythrus	Haplorhini > Simiiformes > Catarrhini > Cercopithecoidea > Cercopithecinae	1
Chlorocebus aethiops	Haplorhini > Simiiformes > Catarrhini > Cercopithecoidea > Cercopithecinae	1
Erythrocebus patas	Haplorhini > Simiiformes > Catarrhini > Cercopithecoidea > Cercopithecinae	2
Cercopithecus mitis	Haplorhini > Simiiformes > Catarrhini > Cercopithecoidea > Cercopithecinae	3
Semnopithecus entellus	Haplorhini > Simiiformes > Catarrhini > Cercopithecoidea > Colobinae	1
Trachypithecus cristatus	Haplorhini > Simiiformes > Catarrhini > Cercopithecoidea > Colobinae	1
Trachypithecus obscurus	Haplorhini > Simiiformes > Catarrhini > Cercopithecoidea > Colobinae	2
Nasalis larvatus	Haplorhini > Simiiformes > Catarrhini > Cercopithecoidea > Colobinae	3
Pygathrix nemaeus	Haplorhini > Simiiformes > Catarrhini > Cercopithecoidea > Colobinae	2
Presbytis melalophos	Haplorhini > Simiiformes > Catarrhini > Cercopithecoidea > Colobinae	2
Piliocolobus foai	Haplorhini > Simiiformes > Catarrhini > Cercopithecoidea > Colobinae	2
Colobus guereza	Haplorhini > Simiiformes > Catarrhini > Cercopithecoidea > Colobinae	2
Galeopterus variegatus	Euarchonta > Dermoptera > Cynocephalidae	1
Tupaia glis	Euarchonta > Scandentia > Tupaiidae	1
Ptilocercus lowii	Euarchonta > Scandentia > Ptilocercidae	1
Chiropodomys gliroides	Glires > Rodentia > Myomorpha > Muridae	1

Table 3.10. Principal components.
The eigenvalues, percentage of variance explained (% Variance) and the cumulative (cum.) variance for each principal component from two analyses. PCA (All rays) is the analysis run on all ray-specific species means and all fossil specimens. PCA (P2s) is the analysis run on species means of second pedal distal phalanges from extant taxa and fossil grooming phalanges.

PCA (All rays)			
PC	**Eigenvalue**	**% Variance**	**Cum. variance**
1	6.3	42.3%	42.3%
2	2.1	13.7%	56.0%
3	1.6	10.6%	66.6%
PCA (P2s)			
PC	**Eigenvalue**	**% Variance**	**Cum. variance**
1	3.5	26.8%	26.8%
2	3.1	24.1%	47.9%
3	1.7	12.9%	60.8%

Table 3.11. Loadings for PCA (All rays).
The Pearson's correlation coefficients from correlations of each variable with principal components 1-3 from the PCA on all ray-specific species means and all fossil specimens.

PC1		PC2		PC3	
Variable	**Correlation**	**Variable**	**Correlation**	**Variable**	**Correlation**
MSH	-0.89	MSW	-0.54	MPL	-0.54
FTH	-0.82	FSA	-0.44	ETH	-0.31
SIA	-0.81	ATW	-0.44	MSH	-0.17
FH	-0.68	FTH	-0.37	ATW	-0.13
ATH	-0.56	FIA	-0.36	FH	-0.12
FIA	-0.51	SIA	-0.24	MSW	-0.06
ETH	-0.49	BW	-0.22	BW	0.04
MPL	-0.42	ETH	-0.19	SIA	0.15
FSA	-0.18	MSH	-0.18	FTH	0.17
WIM	0.10	FH	0.25	VPL	0.21
VPL	0.47	ATH	0.32	ATH	0.23
WSM	0.64	MPL	0.33	WSM	0.24
MSW	0.71	WSM	0.36	WIM	0.55
ATW	0.82	VPL	0.47	FIA	0.55
BW	0.89	WIM	0.56	FSA	0.60

Table 3.12. Canonical variates.
The singular values (SV), percentage of between-group variance explained (% b-g Variance) and the cumulative (cum.) variance for each canonical variate (CV) from two analyses. DFA (Anth P2s) is the analysis used to classify anthropoid second pedal distal phalanges. DFA (Fossils) is the analysis used to classify fossil distal phalanges.

DFA (Anth P2s)			
CV	**SV**	**% b-g Variance**	**Cum. variance**
1	42.0	50.1%	50.1%
2	34.7	34.2%	84.3%
3	19.2	10.5%	94.8%
4	13.6	5.2%	100%
DFA (Fossils)			
CV	**SV**	**% b-g Variance**	**Cum. variance**
1	38.9	53.0%	53.0%
2	29.8	31.2%	84.2%
3	16.7	9.8%	94.0%
4	11.9	5.0%	99.0%
5	5.47	1.0%	100%

Table 3.13. Loadings for DFA (Anth P2s).
The Pearson's correlation coefficients from correlations of each variable with canonical variates 1-2 from the DFA (structure coefficients) used to classify anthropoid second pedal distal phalanges.

CV1		CV2	
Variable	**Correlation**	**Variable**	**Correlation**
MSH	-0.86	MPL	-0.47
FTH	-0.74	ETH	-0.18
SIA	-0.68	ATW	-0.16
FH	-0.66	BW	-0.12
ETH	-0.52	WSM	-0.12
MPL	-0.43	FH	-0.12
FIA	-0.41	MSW	-0.03
ATH	-0.16	MSH	-0.01
FSA	-0.07	WIM	0.21
MSW	0.29	VPL	0.21
WIM	0.33	ATH	0.19
ATW	0.56	SIA	0.33
WSM	0.60	FTH	0.37
BW	0.62	FSA	0.68
VPL	0.85	FIA	0.71

Table 3.14. Loadings for DFA (Fossils).
The Pearson's correlation coefficients from correlations of each variable with canonical variates 1-2 from the DFA (structure coefficients) used to classify fossil phalanges.

CV1		CV2	
Variable	**Correlation**	**Variable**	**Correlation**
MSH	-0.87	MPL	-0.52
FTH	-0.80	ETH	-0.33
SIA	-0.73	FH	-0.28
FH	-0.63	MSH	-0.27
FIA	-0.51	ATW	0.01
ETH	-0.48	MSW	0.04
MPL	-0.35	BW	0.06
FSA	-0.18	WSM	0.07
ATH	-0.17	SIA	0.08
MSW	0.27	FTH	0.10
WIM	0.31	ATH	0.23
ATW	0.56	WIM	0.29
WSM	0.62	VPL	0.46
BW	0.63	FIA	0.49
VPL	0.82	FSA	0.57

Table 3.15. Classifications of fossil distal phalanges based on DFA.
The groups (Class) and the probability (Prob.) of group memberships for each fossil specimen. Anth Groom, anthropoid grooming phalanx group; Groom, strepsirrhine/tarsier grooming phalanx group; Ungula, ungular phalanx group.

Species	Specimen	Class	Prob.
Notharctus tenebrosus	AMNH FM 129382	Anth Groom	0.84
Notharctus tenebrosus	AMNH FM 143612_3	Groom	0.97
?Cantius/Notharctus venticolis	UCMP 217911	Anth Groom	0.37
?Cantius/Notharctus venticolis	UCMP 217911_est	Anth Groom	0.82
Cantius nunienus	UM 112882	Anth Groom	0.81
Notharctus tenebrosus	AMNH FM 11474	Anth Groom	1.00
Notharctus tenebrosus	AMNH FM 131764 (a)	Anth Groom	1.00
Notharctus tenebrosus	AMNH FM 131764 (b)	Anth Groom	0.82
Notharctus tenebrosus	AMNH FM 143612_2	Anth Groom	1.00
Notharctus tenebrosus	AMNH FM 143612_4	Anth Groom	0.61
Smilodectes gracilis	AMNH FM 131763	Ungula	0.92
Indet Adapiform	UCMP 236082	Anth Groom	1.00
Indet Adapiform	AMNH FM 131766	Anth Groom	0.98
Indet Adapiform	UCMP 147533	Ungula	0.98
Indet Adapiform	UCMP 147534	Ungula	0.97
Indet Adapiform	UCMP 217913	Anth Groom	0.94
Indet Adapiform	UCMP 217971	Anth Groom	1.00
Indet Adapiform	UCMP 218139	Ungula	0.72
Indet Adapiform	UCMP 218367	Ungula	0.95
Indet Adapiform	UCMP 218402	Ungula	1.00
?Tetonius	UCMP 217999	Groom	1.00
?Tetonius	UCMP 217999_est	Groom	1.00
?*Arapahovius*	UCMP 218000	Groom	0.83
?*Arapahovius*	UCMP 218000_est	Groom	0.94
Omomys carteri	UM 32258	Ungula	1.00
Teilhardina brandti	USNM 540587	Ungula	1.00
Indet Omomyiform	UCMP 134993	Ungula	1.00
Indet Omomyiform	UCMP 218183	Ungula	1.00
Indet Omomyiform	UCMP 218244	Ungula	1.00
Indet Omomyiform	UCMP 218261	Ungula	1.00
Indet Omomyiform	UCMP 218295	Ungula	1.00
Indet Omomyiform	UCMP 218301	Ungula	1.00
Indet Omomyiform	UCMP 218368	Ungula	1.00
Indet Omomyiform	UCMP 218416	Ungula	1.00
Indet Omomyiform	UCMP 218432	Ungula	1.00
Indet Omomyiform	UCMP 218436	Ungula	1.00
Indet Omomyiform	UM 31624	Ungula	1.00
Indet Omomyiform	UM 32129	Ungula	1.00
Indet Omomyiform	UM 32146 (a)	Ungula	1.00
Indet Omomyiform	UM 32146 (b)	Ungula	1.00
Indet Omomyiform	UM 32274	Ungula	1.00
Indet Omomyiform	UM 32186	Ungula	1.00

Indet Omomyiform	UM 32249 (a)	Ungula	1.00
Indet Omomyiform	UM 32249 (b)	Ungula	1.00
Indet Omomyiform	UM 32249 (c)	Ungula	1.00
Indet Omomyiform	UM 32249 (d)	Ungula	1.00
Indet Omomyiform	UM 32249 (e)	Ungula	1.00
Indet Omomyiform	AMNH FM 126631	Ungula	1.00
Indet Omomyiform	AMNH FM 126632	Ungula	1.00
Indet Omomyiform	AMNH FM 126637	Ungula	1.00
Indet Omomyiform	AMNH FM 126659	Ungula	1.00
Indet Omomyiform	AMNH FM 126663	Ungula	1.00
Indet Omomyiform	AMNH FM 126664	Ungula	1.00
Indet Omomyiform	AMNH FM 126665	Ungula	1.00
Indet Omomyiform	AMNH FM 126674	Ungula	1.00
Indet Omomyiform	AMNH FM 126735	Ungula	1.00

Table 3.16. Group means and standard deviations.
Group means and standard deviations (in parentheses) for each size-adjusted shape variable and angular variable.

	Falcular	**Non-primate Grooming**	**Tegular**	**Strep./Tarsier Grooming**	**Anthropoid Grooming**	**Ungular**
FH	1.11 (0.15)	1.16 (0.12)	1.06 (0.10)	1.09 (0.22)	0.87 (0.09)	0.88 (0.10)
ETH	0.31 (0.14)	0.32 (0.14)	0.17 (0.03)	0.32 (0.08)	0.23 (0.03)	0.21 (0.04)
FTH	0.72 (0.21)	0.76 (0.17)	0.64 (0.19)	0.29 (0.09)	0.29 (0.04)	0.28 (0.06)
MPL	3.74 (0.40)	4.20 (0.66)	4.63 (0.16)	4.69 (0.53)	4.37 (0.39)	3.58 (0.51)
VPL	1.57 (0.24)	1.25 (0.18)	3.02 (0.19)	1.60 (0.33)	2.62 (0.54)	3.21 (0.51)
MSH	1.80 (0.32)	1.50 (0.17)	1.58 (0.16)	1.43 (0.30)	1.10 (0.07)	0.91 (0.11)
ATH	0.89 (0.29)	0.84 (0.20)	0.84 (0.08)	0.66 (0.06)	0.70 (0.08)	0.76 (0.14)
BW	1.40 (0.23)	1.27 (0.10)	1.30 (0.07)	1.74 (0.32)	1.84 (0.08)	1.90 (0.25)
MSW	0.73 (0.24)	0.80 (0.14)	0.66 (0.07)	0.81 (0.16)	0.87 (0.07)	0.87 (0.16)
ATW	0.54 (0.22)	0.70 (0.20)	0.65 (0.09)	0.98 (0.19)	1.00 (0.16)	1.09 (0.29)
WSM	0.95 (0.19)	0.88 (0.09)	0.78 (0.09)	1.15 (0.15)	1.14 (0.12)	1.25 (0.14)
WIM	1.23 (0.19)	1.15 (0.16)	1.19 (0.09)	1.15 (0.13)	1.21 (0.24)	1.30 (0.13)
SIA	85.41 (30.13)	59.47 (10.42)	74.41 (11.40)	23.66 (19.32)	31.19 (10.66)	19.04 (13.88)
FIA	123.13 (20.02)	104.34 (22.72)	58.96 (14.49)	21.73 (23.40)	45.47 (14.14)	60.59 (15.91)
FSA	92.68 (12.21)	84.33 (12.29)	79.22 (6.37)	63.23 (8.06)	71.30 (2.77)	80.28 (6.67)

Table 3.17. Loadings for PCA (P2s).
The Pearson's correlation coefficients from correlations of each variable with principal components 1-2 from the PCA of second pedal distal phalanges and fossil grooming phalanges.

PC1		PC2	
Variable	**Correlation**	**Variable**	**Correlation**
MSH	-0.88	ATW	-0.58
SIA	-0.63	MSW	-0.51
FTH	-0.59	MPL	-0.50
FH	-0.54	BW	-0.48
ETH	-0.45	ETH	-0.37
MPL	-0.42	WSM	-0.31
ATH	-0.10	MSH	-0.11
FIA	-0.09	FH	0.03
FSA	0.10	SIA	0.29
VPL	0.45	WIM	0.34
ATW	0.48	FTH	0.49
MSW	0.50	VPL	0.63
WIM	0.54	FSA	0.68
BW	0.65	ATH	0.71
WSM	0.72	FIA	0.74

4. Chapter 4: Nail Origins – Implications for Primate Origins

4.1 Abstract

The typical primate condition of having nails on postaxial digits is rare among non-primate mammals and especially those that are arboreal. Some arboreal mammals have a primate-like grasping hallux, but still retain claws on postaxial digits. Claws are advantageous for an arboreal mammal as they assist in clinging and climbing on relatively large diameter vertical supports, so the question as to why a primarily arboreal lineage possesses nails rather than claws is unclear. Most hypotheses of primate origins links the presence of nails to grasping in a terminal branch niche. However, at least one non-primate species (the woolly opossum) that utilizes a terminal branch niche possesses claws on all postaxial rays. Others (e.g., pygmy and honey possums) have been described in the literature as possessing reduced claws, but this morphology has not been illustrated or quantified so it is unclear as to how they compare to primates. The goals of this chapter are to determine if and which non-primate arboreal mammals possess primate-like morphology of the distal phalanx (which supports the claw or nail), to assess the distal phalanx morphology of early fossil primates, and to explore the significance of the results for the origin of the primate nail. Distal phalanx morphology is shown to covary with the presence of pedal-grasping, small body size, and reduced claws or nails. Small-bodied pedal graspers (that weigh less than 100g) tend to have reduced claws, while the tiny honey possum possesses nails on postaxial digits. Of early fossil primates, *Notharctus tenebrosus* most closely resembles the reduced claws of small pedal grasping non-primates. However, earlier occurring adapiforms have distal phalanges that are more nail-like and the structures in *Notharctus* are interpreted as derived towards a more tegula- or claw-like state. The association of nail-like morphology and small body size in pedal grasping non-primates suggests that small body size may have facilitated the evolution of nails very early in primate evolution.

4.2 Introduction

Ungulae (nails) are one of the few traits that unite all living primates (e.g., Mivart, 1873). They are thought to have been derived from falculae (claws) at some point early in primate evolution (e.g., Cartmill, 1974). **Fig. 4.1** demonstrates the major differences between the

keratinized structures (falculae and ungulae) and the bones that support them (distal phalanges). All primates possess a hallux that is ungula-bearing and most primates possess ungulae on all or most postaxial (non-pollical and non-hallucal) digits. Such a condition is rare among non-primate mammals, and especially among those that are arboreal. Some arboreal non-primates like diprotodont possums and didelphid opossums possess a primate-like grasping hallux that lacks a falcula, but falculae are retained on postaxial digits (Szalay, 1994). Further these marsupials lack ungulae on their halluces, which in most cases are ununguiculate (lacking any vestige of a keratinized structure).

Falculae have long been considered an asset to an arboreal mammal. By interlocking their tips with the substrate, falculae allow a mammal to cling and climb on vertical supports that have relatively large diameters when compared to the animal's body size (Cartmill, 1974; Cartmill, 1985). A mammal that possesses ungulae rather than falculae, like most primates, must generate an adductor force either between two opposing appendages or by grasping to utilize vertical substrates (Cartmill, 1985). This has the effect of severely limiting the substrate sizes available to them as an ungula-bearing mammal cannot use a smooth substrate that is too big for it to grasp with a hand or foot or to grip between limbs. Therefore, it is unclear as to why arboreal primates lack falculae and possess ungulae in their place.

Several theories of primate origins link the presence of ungulae (or absence of falculae) to grasping, and more specifically, grasping in a terminal branch niche (Cartmill, 1972; Cartmill, 1974; Sussman and Raven, 1978; Hamrick, 1998). These theories suggest that an adaptive shift that involves foraging or hunting on terminal branches is assisted by prehensile hands and feet with enlarged volar pads. In such scenarios, ungulae are usually considered to be the passive byproduct of an expanded apical pad. However, some researchers have suggested that ungulae may convey an adaptive advantage for grasping, either to support the apical pad or redistribute forces placed on the digit tip (Le Gros Clark, 1936; Baden, 1970; Preuschoft, 1970, 1973; Napier, 1993). Recently, the link between grasping, ungulae, and a terminal branch niche has been challenged based on the observation that non-grasping, falcula-bearing mammals like squirrels are capable of climbing and foraging on terminal branches (Orkin and Pontzer, 2011). Additionally, at least one mammal with a grasping hallux that inhabits a terminal branch niche possesses falculae on all postaxial digits (*Caluromys*, the woolly opossum; Rasmussen, 1990; Rasmussen and Sussman, 2007). These observations demonstrate that grasping or grasping with

ungula-bearing digits are not necessary requirements for the utilization of a terminal branch niche. However, these observations do not actually conflict with the idea that performance within a terminal branch niche is improved by prehensile grasping and/or ungulae; rather falculae in terminal branch specialists may be resultant of mammals balancing selective pressures to retain falculae (the utilization of relatively large diameter vertical supports) with pressures for better performance in a terminal branch niche (Hamrick, 1998; Orkin and Pontzer, 2011).

Interestingly, some mammals that inhabit a terminal branch niche (pygmy possums, honey possums, several muroid rodents) are described in the literature as having "reduced claws" (Cartmill, 1974; Russell, 1986; Godinot, 2007; Rasmussen and Sussman, 2007). However, this morphology has not been illustrated, studied, or quantified so it is not clear as to how it compares to that of ungula-bearing primates (Godinot, 2007). Further, the morphology of falculae of mammals that have a grasping hallux, like the woolly opossum, has not been explored. It is possible that they possess "reduced claws" in comparison to those of mammals that do not grasp.

The earliest known primates, adapiforms and omomyiforms, have distal phalanges that indicate the presence of ungulae. In fact, the earliest ungula-bearing distal phalanx is from the Early Eocene (Wa-0) of North America and has been attributed to the omomyiform, *Teilhardina brandti* (Rose et al., 2011). It strongly resembles the ungula-bearing distal phalanges of living primates. On the other hand, adapiform distal phalanges have been described as proximally falcula-like (dorso-ventrally deep) and distally ungula-like (medio-laterally wide). They also possess somewhat proximally restricted volar processes and enlarged bilaterally occurring nutrient foramina, characteristics that are reminiscent of distal phalanges that bear falculae (**Fig. 4.2**). Some have suggested that adapiform distal phalanges are transitional in form between those that bear falculae and those that bear ungulae (Godinot and Beard, 1991; Godinot, 1992; Godinot and Beard, 1993). If this is the case, it would imply that the evolution of ungulae differed in the two major radiations of early primates; omomyiforms would have attained extant primate-like ungulae much earlier than did adapiforms.

The goals of the current study are to determine if and which arboreal non-primates possess primate-like distal phalanges, to determine if the distal phalanges of some fossil primates represent an intermediate stage in the evolution of ungulae from falculae, and to evaluate results for the understanding of the origin of primate ungulae. Distal phalanges are studied because they

are related to the shape of the unguis (e.g., falcula or ungula) and the apical pad, and are preserved in the fossil record.

4.3 Materials and Methods

Data were collected from distal phalanges (n=391) of both extant primates and non-primates and were divided into four groups based on unguis form, climbing mode, and/or phylogenetic group: claw climbing non-primates, pedal grasping non-primates, tegula-bearing primates, and ungula-bearing primates. See **Table 4.1** for sample, **Table 4.2** for group designations, **Table 4.3** for institutional abbreviations, and **Table 4.4** for sample sizes of each group. Non-primate claw climbers are climbing mammals that possess falculae which are used to cling and climb on relatively large diameter supports. Some of these taxa may have some rudimentary prehensile capabilities or a somewhat divergent hallux, but the hallux still possesses a falcula. Non-primate pedal graspers possess a grasping or opposable hallux that lacks a falcula and is either ununguiculate or bears an ungula. Tegula-bearing primates are callitrichines and aye-ayes that possess tegulae on postaxial digits. Tegulae are claw-like structures modified from an ancestral nail and used to cling and climb on relatively large diameter vertical supports in a similar manner to non-primate claw climbers. Ungula-bearing primates are primates that possess ungulae on postaxial digits. This group contains tarsiers and strepsirrhines that can be divided into three locomotor categories: vertical clinging and leaping, generalized arboreal quadrupeds, and slow climbing arboreal quadrupeds. Vertical clinging and leaping taxa are species like tarsiers and indris that cling to and leap between vertical supports using orthograde postures. Generalized arboreal quadrupeds are species with a varied locomotor repertoire that may contain some vertical clinging and leaping, quadrupedal leaping, and quadrupedal walking and running. Slow climbing arboreal quadrupeds are lorisids that primarily locomote on small branches using quiet, slow climbing. These species are capable of more rapid climbing, but primarily move slowly and rarely or never leap. Locomotor designations are based on the literature (Clark, 1924; Musser, 1972; Walker, 1974; Charles-Dominique, 1977; Charles-Dominique and Bearder, 1979; Musser, 1979; Walker, 1979; Crompton, 1983; Gebo, 1987; Musser and Dagosto, 1987; Rasmussen, 1990; Dagosto, 1995; Terranova, 1995, 1996; Bradshaw et al., 2007; Rasmussen and Sussman, 2007; Dieterlen, 2009; Grow and Gursky-Doyen, 2010). Body sizes for pedal grasping

non-primates are also taken from the literature (Breed and Taylor, 2000; Denys et al., 2006; Freudenthal and Martin-Suárez, 2013; Weisbecker et al., 2013).

Data were also collected from distal phalanges of Eocene adapiforms and omomyiforms (n=48; **Table 4.5**). UCMP fossils are known from a number of localities within the Washakie Basin, WY. These specimens are isolated distal phalanges that have not been attributed to a species. Adapiform and omomyiform distal phalanges in this assemblage are easily distinguished from one another on the basis of size as well as morphology. Overall, the omomyiform postaxial distal phalanges from the Washakie Basin are smaller than those of the adapiforms as they range from about 1.61mm in length to about 3.2mm in length while the adapiforms range from about 5.14mm to about 6.43mm. Further, the adapiform distal phalanges are distinct in having more rugous apical tufts, dorso-ventrally deeper shafts, and much larger nutrient foramina than the omomyiforms (compare fossil specimens in **Fig. 4.2**). **Tables 4.6** and **4.7** provide a list of the dentally known taxa at each locality as it is likely that the distal phalanx specimens are from these species. The AMNH fossils are from several localities within the Bridger (Green River) Basin, WY and most adapiform specimens are associated with other skeletal elements which have been attributed to a taxon. The AMNH omomyiforms are all isolated specimens, some of which were figured and discussed by Dagosto (1988). Based on other postcranial elements from the same regions as the distal phalanges, three omomyid taxa are suggested to be present, the largest and most common being *Hemiacodon gracilis* or a similar species. Dagosto suggests that most of the distal phalanges in this collection are attributable to *Hemiacodon* (or a similar species). The UM specimens are also from the Bridger Basin, WY. Most of the indet omomyiform specimens are isolated, but are most likely from either *Hemiacodon gracilis* or *Omomys carteri* (pers. comm. Gregg Gunnell).

Each specimen was sampled in one of two ways. Many extant primates and non-primates were sampled using a high resolution digital SLR camera (Nikon D5100) with a macro lens (Nikon AF-S Micro NIKKOR 40mm 1:2.8G). Photos were taken in dorsal, lateral, volar, and proximal views; a millimeter scale was placed in the same plane as each specimen. Some extant species and all fossil specimens were sampled using micro computed tomography. Most extant specimens were scanned using either a VivaCT 75 Scanco microCT scanner at SBU, a GE phoenix v|tome|x s240 at the AMNH, or a Nikon XT H 225 ST micro x-ray computed tomography scanner at Duke University. Voxel sizes ranged from 10µ (smallest specimens) to

70µ (large specimens). Many of these specimens are left in preserved skins, and microCT scanning of them allows for non-destructive recovery of osteological information. All fossils (except AMNH FM 11474 which was acquired earlier) were scanned with voxel sizes of 4µ to 10µ using a VivaCT 40 Scanco microCT scanner at SBU or the Nikon XT H 225 ST micro x-ray computed tomography scanner at Duke University. Such a range of resolutions was necessary to create comparable 3D reconstructions from very tiny and very large specimens. The resulting scan data was segmented using Avizo 7.1 to generate 3D digital models of each bone. Screen shots with scales were taken of each in dorsal, lateral, volar, and proximal views. Morphological terms referred to in this study are illustrated in **Fig.4.3**.

A set of 15 measurements was taken from the photos or screenshots of each bone (**Figs. 4.4, 4.5; Table 4.8**). Measurements were taken using the ruler tool in Adobe Photoshop CS6 Extended Edition. All measurements with the exception of SIA, FIA, and FSA were taken in millimeters; SIA, FIA, and FSA are in degrees. Calculations of included angles (**Fig. 4.5**) were modified from Jungers et al (1997). All non-angular measurements were converted to size-adjusted shape variables through division of their geometric mean (Jungers et al., 1995). After size-adjustment, species means were calculated for each ray [Mdp2, Mdp3/4, Mdp5, Pdp2, Pdp3/4 (pooled only when the same unguis form is present on both rays), and Pdp5]. Finally, each measurement was converted into a z-score (subtracting by the variable mean and dividing by the variable's standard deviation) to create a set of variables that each have a mean of 0 and a standard deviation of 1 for use in ordination methods that expect variables to have similar variances.

Analyses of data were run in R v3.0.3 (R Core Team, 2014). Principal components analyses (PCA) were run using the princomp function in the base stats package of R and linear discriminant function analyses (DFA) were run using the lda function in the MASS package (Venables and Ripley, 2002). Loadings of each variate were assessed by calculating the Pearson's correlation coefficient between each variable and each variate using the corr function in the basic stats package. PCAs were used to summarize the maximum amount of variation observed in the dataset while DFAs were used to determine the combinations of variables which best distinguish among groups and to classify unknown specimens into these groups. The classification ability of each analysis was tested by classifying all training cases based on the

original analysis and through leave-one-out cross validation in which each training case is in turn left out of an analysis and then classified based on this newly run analysis.

4.4 Results

4.4.1 PCA of Ungulae, Falculae, and Tegulae

A PCA analyzing species means from all taxa shows a sharp morphological divide between the distal phalanges of claw climbing non-primates and ungula-bearing primates (**Table 4.9; Fig. 4.6**). Those of tegula-bearing primates are more intermediate. Loadings along PC1 (**Table 4.10**) show that ungula-bearing primates have relatively dorso-ventrally shallower (MSH, ATH), medio-laterally wider (BW, ATW, MSW), less dorsally convex (SIA) distal phalanges with dorso-ventrally shallower flexor and extensor tubercles (FTH, ETH) and proximo-distally longer volar processes (VPL) than other forms. The distal phalanges of pedal grasping non-primates that weigh more than 100g (**Table 4.2**) cluster near those of claw climbing non-primates. Interestingly the distal phalanges of pedal grasping non-primates that weight less than 100g (**Table 4.2**) show a diversity of morphologies and tend to fall between the claw climbing morphospace and primate morphospaces. Adapiforms and omomyiforms plot near extant ungula-bearing primates, though the two fossil groups tend to cluster apart from one another.

4.4.2 DFA of Ungulae, Falculae, and Tegulae

A DFA discriminating among the distal phalanges of claw climbing non-primates, tegula-bearing primates, and ungula-bearing primates show similar results to the PCA (**Table 4.9, 4.11; Fig. 4.7**). In this analysis, pedal grasping non-primates and fossil primates were treated as unknowns in order to assess their variation in comparison to the other groups. This analysis differs from the PCA in that many adapiform distal phalanges fall further away from extant primate morphospace and overlap considerably with pedal grasping non-primates that weigh less than 100g. This analysis classified 100% of cases correctly based on both the original analysis and leave-one-out cross validation. **Table 4.12** lists classifications of pedal grasping non-primates and fossil specimens demonstrating which groups they are most morphologically similar to. All pedal grasping non-primate cases from species that weigh more than 100g were classified as claw climbing, with one exception; the manual third/fourth ray of *Didelphis sp* was

classified as tegula-bearing. In fact, the distal phalanges from the manual rays of the didelphids *Didelphis* and *Philander* have the highest scores along CV 1 of the pedal grasping non-primates that weigh more than 100g. Most cases from pedal grasping non-primates that weigh less than 100g were classified as tegula-bearing, but several were classified as claw climbing (pedal distal phalanges of *Chiropodomys* and *Cercartetus*) or ungula-bearing (manual and pedal distal phalanx V from *Hapalomys* and all distal phalanges of *Tarsipes*). Of these, *Tarsipes* is plots nearest to the ungula-bearing group, one specimen even falling within this morphospace. **Fig. 4.8** illustrates the distal phalanx morphology of *Tarsipes* and other tiny bodied pedal grasping non-primates in comparison to those of the other groups. Pedal grasping non-primates as a whole tend to have relatively longer volar processes than claw climbing non-primates, but this is taken to the most extreme in taxa that weigh less than 100g. All fossil specimens were classified as ungula-bearing with the exception of AMNH FM 143612_2 (*Notharctus tenebrosus*) which was classified as tegula-bearing. Adapiforms tend to have relatively shorter volar processes and dorso-ventrally deeper shafts than omomyiforms, and this is most pronounced in *Notharctus tenebrosus* (**Fig 4.9**). See **Figs. 4.10-4.17** for group summaries of each variable demonstrated as boxplots and **Table 4.13** for group means and standard deviations.

4.4.3 DFA of Locomotor Groups

A second DFA was run discriminating among the three groups of ungula-bearing primates: those that primarily locomote utilizing vertical clinging and leaping, generalized arboreal quadrupedalism, and slow climbing arboreal quadrupedalism (**Table 4.9; 4.14; Fig. 4.18**). 89.9% of the cases were classified correctly based on the original analysis and 83.5% under leave-one-out cross validation. In this analysis, pedal grasping non-primates and fossil primates were treated as unknowns. Of the non-primates, only *Tarsipes* is plotted in **Fig. 4.18** as it is the only non-primate to possess distal phalanges that fall within ungula-bearing morphospace (**Fig. 4.7**). It was classified as a slow climbing quadrupedalist (**Table 4.12**). CV1 separates slow climbing quadrupedal primates from the other groups; these distals differ in that they tend to have relatively medio-laterally narrower (ATW) and dorso-ventrally deeper apical tufts (ATH). CV2 separates vertical clinging and leaping primates from generalized arboreal quadrupeds albeit with some overlap. Loadings show that generalized arboreal quadrupeds tend to have relatively shorter distal phalanges (MPL) with wider bases (BW) and shorter volar

processes (VPL). When the same two variates are plotted, but symbols are colored according to phylogenetic groups, it can be seen that some of the overlap between the vertical clinging and leaping and generalized arboreal group is due in part to some similarities in galagid arboreal quadrupedal distal phalanges and lemurid vertical clinging and leaping distal phalanges (**Fig. 4.19**). However, the locomotor groups are well separated within each family. Lepilemurids present an interesting case as the manual distal phalanx falls with lemurid arboreal quadrupeds and the pedal with vertical clinging and leaping though it is unclear why this might be the case. **Figure 4.2** demonstrates the morphologies associated with groups. Returning to fossils, all middle Eocene adapiforms were classified as generalized arboreal quadrupeds, while classifications of early Eocene adapiforms were more varied (**Table 4.12**). Most middle Eocene omomyiforms were also classified as generalized arboreal quadrupeds, while most early Eocene specimens were classified as vertical clingers and leapers. Interestingly, the earliest known ungula-bearing distal phalanx (*Teilhardina brandti*) was classified as a vertical clinger and leaper. Most of the overlap of fossil adapiform and omomyiform morphospaces is between early Eocene specimens as there is less overlap among those from the middle Eocene (**Fig. 4.18**). See **Figs. 4.10-4.17** for group summaries of each variable demonstrated as boxplots and **Table 4.15** for group means and standard deviation.

4.5 Discussion

4.5.1 Primate-like Morphology in Non-primate Pedal Graspers

These results demonstrate a relationship between very small body size and primate-like morphology of the distal phalanx. Overall, the distal phalanges of pedal grasping non-primates that weigh more than 100g are morphologically similar to those of claw climbing non-primates. There is a trend in which the volar process tends to be relatively longer in grasping taxa, but this is not seen in all taxa. On the other hand, pedal grasping non-primates that weigh less than 100g tend to resemble primates more strongly than do larger ones. These mammals have elongated volar processes and distal phalanges that are medio-laterally wider than their larger bodied counterparts. The volar process lies embedded within the apical pad and a longer process is related to an apical pad that extends further distally along the volar surface of the phalanx (See Chapter 2; Maiolino et al., 2011); tiny bodied pedal graspers tend to have more extensive apical

pads relative to the size of the distal phalanx than larger pedal graspers and claw climbers. Morphologically they fill the gap between falcula-bearing and ungula-bearing distal phalanges creating a morphocline with falcula-bearing and ungula-bearing distal phalanges at the extremes (**Fig. 4.7**). Examination of the external tissues of the digits of tiny bodied pedal graspers reveals that all (with one exception) possess falculae that are relatively smaller (when compared to the apical pad) and do not project as far beyond the apical pad as seen in claw climbing non-primates (**Fig 4.21**); this condition may be referred to as "reduced." The one exception is the honey possum (*Tarsipes rostratus*) which actually possesses ungulae like those of primates! In fact, it possesses ungulae on all postaxial digits with the exception of pedal rays II and III, which are syndactylus and possess grooming ungues. Its pollex also possesses a nail, but its hallux (like those of other diprotodonts) lacks a keratinized structure. Honey possums are exceedingly small (~9g, the smallest in the sample), inhabit a terminal branch niche, and subsist upon nectars (Russell, 1986; Rasmussen and Sussman, 2007; Weisbecker et al., 2013). Among ungula-bearing primates, its distal phalanges most strongly resemble those of slow climbing arboreal quadrupeds although its movements are described to differ from those of the slow climbing primates. Captive observations demonstrate that honey possums run and climb rapidly, but can also move slowly when feeding (Russell, 1986).

4.5.2 Early Primate Distal Phalanx Morphology

There are striking differences in the distal phalanges of omomyiforms and adapiforms. Adapiforms have distal phalanges that are dorso-ventrally deep proximally with somewhat proximally restricted volar processes and large bilaterally occurring nutrient foramina causing them to more closely resemble falcula-bearing distal phalanges than do omomyiforms. However, later occurring species (e.g., Middle Eocene *Notharctus tenebrosus*) tend to have even shorter volar processes than do earlier ones. It seems most likely that 1) all adapiforms retain features (albeit somewhat modified) that are reminiscent of their falcula-bearing ancestry (proximally restricted volar processes, large nutrient foramina, deep proximal shafts) and 2) volar processes were secondarily reverted back to an even shorter (more falcula-like) state in *Notharctus tenebrosus*. This implies that a larger portion of the distal phalanx shaft (and therefore the unguis) of *Notharctus tenebrosus* projected beyond the apical pad than in other species. This

may have been an adaptation for vertical clinging in this larger species, similar to but less pronounced than the tegulae of aye-ayes and callitrichines.

The earliest known primate distal phalanx (*Teilhardina brandti*) closely resembles those of vertical clinging and leaping extant primates and lacks the proximo-distally restricted volar process and dorso-ventrally deep proximal shaft of adapiforms. In fact, all omomyiforms studied lacked these features. This suggests that a modern ungula-like state was achieved earlier in the omomyiform radiation than in the adapiform radiation.

4.5.3 The Transition from Falculae to Ungulae

Since a morphological continuum between falcula-bearing and ungula-bearing distal phalanges has been established, the process by which one might be morphed into the other is clarified. Evolution towards an ungula-bearing state would simply involve the proximo-distal elongation of the volar process and/or reduction of the shaft of the distal phalanx related to a more expansive apical pad in conjunction with a medio-lateral widening and dorso-ventral shortening of the phalanx. Exactly why these changes occurred is less clear, but results suggest that there is a relationship between grasping on terminal branches, small body size, and reduced falculae or ungulae.

Small body size in extant mammals (< 100g) may be related to reduced claws and nails as it may relax the strong selective pressure to retain falculae for clinging on relatively large diameter vertical supports. A small grasping mammal may be able to use crenulations and ridges in bark as toeholds and therefore would only be restricted from climbing on smooth barked trees of relatively large diameter. Utilization of crenulations in bark is not a behavior that is described, but images of small mammals doing so can be found: honey possums can climb on mesh walls without falculae (Russell, 1986, Fig. 2); the western pygmy possum (*Cercartetus concinnus*) can grasp crenulations of bark with its foot (http://bird.net.au/bird/index.php?title=File:Western_Pygmy-possum_341_Lindy_Lumsden1.jpg) and mouse lemurs (which do not have pointed or keeled ungulae; pers obs) can descend head first on relatively large diameter vertical supports that have rough/crenulated bark (http://www.enviroreach.com/wp-content/uploads/2014/11/IMG_2065.jpg). Further, ungula-bearing honey possums have been described as running up and down tree trunks despite their lack of falculae (Russell, 1986). The

ancestor of living primates has recently been reconstructed to be quite small (~55g, Steiper and Seiffert, 2012) and has been suggested to be even smaller (10-15g, Gebo, 2004). If this is the case, then small body size may have facilitated the evolution of ungulae by relieving the pressure to retain falculae.

A positive selective pressure for ungulae is still unclear, but it does appear to be related to climbing among terminal branches (e.g., honey possum). While ungulae are not necessary for a terminal branch niche, they may still convey an advantage. For example broadened apical pads may play a role in increasing the stability of slow, quiet climbing to avoid detection of predators; ungulae would either assist with this (e.g., by supporting the apical pad) or be a passive result of an enlarged apical pad. Further, different ungula shapes likely play different roles in locomotion, prehension, or tactile sensation. For example, *Phaner* and *Euoticus* have keeled ungulae which actually assist them in vertical clinging (Charles-Dominique, 1977). *Tarsius pumilus*, a very small primate (~50g) also has keeled nails and lives in an extreme habitat (Grow and Gursky-Doyen, 2010). The trees it utilizes are described as being covered in slippery moss (pers. comm. Sharon Gursky) and it may require pointed ungulae to gain traction upon it. The shape of ungulae certainly plays a role in some forms of primate locomotion, but it is unclear as to what role it plays in a terminal branch niche.

It is clear that ungulae evolved early on within the omomyiform radiation as *Teilhardina brandti* already had modern ungula-bearing distal phalanges. The evolution of these structures may have been facilitated by small body size combined with the utilization of terminal branches. Most early omomyiforms were small (sizes reported in Fleagle, 2013) suggesting that the ancestor of the group was also small in size. The story for adapiforms is less clear due to the retention of falcula-like morphology and potential reversals. Additional factors may have driven the evolution of ungulae in adapiforms.

4.6 Figures

Fig. 4.1. Nails and claws.
A comparison of ungulae (nails) and falculae (claws). Top: elements of the digit tip of *Chlorocebus*: (left) isolated distal phalanx shown in dorsal and lateral views and (right) external tissue rendered transparent to show the relationship of the bone to apical pad and unguis. Bottom: the same elements shown for the opossum, *Didelphis*. Ungula and falcula refer to the keratinized structure that drapes over the distal phalanx (highlighted in grey). Ungular phalanges (those that bear ungulae) are medio-laterally wide and dorso-ventrally shallow when compared to falcular phalanges (those that bear falculae). Ungular phalanges have volar processes that are more proximo-distally elongated than those of falcular phalanges. The volar process lies embedded in the apical pad; the portion of the shaft distal to it projects above and/or beyond the pad where it is surrounded only by the unguis (e.g., ungula, falcula) and its associated tissues.

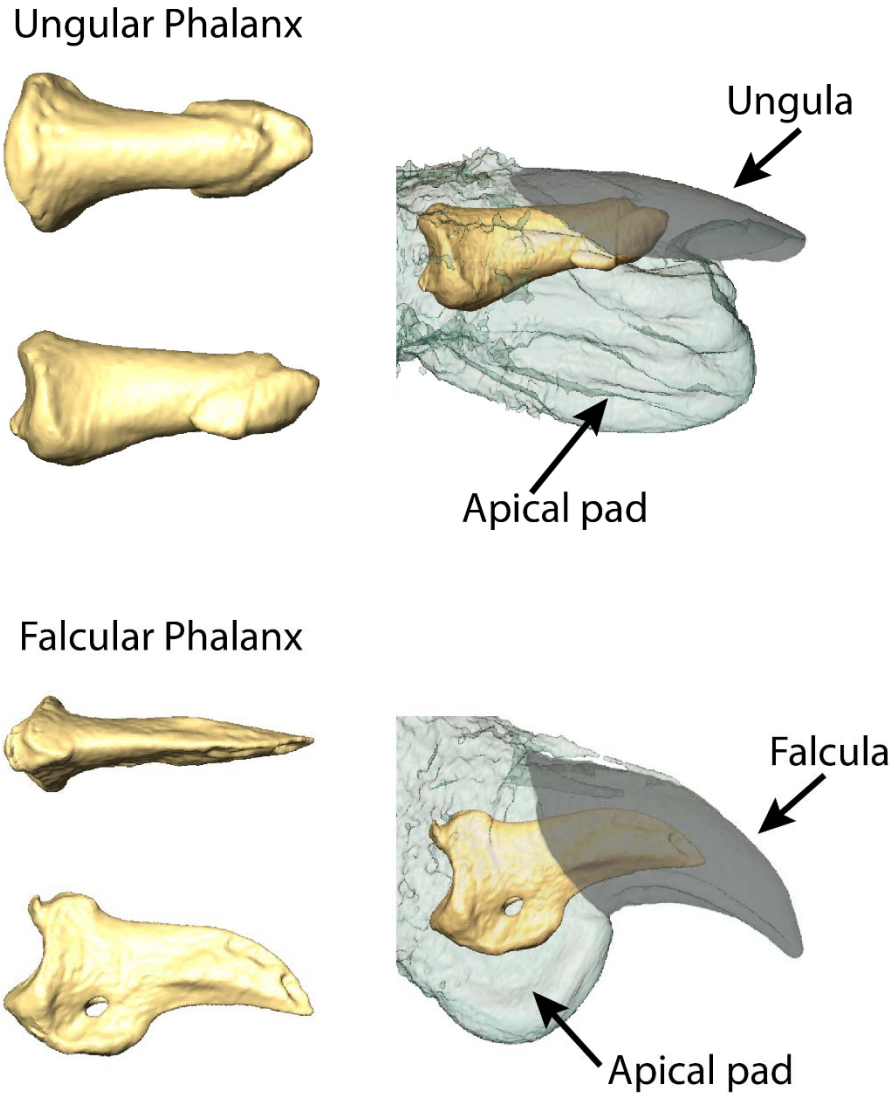

Fig. 4.2. Extant and fossil distal phalanges.
Extant phalanges shown in light colors, fossils in grey. Red lines denote the regions of the volar process; arrows point to nutrient foramina. The volar process of *Notharctus* resembles those of falcular phalanges in being more proximally restricted. Both *Notharctus* and *Teilhardina* possess bilaterally occurring nutrient foramina similar to those of non-primate falcular phalanges and unlike extant primate ungular phalanges which typically lack these foramina.

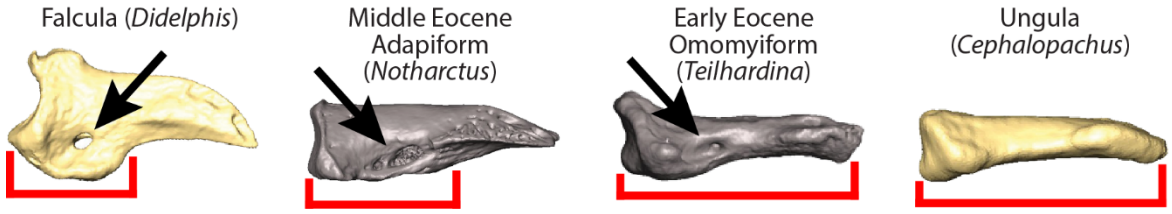

Fig. 4.3. Anatomical terminology illustrated.
Morphological features discussed in this chapter are demonstrated on distal phalanges that bear different unguis forms shown (from left to right) in dorsal, lateral, volar, and proximal views. Unmarked images of each specimen are shown directly above those that are highlighted.

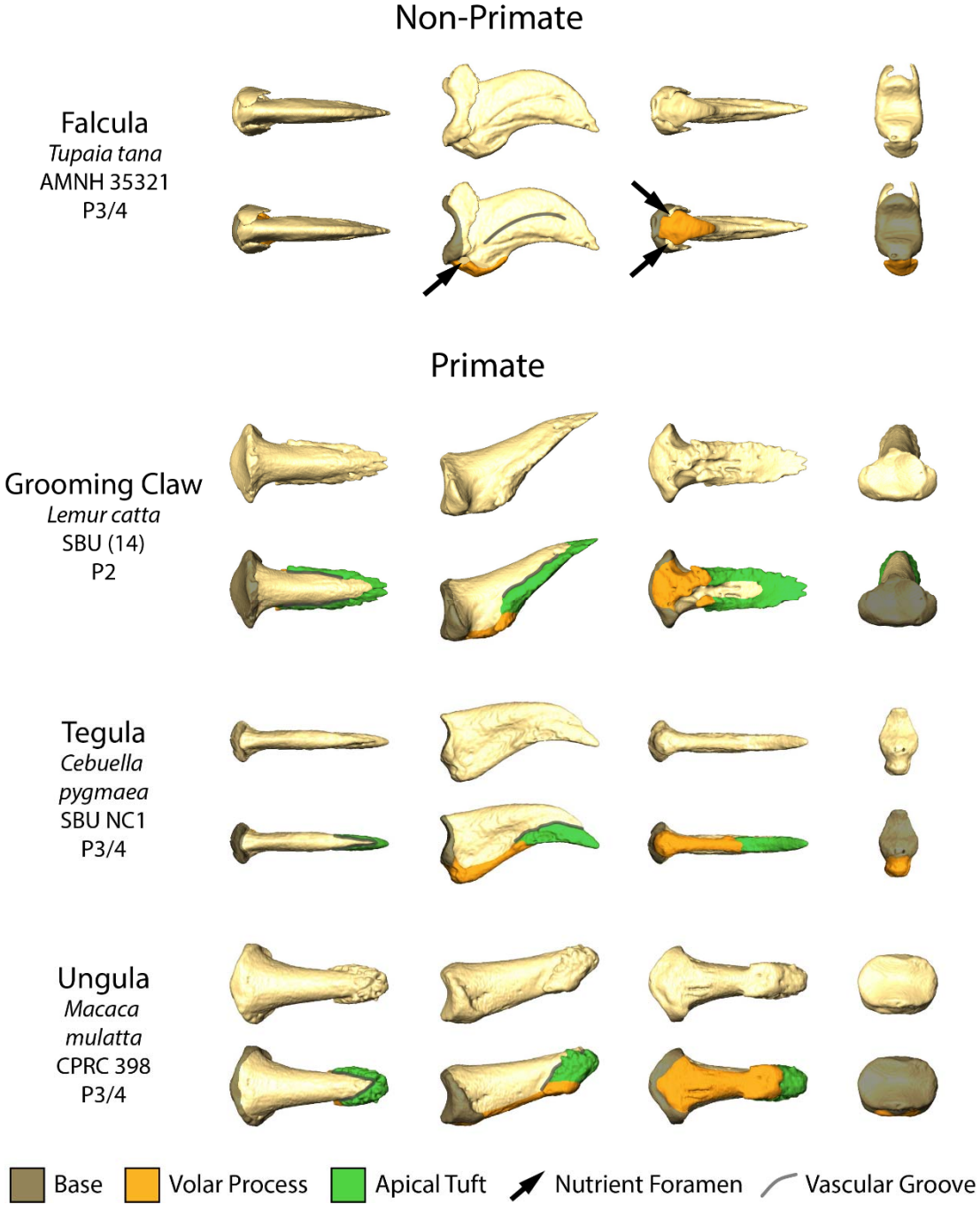

Fig. 4.4. Measurements used in analyses (1).
Illustrations of measurements ETH, FTH, VPL, MSH, ATH, WSM, and WIM taken on a range of distal phalanx shapes. See **Table 4.8** for measurement abbreviations and definitions.

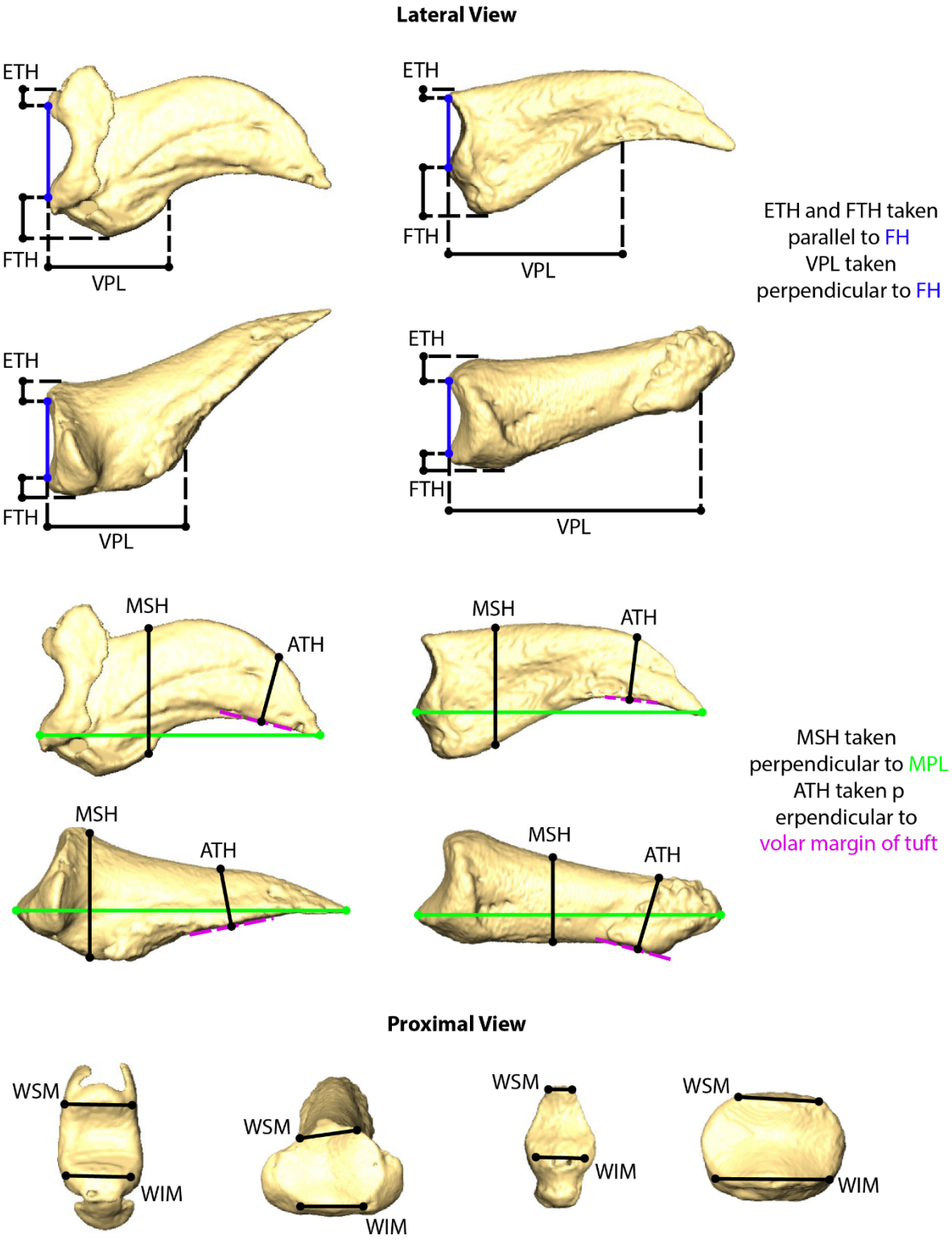

Fig. 4.5. Measurements used in analyses (2).
Illustrations of measurements FH, FIA, SIA, MPL, BW, MSW, and ATW taken on a range of distal phalanx shapes. See **Table 4.8** for measurement abbreviations and definitions.

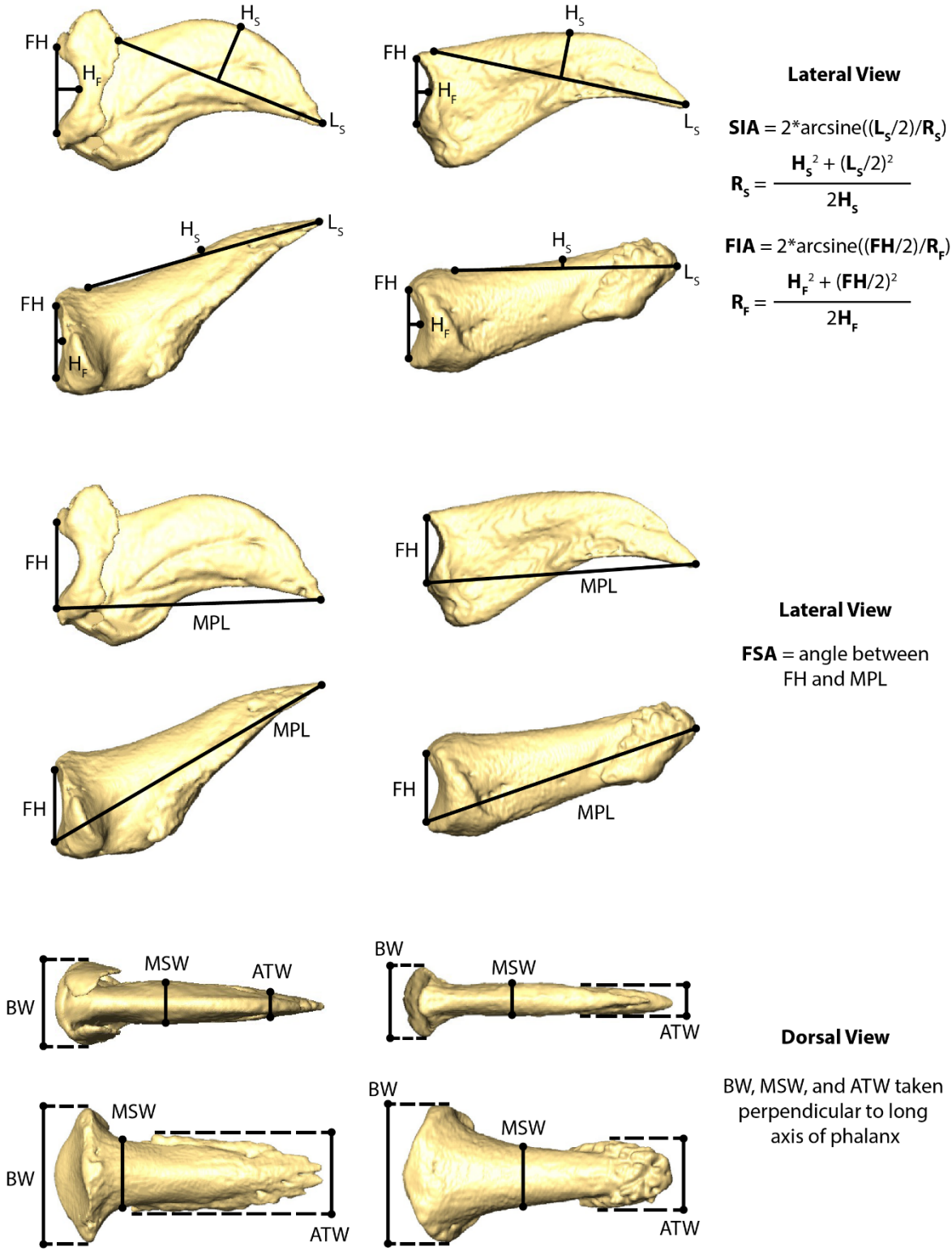

Fig. 4.6. PCA of ungulae, falculae, and tegulae.
PCA of ray-specific species means of extant taxa and fossil specimens. Variables with the highest loadings along each axis are listed along the top and right side of the graph. T denotes *Tarsipes rostratus*, the only non-primate to fall within ungula-bearing primate morphospace.

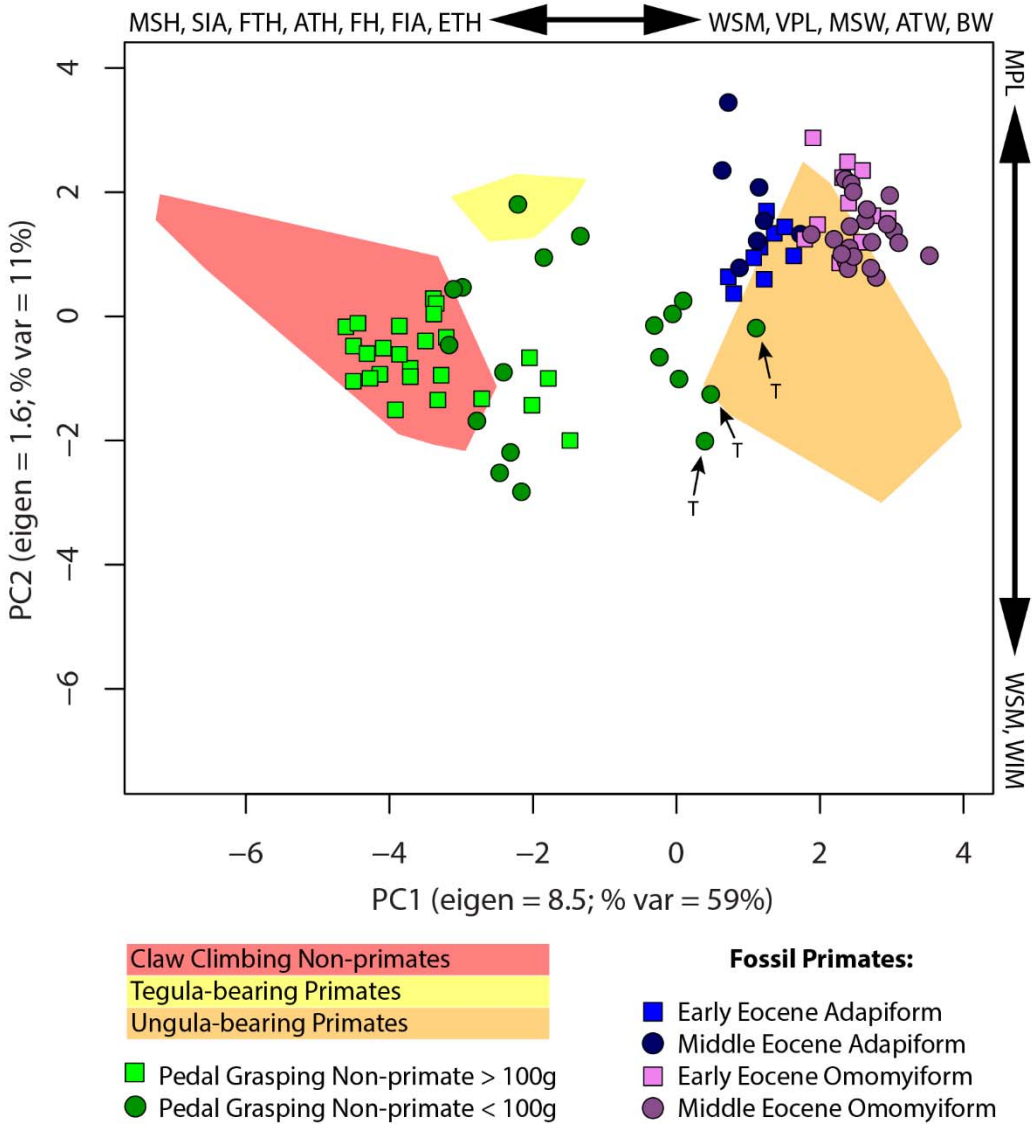

Fig. 4.7. DFA of ungulae, falculae, and tegulae.
DFA discriminating among claw climbing non-primates, tegula-bearing primates and ungula-bearing primates. Variables with the highest loadings along each axis are listed along the top and right side of the graph. T denotes *Tarsipes rostratus*, the only non-primate to fall within ungula-bearing primate morphospace. N denotes *Notharctus tenebrosus*, the adapiform which falls furthest from extant ungula-bearing primates. Other fossils attributed to species are indicated: C, *Cantius nunienus*; S, *Smilodectes gracilis*; O, *Omomys carteri*; Te, *Teilhardina brandti*.

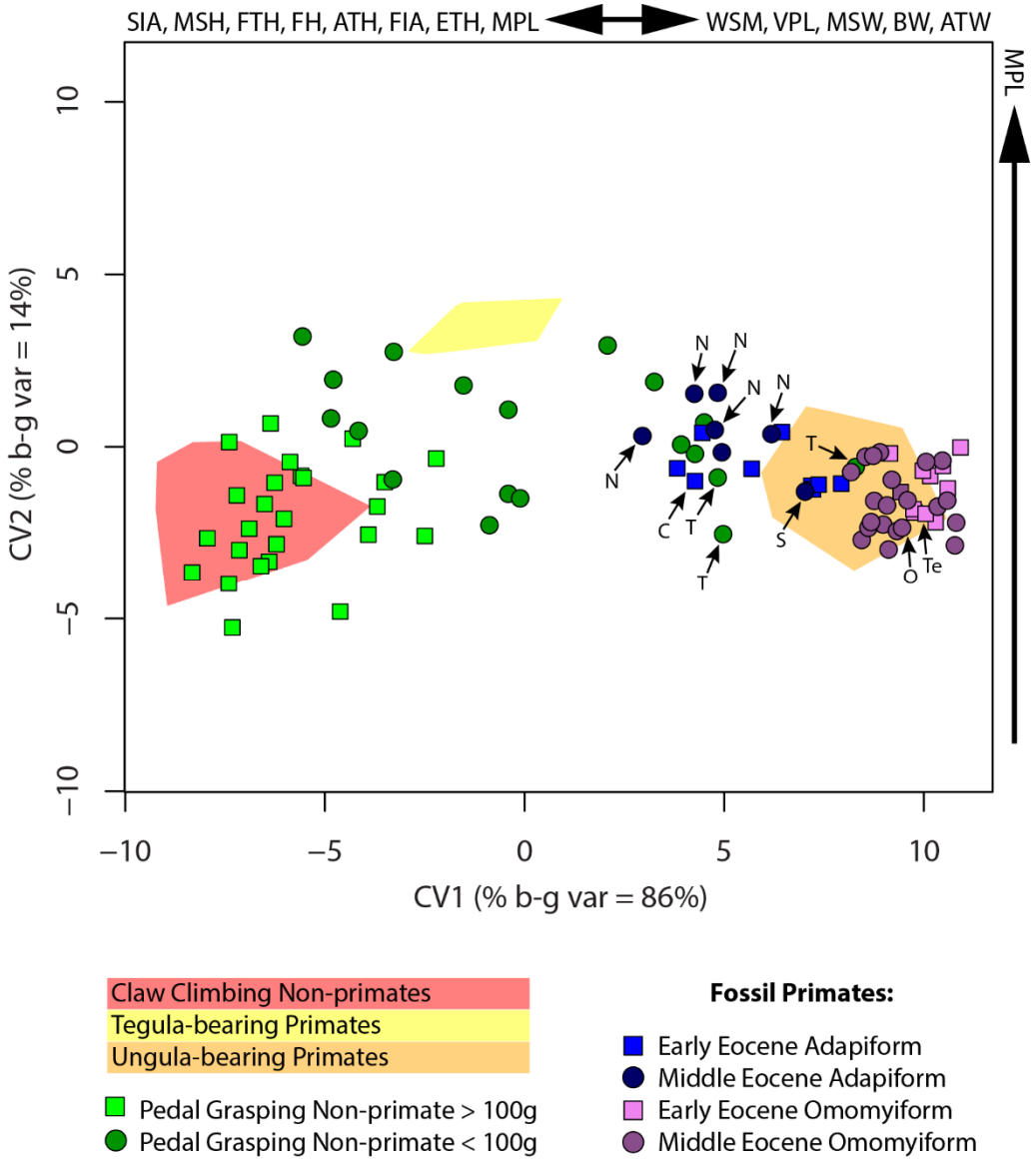

Fig. 4.8. Comparison of distal phalanx morphology.
The distal phalanges of pedal grasping non-primates compared to those of claw climbing non-primates, tegula-bearing primates, and ungula-bearing primates. Distal phalanges from pedal graspers tend to have relatively longer volar processes than do those of claw climbing mammals. This is most apparent in pedal graspers that weigh less than 100g. Of these species, *Tarsipes*, the honey possum, most closely resembles ungula-bearing primates as its postaxial digits (with the exceptions of grooming ungues) bear ungulae. Each phalanx is shown in dorsal (top) and lateral (bottom) views.

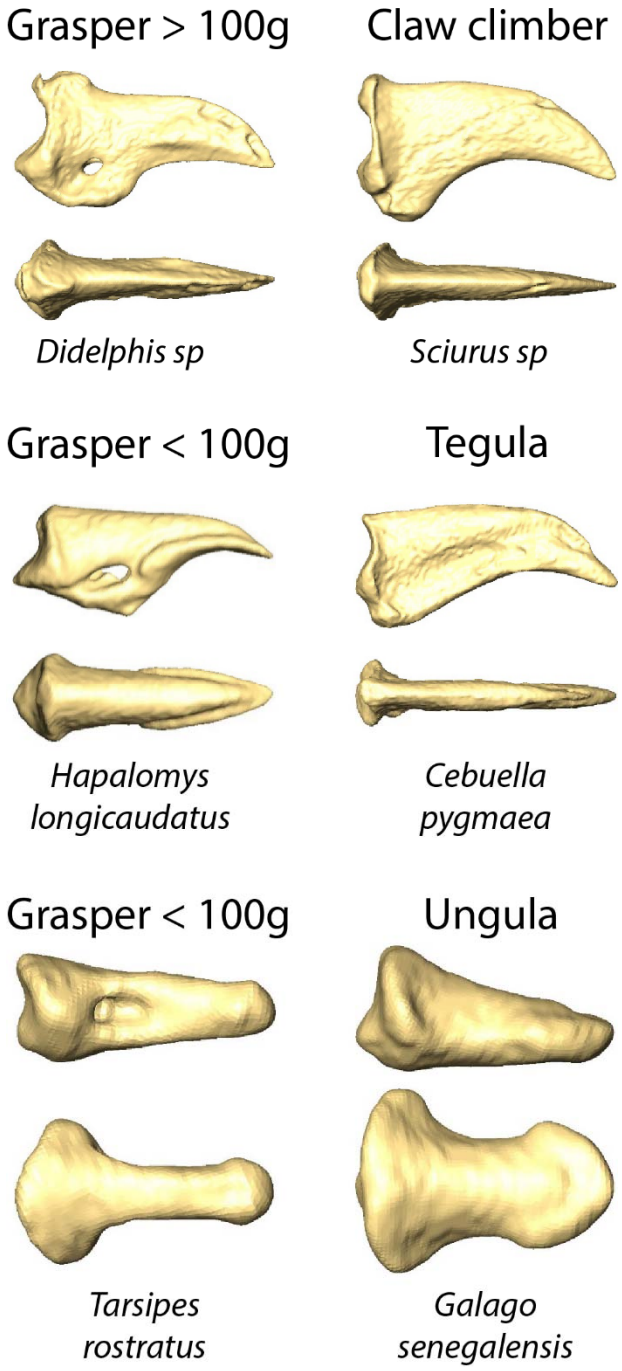

Fig. 4.9. Eocene primate distal phalanges.
An example of the variation among adapiforms and omomyiforms from the Early and Middle Eocene. Adapiforms as a whole tend to have relatively short volar processes and enlarged bilaterally occurring nutrient foramina. Of the adapiforms, *Notharctus tenebrosus* has the most proximally restricted volar process. Omomyiform distal phalanges tend to be dorso-volarly shallower and do not always possess clearly defined nutrient foramina. Each phalanx is shown in dorsal (left) and lateral (right) views.

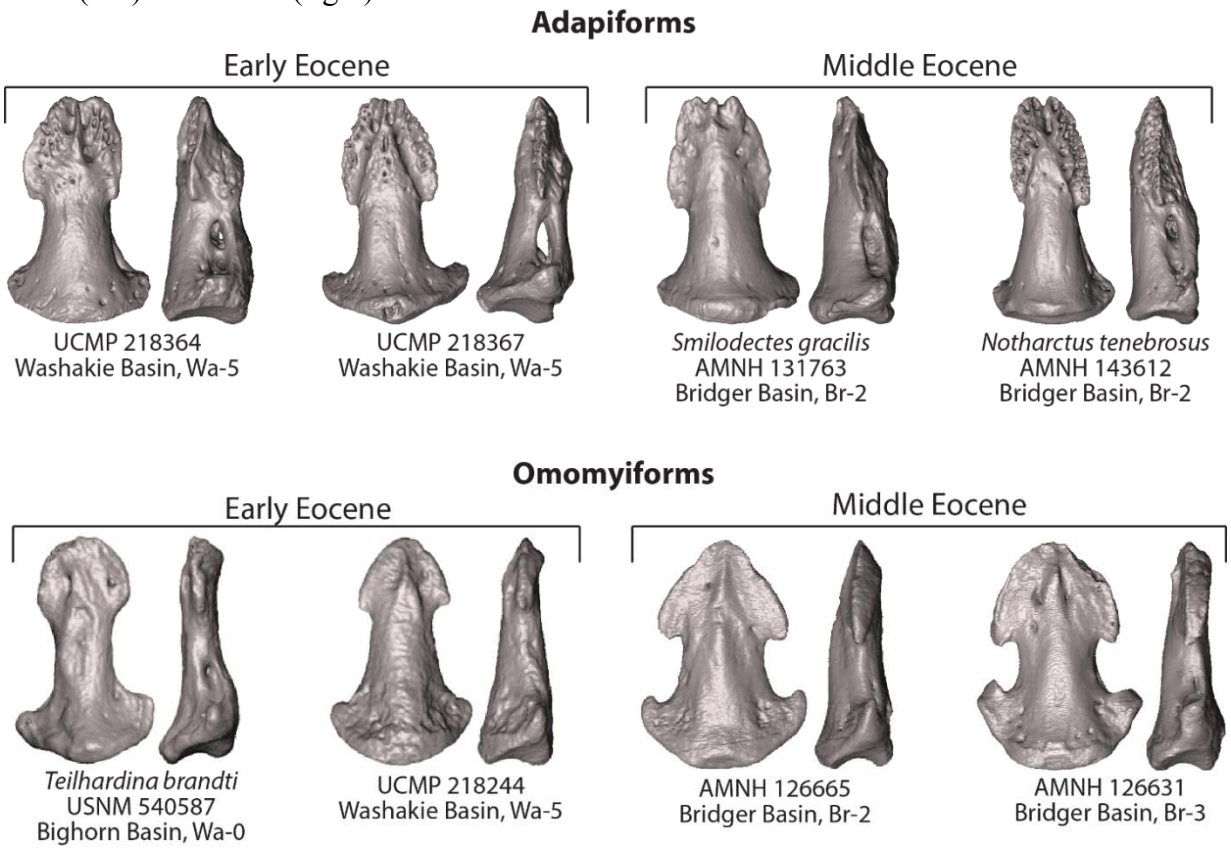

Fig. 4.10. Boxplots of FH and ETH.
Boxplots of Z-scores of FH (top) and ETH (bottom) indicating interquartile range and median with whiskers extending to the most extreme case that is not greater than 1.5x the interquartile range. Data points that fall outside of this are represented by open circles. Colors: non-primates are represented by white boxes, tegula-bearing primates by light grey, extant ungula-bearing primates (divided into locomotor groups) by medium grey, and fossil primates by dark grey.

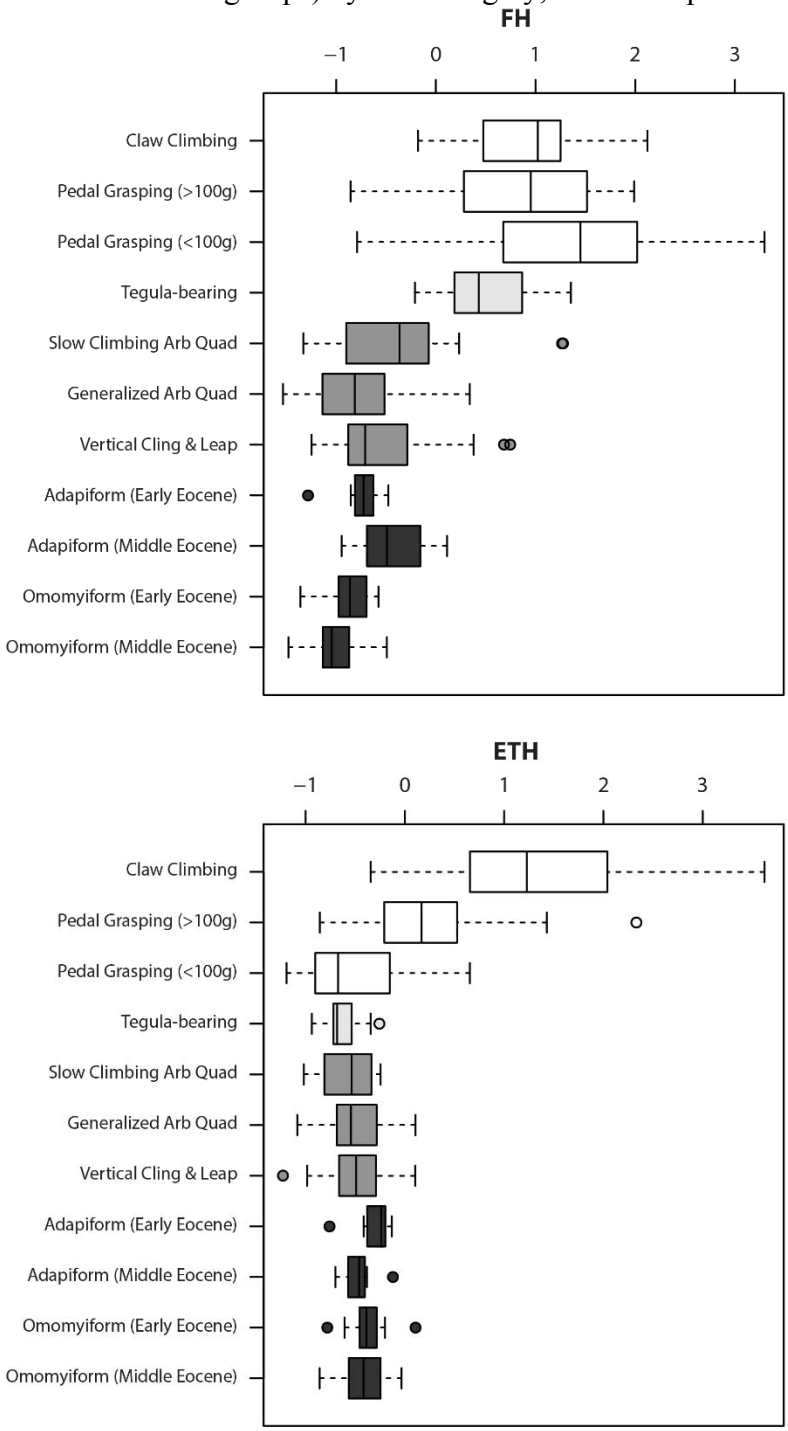

Fig. 4.11. Boxplots of FTH and MPL.
Boxplots of Z-scores of FTH (top) and MPL (bottom) indicating interquartile range and median with whiskers extending to the most extreme case that is not greater than 1.5x the interquartile range. Data points that fall outside of this are represented by open circles. Colors: non-primates are represented by white boxes, tegula-bearing primates by light grey, extant ungula-bearing primates (divided into locomotor groups) by medium grey, and fossil primates by dark grey.

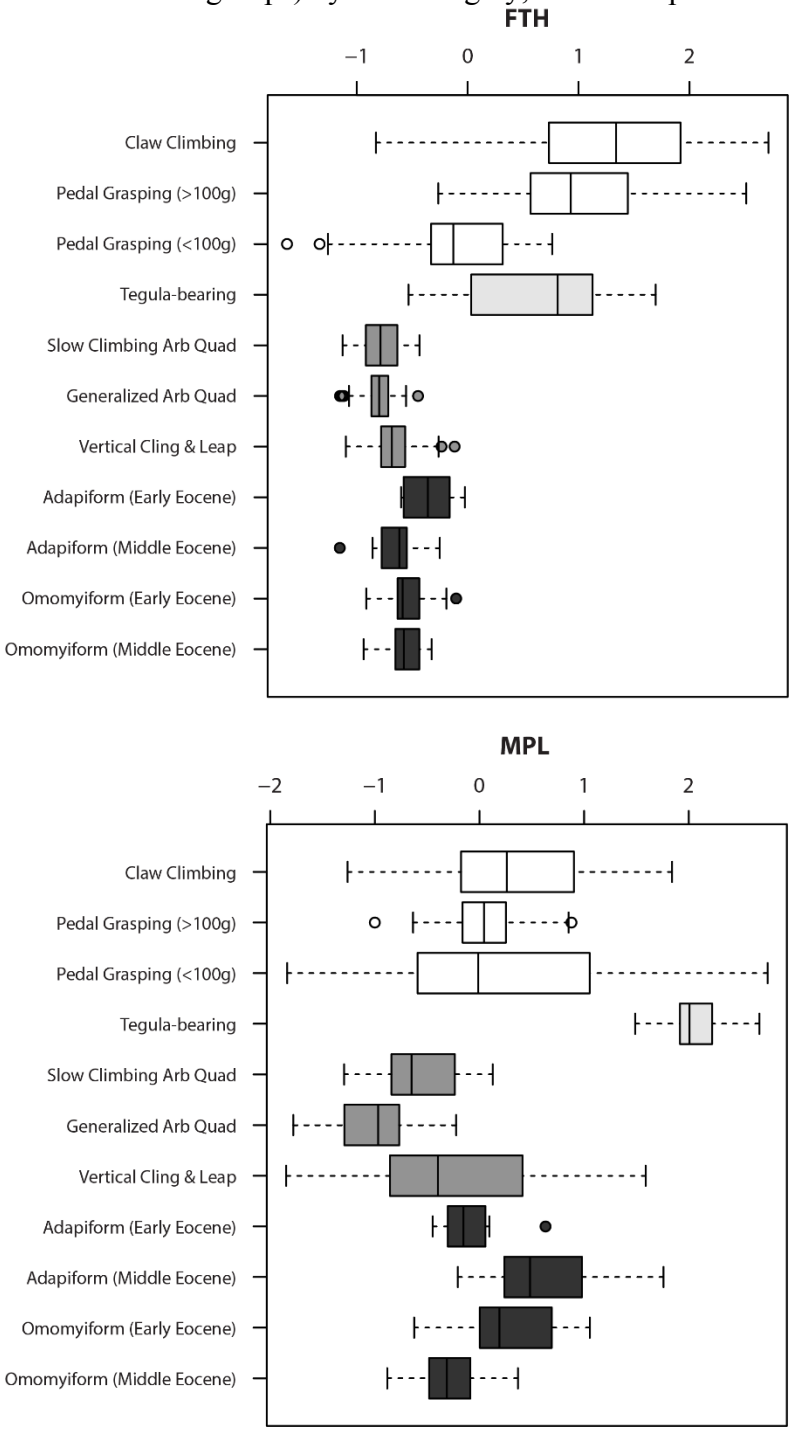

Fig. 4.12. Boxplots of VPL and MSH.
Boxplots of Z-scores of VPL (top) and MSH (bottom) indicating interquartile range and median with whiskers extending to the most extreme case that is not greater than 1.5x the interquartile range. Data points that fall outside of this are represented by open circles. Colors: non-primates are represented by white boxes, tegula-bearing primates by light grey, extant ungula-bearing primates (divided into locomotor groups) by medium grey, and fossil primates by dark grey.

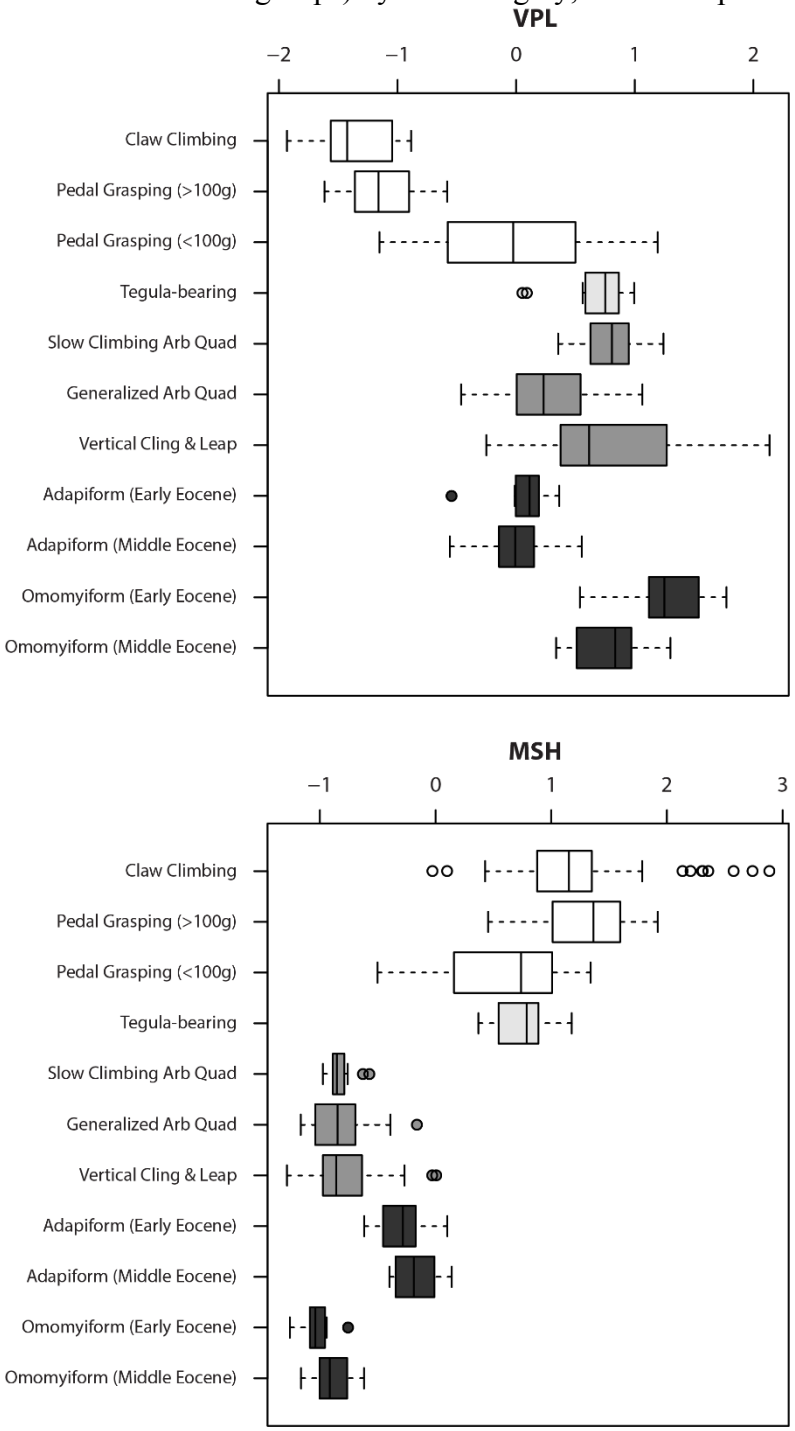

Fig. 4.13. Boxplots of ATH and BW.
Boxplots of Z-scores of ATH (top) and BW (bottom) indicating interquartile range and median with whiskers extending to the most extreme case that is not greater than 1.5x the interquartile range. Data points that fall outside of this are represented by open circles. Colors: non-primates are represented by white boxes, tegula-bearing primates by light grey, extant ungula-bearing primates (divided into locomotor groups) by medium grey, and fossil primates by dark grey.

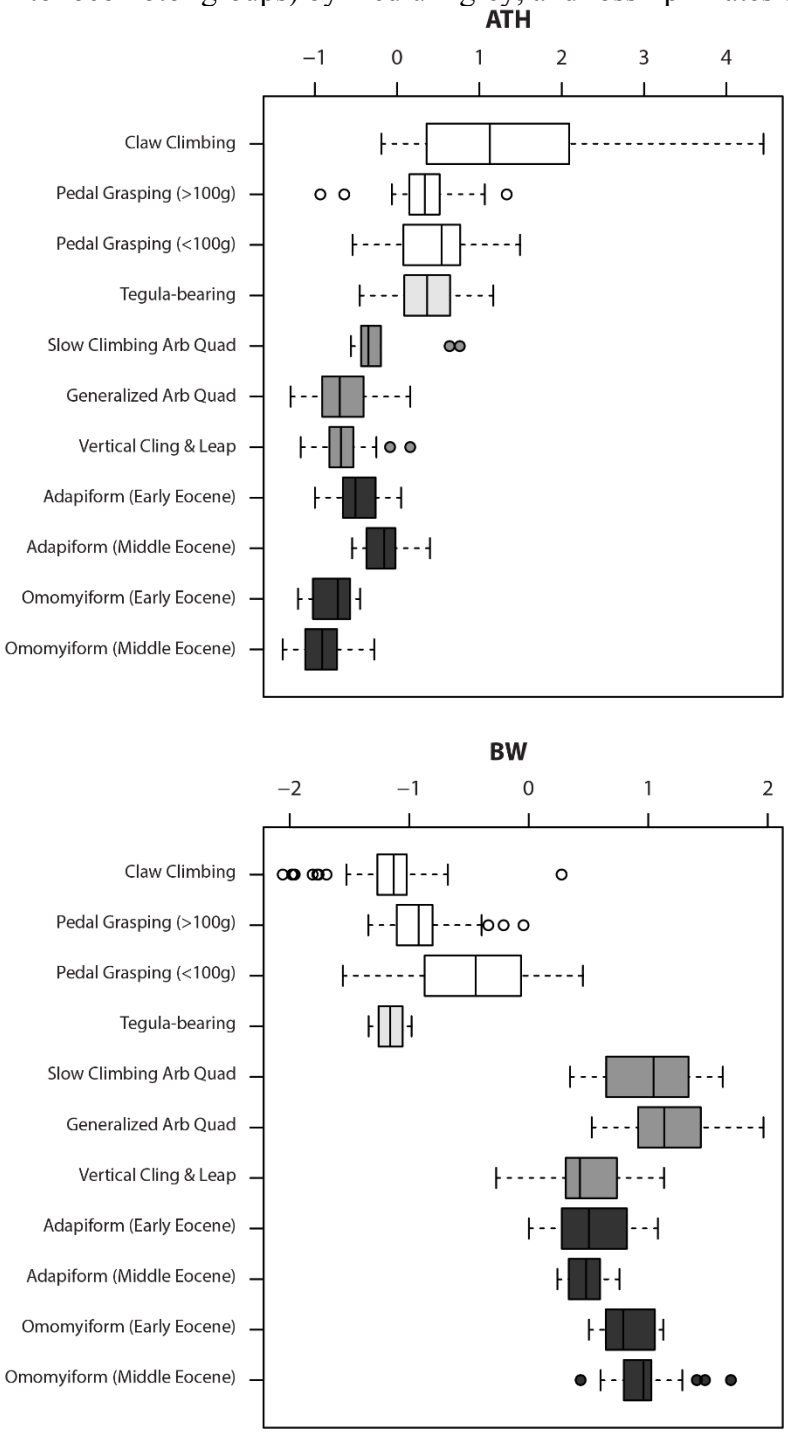

Fig. 4.14. Boxplots of MSW and ATW.
Boxplots of Z-scores of MSW (top) and ATW (bottom) indicating interquartile range and median with whiskers extending to the most extreme case that is not greater than 1.5x the interquartile range. Data points that fall outside of this are represented by open circles. Colors: non-primates are represented by white boxes, tegula-bearing primates by light grey, extant ungula-bearing primates (divided into locomotor groups) by medium grey, and fossil primates by dark grey.

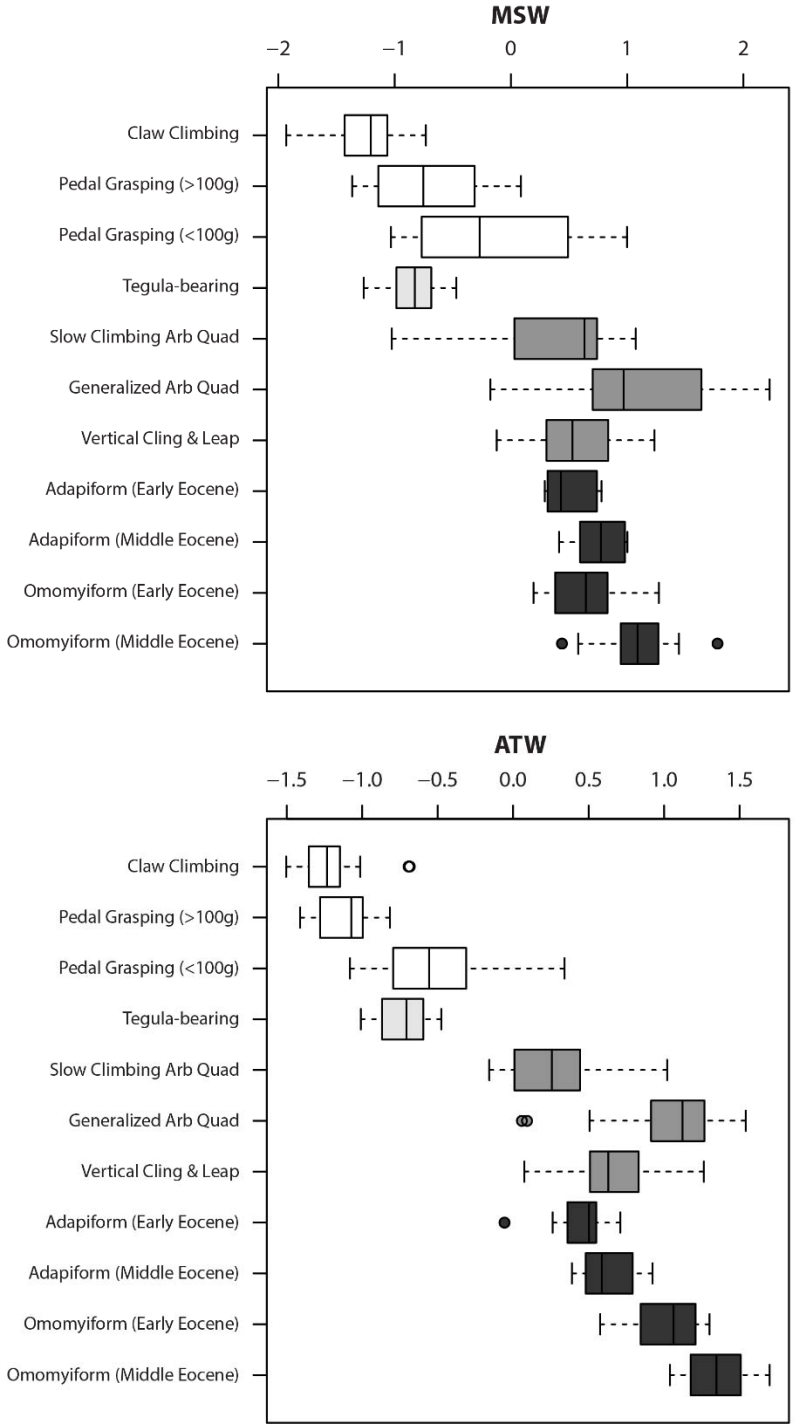

Fig. 4.15. Boxplots of WSM and WIM.
Boxplots of Z-scores of WSM (top) and WIM (bottom) indicating interquartile range and median with whiskers extending to the most extreme case that is not greater than 1.5x the interquartile range. Data points that fall outside of this are represented by open circles. Colors: non-primates are represented by white boxes, tegula-bearing primates by light grey, extant ungula-bearing primates (divided into locomotor groups) by medium grey, and fossil primates by dark grey.

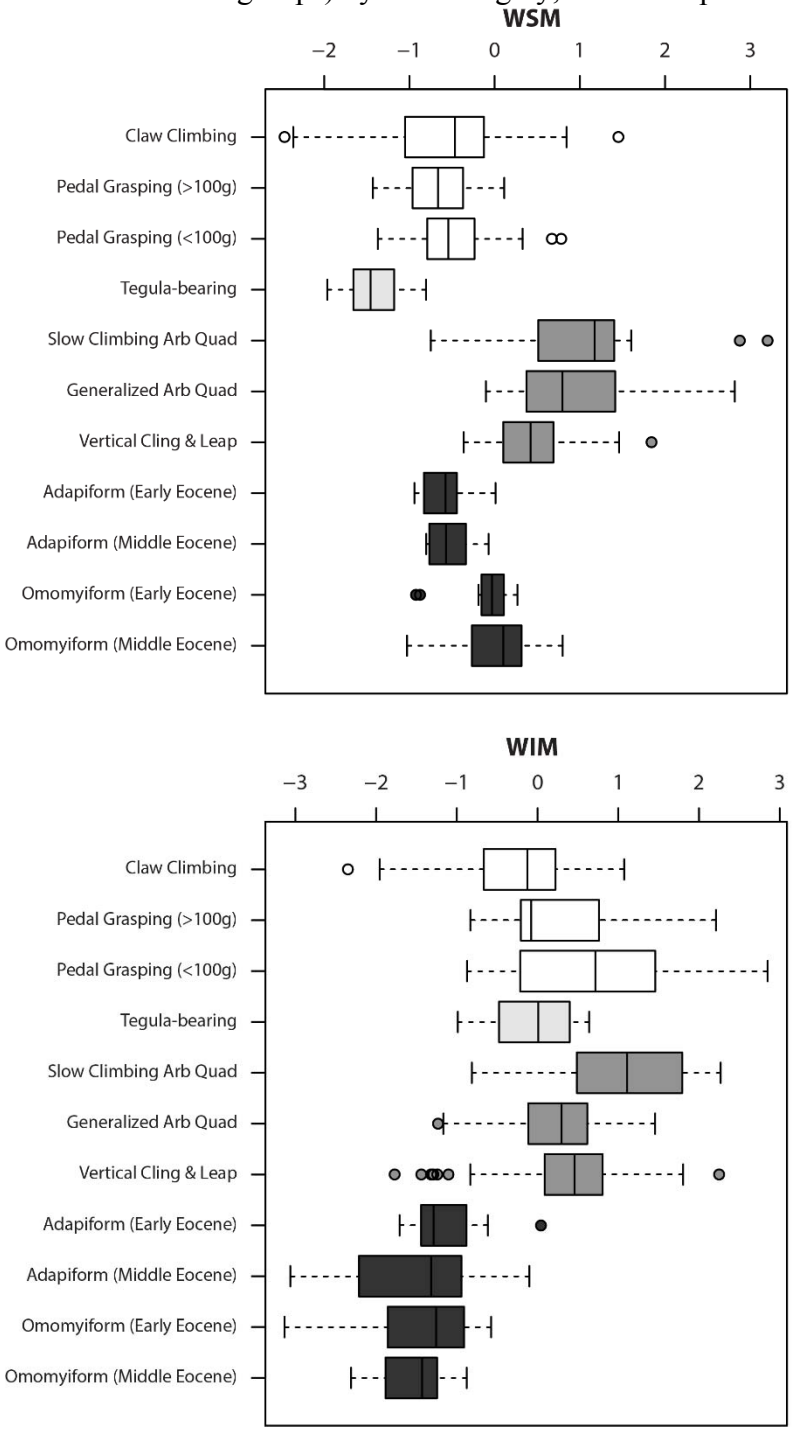

Fig. 4.16. Boxplots of SIA and FIA.
Boxplots of Z-scores of SIA (top) and FIA (bottom) indicating interquartile range and median with whiskers extending to the most extreme case that is not greater than 1.5x the interquartile range. Data points that fall outside of this are represented by open circles. Colors: non-primates are represented by white boxes, tegula-bearing primates by light grey, extant ungula-bearing primates (divided into locomotor groups) by medium grey, and fossil primates by dark grey.

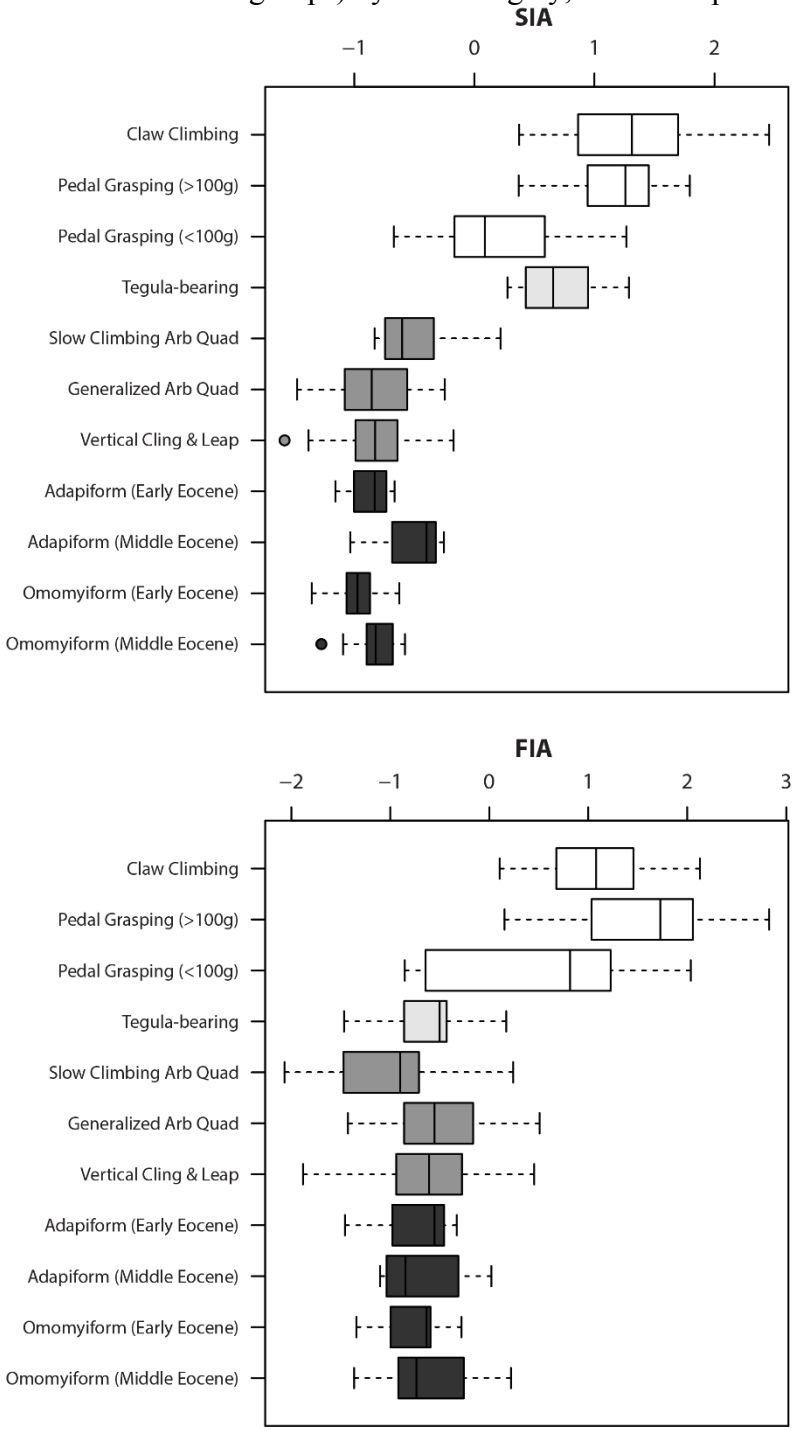

Fig. 4.17. Boxplots of FSA.
Boxplot of Z-scores of FSA indicating interquartile range and median with whiskers extending to the most extreme case that is not greater than 1.5x the interquartile range. Data points that fall outside of this are represented by open circles. Colors: non-primates are represented by white boxes, tegula-bearing primates by light grey, extant ungula-bearing primates (divided into locomotor groups) by medium grey, and fossil primates by dark grey.

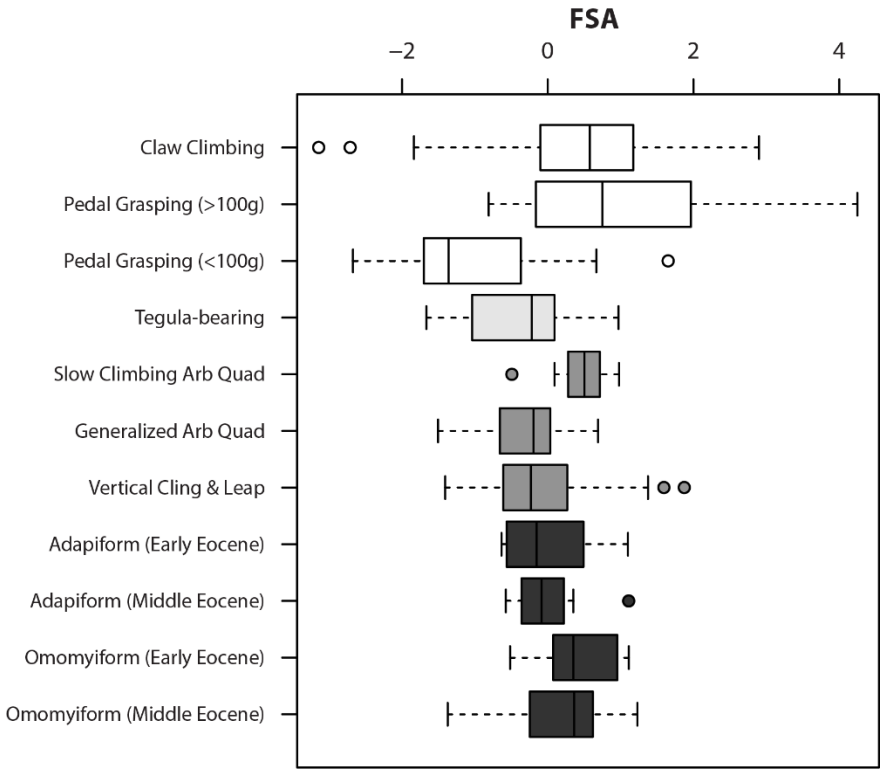

Fig. 4.18. DFA of locomotor groups.
DFA discriminating among ungula-bearing primates that primarily utilize vertical clinging and leaping, generalized arboreal quadrupedalism, and slow climbing arboreal quadrupedalism. Variables with the highest loadings along each axis are listed along the top and right side of the graph. Dotted lines are convex hulls drawn around Middle Eocene Adapiforms and Middle Eocene Omomyiforms. Fossils attributed to a species are indicated by letters N, *Notharctus tenebrosus*; C, *Cantius nunienus*; S, *Smilodectes gracilis*; O, *Omomys carteri*; Te, *Teilhardina brandti*.

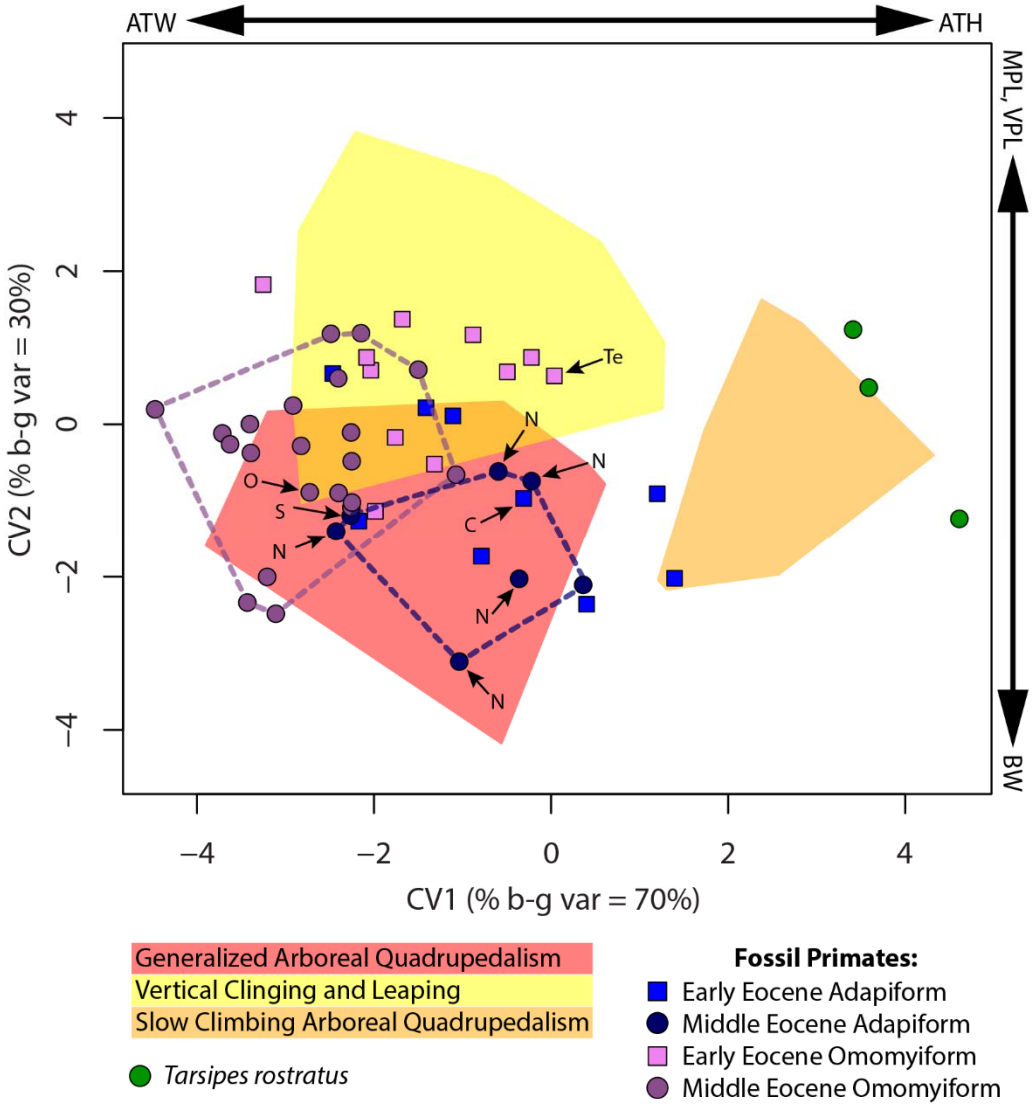

Fig. 4.19. Phylogeny in DFA of locomotor groups.
DFA discriminating among ungula-bearing primates that primarily utilize vertical clinging and leaping, generalized arboreal quadrupedalism, and slow climbing arboreal quadrupedalism with symbols denoting phylogenetic group. Variables with the highest loadings along each axis are listed along the top and right side of the graph. Shaded convex hulls (blue and purple) surround vertical clinging and leaping lemurids, generalized arboreal quadrupedalist lemurids, vertical clinging and leaping galagids, and generalized arboreal quadrupedalist galagids.

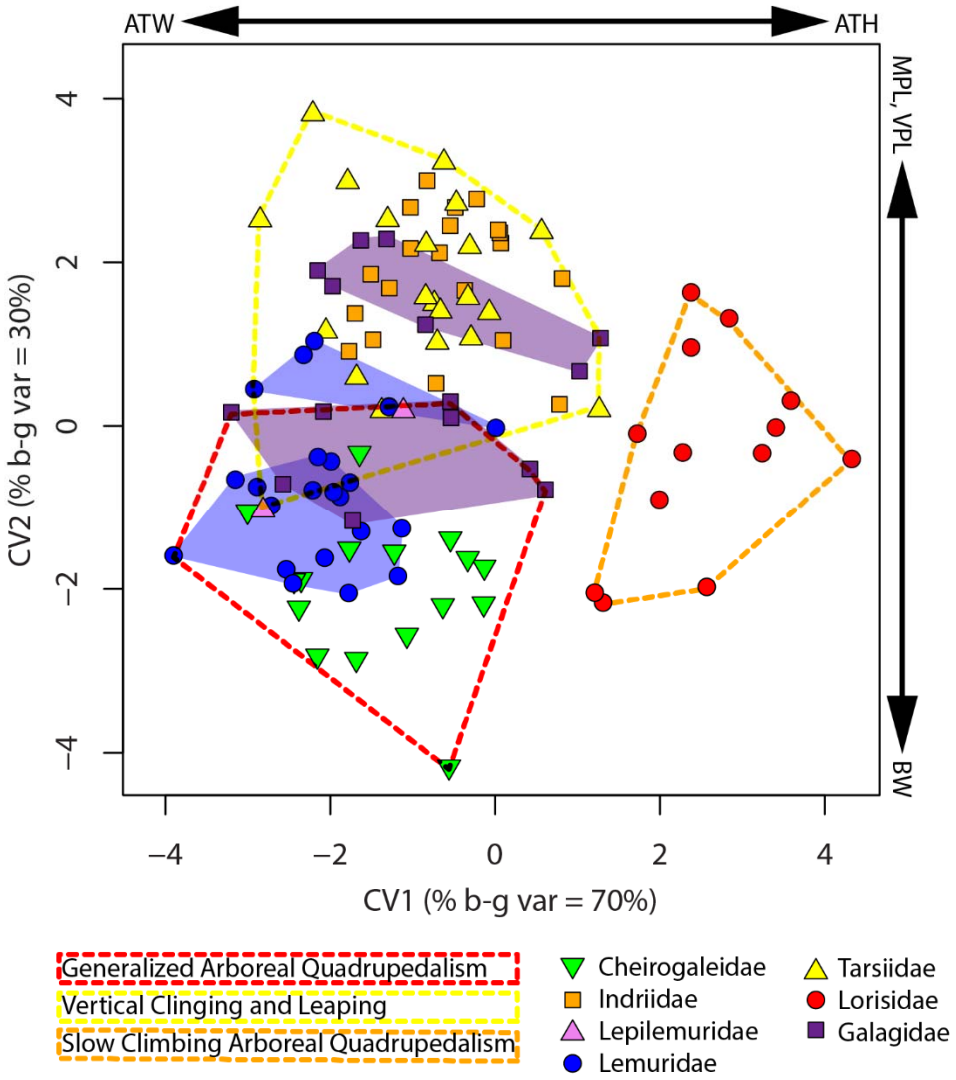

Fig. 4.20. Primate ungular phalanges.
Left column: distal phalanges from generalized arboreal quadrupeds; Middle: distal phalanges from vertical clingers and leapers; Right: distal phalanx from a slow climbing arboreal quadruped. Each phalanx is shown in dorsal (top) and lateral (bottom) views. The distal phalanges of slow climbing arboreal quadrupeds tend to be medio-laterally narrower with dorso-ventrally deeper apical tufts than the other two groups. Generalized arboreal quadrupeds tend to have distal phalanges that are relatively shorter and have medio-laterally wider bases and shorter volar processes than those of vertical clinging and leaping species.

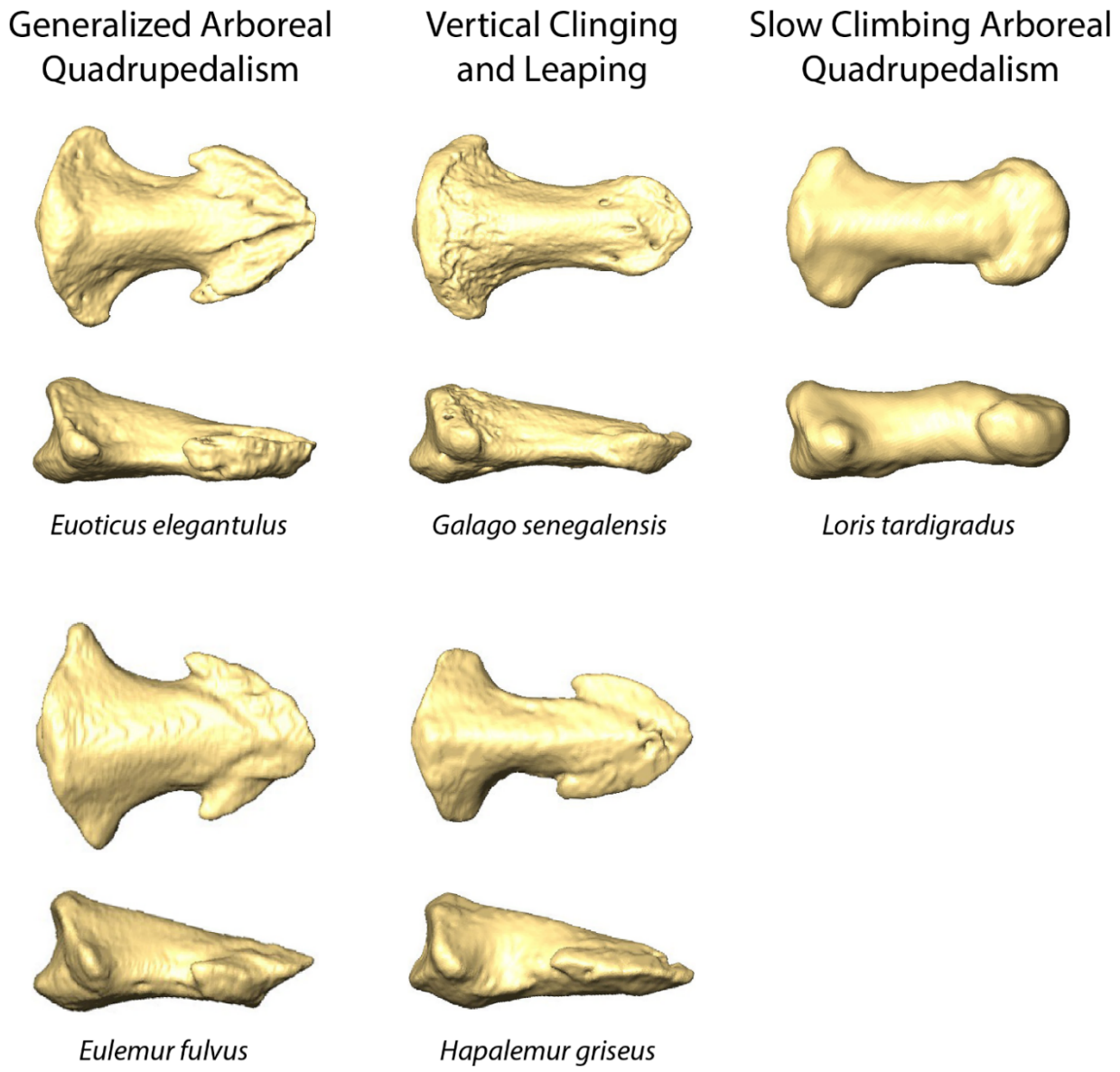

Fig. 4.21. Reduced falculae in small-bodied pedal graspers.
The falculae of tiny bodied pedal graspers (middle row) are smaller when compared to the apical pad and do not project beyond it as far as those of claw climbers do (top row). The honey possum, *Tarsipes rostratus*, possesses ungulae like those of primates (bottom row). Digit tips of each species are shown in dorsal (top) and lateral views (bottom) in which external tissue is rendered both opaque (left) and transparent (right). The external portion of the unguis is shaded in grey.

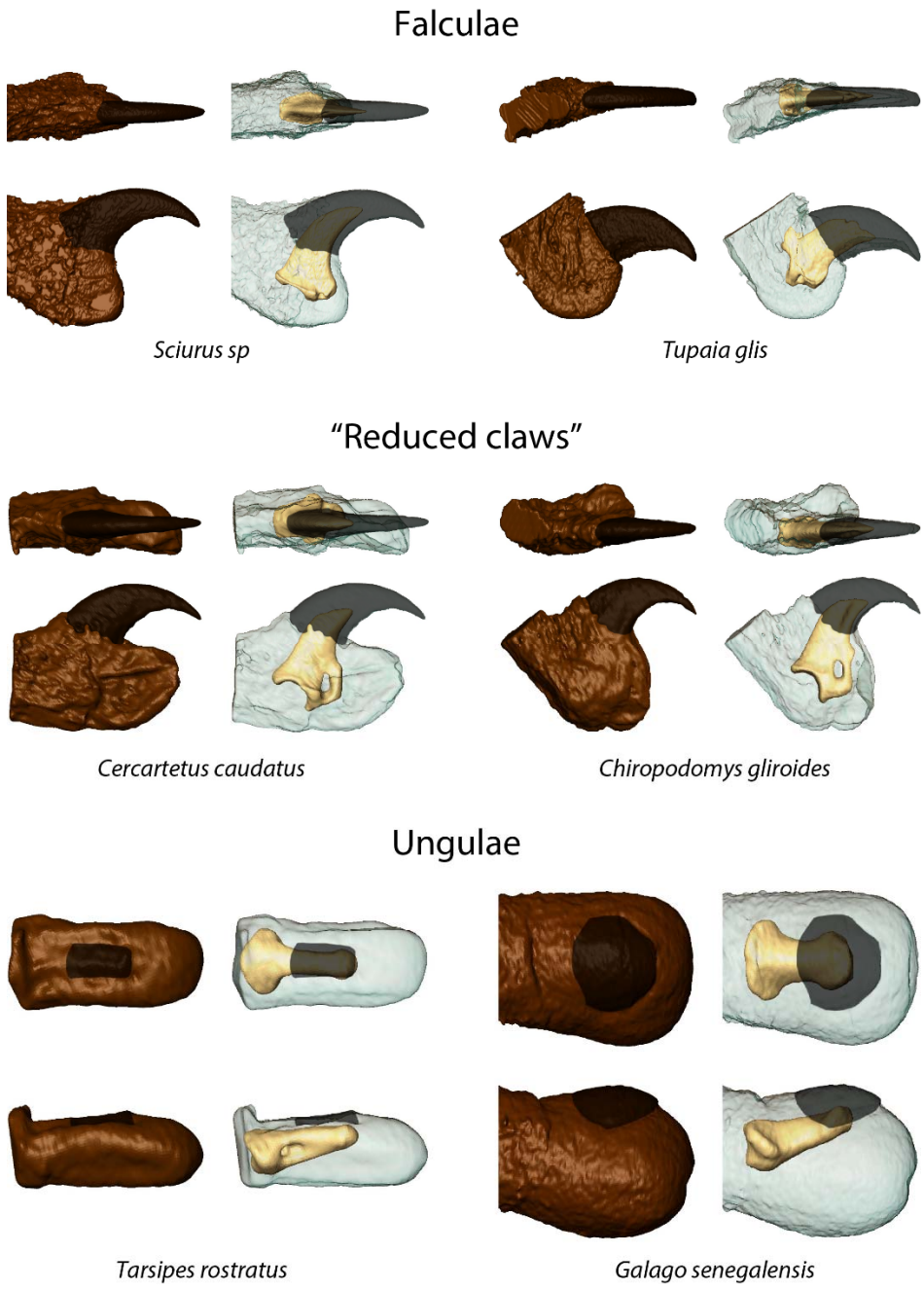

4.7 Tables

Table 4.1. Extant sample.
The elements sampled from each individual listed by institutional abbreviation and specimen number. See **Table 4.2** for institutional abbreviations. Rays: the rays from which distal phalanges were sampled; M, manual; P, pedal.

Specimen	Order/ Suborder	Infraorder/ Suborder	Parvorder/ Superfamily/ Family	Species	Rays
SBU nn	Haplorhini	Simiiformes	Platyrrhini	*Callimico goeldii*	M3/4, P3/4
AMNH 17574	Haplorhini	Simiiformes	Platyrrhini	*Callithrix sp.*	M3/4, P3/4
AMNH 22994	Haplorhini	Simiiformes	Platyrrhini	*Callithrix sp.*	M3/4, P3/4
SBU NCx1	Haplorhini	Simiiformes	Platyrrhini	*Callithrix sp.*	M3/4, P3/4
SBU NCx2	Haplorhini	Simiiformes	Platyrrhini	*Callithrix sp.*	M3/4
AMNH 244101	Haplorhini	Simiiformes	Platyrrhini	*Cebuella pygmaea*	P3/4, P3/4, P3/4
SBU NC1	Haplorhini	Simiiformes	Platyrrhini	*Cebuella pygmaea*	P3/4, P3/4, P3/4, P3/4
SBU NLe1	Haplorhini	Simiiformes	Platyrrhini	*Leontopithecus rosalia*	M3/4
SBU NLe2	Haplorhini	Simiiformes	Platyrrhini	*Leontopithecus rosalia*	M3/4, P3/4, P3/4
AMNH 235275	Haplorhini	Simiiformes	Platyrrhini	*Leontopithecus sp.*	M3/4, P3/4
SBU NSg9	Haplorhini	Simiiformes	Platyrrhini	*Saguinus fuscicollis*	M3/4, P3/4
SBU NSg1	Haplorhini	Simiiformes	Platyrrhini	*Saguinus sp.*	M3/4, P3/4
SBU NSg2	Haplorhini	Simiiformes	Platyrrhini	*Saguinus sp.*	M3/4, P3/4
AMNH 166856	Haplorhini	Tarsiiformes	Tarsiidae	*Carlito syrichta*	M2, M3/4, M3/4, M5, P4, P5
AMNH 203296	Haplorhini	Tarsiiformes	Tarsiidae	*Carlito syrichta*	M3/4, P4
AMNH 203297	Haplorhini	Tarsiiformes	Tarsiidae	*Carlito syrichta*	M3/4, P4, P5
AMNH 242091	Haplorhini	Tarsiiformes	Tarsiidae	*Carlito syrichta*	M3/4
AMNH 106649	Haplorhini	Tarsiiformes	Tarsiidae	*Cephalopachus bancanus*	M3/4, P4
AMNH 106010	Haplorhini	Tarsiiformes	Tarsiidae	*Cephalopachus bancanus*	M3/4, P4
AMNH 106754	Haplorhini	Tarsiiformes	Tarsiidae	*Cephalopachus bancanus*	M2, M3/4, M5, P4, P4, P5
AMNH 109216	Haplorhini	Tarsiiformes	Tarsiidae	*Tarsius pelengensis*	M3/4, P4
AMNH 109367	Haplorhini	Tarsiiformes	Tarsiidae	*Tarsius pelengensis*	M2, M3/4, M5, P4, P4, P5
AMNH 109368	Haplorhini	Tarsiiformes	Tarsiidae	*Tarsius pelengensis*	M3/4, P4
AMNH 109369	Haplorhini	Tarsiiformes	Tarsiidae	*Tarsius pelengensis*	M3/4, P4
AMNH 196477	Haplorhini	Tarsiiformes	Tarsiidae	*Tarsius pumilus*	M2, M3/4, M3/4, M5, P4, P5
USNM 199694	Strepsirrhini	Chiromyiformes	Daubentoniidae	*Daubentonia madagascariensis*	M2, M3/4, M5, P3/4, P3/4, P5
AMNH 100654	Strepsirrhini	Lemuriformes	Cheirogaleidae	*Cheirogaleus medius*	M3/4, P3/4, P3/4, P5
DPC 1285	Strepsirrhini	Lemuriformes	Cheirogaleidae	*Cheirogaleus medius*	P3/4
DPC 130	Strepsirrhini	Lemuriformes	Cheirogaleidae	*Cheirogaleus medius*	P3/4
AMNH 174424	Strepsirrhini	Lemuriformes	Cheirogaleidae	*Microcebus murinus*	M3/4, P3/4
AMNH 185627	Strepsirrhini	Lemuriformes	Cheirogaleidae	*Microcebus murinus*	M3/4, P3/4
AMNH 185628	Strepsirrhini	Lemuriformes	Cheirogaleidae	*Microcebus murinus*	M3/4, P3/4
DPC 035	Strepsirrhini	Lemuriformes	Cheirogaleidae	*Microcebus murinus*	P3/4
DPC 7017	Strepsirrhini	Lemuriformes	Cheirogaleidae	*Microcebus murinus*	P3/4, P5
DPC 097	Strepsirrhini	Lemuriformes	Cheirogaleidae	*Mirza coquereli*	P3/4
DPC 137	Strepsirrhini	Lemuriformes	Cheirogaleidae	*Mirza coquereli*	M2, M3/4, M3/4, M5, P5
DPC 2301	Strepsirrhini	Lemuriformes	Cheirogaleidae	*Mirza coquereli*	P3/4, P3/4
AMNH 100645	Strepsirrhini	Lemuriformes	Cheirogaleidae	*Phaner furcifer*	M2, M3/4, M5, P3/4, P3/4, P5

AMNH 100831	Strepsirrhini	Lemuriformes	Cheirogaleidae	*Phaner furcifer*	M3/4
USNM 18437	Strepsirrhini	Lemuriformes	Indriidae	*Avahi laniger*	P3/4, P3/4, P5
USNM 83651	Strepsirrhini	Lemuriformes	Indriidae	*Avahi laniger*	M3/4
USNM 83652	Strepsirrhini	Lemuriformes	Indriidae	*Avahi laniger*	M3/4
AMNH 170494	Strepsirrhini	Lemuriformes	Indriidae	*Avahi laniger*	M2, M3/4, P3/4, P3/4, P5
CMNH B343	Strepsirrhini	Lemuriformes	Indriidae	*Indri indri*	M2, M3/4, M3/4, M5, P3/4, P3/4, P5
DPC 6273	Strepsirrhini	Lemuriformes	Indriidae	*Propithecus coquereli*	P3/4, P5
CMNH B1155	Strepsirrhini	Lemuriformes	Indriidae	*Propithecus diadema*	M3/4, M3/4, M5, P3/4, P5
AMNH 170463	Strepsirrhini	Lemuriformes	Indriidae	*Propithecus verreauxi*	M3/4, P3/4
AMNH 170489	Strepsirrhini	Lemuriformes	Indriidae	*Propithecus verreauxi*	M2, M3/4, M5, P3/4, P5, P5
AMNH 170491	Strepsirrhini	Lemuriformes	Indriidae	*Propithecus verreauxi*	M3/4, P3/4
AMNH 31255	Strepsirrhini	Lemuriformes	Indriidae	*Propithecus verreauxi*	P3/4
DPC 1397	Strepsirrhini	Lemuriformes	Indriidae	*Propithecus verreauxi*	P3/4
AMNH 170708	Strepsirrhini	Lemuriformes	Lemuridae	*Eulemur albifrons*	M3/4, P3/4
AMNH 170711	Strepsirrhini	Lemuriformes	Lemuridae	*Eulemur albifrons*	M5
AMNH 170717	Strepsirrhini	Lemuriformes	Lemuridae	*Eulemur albifrons*	M3/4, P3/4
SBU (13)	Strepsirrhini	Lemuriformes	Lemuridae	*Eulemur fulvus*	M3/4, P3/4
DPC 6793	Strepsirrhini	Lemuriformes	Lemuridae	*Eulemur macaco*	P3/4, P3/4, P5
DPC 6287	Strepsirrhini	Lemuriformes	Lemuridae	*Eulemur rufus*	P3/4, P5
AMNH 170675	Strepsirrhini	Lemuriformes	Lemuridae	*Hapalemur griseus*	M2, M3/4, P3/4
AMNH 170680	Strepsirrhini	Lemuriformes	Lemuridae	*Hapalemur griseus*	M3/4, P3/4
AMNH 170689	Strepsirrhini	Lemuriformes	Lemuridae	*Hapalemur griseus*	P3/4, P5
DPC 1359	Strepsirrhini	Lemuriformes	Lemuridae	*Hapalemur griseus*	P3/4, P5
SBU (12)	Strepsirrhini	Lemuriformes	Lemuridae	*Hapalemur griseus*	P3/4
AMNH 200881	Strepsirrhini	Lemuriformes	Lemuridae	*Lemur catta*	M2, M3/4, M3/4, M5, P3/4, P3/4, P5
SBU (14)	Strepsirrhini	Lemuriformes	Lemuridae	*Lemur catta*	M3/4, P3/4
CMNH 1382	Strepsirrhini	Lemuriformes	Lemuridae	*Varecia sp.*	M3/4, M3/4
CMNH 1383	Strepsirrhini	Lemuriformes	Lemuridae	*Varecia sp.*	M2, M5
AMNH 17338	Strepsirrhini	Lemuriformes	Lemuridae	*Varecia variegata*	M3/4, P3/4
AMNH 18040	Strepsirrhini	Lemuriformes	Lemuridae	*Varecia variegata*	M3/4
AMNH 22897	Strepsirrhini	Lemuriformes	Lemuridae	*Varecia variegata*	M3/4, M3/4
AMNH 170557	Strepsirrhini	Lemuriformes	Lepilemuridae	*Lepilemur leucopus*	M3/4, P3/4
AMNH 170560	Strepsirrhini	Lemuriformes	Lepilemuridae	*Lepilemur leucopus*	M3/4
AMNH 170562	Strepsirrhini	Lemuriformes	Lepilemuridae	*Lepilemur leucopus*	P3/4
AMNH 170565	Strepsirrhini	Lemuriformes	Lepilemuridae	*Lepilemur leucopus*	P3/4
USNM 598551	Strepsirrhini	Lorisiformes	Galagidae	*Euoticus elegantulus*	M3/4, M5, P3/4, P3/4
AMNH 86502	Strepsirrhini	Lorisiformes	Galagidae	*Galago moholi*	M3/4
AMNH 87065	Strepsirrhini	Lorisiformes	Galagidae	*Galago moholi*	M3/4, P3/4
DPC 3190	Strepsirrhini	Lorisiformes	Galagidae	*Galago moholi*	M2, M3/4, M3/4, M5
DPC 003	Strepsirrhini	Lorisiformes	Galagidae	*Galago senegalensis*	P3/4
DPC 1063	Strepsirrhini	Lorisiformes	Galagidae	*Galago senegalensis*	P3/4
SBU (15)	Strepsirrhini	Lorisiformes	Galagidae	*Galago senegalensis*	M3/4, M3/4, M5, P3/4, P3/4, P5
SBU PGa4	Strepsirrhini	Lorisiformes	Galagidae	*Galago senegalensis*	M3/4, P3/4
AMNH 215180	Strepsirrhini	Lorisiformes	Galagidae	*Galagoides demidovii*	M3/4, P3/4
AMNH 80801	Strepsirrhini	Lorisiformes	Galagidae	*Otolemur crassicaudatus*	M3/4
SBU PGa1163	Strepsirrhini	Lorisiformes	Galagidae	*Otolemur crassicaudatus*	M3/4, P3/4
AMNH 212576	Strepsirrhini	Lorisiformes	Lorisidae	*Arctocebus calabarensis*	M3/4, P3/4
AMNH 212954	Strepsirrhini	Lorisiformes	Lorisidae	*Arctocebus calabarensis*	P3/4
AMNH 34257	Strepsirrhini	Lorisiformes	Lorisidae	*Loris tardigradus*	M3/4, P3/4
DPC 2925	Strepsirrhini	Lorisiformes	Lorisidae	*Loris tardigradus*	M5, P3/4, P5
AMNH 90381	Strepsirrhini	Lorisiformes	Lorisidae	*Nycticebus coucang*	M3/4, P3/4

AMNH 102027	Strepsirrhini	Lorisiformes	Lorisidae	*Nycticebus coucang*	M3/4
AMNH 16591	Strepsirrhini	Lorisiformes	Lorisidae	*Nycticebus coucang*	M3/4, P3/4
DPC 1906	Strepsirrhini	Lorisiformes	Lorisidae	*Nycticebus coucang*	M3/4, M5, P5
AMNH 52682	Strepsirrhini	Lorisiformes	Lorisidae	*Perodicticus potto*	M3/4, P3/4
AMNH 52685	Strepsirrhini	Lorisiformes	Lorisidae	*Perodicticus potto*	M3/4, P5
AMNH 52698	Strepsirrhini	Lorisiformes	Lorisidae	*Perodicticus potto*	M3/4, P3/4
AMNH 170605	Afrosoricida	Tenrecomorpha	Tenrecidae	*Echinops telfairi*	P2
AMNH 170607	Afrosoricida	Tenrecomorpha	Tenrecidae	*Echinops telfairi*	P3/4
AMNH 212918	Afrosoricida	Tenrecomorpha	Tenrecidae	*Echinops telfairi*	M3/4, P3/4
AMNH 119675	Carnivora	Caniformia	Ailuridae	*Ailurus fulgens*	P3/4, P5
AMNH 81064	Carnivora	Caniformia	Ailuridae	*Ailurus fulgens*	M3/4, P3/
AMNH 85346	Carnivora	Caniformia	Ailuridae	*Ailurus fulgens*	P3/4
AMNH 15069	Carnivora	Caniformia	Mustelidae	*Martes americana*	M2, M3/4, M5, P3/4
AMNH 29057	Carnivora	Caniformia	Mustelidae	*Martes americana*	M3/4
AMNH 35639	Carnivora	Caniformia	Mustelidae	*Martes americana*	P3/4, P3/4
AMNH 266597	Carnivora	Caniformia	Procyonidae	*Potos flavus*	M3/4, P3/4
AMNH 266598	Carnivora	Caniformia	Procyonidae	*Potos flavus*	M3/4, P3/4
AMNH 266599	Carnivora	Caniformia	Procyonidae	*Potos flavus*	M3/4, P3/4
AMNH 267053	Carnivora	Caniformia	Procyonidae	*Potos flavus*	P3/4, P3/4
AMNH 146544	Carnivora	Caniformia	Procyonidae	*Procyon lotor*	M3/4, P3/4
AMNH 245620	Carnivora	Caniformia	Procyonidae	*Procyon lotor*	P3/4, P3/4
AMNH 35890	Carnivora	Caniformia	Procyonidae	*Procyon lotor*	M3/4, P3/4
AMNH 181	Carnivora	Feliformia	Viverridae	*Arctictis binturong*	P3/4
AMNH 22906	Carnivora	Feliformia	Viverridae	*Arctictis binturong*	M3/4, P3/4
AMNH 80162	Carnivora	Feliformia	Viverridae	*Arctictis binturong*	M3/4, P3/4
AMNH 80163	Carnivora	Feliformia	Viverridae	*Arctictis binturong*	M3/4, P3/4
USNM 144662	Dermoptera		Cynocephalidae	*Cynocephalus volans*	M3/4
YPM 963	Dermoptera		Cynocephalidae	*Cynocephalus volans*	P5
USNM 15502	Dermoptera		Cynocephalidae	*Galeopterus variegatus*	M3/4, P2, P3/4
AMNH 160105	Diprotodontia	Phalangeriformes	Petauroidea	*Dactylopsila trivirgata*	M3/4, P4
AMNH 42993	Diprotodontia	Phalangeriformes	Petauroidea	*Petaurus breviceps*	M3/4, P4
AMNH 237507	Diprotodontia	Phalangeriformes	Petauroidea	*Petaurus sp.*	M3/4, P4
AMNH 196925	Diprotodontia	Phalangeriformes	Petauroidea	*Tarsipes rostratus*	M3/4, M5, P4
AMNH 109803	Diprotodontia	Phalangeriformes	Phalangeroidea	*Cercartetus caudatus*	M2, M3/4, M3/4, M5, P4
AMNH 104089	Diprotodontia	Phalangeriformes	Phalangeroidea	*Phalanger gymnotis*	P4, P4
AMNH 79864	Diprotodontia	Phalangeriformes	Phalangeroidea	*Phalanger orientalis*	M3/4, M3/4, P4, P4
AMNH 35698	Diprotodontia	Phalangeriformes	Phalangeroidea	*Trichosurus vulpecula*	P4
AMNH 35708	Diprotodontia	Phalangeriformes	Phalangeroidea	*Trichosurus vulpecula*	M3/4, P4
AMNH 42996	Diprotodontia	Phalangeriformes	Phalangeroidea	*Trichosurus vulpecula*	M3/4, P4, P4
AMNH 65611	Diprotodontia	Vombatiformes	Phascolarctidae	*Phascolarctos cinereus*	M2, M3/4, P4
AMNH 234979	Didelphimorphia		Didelphidae	*Caluromys philander*	P3/4
AMNH 234986	Didelphimorphia		Didelphidae	*Caluromys philander*	P3/4, P3/4
AMNH 48188	Didelphimorphia		Didelphidae	*Caluromys philander*	M2, P3/4, P3/4
SBU (3)	Didelphimorphia		Didelphidae	*Didelphis sp.*	M3/4, P3/4
AMNH 146514	Didelphimorphia		Didelphidae	*Didelphis virginiana*	M3/4, P3/4
AMNH 146532	Didelphimorphia		Didelphidae	*Didelphis virginiana*	M3/4
AMNH 146551	Didelphimorphia		Didelphidae	*Didelphis virginiana*	M3/4, M3/4, P5
AMNH 90435	Didelphimorphia		Didelphidae	*Didelphis virginiana*	P2
AMNH 133098	Didelphimorphia		Didelphidae	*Philander opossum*	M2, P3/4
AMNH 133182	Didelphimorphia		Didelphidae	*Philander opossum*	M3/4, P3/4, P3/4
AMNH 241147	Rodentia	Anomaluromorpha	Anomaluridae	*Anomalurus derbianus*	P5
AMNH 50606	Rodentia	Anomaluromorpha	Anomaluridae	*Idiurus macrotis*	M3/4, P3/4

AMNH 102119	Rodentia	Myomorpha	Muridae	*Chiropodomys gliroides*	M3/4, P2 P3/4, P3/4, P5
AMNH 54754	Rodentia	Myomorpha	Muridae	*Hapalomys longicaudatus*	M3/4, M5, P3/4, P5
AMNH 181037	Rodentia	Myomorpha	Nesomyidae	*Dendromus insignis*	M3/4, P3/4, P5
AMNH 241344	Rodentia	Myomorpha	Nesomyidae	*Prionomys batesi*	P3/4
AMNH 51017	Rodentia	Sciuromorpha	Sciuridae	*Heliosciurus rufobrachium*	M2, P3/4, P3/4
AMNH 184935	Rodentia	Sciuromorpha	Sciuridae	*Petaurista petaurista*	P3/4, P3/4
AMNH 184939	Rodentia	Sciuromorpha	Sciuridae	*Petaurista petaurista*	M3/4, P3/4
AMNH 184942	Rodentia	Sciuromorpha	Sciuridae	*Petaurista petaurista*	P3/4, P3/4
AMNH 51173	Rodentia	Sciuromorpha	Sciuridae	*Protoxerus strangeri*	P3/4, P3/4, P5
AMNH 52098	Rodentia	Sciuromorpha	Sciuridae	*Protoxerus strangeri*	M3/4, M3/4, P3/4
AMNH 22837	Rodentia	Sciuromorpha	Sciuridae	*Ratufa indica*	M3/4
AMNH 70208	Rodentia	Sciuromorpha	Sciuridae	*Ratufa indica*	P3/4
AMNH 60792	Rodentia	Sciuromorpha	Sciuridae	*Sciurus carolinensis*	M3/4, P3/4
AMNH 35863	Rodentia	Sciuromorpha	Sciuridae	*Sciurus sp.*	M3/4, P3/4
SBU (2)	Rodentia	Sciuromorpha	Sciuridae	*Sciurus sp.*	M3/4, P3/4
SBU MRd10	Rodentia	Sciuromorpha	Sciuridae	*Sciurus sp.*	M3/4, P3/4
USNM 481106	Scandentia		Ptilocercidae	*Ptilocercus lowii*	M3/4, P3/4
USNM 488055	Scandentia		Ptilocercidae	*Ptilocercus lowii*	M3/4, P3/4
USNM 488058	Scandentia		Ptilocercidae	*Ptilocercus lowii*	M3/4, P3/4
USNM 488067	Scandentia		Ptilocercidae	*Ptilocercus lowii*	M3/4, P3/4
USNM 488069	Scandentia		Ptilocercidae	*Ptilocercus lowii*	M3/4, P2, P3/4
USNM 488072	Scandentia		Ptilocercidae	*Ptilocercus lowii*	M3/4, P3/4
AMNH 215175	Scandentia		Tupaiidae	*Tupaia glis*	M3/4, P3/4
AMNH 215176	Scandentia		Tupaiidae	*Tupaia glis*	M3/4, P2
AMNH 215177	Scandentia		Tupaiidae	*Tupaia glis*	M3/4, P3/4
AMNH 35921	Scandentia		Tupaiidae	*Tupaia tana*	M3/4, M3/4, P2, P3/4, P3/4, P3/4, P5

Table 4.2. Group designations for extant species sample.
See text for explanations of groups and citations. Locomotor groupings are provided for ungula-bearing primates and size categories for pedal-grasping non-primates.

Clade	Species	Group
Primates > Haplorhini > Simiiformes > Platyrrhini > Callitrichinae	*Callimico goeldii*	Tegula-bearing
	Callithrix sp	Tegula-bearing
	Cebuella pygmaea	Tegula-bearing
	Leontopithecus rosalia	Tegula-bearing
	Leontopithecus sp	Tegula-bearing
	Saguinus fuscicollis	Tegula-bearing
	Saguinus sp	Tegula-bearing
Primates > Haplorhini > Tarsiiformes	*Carlito syrichta*	Ungula-bearing Vertical clinging and leaping
	Cephalopachus bancanus	Ungula-bearing Vertical clinging and leaping
	Tarsius pelengensis	Ungula-bearing Vertical clinging and leaping
	Tarsius pumilus	Ungula-bearing Vertical clinging and leaping
Primates > Strepsirrhini > Chiromyiformes	*Daubentonia madagascariensis*	Tegula-bearing
Primates > Strepsirrhini > Lemuriformes > Cheirogaleidae	*Cheirogaleus medius*	Ungula-bearing Generalized arboreal quadrupedalism
	Microcebus murinus	Ungula-bearing Generalized arboreal quadrupedalism
	Mirza coquereli	Ungula-bearing Generalized arboreal quadrupedalism
	Phaner furcifer	Ungula-bearing Generalized arboreal quadrupedalism
Primates > Strepsirrhini > Lemuriformes > Indriidae	*Avahi laniger*	Ungula-bearing Vertical clinging and leaping
	Indri indri	Ungula-bearing Vertical clinging and leaping
	Propithecus coquereli	Ungula-bearing Vertical clinging and leaping
	Propithecus diadema	Ungula-bearing Vertical clinging and leaping
	Propithecus verreauxi	Ungula-bearing Vertical clinging and leaping
Primates > Strepsirrhini > Lemuriformes > Lemuridae	*Eulemur albifrons*	Ungula-bearing Generalized arboreal quadrupedalism
	Eulemur fulvus	Ungula-bearing Generalized arboreal quadrupedalism
	Eulemur macaco	Ungula-bearing Generalized arboreal quadrupedalism
	Eulemur rufus	Ungula-bearing Generalized arboreal quadrupedalism
	Hapalemur griseus	Ungula-bearing Vertical clinging and leaping
	Lemur catta	Ungula-bearing Generalized arboreal quadrupedalism
	Varecia sp	Ungula-bearing Generalized arboreal quadrupedalism

	Varecia variegata	Ungula-bearing Generalized arboreal quadrupedalism
Primates > Strepsirrhini > Lemuriformes > Lepilemuridae	*Lepilemur leucopus*	Ungula-bearing Vertical clinging and leaping
Primates > Strepsirrhini > Lorisiformes >Galagidae	*Euoticus elegantulus*	Ungula-bearing Generalized arboreal quadrupedalism
	Galago moholi	Ungula-bearing Vertical clinging and leaping
	Galago senegalensis	Ungula-bearing Vertical clinging and leaping
	Galagoides demidovii	Ungula-bearing Generalized arboreal quadrupedalism
	Otolemur crassicaudatus	Ungula-bearing Generalized arboreal quadrupedalism
Primates > Strepsirrhini > Lorisiformes >Lorisidae	*Arctocebus calabarensis*	Ungula-bearing Slow climbing arboreal quadrupedalism
	Loris tardigradus	Ungula-bearing Slow climbing arboreal quadrupedalism
	Nycticebus coucang	Ungula-bearing Slow climbing arboreal quadrupedalism
	Perodicticus potto	Ungula-bearing Slow climbing arboreal quadrupedalism
Non-Primate > Afrosoricida	*Echinops telfairi*	Claw climbing
	Ailurus fulgens	Claw climbing
Non-Primate > Carnivora	*Arctictis binturong*	Claw climbing
	Martes americana	Claw climbing
	Potos flavus	Claw climbing
	Procyon lotor	Claw climbing
Non-Primate > Dermoptera	*Cynocephalus volans*	Claw climbing
	Galeopterus variegatus	Claw climbing
Non-Primate > Diprotodontia	*Cercartetus caudatus*	Pedal grasping < 100g
	Dactylopsila trivirgata	Pedal grasping > 100g
	Petaurus breviceps	Pedal grasping > 100g
	Petaurus sp	Pedal grasping > 100g
	Phalanger gymnotis	Pedal grasping > 100g
	Phalanger orientalis	Pedal grasping > 100g
	Phascolarctos cinerus	Pedal grasping > 100g
	Tarsipes rostratus	Pedal grasping < 100g
	Trichosurus vulpecula	Pedal grasping > 100g
Non-Primate > Didelphimorphia	*Caluromys philander*	Pedal grasping > 100g
	Didelphis sp	Pedal grasping > 100g

	Didelphis virginiana	Pedal grasping > 100g
	Philander opossum	Pedal grasping > 100g
Non-Primate > Rodentia	*Anomalurus derbianus*	Claw climbing
	Chiropodomys gliroides	Pedal grasping < 100g
	Dendromus insignis	Pedal grasping < 100g
	Hapalomys longicaudatus	Pedal grasping < 100g
	Heliosciurus rufobrachium	Claw climbing
	Idiurus macrotis	Claw climbing
	Petaurista petaurista	Claw climbing
	Prionomys batesi	Pedal grasping < 100g
	Protoxerus strangeri	Claw climbing
	Ratufa indica	Claw climbing
	Sciurus carolinensis	Claw climbing
	Sciurus sp	Claw climbing
Non-Primate > Scandentia	*Ptilocercus lowii*	Claw climbing
	Tupaia glis	Claw climbing
	Tupaia tana	Claw climbing

Table 4.3. Institutional abbreviations.
Abbreviations for institutions from which specimens were sampled.

Abbreviation	Institution
AMNH	American Museum of Natural History, New York, NY, USA
CMNH	Cleveland Museum of Natural History, Cleveland, OH, USA
DPC	Duke Lemur Center, Durham, NC, USA
SBU	Stony Brook University, Stony Brook, NY, USA
UCMP	University of California Museum of Paleontology, Berkeley, CA, USA
UM	University of Michigan Museum of Paleontology, Ann Arbor, MI, USA
USNM	National Museum of Natural History, Smithsonian Institution, Washington, DC, USA

Table 4.4. Group sample sizes.
The number of specimens, individuals, species, and ray-specific species means sampled for each group. Ungula-bearing primates (total) is the sum of the three ungula-bearing locomotor groups (vertical clinging and leaping, generalized arboreal quadrupedalism, and slow-climbing quadrupedalism).

Group	Specimens	Individuals	Species	Means (n)
Claw climbing non-primates	96	47	19	47
Pedal grasping non-primates (> 100g)	41	19	11	25
Pedal grasping non-primates (< 100g)	21	6	6	19
Tegula bearing primates	34	14	8	18
Vertical clinging and leaping	108	40	13	54
Generalized arboreal quadrupedalism	69	30	14	42
Slow climbing arboreal quadrupedalism	22	11	4	13
Ungula bearing primates (total)	199	81	31	109

Table 4.5. Fossil sample.

Specimen	Taxon	Species	Region/Locality	Relative Age
UM 112882	Adapiform	*Cantius nunienus*	Bridger Basin, WY (SP-98)	Bridgerian (Br-1a)
AMNH FM 11474	Adapiform	*Notharctus tenebrosus*	Bridger Basin, WY (Little Dry Creek)	Bridgerian (Br-2)
AMNH FM 131764 (a)	Adapiform	*Notharctus tenebrosus*	Bridger Basin, WY (Forbidden City)	Bridgerian (Br-2)
AMNH FM 131764 (b)	Adapiform	*Notharctus tenebrosus*	Bridger Basin, WY (Forbidden City)	Bridgerian (Br-2)
AMNH FM 143612_2	Adapiform	*Notharctus tenebrosus*	Bridger Basin, WY (ALX-00-02)	Bridgerian (Br-2)
AMNH FM 143612_4	Adapiform	*Notharctus tenebrosus*	Bridger Basin, WY (ALX-00-02)	Bridgerian (Br-2)
AMNH FM 131763	Adapiform	*Smilodectes gracilis*	Bridger Basin, WY (Hermes Hill)	Bridgerian (Br-2)
AMNH FM 131766	Adapiform	Indet	Bridger Basin, WY (Leahanne's Lintel)	Bridgerian (Br-2)
UCMP 236082	Adapiform	Indet	Mutigny, France (v6167)	Ypresian
UCMP 147533	Adapiform	Indet	Washakie Basin, WY (v70243)	Wasatchian (Wa-3)
UCMP 147534	Adapiform	Indet	Washakie Basin, WY (v70243)	Wasatchian (Wa-3)
UCMP 217913	Adapiform	Indet	Washakie Basin, WY (v70243)	Wasatchian (Wa-3)
UCMP 217971	Adapiform	Indet	Washakie Basin, WY (v74022)	Wasatchian (Wa-5)
UCMP 218139	Adapiform	Indet	Washakie Basin, WY (v74022)	Wasatchian (Wa-5)
UCMP 218367	Adapiform	Indet	Washakie Basin, WY (v71231)	Wasatchian
UCMP 218402	Adapiform	Indet	Washakie Basin, WY (v70215)	Wasatchian (~Wa-3)
UM 32258	Omomyiform	*Omomys carteri*	Bridger Basin, WY (BRW-139)	Bridgerian (Br-3)
USNM 540587	Omomyiform	*Teilhardina brandti*	Bighorn Basin, WY	Wasatchian (Wa-0)
UM 31624	Omomyiform	Indet	Bridger Basin, WY (BRW-14)	Bridgerian (Br-2)
UM 32129	Omomyiform	Indet	Bridger Basin, WY (BRW-14)	Bridgerian (Br-2)
UM 32146 (a)	Omomyiform	Indet	Bridger Basin, WY (BRW-14)	Bridgerian (Br-2)
UM 32146 (b)	Omomyiform	Indet	Bridger Basin, WY (BRW-14)	Bridgerian (Br-2)
UM 32274	Omomyiform	Indet	Bridger Basin, WY (BRW-35)	Bridgerian (Br-2)
UM 32186	Omomyiform	Indet	Bridger Basin, WY (BRW-12)	Bridgerian (Br-3)
UM 32249 (a)	Omomyiform	Indet	Bridger Basin, WY (BRW-10)	Bridgerian (Br-3)
UM 32249 (b)	Omomyiform	Indet	Bridger Basin, WY (BRW-10)	Bridgerian (Br-3)
UM 32249 (c)	Omomyiform	Indet	Bridger Basin, WY (BRW-10)	Bridgerian (Br-3)
UM 32249 (d)	Omomyiform	Indet	Bridger Basin, WY (BRW-10)	Bridgerian (Br-3)
UM 32249 (e)	Omomyiform	Indet	Bridger Basin, WY (BRW-10)	Bridgerian (Br-3)
AMNH FM 126631	Omomyiform	Indet	Bridger Basin, WY (LSV-A)	Bridgerian (Br-3)
AMNH FM 126632	Omomyiform	Indet	Bridger Basin, WY (LSV-A)	Bridgerian (Br-3)
AMNH FM 126637	Omomyiform	Indet	Bridger Basin, WY (LSV-A)	Bridgerian (Br-3)
AMNH FM 126659	Omomyiform	Indet	Bridger Basin, WY (Sage Creek)	Bridgerian (Br-2)
AMNH FM 126663	Omomyiform	Indet	Bridger Basin, WY (Sage Creek)	Bridgerian (Br-2)
AMNH FM 126664	Omomyiform	Indet	Bridger Basin, WY (Sage Creek)	Bridgerian (Br-2)

AMNH FM 126665	Omomyiform	Indet	Bridger Basin, WY (Sage Creek)	Bridgerian (Br-2)
AMNH FM 126674	Omomyiform	Indet	Bridger Basin, WY (Sage Creek)	Bridgerian (Br-2)
AMNH FM 126735	Omomyiform	Indet	Bridger Basin, WY (Mac's Hole)	Bridgerian (~Br-2/3)
UCMP 134993	Omomyiform	Indet	Washakie Basin, WY (v70220)	Wasatchian
UCMP 218416	Omomyiform	Indet	Washakie Basin, WY (v70220)	Wasatchian
UCMP 218183	Omomyiform	Indet	Washakie Basin, WY (v74022)	Wasatchian (Wa-5)
UCMP 218244	Omomyiform	Indet	Washakie Basin, WY (v74022)	Wasatchian (Wa-5)
UCMP 218261	Omomyiform	Indet	Washakie Basin, WY (v74022)	Wasatchian (Wa-5)
UCMP 218295	Omomyiform	Indet	Washakie Basin, WY (v74022)	Wasatchian (Wa-5)
UCMP 218301	Omomyiform	Indet	Washakie Basin, WY (v74022)	Wasatchian (Wa-5)
UCMP 218368	Omomyiform	Indet	Washakie Basin, WY (v71231)	Wasatchian
UCMP 218432	Omomyiform	Indet	Washakie Basin, WY (v70229)	Wasatchian
UCMP 218436	Omomyiform	Indet	Washakie Basin, WY (v70246)	Wasatchian (Wa-3)

Table 4.6. Dentally known adapiforms from Washakie Basin localities.
Lists of the known adapiform taxa and the number of dental specimens attributed to them for each locality (listed along the top). Information was taken from the UCMP online database.

v6167		**v70215**		**v70243**		**v71231**		**v74022**	
*Cantius sp.**	30	*Cantius sp.**	3	*Cantius sp.**	31	*Cantius sp.**	1	*Cantius sp.**	3
Cantius savagei	11			*Copelemur sp.*	18	*Copelemur sp.*	1	*Copelemur australotutus*	4
				Copelemur praetutus	2			*Copelemur feretutus*	2
								Copelemur sp.	2
								Notharctus sp.	1

*These specimens may also be attributed to *Notharctus venticolis* (pers. comm., Doug Boyer)

Table 4.7. Dentally known omomyiforms from Washakie Basin localities.
Lists of the known omomyiform taxa and the number of dental specimens attributed to them for each locality (listed along the top). Information was taken from the UCMP online database.

v70214		**v70220**		**v70229**		**v70246**		**v74022**	
Tetonius sp.	134	*Anemorhysis pearcei*	9	*Anemorhysis sp.*	5	*Arapahovius gazini*	45	*Arapahovius sp.*	93
Anemorhysis sp.	1	*Anemorhysis sp.*	1	*Tetonius sp.*	1	*Arapahovius sp.*	10	*Anemorhysis savagei*	70
Anemorhysis pearcei	1	*Tetonius sp.*	1	*Loveina zephyri*	1	*Anemorhysis sp.*	2	*Arapahovius gazini*	39
								Anemorhysis sp.	5
								Steinius sp.	4
								Tetonius sp.	4

Table 4.8. Measurements used in this study.
See **Fig. 4.3** for illustrations of anatomical terminology and **Figs. 4.4, 4.5** for illustrations of measurements.

Measurement (Abbreviation)	**Definition**	**Significance**
Facet height (FH)	Distance between most proximal point on superior margin of articular facet and that of the inferior margin; Taken in lateral view	Height of articular facet
Extensor tubercle height (ETH)	Distance between most proximal point on superior margin of articular facet and most dorsal point of extensor tubercle; ∥ to FH and taken in lateral view	Related to leverage of long digital extensor tendon; higher values reflect increased lever arm
Flexor tubercle height (FTH)	Distance between most proximal point on inferior margin of articular facet and most volar point of flexor tubercle; ∥ to FH and taken in lateral view	Related to leverage of long digital flexor tendon; higher values reflect increased lever arm
Maximum phalangeal length (MPL)	Distance between most proximal point on inferior margin of articular facet and most distal point on distal tip of phalanx; Taken in lateral view	Total length of the phalanx
Volar process length (VPL)	Distance between most proximal point on inferior margin of articular facet and most distal point of volar process; ⊥ to FH and taken in lateral view	Estimate of the portion of the bone that lies embedded within the apical pad
Mid-shaft height (MSH)	For specimens that have apical tufts: Height of shaft at midpoint between base and tuft For specimens that do not have apical tufts: Height of shaft taken at ¼ of its length (shaft length is considered to be the length of MPL distal to the base of the phalanx); in both cases ⊥ to MPL and taken in lateral view	Higher values are suggested to reflect a shaft that is more resistant to dorso-ventral bending
Apical tuft height (ATH)	For specimens that have apical tufts: Height of shaft at midpoint of apical tuft For specimens that do not have apical tufts: Height of shaft taken at ¾ of its length (shaft length is considered to be the length of MPL distal to the base of the phalanx); in both cases ⊥ to volar margin of tuft/shaft in region where measurement is taken and taken in lateral view	Height of the apical tuft
Base width (BW)	Maximum, medio-lateral width of base; ⊥ to long axis of shaft and taken in dorsal view	May be related to width of unguis
Mid-shaft width (MSW)	For specimens that have apical tufts: Width of shaft at midpoint between base and tuft For specimens that do not have apical tufts: Width of shaft taken at ¼ of its length (shaft length is considered to be the length of MPL distal to the base of the phalanx); in both cases ⊥ to long axis of shaft and taken in dorsal view	Higher values are suggested to reflect a shaft that is more resistant to medio-lateral bending

Apical tuft width (ATW)	For specimens that have apical tufts: Maximum width of apical tuft For specimens that do not have apical tufts: Width of shaft taken at ¾ of its length (shaft length is considered to be the length of MPL distal to the base of the phalanx); in both cases ⊥ to long axis of shaft and taken in dorsal view	May be related to width of unguis
Width of superior margin of articular facet (WSM)	Width of superior margin of articular facet taken in proximal view	Describes shape of facet
Width of inferior margin of articular facet (WIM)	Width of inferior margin of articular facet taken in proximal view	Describes shape of facet
Included angle of shaft (SIA)	Included angle of dorsal surface of shaft calculated based on measurements L_s and H_s as in **Fig. 4.5** L_s = distance from point on dorsal margin where shaft meets base to distalmost tip of shaft H_s = distance from midpoint of L_s to dorsal margin of shaft; ⊥ to L_s If L_s is positioned volar to H_s; angle is scored as positive (dorsally convex) If L_s is position dorsal to H_s, angle is scored as negative (dorsally concave) All measurements taken in lateral view	Curvature of the dorsum of shaft; unguis tends to follow shape of dorsum of shaft; higher degrees of curvature indicative of a more strongly keeled unguis
Included angle of articular facet (FIA)	Included angle of dorsal surface of shaft calculated based on measurements FH and H_F as in **Fig. 4.5** H_F = distance from midpoint of FH to proximal margin of articular surface; ⊥ to FH If FH is positioned proximal to H_F; angle is scored as positive (proximally concave) If FH is positioned distal to H_F, angle is scored as negative (proximally convex) All measurements taken in lateral view	Describes shape of facet
Facet-shaft angle (FSA)	Angle between FH and MPL	Reflects the degree to which the shaft (and unguis) projects dorsally or volarly with respect to the base of the phalanx

Table 4.9. Principal components and canonical variates.
The eigenvalues, percentage of variance explained (% Variance) and the cumulative (cum.) variance for each principal component from one analysis: PCA (Ungulae, Falculae, and Tegulae) is the analysis run on all ray-specific species means and all fossil specimens. The singular values (SV), percentage of between-group variance explained (% b-g Variance) and the cumulative (cum.) variance for each canonical variate (CV) from two analyses: DFA (Ungulae, Falculae, and Tegulae) is the analysis discriminating among claw climbing non-primates, tegula-bearing primates and ungula-bearing primates; DFA (Locomotor Group) is the analysis among ungula-bearing primates that primarily utilize vertical clinging and leaping, generalized arboreal quadrupedalism, and slow climbing arboreal quadrupedalism.

PCA (Ungulae, Falculae, and Tegulae)			
PC	**Eigenvalue**	**% Variance**	**Cum. variance**
1	8.5	58.5%	58.5%
2	1.6	10.9%	69.4%
DFA (Ungulae, Falculae, and Tegulae)			
CV	**SVD**	**% Variance**	**Cum. variance**
1	59.9	86.2%	86.2%
2	23.9	13.8%	100.0%
DFA (Locomotor Group)			
CV	**SVD**	**% Variance**	**Cum. variance**
1	13.6	70.3%	70.3%
2	8.8	29.7%	100.0%

Table 4.10. Loadings for PCA (ungulae, falculae, and tegulae).
The Pearson's correlation coefficients from correlations of each variable with principal components 1-2 from the PCA on all ray-specific species means and all fossil specimens.

PC1		PC2	
Variable	**Correlation**	**Variable**	**Correlation**
MSH	-0.96	WIM	-0.78
SIA	-0.93	WSM	-0.55
FTH	-0.89	FIA	-0.21
ATH	-0.82	FH	-0.14
FH	-0.79	BW	-0.12
FIA	-0.79	ETH	-0.08
ETH	-0.63	SIA	-0.05
MPL	-0.45	ATH	-0.01
FSA	-0.25	MSH	0.01
WIM	0.03	FSA	0.06
WSM	0.67	FTH	0.06
VPL	0.78	MSW	0.07
MSW	0.91	ATW	0.14
ATW	0.94	VPL	0.37
BW	0.94	MPL	0.64

Table 4.11. Loadings for DFA (ungulae, falculae, and tegulae).
The Pearson's correlation coefficients from correlations of each variable with canonical variates 1-2 from the DFA (structure coefficients) discriminating among claw climbing non-primates, tegula-bearing primates and ungula-bearing primates.

CV1		CV2	
Variable	**Correlation**	**Variable**	**Correlation**
SIA	-0.94	WSM	-0.42
MSH	-0.92	ETH	-0.41
FTH	-0.88	FIA	-0.35
FH	-0.80	BW	-0.27
ATH	-0.79	FSA	-0.23
FIA	-0.78	MSW	-0.14
ETH	-0.74	ATW	-0.13
MPL	-0.50	ATH	-0.05
FSA	-0.24	WIM	-0.01
WIM	0.39	FTH	0.09
WSM	0.63	FH	0.10
VPL	0.80	SIA	0.11
MSW	0.88	MSH	0.14
BW	0.89	VPL	0.44
ATW	0.95	MPL	0.70

Table 4.12 Classifications of pedal grasping non-primates and fossil specimens.
Classifications and probabilities of classification (Prob.) of specimens treated as unknowns in two discriminant function analyses. DFA (U, F, T) is the analysis discriminating among claw climbing non-primates, tegula-bearing primates and ungula-bearing primates. DFA (LG) is the analysis discriminating among ungula-bearing primates that primarily utilize vertical clinging and leaping (VCL), generalized arboreal quadrupedalism (Gen arb quad), and slow climbing arboreal quadrupedalism (Slow arb quad).

		DFA (U, F, T)		**DFA (LG)**	
Pedal grasping non-primates > 100g					
Taxon	**Ray/Specimen**	**Classification**	**Prob.**	**Classification**	**Prob.**
Caluromys philander	M2	Claw climbing	1.00	Gen arb quad	0.99
Caluromys philander	P3/4	Claw climbing	1.00	Gen arb quad	0.94
Dactylopsila trivirgata	M3/4	Claw climbing	1.00	Gen arb quad	1.00
Dactylopsila trivirgata	P4	Claw climbing	1.00	Gen arb quad	1.00
Didelphis sp.	M3/4	Tegula-bearing	1.00	Slow arb quad	0.96
Didelphis sp.	P3/4	Claw climbing	0.98	Gen arb quad	0.99
Didelphis virginiana	M3/4	Claw climbing	1.00	Gen arb quad	0.97
Didelphis virginiana	P2	Claw climbing	1.00	Gen arb quad	0.74
Didelphis virginiana	P3/4	Claw climbing	1.00	Gen arb quad	1.00
Didelphis virginiana	P5	Claw climbing	1.00	Gen arb quad	0.92
Petaurus breviceps	M3/4	Claw climbing	1.00	Gen arb quad	1.00
Petaurus breviceps	P4	Claw climbing	1.00	Gen arb quad	1.00
Petaurus sp.	M3/4	Claw climbing	1.00	Gen arb quad	0.93
Petaurus sp.	P4	Claw climbing	1.00	Gen arb quad	1.00
Phalanger gymnotis	P4	Claw climbing	1.00	Gen arb quad	1.00
Phalanger orientalis	M3/4	Claw climbing	1.00	Slow arb quad	0.93
Phalanger orientalis	P4	Claw climbing	1.00	Gen arb quad	1.00
Phascolarctos cinereus	M2	Claw climbing	1.00	Slow arb quad	1.00
Phascolarctos cinereus	M3/4	Claw climbing	1.00	Slow arb quad	0.89
Phascolarctos cinereus	P4	Claw climbing	1.00	Slow arb quad	0.84
Philander opossum	M2	Claw climbing	1.00	Gen arb quad	0.99
Philander opossum	M3/4	Claw climbing	1.00	Gen arb quad	1.00
Philander opossum	P3/4	Claw climbing	1.00	Gen arb quad	1.00
Trichosurus vulpecula	M3/4	Claw climbing	1.00	Gen arb quad	1.00
Trichosurus vulpecula	P4	Claw climbing	1.00	Gen arb quad	1.00
Pedal grasping non-primates < 100g					
Cercartetus caudatus	M2	Tegula-bearing	1.00	Slow arb quad	1.00
Cercartetus caudatus	M3/4	Tegula-bearing	1.00	Slow arb quad	0.99
Cercartetus caudatus	M5	Tegula-bearing	0.97	Slow arb quad	0.99
Cercartetus caudatus	P3/4	Claw climbing	0.99	Gen arb quad	0.78
Chiropodomys gliroides	M3/4	Tegula-bearing	1.00	Slow arb quad	0.99
Chiropodomys gliroides	P2	Tegula-bearing	0.96	Gen arb quad	0.99
Chiropodomys gliroides	P3/4	Claw climbing	0.98	Gen arb quad	1.00
Chiropodomys gliroides	P5	Claw climbing	0.81	Slow arb quad	0.85
Dendromus insignis	M3/4	Tegula-bearing	1.00	VCL	0.93
Dendromus insignis	P3/4	Tegula-bearing	1.00	Gen arb quad	1.00

Dendromus insignis	P5	Tegula-bearing	1.00	VCL	1.00
Hapalomys longicaudatus	M3/4	Ungula-bearing	1.00	Slow arb quad	1.00
Hapalomys longicaudatus	M5	Ungula-bearing	1.00	Slow arb quad	1.00
Hapalomys longicaudatus	P3/4	Tegula-bearing	1.00	Gen arb quad	1.00
Hapalomys longicaudatus	P5	Ungula-bearing	1.00	Slow arb quad	1.00
Prionomys batesi	P3/4	Tegula-bearing	1.00	Gen arb quad	0.99
Tarsipes rostratus	M3/4	Ungula-bearing	1.00	Slow arb quad	1.00
Tarsipes rostratus	M5	Ungula-bearing	1.00	Slow arb quad	1.00
Tarsipes rostratus	P3/4	Ungula-bearing	1.00	Slow arb quad	1.00
Early Eocene Adapiforms					
Cantius nunienus	UM 112882	Ungula-bearing	1.00	Gen arb quad	0.89
Indet	UCMP 147533	Ungula-bearing	1.00	Slow arb quad	0.95
Indet	UCMP 147534	Ungula-bearing	1.00	Gen arb quad	0.84
Indet	UCMP 217913	Ungula-bearing	1.00	VCL	0.51
Indet	UCMP 217971	Ungula-bearing	1.00	VCL	0.62
Indet	UCMP 218139	Ungula-bearing	1.00	VCL	0.50
Indet	UCMP 218367	Ungula-bearing	1.00	Gen arb quad	0.99
Indet	UCMP 218402	Ungula-bearing	1.00	Slow arb quad	0.94
Indet	UCMP 236082	Ungula-bearing	1.00	Gen arb quad	0.99
Middle Eocene Adapiforms					
Notharctus tenebrosus	AMNH FM 11474	Ungula-bearing	0.96	Gen arb quad	0.99
Smilodectes gracilis	AMNH FM 131763	Ungula-bearing	1.00	Gen arb quad	0.99
Notharctus tenebrosus	AMNH FM 131764 (a)	Ungula-bearing	1.00	Gen arb quad	1.00
Notharctus tenebrosus	AMNH FM 131764 (b)	Ungula-bearing	1.00	Gen arb quad	0.80
Notharctus tenebrosus	AMNH FM 143612_2	Tegula-bearing	0.94	Gen arb quad	1.00
Notharctus tenebrosus	AMNH FM 143612_4	Ungula-bearing	1.00	Gen arb quad	0.83
Indet	AMNH FM 131766	Ungula-bearing	1.00	Gen arb quad	0.82
Early Eocene Omomyiforms					
Teilhardina brandti	USNM 540587	Ungula-bearing	1.00	VCL	0.87
Indet	UCMP 134993	Ungula-bearing	1.00	VCL	0.96
Indet	UCMP 218183	Ungula-bearing	1.00	Gen arb quad	0.99
Indet	UCMP 218244	Ungula-bearing	1.00	VCL	0.94
Indet	UCMP 218261	Ungula-bearing	1.00	VCL	0.96
Indet	UCMP 218295	Ungula-bearing	1.00	VCL	0.96
Indet	UCMP 218301	Ungula-bearing	1.00	VCL	0.89
Indet	UCMP 218368	Ungula-bearing	1.00	Gen arb quad	0.88
Indet	UCMP 218416	Ungula-bearing	1.00	Gen arb quad	0.79
Indet	UCMP 218432	Ungula-bearing	1.00	VCL	0.72
Indet	UCMP 218436	Ungula-bearing	1.00	VCL	0.80
Middle Eocene Omomyiforms					
Omomys carteri	UM 32258	Ungula-bearing	1.00	Gen arb quad	0.99
Indet	AMNH FM 126631	Ungula-bearing	1.00	Gen arb quad	1.00
Indet	AMNH FM 126632	Ungula-bearing	1.00	Gen arb quad	1.00
Indet	AMNH FM 126637	Ungula-bearing	1.00	Gen arb quad	0.93
Indet	AMNH FM 126659	Ungula-bearing	1.00	Gen arb quad	0.93
Indet	AMNH FM 126663	Ungula-bearing	1.00	Gen arb quad	0.90
Indet	AMNH FM 126664	Ungula-bearing	1.00	Gen arb quad	0.90
Indet	AMNH FM 126665	Ungula-bearing	1.00	Gen arb quad	1.00

Indet	AMNH FM 126674	Ungula-bearing	1.00	Gen arb quad	0.93
Indet	AMNH FM 126735	Ungula-bearing	1.00	Gen arb quad	0.83
Indet	UM 31624	Ungula-bearing	1.00	Gen arb quad	0.99
Indet	UM 32129	Ungula-bearing	1.00	Gen arb quad	0.98
Indet	UM 32146 (a)	Ungula-bearing	1.00	VCL	0.59
Indet	UM 32146 (b)	Ungula-bearing	1.00	VCL	0.91
Indet	UM 32186	Ungula-bearing	1.00	VCL	0.80
Indet	UM 32249 (a)	Ungula-bearing	1.00	Gen arb quad	0.75
Indet	UM 32249 (b)	Ungula-bearing	1.00	Gen arb quad	0.99
Indet	UM 32249 (c)	Ungula-bearing	1.00	Gen arb quad	0.94
Indet	UM 32249 (d)	Ungula-bearing	1.00	VCL	0.88
Indet	UM 32249 (e)	Ungula-bearing	1.00	Gen arb quad	0.96
Indet	UM 32274	Ungula-bearing	1.00	Gen arb quad	0.96

Table 4.13. Group (ungulae, falculae, and tegulae) means and standard deviations.
Group means and standard deviations (in parentheses) for each size-adjusted shape variable and angular variable.

	Claw climbing Non-primate	**Pedal Grasping Non-primate (>100g)**	**Pedal Grasping Non-primate (<100g)**	**Tegula-bearing Primate**	**Ungula-bearing Primate**
FH	1.13 (0.11)	1.12 (0.15)	1.22 (0.22)	1.05 (0.09)	0.82 (0.11)
ETH	0.49 (0.16)	0.33 (0.11)	0.21 (0.09)	0.18 (0.03)	0.20 (0.04)
FTH	0.78 (0.21)	0.73 (0.20)	0.40 (0.17)	0.63 (0.18)	0.27 (0.05)
MPL	3.72 (0.36)	3.59 (0.21)	3.72 (0.63)	4.62 (0.16)	3.26 (0.37)
VPL	1.49 (0.23)	1.63 (0.23)	2.48 (0.51)	3.04 (0.20)	2.96 (0.41)
MSH	1.84 (0.32)	1.88 (0.19)	1.50 (0.27)	1.62 (0.11)	0.84 (0.12)
ATH	1.06 (0.27)	0.84 (0.10)	0.87 (0.12)	0.84 (0.08)	0.63 (0.08)
BW	1.26 (0.19)	1.41 (0.16)	1.57 (0.27)	1.28 (0.05)	2.18 (0.22)
MSW	0.53 (0.08)	0.66 (0.11)	0.81 (0.17)	0.64 (0.06)	1.03 (0.15)
ATW	0.40 (0.10)	0.45 (0.09)	0.76 (0.19)	0.65 (0.09)	1.44 (0.20)
WSM	0.94 (0.22)	0.94 (0.10)	0.99 (0.13)	0.76 (0.08)	1.26 (0.18)
WIM	1.13 (0.14)	1.23 (0.13)	1.32 (0.20)	1.18 (0.09)	1.26 (0.14)
SIA	97.97 (19.89)	93.60 (14.57)	54.96 (19.80)	75.48 (11.94)	15.17 (12.67)
FIA	116.42 (16.15)	134.02 (23.50)	93.88 (32.69)	62.79 (13.31)	59.96 (17.84)
FSA	87.13 (11.02)	91.49 (11.16)	74.35 (9.35)	80.00 (6.56)	82.22 (5.52)

Table 4.14. Loadings for DFA (locomotor group).
The Pearson's correlation coefficients from correlations of each variable with canonical variates 1-2 from the DFA (structure coefficients) discriminating among ungula-bearing primates that primarily utilize vertical clinging and leaping, generalized arboreal quadrupedalism, and slow climbing arboreal quadrupedalism.

CV1		CV2	
Variable	**Correlation**	**Variable**	**Correlation**
ATW	-0.72	BW	-0.84
MSW	-0.42	MSW	-0.48
FIA	-0.30	WSM	-0.45
ETH	-0.13	ATW	-0.43
BW	-0.03	ATH	-0.11
FTH	-0.01	SIA	-0.06
MSH	0.00	FIA	-0.04
WSM	0.10	WIM	-0.03
MPL	0.15	MSH	0.06
VPL	0.32	FSA	0.08
FH	0.33	ETH	0.09
WIM	0.39	FH	0.21
SIA	0.40	FTH	0.45
FSA	0.43	VPL	0.55
ATH	0.52	MPL	0.58

Table 4.15. Group (locomotor mode) means and standard deviations.
Group means and standard deviations (in parentheses) for each size-adjusted shape variable and angular variable.

	Slow Climbing Arboreal Quadruped	**Generalized Arboreal Quadruped**	**Vertical Clinging and Leaping**
FH	0.88 (0.17)	0.78 (0.09)	0.83 (0.09)
ETH	0.19 (0.04)	0.20 (0.05)	0.21 (0.04)
FTH	0.25 (0.05)	0.25 (0.04)	0.28 (0.05)
MPL	3.26 (0.22)	3.04 (0.20)	3.43 (0.42)
VPL	3.11 (0.21)	2.70 (0.25)	3.12 (0.45)
MSH	0.84 (0.06)	0.83 (0.11)	0.84 (0.13)
ATH	0.72 (0.09)	0.62 (0.08)	0.62 (0.05)
BW	2.26 (0.21)	2.34 (0.17)	2.03 (0.15)
MSW	0.94 (0.15)	1.12 (0.16)	0.98 (0.09)
ATW	1.17 (0.18)	1.58 (0.17)	1.38 (0.13)
WSM	1.34 (0.27)	1.32 (0.18)	1.19 (0.11)
WIM	1.37 (0.16)	1.23 (0.11)	1.24 (0.15)
SIA	26.21 (12.13)	13.40 (12.97)	13.89 (11.38)
FIA	48.98 (22.13)	63.12 (15.48)	60.14 (17.75)
FSA	86.94 (3.33)	80.69 (4.49)	82.28 (6.06)

5. Chapter 5: Discussion

5.1 Summary of Results

The first major finding of this dissertation is that of the presence and significance of the volar process. A volar process is clearly present on almost all distal phalanx specimens observed and is modified in relation to digit form. Further, this process can be used to indicate the relative portion of the distal phalanx that lies embedded within the apical pad in comparison to the portion that projects beyond the pad where it is surrounded solely by the unguis and its associated tissues. These are features that directly relate to major external differences among digits that bear claws, nails, tegulae, or grooming ungues. Therefore, it allows for the construction of distal phalanx measurements that are informative for the identification of unguis forms and morphology that is transitional between unguis forms. This result has been utilized to inform the findings enumerated below.

Distribution of grooming ungues among living and fossil primates:

- Three lineages of platyrrhine monkeys possess grooming ungues on their second pedal digits: *Callicebus*, *Aotus*, and *Pithecia*.
- At least two Early Eocene omomyiform species possessed grooming ungues.
- An additional adapiform grooming unguis has been identified from the Early Eocene and likely belonged to the genus *Cantius* or *Notharctus venticolis*.

Grooming unguis variations, homologies, and polarity:

- Extant anthropoid grooming ungues are morphologically different from those of strepsirrhines and tarsiers. They were likely derived independently but in parallel along the three platyrrhine lineages that possess them.
- The ancestor of all living primates likely possessed a grooming unguis on its second pedal digit that resembled those of living strepsirrhines and tarsiers. Strepsirrhines and haplorhines likely inherited this morphology from a common ancestor; the differences among strepsirrhine and tarsier grooming ungues are related to independent changes in grooming unguis form that occurred in the respective lineages.

- The distribution of morphology in extant taxa suggest that the ancestor of living anthropoids possessed a nail on its second pedal digit rather than a grooming unguis.

The origins of primate nails:

- The honey possum (*Tarsipes rostratus*), a terminal branch specialist that weighs ~9g, has nails on its postaxial digits.
- There is a relationship between primate-like distal phalanges and small body size (<100g) among pedal grasping non-primates.
- Adapiform distal phalanges differ from those of omomyiforms as they are claw-like in the retention of shorter volar processes associated with bilaterally occurring nutrient foramina. This is likely inherited from a claw-bearing ancestor and suggests that the evolution of nails differed somewhat along the two lineages as adapiforms retained a portion (albeit small) of the distal phalanx that projected above and beyond the apical pad while omomyiforms did not.
- Small body size in conjunction with pedal grasping in a terminal branch milieu likely facilitated the origins of primate nails.

North American Eocene primate paleobiology:

- Extant strepsirrhine and tarsier distal phalanx morphology is associated with locomotor mode.
- The earliest known nail-bearing distal phalanx (from *Teilhardina brandti*) is morphologically most similar to extant species that engage in vertical clinging and leaping.
- *Notharctus tenebrosus* appears to have secondarily shortened its volar processes (increasing the length of the phalanx that projects above and beyond the apical pad) and may be derived in a direction towards tegulae.

5.2 Significance

5.2.1 Grooming Ungues in Eocene Primate Phylogenetics

As grooming ungues are now shown to be present in adapiforms and omomyiforms and were likely the ancestral condition for primates, haplorhines, strepsirrhines, and tarsiers, the presence of grooming ungues on the second pedal digit of strepsirrhines and tarsiers is best viewed as a symplesiomorphy. There is some variation among grooming unguis-bearing distal phalanges of tarsiers and strepsirrhines; those of lemuriform strepsirrhines form a morphological cluster while those of tarsiers and lorisiform strepsirrhines form another cluster. Interestingly, the omomyiform grooming specimens are most similar to those of lorisiforms and tarsiers while those of adapiforms are more similar to lemuriforms. However, because there is no sharp divide between tarsiers and strepsirrhines, grooming phalanx morphology of the second pedal digit cannot be used to assign phylogenetic affinity to tarsiers or a phylogenetic position as a stem strepsirrhine.

Of extant primates, tarsiers alone possess a grooming unguis on the third pedal digit. Therefore, the presence of a grooming unguis on the third digit might be a good indicator of tarsier phylogenetic affinity. The recently described *Archicebus achilles* currently represents the only articulated foot of an early species of haplorhine primate (Ni et al., 2013). It was originally described as possessing scutiform distal phalanges on its second and third pedal digits (suggesting nails). If this is the case, then the reconstruction of a grooming unguis for the haplorhine ancestor might be incorrect and both the second and third pedal grooming ungues would have been independently acquired in tarsiers. However, the images presented in both the main text and supplementary material do not allow for an assessment of the presence of grooming unguis-bearing or nail-bearing distal phalanges. A lateral view is required to diagnose the presence of a grooming unguis by allowing the determination of the relative length of the volar process and the degree to which the shaft projects dorsally relative to the articular facet. Additional omomyiform specimens with phalanges attributable to specific pedal rays is required to elucidate his question.

5.2.2 The Origins of Primate Nails

Nails and reduced claws are associated with pedal grasping and a body mass of less than 100 grams. Currently, the only known arboreal mammal to possess nails like those of primates is *Tarsipes rostratus*, the honey possum. Honey possums are extremely small (~9g), subsist upon nectars in a terminal branch niche, and are described in the literature to run up and down tree trunks despite their lack of claws (Russell, 1986). One way in which small body size may facilitate the evolution of nails is by reducing the strong selective pressure to retain claws as a very tiny mammal may be able to utilize crenulations and ridges in bark as toeholds. Photographic images of mammals engaging in this behavior can be found using a simple google image search, but this behavior is not described in the literature. Further, it is not clear how efficient such a behavior would be nor if it would incur significant restrictions in speed. Additional studies and behavioral observations are required to assess this. It is also possible that the relationship between body size and primate-like morphology is due to an intermediate factor rather than a causal relationship. A terminal branch niche may be capable of exerting a selective pressure for a decrease in body size while a different factor concurrently reduces the selective pressure to retain claws. It has been shown that smaller mammals can utilize smaller substrates to support themselves (Shapiro et al., 2014), so it is certainly feasible that access to resources on tiny branches might select for small body size. Further, it has been suggested that a reduction of time spent on relatively large diameter vertical supports may reduce the selective pressure to retain claws (Hamrick, 1998; Orkin and Pontzer, 2011). These two pressures working together would also explain the pattern observed among extant mammals. Additional work is clearly needed to better understand the relationship between body size and distal phalanx morphology.

A number of studies now show that there is a link between grasping and the use of terminal or slender branches (e.g., Sargis, 2001; Byron et al., 2011; Youlatos et al., 2015). While claw-bearing and non-grasping mammals can utilize terminal branches (Rasmussen, 1990; Orkin and Pontzer, 2011), it is likely that some aspect of performance is enhanced by the ability to grasp. However, it is still unclear as to what role if any a nail may play during grasping behaviors. They may help redistribute forces or support the pad while grasping (Clark, 1936; Baden, 1970; Preuschoft, 1970, 1973; Napier, 1993), or perhaps are retained for the utility of the distal edge of the nail when climbing on larger supports (similar to those of *Eouticus* and *Phaner*), scratching, or foraging tasks (Spearman, 1985; Napier, 1993). They may also play a

sensory role (Lemelin and Grafton, 1998) as, at least in humans, specialized mechanoreceptors a present in the folds of skin surrounding the nail that are triggered by compression against the nail (Birznieks et al., 2009). This configuration detects the directions of forces placed upon the digit tip. However, it remains to be seen if non-human primates possess such mechanoreceptors. Regardless, it is likely that nails play different roles in different primates and a better understanding of their morphological diversity will help to elucidate the nail's role in different behaviors.

Since nails differentiate primates from most other mammals, they are particularly useful for understanding primate origins. Nails are likely related to some adaptive shift that occurred early in primate evolution and understanding the circumstances that lead to nails has the potential to support or refute major hypotheses of primate origins. Data from this dissertation is in accord with the idea that primates underwent an adaptive shift towards a terminal branch niche if body size was also small (less than 100g). Some have suggested that nails may be related to insect catching (Godinot, 2007), however, the one known non-primate that does possess nails does not catch insects. Rather it is the only non-volant mammal to subsist entirely upon nectars (Bradshaw et al., 2007). Therefore insect catching is not a necessary requirement for the evolution of nails, but it is unclear if nails assist with this behavior. Grasp leaping and vertical clinging and leaping have also been suggested to be an impetus for claw loss or nail origins (Napier and Walker, 1967; Szalay and Dagosto, 1980). Along the same line of reasoning as for insect catching, leaping and particularly vertical clinging and leaping are not necessary for the evolution of nails. *Tarsipes* is capable of some leaping, but is described as avoiding leaping when possible (Russell, 1986). But again, it is not clear if nails enhance these behaviors or not. One hypothesis suggests that claw climbing is too physiologically expensive for a large mammal, implying that nails are the result of enlarged body size (Soligo and Müller, 1999; Soligo and Martin, 2006). However, there does not appear to be a relationship between large body size and reduction of claws, while there is one between small body size and reduction of claws. Further, there is currently no evidence to suggest that an early primate ancestor was large bodied (Hamrick, 1999), and rather it has been suggested to be ~55g or smaller (Steiper and Seiffert, 2012). Therefore, it seems unlikely that large body size was a factor in the origin of primate nails. To conclude, it is plausible that nails in primate evolution are evidence of the inhabitation of a terminal branch niche at a small body size. However, it is also possible that nails may be

related to other behaviors and a better understanding of the morphological variation in extant nails may help to elucidate potential relationships.

5.3 Future Directions

Future work will build upon these results by seeking to:

- Utilize and compare the results of different methods for reconstructing ancestral states of primate second pedal distal phalanges.
- Compare the relationship of morphology and behavior between manual and pedal distal phalanges.
- Explore the morphological diversity in extant primate nail form and determine what aspects of nail morphology can be reconstructed based on distal phalanx shape.
- More rigorously investigate the relationship between distal phalanx morphology and body size in extant and fossil primates and among a broader sample of pedal grasping and claw-climbing non-primates.
- Determine if and what other aspects of small bodied non-primate pedal grasper cheiridial morphology follow a similar pattern of variation as do distal phalanges, and in particular to study joint surfaces and how they related to phalangeal position.
- Further explore the morphology of the hands and feet of non-primates with nails and reduced claws to determine if the morphology of other cheiridial bones follows the same primate-like pattern.
- Assess the morphological diversity among anthropoid nail-bearing distal phalanges in relation to locomotor mode and other behaviors.

Works Cited

Aiello, L., Dean, C., 1990. An Introduction to Human Evolutionary Anatomy. Academic Press, New York.

Almécija, S., Shrewsbury, M., Rook, L., Moyà-Solà, S., 2014. The morphology of *Oreopithecus bambolii* pollical distal phalanx. American Journal of Physical Anthropology 153, 582-597.

Aversi-Ferreira, T.A., Maior, R.S., Carneiro-e-Silva, F.O., Aversi-Ferreira, R.A.G.M.F., Tavares, M.C., Nishijo, H., Tomaz, C., 2011. Comparative anatomical analyses of the forearm muscles of *Cebus libidinosus* (Rylands et al. 2000):Manipulatory behavior and tool use. PLoS ONE 6, e22165.

Baden, H.P., 1970. The physical properties of nail. J Invest Dermatol 55, 115-122.

Bininda-Emonds, O.R.P., Cardillo, M., Jones, K.E., MacPhee, R.D., Beck, R.M.D., Grenyer, R., Price, S.A., Vos, R.A., Gittleman, J.L., Purvis, A., 2007. The delayed rise of present-day mammals. Nature 446, 507-512.

Birznieks, I., Macefield, V.G., Westling, G., Johansson, R.S., 2009. Slowly adapting mechanoreceptors in the borders of the human fingernail encode fingertip forces. J Neurosci 29, 9370-9379.

Bluntschli, H., 1929. Ein eigenartiges an Prosimierbefunde erinnerndes Nagelverhalten am Fuss von platyrrhinen Affen. Dev Genes Evol 118, 1-10.

Boyer, D.M., Seiffert, E.R., 2013. Patterns of astragalar fibular facet orientation in extant and fossil primates and their evolutionary implications. American Journal of Physical Anthropology 151, 420-447.

Boyer, D.M., Yapuncich, G.S., Chester, S.G.B., Bloch, J.I., Godinot, M., 2013. Hands of early primates. American Journal of Physical Anthropology 57, 33-78.

Bradshaw, D., Phillips, R., Tomlinson, S., Holley, R., Jennings, S., Bradshaw, F., 2007. Ecology of the honey possum, *Tarsipes rostratus* in Scott National Park, Western Australia. Australian Mammalogy 29, 25-38.

Breed, W.G., Taylor, J., 2000. Body mass, testes mass, and sperm size in murine rodents. Journal of Mammalogy 81, 758-768.

Bruhns, F., 1910. Der nagel der halbaffen und affen. Gegenbaurs Morphologisches Jahrbuch 40, 501-609.

Byron, C., Kunz, H., Matuszek, H., Lewis, S., Van Valkinburgh, D., 2011. Rudimentary pedal grasping in mice and implications for terminal branch arboreal quadrupedalism. Journal of Morphology 272, 230-240.

Cartmill, M., 1972. Arboreal adaptations and the origin of the order Primates, in: Tuttle, R. (Ed.), The Functional and Evolutionary Biology of Primates. Aldine-Atherton, Chicago, pp. 97-122.

Cartmill, M., 1974. Pads and claws in arboreal locomotion, in: Jr., F.A.J. (Ed.), Primate Locomotion. Academic Press, New York, pp. 45-83.

Cartmill, M., 1985. Climbing, in: Hildebrand, M., Bramble, D., Liem, K., Wake, D. (Eds.), Functional Vertebrate Morphology. Harvard University Press, Cambridge, pp. 73 - 88.

Cartmill, M., 1992. New views on primate origins. Evol Anthropol 1, 105-111.

Case, D.T., Heilman, J., 2006. New siding techniques for the manual phalanges: a blind test. International Journal of Osteoarchaeology 16, 338-346.

Charles-Dominique, P., 1977. Ecology and Behaviour of Nocturnal Primates. Columbia University Press, New York.

Charles-Dominique, P., Bearder, S.K., 1979. Field studies of lorisid behavior: methodological aspects, in: Doyle, G.A., Martin, R.D. (Eds.), The Study of Prosimian Behavior. Academic Press, New York, pp. 567-629.

Clark, W.E.L.G., 1924. Notes on the living Tarsier (*Tarsius spectrum*). Proceedings of the Zoological Society of London 94, 217-223.

Clark, W.E.L.G., 1936. The problem of the claw in primates. Proceedings of the Zoological Society of London 106, 1-24.

Clark, W.E.L.G., 1959. The Antecedents of Man. Edinburgh University Press, Edinburgh.

Crompton, R.H., 1983. Age Differences in Locomotion of Two Subtropical Galaginae. Primates 24, 241-259.

Dagosto, M., 1988. Implications of postcranial evidence for the origins of euprimates. J Hum Evol 17, 35-56.

Dagosto, M., 1990. Models for the origin of the anthropoid postcranium. J Hum Evol 19, 121-139.

Dagosto, M., 1995. Seasonal variation in positional behavior of Malagasy lemurs. Int J Primatol 16, 807-833.

Dagosto, M., 2007. The postcranial morphotype of primates, in: Ravosa, M.J., Dagosto, M. (Eds.), Primate Origins: Adaptations and Evolution. Springer US, New York, pp. 489-534.

Day, M.H., Napier, J.R., 1966. A hominid toe bone from Bed I Olduvai Gorge Tanzania. Nature 211, 929-930.

Denys, C., Colyn, M., Nicolas, V., 2006. First record of the Dollman's tree mouse (*Prionomys batesi*; Mammalia: Nesomyidae) in the Republic of Congo and additional description of this rare Central African rodent. Zootaxa 1318, 59-68.

Dieterlen, F., 2009. Climbing mice of the genus *Dendromus* (Nesomyidae, Dendromurinae) in Sudan and Ethiopia, with the description of a new species. Bonner zoologische Beiträge 56, 185-200.

Diogo, R., Richmond, B.G., Wood, B., 2012. Evolution and homologies of primate and modern human hand and forearm muscles, with notes on thumb movements and tool use. Journal of Human Evolution 63, 64-78.

Fleagle, J.G., 2013. Primate Adaptation and Evolution. Elsevier, New York.

Franzen, J.L., Frey, E., 1993. *Europolemur* completed. Kaupia 3, 113-130.

Franzen, J.L., Gingerich, P.D., Habersetzer, J., Hurum, J.H., von Koenigswald, W., Smith, B.H., 2009. Complete primate skeleton from the middle Eocene of Messel in Germany: morphology and paleobiology. PLoS ONE 4, 1-27.

Freudenthal, M., Martin-Suárez, E., 2013. Estimating body mass of fossil rodents. Scripta Geologica 145, 1-130.

Garber, P.A., 1980. Locomotor behavior and feeding ecology of the Panamanian tamarin (*Saguinus oedipus geoffroyi*, Callitrichidae, Primates). International Journal of Primatology 1, 185-201.

Gebo, D.L., 1987. Locomotor diversity in prosimian primates. Am J Primatol 13, 271-281.

Gebo, D.L., 2004. A shrew-sized origin for primates. American Journal of Physical Anthropology 47, 40-62.

Gebo, D.L., Dagosto, M., Rose, K.D., 1991. Foot morphology and evolution in early Eocene *Cantius*. American Journal of Physical Anthropology 86, 51-73.

Gilbert, C.C., Maiolino, S.A., 2015. Comment to "Primates in the Eocene" by Gingerich (21012). Palaeobiodiversity and Palaeoenvironments In press.

Gingerich, P.D., 2012. Primates in the Eocene. Palaeobiodiversity and Palaeoenvironments 92, 649-663.

Gingerich, P.D., Jens L. Franzen, J.L., Habersetzer, J., Hurum, J.H., Smith, B.H., 2010. *Darwinius masillae* is a haplorhine - reply to Williams et al. (2010). Journal of Human Evolution 59, 574-579.

Godinot, M., 1992. Early euprimate hands in evolutionary perspective. J Hum Evol 22, 267-283.

Godinot, M., 2007. Primate origins: reappraisal of historical data favoring tupaiid affinities, in: Ravosa, M.J., Dagosto, M. (Eds.), Primate Origins: Adaptations and Evolution. Springer US, New York, pp. 403-435.

Godinot, M., Beard, K.C., 1991. Fossil primate hands: a review and an evolutionary inquiry emphasizing early forms. J Hum Evol 6, 307-354.

Godinot, M., Beard, K.C., 1993. A survey of fossil primate hands, in: Preuschoft, H., Chivers, D.J. (Eds.), Hands of Primates. Springer-Verlag/Wien, New York.

Gregory, W.K., 1920. On the structure and relations of *Notharctus*, an American Eocene primate. Mem Am Mus Nat Hist 3, 49-243.

Grow, N., Gursky-Doyen, S., 2010. Preliminary data on the behavior, ecology, and morphology of pygmy tarsiers (*Tarsius pumilus*). International Journal of Primatology 31, 1174-1191.

Gunnell, G.F., 2002. Notharctine primates (Adapiformes) from the early to middle Eocene (Wasatchian-Bridgerian) of Wyoming: transitional species and the origins of *Notharctus* and *Smilodectes*. Journal of Human Evolution 43, 353-380.

Hamrick, M.W., 1998. Functional and adaptive significance of primate pads and claws: evidence from new world anthropoids. Am J Phys Anth 106, 113-127.

Hamrick, M.W., 1999. Pattern and process in the evolution of primate nails and claws. Journal of Human Evolution 37, 293-297.

Hamrick, M.W., 2001. Development and evolution of the mammalian limb: adaptive diversification of nails, hooves, and claws. Evol Dev 3, 355-363.

Hamrick, M.W., Alexander, J.P., 1996. The hand skeleton of *Notharctus tenebrosus* (Primates, Notharctidae) and its significance for the origin of the primate hand. American Museum Novitates 3182, 1-20.

Hershkovitz, P., 1977. Living new world monkeys (Platyrrhini), volume 1. The University of Chicago Press, Chicago.

Hill, W.C.O., 1953. Primates: comparative anatomy and taxonomy I - Strepsirhini. Interscience Publishers, Inc., New York.

Hill, W.C.O., 1955. Primates: comparative anatomy and taxonomy II - Haplorhini: Tasioidea. Interscience Publishers, Inc., New York.

Hill, W.C.O., 1960. Primates: comparative anatomy and taxonomy IV - Cebidae, part A. Interscience Publishers, Inc., New York.

Homberger, D.G., Ham, K., Ogunbakin, T., Bonin, J.A., Hopkins, B.A., Osborn, M.L., Hossain, I., Barnett, H.A., Matthews, K.L., II, Butler, L.G., Bragulla, H.H., 2009. The structure of the

cornified claw sheath in the domesticated cat (*Felis catus*): Implications for the claw-shedding mechanism and the evolution of cornified digital end organs. Journal of Anatomy 214.

Iwaniuk, A., Nelson, J., Ivanco, T., Pellis, S., Whishaw, I., 1998. Reaching, grasping and manipulation of food objects by two tree kangaroo species, *Dendrolagus lumholtzi* and *Dendrolagus matschiei*. Aust J Zool 46, 235-248.

Jungers, W., Lemelin, P., Godfrey, L., Wunderlich, R., Burney, D., Simons, E., Chatrath, P., James, H., Randria, G., 2005. The hands and feet of Archaeolemur: metrical affinities and their functional significance. Journal of Human Evolution 49, 36-55.

Jungers, W.L., Falsetti, A.B., Wall, C.E., 1995. Shape, relative size, and size-adjustments in morphometrics. Yearb Phys Anthropol 38, 137-161.

Jungers, W.L., Godfrey, L.R., Simons, E.L., Chatrath, P.S., 1997. Phalangeal curvature and positional behavior in extinct sloth lemurs (Primates, Palaeopropithecidae). Proceedings of the National Academy of Sciences of the United States of America 94, 11998-12001.

Le Gros Clark, W.E., 1936. The problem of the claw in primates. Proc Zool Soc Lond, 1-24.

Lemelin, P., Grafton, B., 1998. Grasping performance in *Saguinus midas* and the evolution of hand prehensility in primates, in: Strasser, E., Fleagle, J., Rosenberger, A., McHenry, H. (Eds.), Primate Locomotion: Recent Advances. Plenum Press, New York, pp. 131-144.

Lewis, O.J., 1962. The comparative morphology of M. flexor accessorius and the associated long flexor tendons. Journal of Anatomy 96, 321-333.

Maiolino, S.A., Boyer, D.M., Bloch, J.I., Gilbert, C.C., Groenke, J., 2012. Evidence for a grooming claw in a North American adapiform primate: implications for anthropoid origins. PLoS ONE 7, e29135.

Maiolino, S.A., Boyer, D.M., Rosenberger, A., 2011. Morphological correlates of the grooming claw in distal phalanges of platyrrhines and other primates: A preliminary study. Anatomical Record 294, 1975-1990.

Marzke, M.W., 1997. Precision grips, hand morphology, and tools. American Journal of Physical Anthropology 102, 91-110.

Marzke, M.W., Toth, N., Schick, K., Steinberg, R.B., Hunt, K., Linscheid, R.L., An, K.-N., 1998. EMG study of hand muscle recruitment during hard hammer percussion manufacture of Oldowan tools. American Journal of Physical Anthropology 105, 315-332.

McClearn, D., Anatomy of raccoon (Procyon lotor) and coati (Nasua narica and N. nasua) forearm and leg muscles: Relations between fiber length, moment-arm length, and joint-angle excursion. Journal of Morphology 183, 87-115.

McEvoy, J.S., 1982. Comparative myology of the pectoral and pelvic appendages of the North American porcupine (*Erethizon dorsatum*) and the prehensile-tailed porcupine (*Coendou prehensilis*). Bulletin of the American Museum of Natural History 173, 337-421.

Meade, A., Pagel, M., 2014. BayesTraitsV2. University of Reading, Reading, UK.

Mittra, E.S., Smith, H.F., Lemelin, P., Jungers, W.L., 2007. Comparative morphometrics of the primate apical tuft. Am J Phys Anth 134, 449-459.

Mivart, S.G., 1873. On *Lepilemur* and *Cheirogaleus* and on the zoological rank of the Lemuroidea. Proceedings of the Zoological Society of London 1873, 484-510.

Moyà-Solà, S., Kohler, M., Rook, L., 1999. Evidence of hominid-like precision grip capability in the hand of the Miocene ape *Oreopithecus*. Proceedings of the National Academy of Sciences of the United States of America 96, 313-317.

Musser, G.G., 1972. The Species of *Hapalomys* (Rodentia, Muridae). American Museum Novitates 1503.

Musser, G.G., 1979. Results of the Archbold Expeditions. No 102. The Species of *Chiropodomys*, Arboreal Mice of Indochina and the Malay Archipelago. Bulletin of the American Musuem of Natural History 162.

Musser, G.G., Dagosto, M., 1987. The identity of *Tarsius pumilis*, a pygmy species endemic to the montane mossy forests of Central Sulawesi. Am Mus Novit 2867, 1-53.

Nakatsukasa, M., Kunimatsu, Y., Nakano, Y., Takano, T., Ishida, H., 2003. Comparative and functional anatomy of phalanges in Nacholapithecus kerioi, a Middle Miocene hominoid from northern Kenya. Primates 44, 371-412.

Napier, J.R., 1993. Hands. Princeton University Press, Princeton.

Napier, J.R., Walker, A.C., 1967. Vertical clinging and leaping – a newly recognized category of locomotor behaviour of primates. Folia Primatologica 6, 204-219.

Ni, X., Gebo, D.L., Dagosto, M., Meng, J., Tafforeau, P., Flynn, J.J., Beard, K.C., 2013. The oldest known primate skeleton and early haplorhine evolution. Nature 498, 60-64.

Orkin, J.D., Pontzer, H., 2011. The narrow niche hypothesis: gray squirrels shed new light on primate origins. Am J Phys Anth 144, 617-624.

Orme, D., 2013. The caper package: comparative analysis of phylogenetics and evolution in R. Available at http://cran.r-project.org/web/packages/caper/vignettes/caper.pdf.

Preuschoft, H., 1970. Functional anatomy of the lower extermity, in: Bourne, G.H. (Ed.), The Chimpanzee, Vol 3. Karger, Basel, pp. 221-294.

Preuschoft, H., 1973. Functional anatomy of the upper extremity, in: Bourne, G.H. (Ed.), The Chimpanzee. Vol. 6. University Park Press, Baltimore, pp. 34-120.

R Core Team, 2014. R: A Language and Environment for Statistical Computing. R Foundation for Statistical Computing, Vienna, Austria.

Rambaut, A., Suchard, M.A., Xie, D., Drummond, A.J., 2014. Tracer v1.6.

Rasmussen, D.T., 1990. Primate origins: lessons from a neotropical marsupial. Am J Primatol 22, 263-277.

Rasmussen, D.T., Sussman, R.W., 2007. Parallelisms Among Primates and Possums, in: Ravosa, M.J., Dagosto, M. (Eds.), Primate Origins: Adaptations and Evolution. Springer, New York, pp. 775-803.

Revell, L.J., 2014. Graphical methods for visualizing comparative data on phylogenies, in: Garamszegi, L.Z. (Ed.), Modern phylogenetic comparative methods and their application in evolutionary biology: Concepts and practice. Springer-Verlag Berlin Heidelberg, New York.

Ricklan, D.E., 1988. A functional and morphological study of the hand bones of early and recent South African hominids. University of Witwatersrand.

Rose, K.D., 1994. The earliest primates. Evolutionary Anthropology 3, 159-172.

Rose, K.D., Chester, S.G.B., Dunn, R.H., Boyer, D.M., Bloch, J.I., 2011. New fossils of the oldest North American euprimate *Teilhardina brandti* (Omomyidae) from the paleocene–eocene thermal maximum. Am J Phys Anth 146, 281-305.

Rosenberger, A., 1979. Phylogeny, evolution and classification of New World Monkeys, Anthropology. City University of New York, New York, p. 603.

Rosenberger, A.L., 1977. *Xenothrix* and ceboid phylogeny. J Hum Evol 6, 461-481.

Russell, E.M., 1986. Observations on the Behavior of the Honey Possum, *Tarsipes rostratus* (Marsupialia: Tarsipedidae) in Captivity. Australian Journal of Zoology 121, 1-63.

Sargis, E.J., 2001. The grasping behaviour, locomotion and substrate use of the tree shrews *Tupaia minor* and *T. tana* (Mammalia, Scandentia). Journal of Zoology 253, 485-490.

Seiffert, E.R., Perry, J.M.G., Simons, E.L., Boyer, D.M., 2009. Convergent evolution of anthropoid-like adaptations in Eocene adapiform primates. Nature 461, 1118-1122.

Shapiro, L.J., Young, J.W., VandeBerg, J.L., 2014. Body size and the small branch niche: Using marsupial ontogeny to model primate locomotor evolution. Journal of Human Evolution 68, 14-31.

Shrewsbury, M., 2003. Pollical oblique ligament in humans and non-human primates. Journal of Anatomy 202, 397-407.

Shrewsbury, M., Johnson, R.K., 1975. The fascia of the distal phalanx. The Journal of Bone and Joint Surgery 57, 784-788.

Shrewsbury, M.M., Marzke, M.W., Linscheid, R.L., Reece, S.P., 2003. Comparative morphology of the pollical distal phalanx. American Journal of Physical Anthropology 121, 30-47.

Shrewsbury, M.M., Sonek, A., 1986. Precision holding in humans, non-human primates, and Plio-Pleistocene hominids. Human Evolution 1, 233-242.

Smith, E.M., Singer, B.S., Carroll, A.R., 2004. Reply: $^{40}Ar/^{39}Ar$ geochronology of the Eocene Green River Formation, Wyoming Discussion. Geological Society of America Bulletin 116, 253-256.

Smith, T., Quesnel, F., De Plöeg, G., De Franceschi, D., Métais, G., De Bast, E., Solé, F., Folie, A., Boura, A., Claude, J., Dupuis, C., Gagnaison, C., Iakovleva, A., Martin, J., Maubert, F., Prieur, J., Roche, E., Storme, J.Y., Thomas, R., Tong, H., Yans, J., Buffetaut, E., 2014. First Clarkforkian equivalent land mammal age in the Latest Paleocene basal Sparnacian facies of Europe: Fauna, flora, paleoenvironment and (bio)stratigraphy. PLoS ONE 9, e86229.

Soligo, C., Martin, R.D., 2006. Adaptive origins of primates revisited. J Hum Evol 50, 414-430.

Soligo, C., Müller, A.E., 1999. Nails and claws in primate evolution. Journal of Human Evolution 36, 97-114.

Spearman, R.I.C., 1985. Phylogeny of the nail. J Hum Evol 14, 57-61.

Springer, M.S., Meredith, R.W., Gatesy, J., Emerling, C.A., Park, J., Rabosky, D.L., Stadler, T., Steiner, C., Ryder, O.A., Janečka, J.E., Fisher, C.A., Murphy, W.J., 2012. Macroevolutionary dynamics and historical biogeography of primate diversification inferred from a species supermatrix. PLoS ONE 7, e49521.

Steiper, M.E., Seiffert, E.R., 2012. Evidence for a convergent slowdown in primate molecular rates and its implications for the timing of early primate evolution. Proceedings of the National Academy of Sciences of the United States of America 109, 6006-6011.

Stöver, B.C., Müller, K.F., 2010. TreeGraph 2: Combining and visualizing evidence from different phylogenetic analyses. BMC Bioinformatics 11.

Susman, R.L., 1979. Comparative and functional morphology of hominoid fingers. American Journal of Physical Anthropology 50, 215-236.

Susman, R.L., 1998. Hand function and tool behavior in early hominids. Journal of Human Evolution 35, 23-46.

Susman, R.L., Creel, N., 1979. Functional and morphological affinities of the subadult hand (O.H. 7) from Olduvai Gorge. American Journal of Physical Anthropology 51, 311-331.

Sussman, R.W., Raven, P.H., 1978. Pollination by Lemurs and Marsupials: An Archaic Coevolutionary System. Science 200, 731-736.

Szalay, F.S., 1972. Paleobiology of the earliest primates, in: Tuttle, R. (Ed.), The Functional and Evolutionary Biology of Primates. Aldine-Atherton, Chicago, pp. 3-35.

Szalay, F.S., 1994. Evolutionary history of the marsupials and an analysis of osteological characters. Cambridge University Press, Cambridge.

Szalay, F.S., 2007. Ancestral locomotor modes, placental mammals, and the origin of euprimates: lessons from history, in: Ravosa, M.J., Dagosto, M. (Eds.), Primate Origins: Adaptations and Evolution. Springer US, New York, pp. 457-487.

Szalay, F.S., Dagosto, M., 1980. Locomotor adaptations as reflected on the humerus of Paleogene primates. Folia Primatologica 34, 1-45.

Terranova, C.J., 1995. Functional morphology of leaping behavior in galagids: associations between landing limb use and diaphyseal geometry, in: Alterman, L., Doyle, G.A., Kay Izard, M. (Eds.), Creatures of the Dark: The Nocturnal Prosimians. Plenum Press, New York, pp. 473-493.

Terranova, C.J., 1996. Variation in the leaping of lemurs. American Journal of Primatology 40, 145-165.

Thorndike, E.E., 1968. A microscopic study of the marmoset claw and nail. American Journal of Physical Anthropology 28, 247-262.

Venables, W.N., Ripley, B.D., 2002. Modern Applied Statistics with S. Fourth Edition. Springer, New York.

von Koenigswald, W., 1979. Ein lemurenrest aus dem eozänen Ölschiefer der Grube Messel bei Darmstadt. Paläontologische Zeitschrift 53, 63-76.

von Koenigswald, W., Habersetzer, J., Gingerich, P.D., 2012. Pedal distal phalanges of the Eocene adapoids *Europolemur* and *Darwinius* compared to phalanges of *Notharctus* and other primates. Palaeobiodiversity and Palaeoenvironments 92, 539-565.

Walker, A., 1974. Locomotor adaptations in past and present prosimian prmates, in: Jenkins, F.A., Jr. (Ed.), Primate Locomotion. Academic Press, New York, pp. 349-381.

Walker, A., 1979. Prosimian locomotor behavior, in: Doyle, G.A., Martin, R.D. (Eds.), The Study of Prosimian Behavior. Academic Press, New York, pp. 543-565.

Walker, M.J., Ortega, J., Lopez, M.V., Parmova, K., Trinkaus, E., 2011. Neandertal postcranial remains From the Sima de las Palomas del Cabezo Gordo, Murcia, Southeastern Spain. American Journal of Physical Anthropology 144, 505-515.

Weber, M., 1904. Die Säugetiere. Einführung in die Anatomie und Systematik der recenten und fossilen Mammalia. Gustav Fisher, Jena.

Weisbecker, V., Ashwell, K., Fisher, D., 2013. An improved body mass dataset for the study of marsupial brain size evolution. Brain, Behavior and Evolution 82, 81-82.

Wilkinson, J.L., 1951. The anatomy of an oblique proximal septum of the pulp space. British Journal of Surgery 38, 454-459.

Williams, B.A., Kay, R.F., Kirk, E.C., Ross, C.F., 2010. *Darwinius masillae* is a strepsirrhine - a reply to Franzen et al. (2009). Journal of Human Evolution 59, 567-573.

Youlatos, D., Karantanis, N.E., Byron, C.D., Panyutina, A., 2015. Pedal grasping in an arboreal rodent relates to above-branch behavior on slender substrates. Journal of Zoology Early View.